Nanostructured gene and drug delivery systems based on molecular self-assembly

by

Kris Cameron Wood

B.S. Chemical Engineering, University of Kentucky, 2002

Submitted to the Department of Chemical Engineering in partial fulfillment of the requirements for the degree of

Doctor of Philosophy in Chemical Engineering
at the
Massachusetts Institute of Technology

June 2007

Signature of Author: _____
Department of Chemical Engineering
May 2, 2007

Certified by: _____
Paula T. Hammond, Ph.D.
Bayer Professor of Chemical Engineering
Thesis Supervisor

Certified by: _____
Robert S. Langer, Sc.D.
Institute Professor
Thesis Supervisor

Accepted by: _____
William M. Deen, Ph.D.
Carbon P. Dubbs Professor of Chemical Engineering
Chairman, Committee for Graduate Students

Nanostructured gene and drug delivery systems based on molecular self-assembly

by

Kris Cameron Wood

Submitted to the Department of Chemical Engineering on May 2, 2007 in partial fulfillment of the requirements for the degree of Doctor of Philosophy in Chemical Engineering

Abstract

Molecular self-assembly describes the assembly of molecular components into complex, supramolecular structures governed by weak, non-covalent interactions. In recent years, molecular self-assembly has been used extensively as a means of creating materials and devices with well-controlled, nanometer-scale architectural features. In this thesis, molecular self-assembly is used as a tool for the fabrication of both gene and drug delivery systems which, by virtue of their well-controlled architectural features, possess advantageous properties relative to traditional materials used in these applications.

The first part of this thesis describes the solution-phase self-assembly of a new family of linear-dendritic "hybrid" polymers with plasmid DNA for applications in gene therapy. It begins with an overview of the design of next-generation, non-viral gene delivery systems and continues through the synthesis and validation of hybrid polymer systems, which possess modular functionalities for DNA binding, endosomal escape, steric stabilization, and tissue targeting. This part of the thesis concludes with applications of these systems to two areas of clinical interest: DNA vaccination and tumor targeted gene therapy.

The second part of this thesis describes the directed self-assembly of polymeric thin films which are capable of degrading in response to either passive or active stimuli to release their contents. It begins with a description of passive release thin films which degrade by basic hydrolysis to release precise quantities of model drug compounds. These systems can be engineered to release their contents on time scales ranging from hours to weeks and can also be designed to release multiple drugs either in series or in parallel. Later, field-activated thin films which release their contents in response to an external, electrical stimulus are described and characterized in detail. Together, these approaches combine rapid and inexpensive processing, the ability to conformally coat any surface regardless of composition, size, or shape, and the ability to release multi-drug or multi-dose schedules, and as such they may find applications in a range of areas.

Thesis Supervisor: Paula T. Hammond
Bayer Professor of Chemical Engineering

Thesis Supervisor: Robert S. Langer
Institute Professor

Table of Contents

List of Figures and Tables

Acknowledgements

This thesis could not have been completed without the generosity and support of many. First, I want to thank my thesis advisors, Professors Paula Hammond and Bob Langer, for their enthusiastic support of both me and my work. They encouraged me to strive for lofty goals and challenged me to take on the most important problems. Paula and Bob have been models of dedication, humility, and generosity that I will strive to emulate in my own career.

I would like to thank the members of my thesis committee, Professors Dane Wittrup and Bruce Zetter, who generously gave their time and advice to help further not only this work but also my own professional development. Also, I would like to thank our collaborators: Professor David Lynn, who was instrumental in laying the groundwork for our research on degradable thin films; Professor Jianzhu Chen, who allowed us access to material and intellectual resources in his group during our DNA vaccine work; and Professors Renata Pasqualini and Wadih Arap, whose group provided us with peptide ligands for GRP78 and assisted with *in vivo* luciferase imaging studies.

I thank the many members of the Hammond and Langer groups who have made helpful contributions not only to the work described in this thesis, but more broadly to my educational experience at MIT. Specifically, I would like to thank the following: Steve Little for helping me shape the direction of our gene delivery work during its early stages; David Nguyen for assisting in every aspect of our work on DNA vaccination; Kris Stokes for helpful advice and suggestions regarding polymer synthesis; Greg Zugates for teaching me most of the experimental tissue culture techniques that were used in this work and, more generally, for being a thoughtful sounding board for my ideas and questions; Dan Schmidt for his helpful insight on electroactive thin films; and Helen Chuang for assisting with our work on multicomponent degradable thin films. I am immensely proud of, and grateful to, the undergraduate researchers who worked with me during the completion of this thesis: James Boedicker, Yun Xie, Brian Andaya, Robert Batten, Stefani Wrightman, Samira Azarin, and Lauren Tashima. I have no doubt that the future will hold wonderful successes for each. I thank the members of the chemical engineering support staff who have aided in so many aspects of my graduate experience: Suzanne Easterly, Don McGaffigan, Linda Mousseau, Connie Beal, and Nancy Parkinson. Finally, none of this work would have been possible without generous financial support from the National Institutes of Health, the National Science Foundation, the National Cancer Institute (through a Ludwig Fellowship in Cancer Research), the Harvard-MIT Center for Cancer Nanotechnology Excellence, and the Deshpande Center for Technological Innovation at MIT.

My decision to attend graduate school, and the opportunity to come to MIT, were made possible by a handful of mentors who, through their patience and dedication, exerted a powerful, positive influence on me as an undergraduate student. Professor Dibakar (D.B.) Bhattacharyya offered me a position in his lab as a sophomore, and for two years continually challenged me to become the best scientist I could be. His concern for my personal development far surpassed his ambitions for the specific projects I worked on in his lab, and for that I owe him a great debt. Professors Paula Hammond and Bob Cohen welcomed me into their labs as an undergraduate summer student, my first experience at MIT. They treated me with kindness and generosity, and

helped instill in me the belief that I could excel in a world-class research environment. My decision to come back to MIT for graduate school was in many ways a reflection of the wonderful experience I had working with them. Finally, as graduate students Drs. Dean DeLongchamp and Steve Ritchie spent long hours patiently teaching me how to conduct experiments in the lab, and I thank them for their investments in me.

Undoubtedly the best memories I will take from my graduate experience stem from the wonderful friendships I made at MIT. Whether things were going well or poorly, my friends were always there to encourage, amuse, and lend valuable perspective. I have been blessed with too many friends to mention individually in this space, but I send my heartfelt thanks to each. In particular, Gregg has been a supportive friend and a great listener; his infectious laughter made even mundane things great fun. Bernat has been a loyal friend who was always ready to get together for something fun at a moment's notice. Jane was and continues to be a constant, loving companion who has wholeheartedly supported me in every step of this journey. She has helped me to expand my horizons in wonderful, unexpected ways and has added important balance to my life as a graduate student. For these things and many more, I thank her.

Finally, this work is only possible because of the love and support of my family. My sister Carmen has set a standard for hard work and dedication that has served as a powerful motivator for me. My brother Kevin, who first convinced me to give science a try, continues to be a mentor and friend whose role in my life is irreplaceable. Most of all, I thank my parents, who so thoroughly dedicated themselves to raising my siblings and me. They taught me to value education and hard work, to love and respect myself and others, and to always do my very best. They have all my love.

Chapter 1: Molecular self-assembly

1.1 Introduction

Self-assembly can be defined as the autonomous organization of discrete components into structures or patterns without human intervention.[1, 2] This general phenomenon occurs on length scales ranging from molecular (i.e. crystals, vesicles) to planetary (i.e. weather systems) and can be driven by a wide range of different physical interactions. In some cases, self-assembly behavior can be governed entirely by properties such as the shape, size, charge, surface characteristics, and polarity of constituent components; in other cases, external forces and fields can also play a role.[1, 2] In recent years, self-assembly has been a topic of significant scientific interest because of its pervasive role in nature and its expanding utility as a tool for developing new technologies.[1-5]

In nature, examples of the abundant materials and systems which exhibit self-assembly behavior include atomic or molecular crystals[2, 6], multi-protein complexes (i.e. organelles, viruses), lipid membranes[7], bacterial colonies[8] , and complex weather patterns[1, 2] (Figure 1.1). The interactions governing self-assembly processes in nature vary with respect to length scale. Small-scale molecular self-assembly of crystals or protein complexes, for example, is governed primarily by non-covalent interactions such as van der Waals forces, electrostatics, hydrophobic interactions, hydrogen and coordination bonds. Self-assembly of larger components such as macroscopic objects can also include gravitational attraction, external electromagnetic fields, and magnetic, capillary, and entropic interactions.[1, 2]

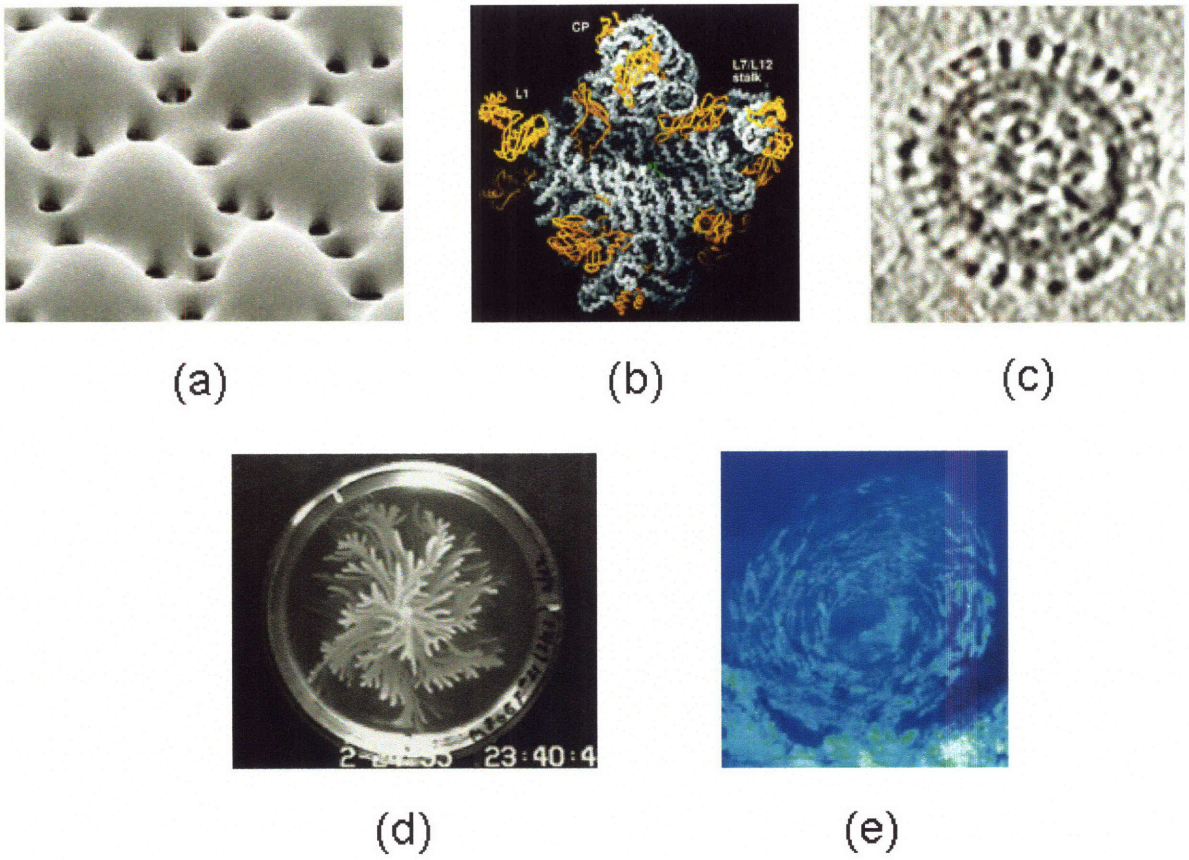

Figure 1.1. Examples of naturally-occurring materials and systems based on self-assembly. (a) Crystalline calcite microlenses from brittlestars[9]; (b) Crystal structure of a ribosome[10]; (c) Micrograph of an individual influenza particle[11]; (d) A colony of Bacillus subtilis[12]; (e) A school of fish[1]

1.2 Synthetic materials and devices based on self-assembly

Driven by an increasing need to produce materials and devices with small-scale, well-controlled, and highly functional architectural features, engineers and scientists have begun to use self-assembly as a powerful fabrication tool.[1-5] Figure 1.2 provides examples of novel materials constructed using the principles of engineering self-assembly, including nanoscale tubes, fibers, and origami-like shapes as well as microscale folded polyhedra and arrayed or aggregated colloids.[13-17]

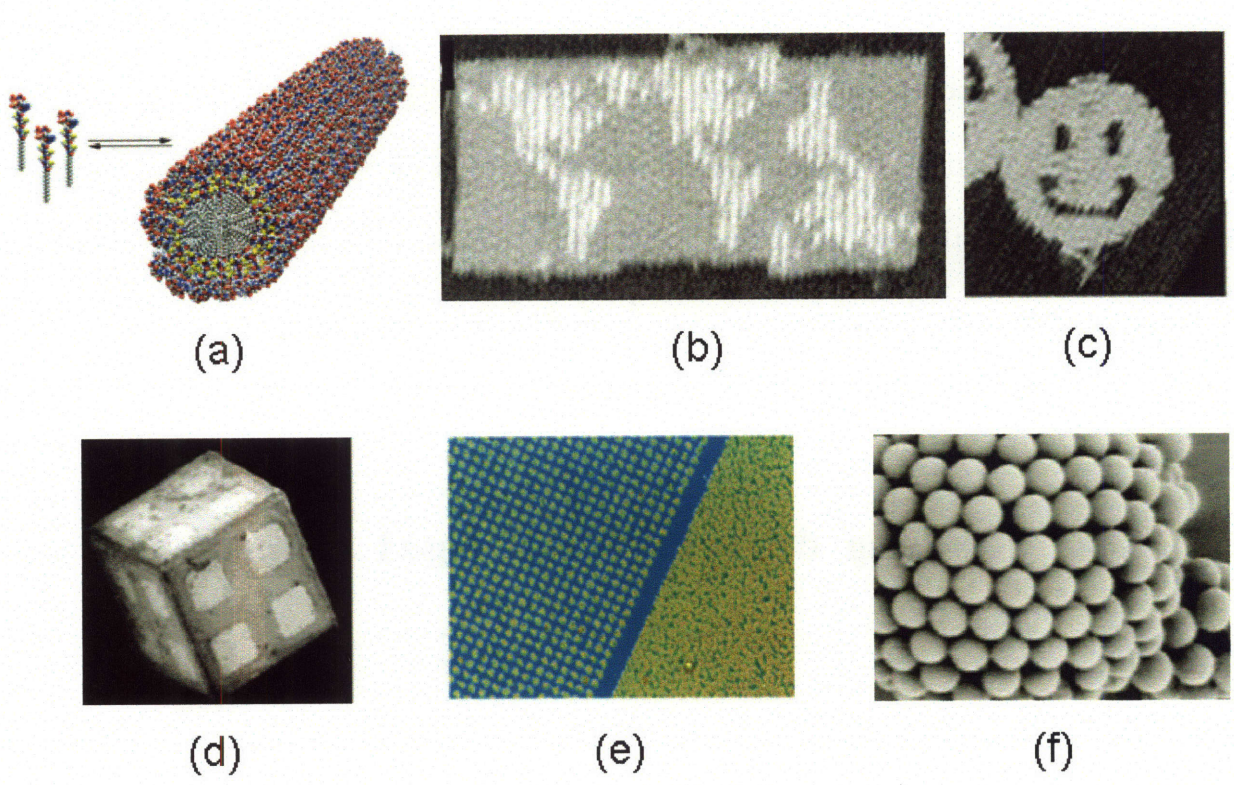

Figure 1.2. Examples of engineered materials based on self-assembly.

(a) Self-assembled peptide-amphiphile nanofibers[13]; (b,c) Two-dimensional self-assembly of DNA "origami" to form complex two-dimensional shapes[14]; (d) Micrometer-scale folded polyhedra[15]; (e) Templated patterning of colloids on a surface[16]; (f) Self-assembly of colloids onto the interface of an emulsion droplet.[17]

Perhaps the most common approach to the design and fabrication of new materials based on self-assembly involves so-called "molecular" self-assembly. As the name implies, molecular self-assembly is the assembly of molecular components into complex, supramolecular structures.[1, 2, 4] This process is usually governed by weak, non-covalent interactions between molecular components. The most significant (and common) applications of molecular self-assembly involve the fabrication of small-scale, ordered structures whose sizes fall between those that can be synthesized using traditional chemistry (individual molecules) and those that

can be manipulated by conventional manufacturing (micrometer to millimeter length scales). Unlike other approaches, self-assembly offers a clear route for assembling individual components into functional ensembles whose sizes range from nano- to micrometers. Molecular self-assembly frequently occurs both in solution and at interfaces (i.e. liquid-liquid, solid-liquid, etc.), and in recent years has yielded a host of interesting new materials such as gels, thin films, periodic two- and three-dimensional structures, and nanoscale wires, fibers, particles, and devices.[1-5]

1.3 Gene and drug delivery systems based on molecular self-assembly

The objective of the research described in this thesis is to use molecular self-assembly as a tool to fabricate gene and drug delivery systems with controlled architectural features and, as a consequence, new and advantageous properties. The first part of this thesis (Chapters 2-5) describes the solution-phase self-assembly of a new family of linear-dendritic "hybrid" polymers with plasmid DNA for applications in gene therapy. Chapters 2-3 describe the design, fabrication, and *in vitro* validation of these systems, and Chapters 4-5 explore their application to two distinct areas of interest in clinical medicine: DNA vaccination and tumor-targeted gene therapy. The second part of this thesis (Chapters 6-9) describes the directed self-assembly of polymeric thin films at a solid-liquid interface. The focus of this work, which is based on the layer-by-layer (LbL) deposition technique, is to construct nanoscale polymeric architectures capable of degrading in response to various stimuli to release their contents. In Chapter 6, an overview of the LbL technique is offered. Chapters 7-8 describe the design, fabrication, and testing of hydrolytically degradable thin films for the controlled release of one or more species. Chapter 9 describes an alternative approach to the fabrication of degradable LbL structures based

on electroactive nanoparticles which trigger film degradation and drug release in response to an electrical stimulus. Finally, Chapter 10 will provide a summary and recommendations for future work based on findings in both parts of this thesis.

1.4 References

1. Whitesides, G.M. & Grzybowski, B. Self-assembly at all scales. *Science* **295**, 2418-2421 (2002).
2. Philip, D. & Stoddart, J.F. Self-assembly in natural and unnatural systems. *Angew Chem Int Ed* **35**, 1154-1196 (1996).
3. Reinhoudt, D.N. & Crego-Calama, M. Synthesis beyond the molecule. *Science* **295**, 2403-2407 (2002).
4. Ikkala, O. & ten Brinke, G. Functional materials based on self-assembly of polymeric supramolecules. *Science* **295**, 2407-2409 (2002).
5. Lehn, J.M. Toward self-organization and complex matter. *Science* **295**, 2400-2403 (2002).
6. Desiraju, G.R. Crystal engineering: The design of organic solids. (Elsevier, New York; 1989).
7. Jones, M.N. & Chapman, D. Micelles, Monolayers, and Biomembranes. (Wiley-Liss, New York; 1995).
8. Shapiro, J.A. Thinking about bacterial populations as multicellular organisms. *Annu Rev Microbiol* **52**, 81-104 (1998).
9. Aizenberg, J., Tkachenko, A., Weiner, S., Addadi, L. & Hendler, G. Calcitic microlenses as part of the photoreceptor system in brittlestars. *Nature* **412**, 819-822 (2001).
10. Ban, N., Nissen, P., Hansen, J., Moore, P.B. & Steitz, T.A. The complete atomic structure of the large ribosomal subunit at 2.4 angstrom resolution. *Science* **289**, 905-920 (2000).
11. Harris, A. et al. Influenza virus pleiomorphy characterized by cryoelectron tomography. *Proc Natl Acad Sci U S A* **103**, 19123-19127 (2006).
12. Mendelson, N.H. Bacillus subtilis macrofibres, colonies and bioconvection patterns use different strategies to achieve multicellular organization. *Environ Microbiol* **1**, 471-477 (1999).
13. Hartgerink, J.D., Beniash, E. & Stupp, S.I. Self-assembly and mineralization of peptide-amphiphile nanofibers. *Science* **294**, 1684-1688 (2001).
14. Rothemund, P.W. Folding DNA to create nanoscale shapes and patterns. *Nature* **440**, 297-302 (2006).
15. Gracias, D.H., Kavthekar, V., Love, J.C., Paul, K.E. & Whitesides, G.M. Fabrication of micrometer-scale, patterned polyhedra by self-assembly. *Advanced Materials* **14**, 235-+ (2002).
16. Lee, I., Zheng, H.P., Rubner, M.F. & Hammond, P.T. Controlled cluster size in patterned particle arrays via directed adsorption on confined surfaces. *Advanced Materials* **14**, 572-577 (2002).
17. Dinsmore, A.D. et al. Colloidosomes: selectively permeable capsules composed of colloidal particles. *Science* **298**, 1006-1009 (2002).

Chapter 2: Designing systems for non-viral gene delivery

2.1 Gene therapy

Gene therapy is conventionally defined as the treatment of disease by introducing exogenous genes, gene segments, or oligonucleotides to appropriate cells.[1, 2] As such, gene therapy aims for the transient or prolonged expression of a therapeutic or corrective gene product in a target cell population. A range of therapeutic approaches for gene therapy have been suggested, and include the expression of replacement genes for single genetic disorders, apoptosis genes to prompt cell "suicide," protective genes for the production of proteins with therapeutic utility (i.e., antiviral or antibacterial), and stimulatory genes for the elicitation of a protective immune response (i.e., DNA vaccines).[1, 2] Further, as our understanding of the genetic and molecular basis of human disease continues to grow, the range of potential applications for gene therapies will follow. Currently, clinical gene therapy trials are underway for illnesses ranging from infectious[3] and cardiovascular[4] diseases to cancer (see Table 2.1).[5, 6] Ultimately, it has been suggested that virtually all human diseases could one day be amenable to some form of treatment using gene therapies.[1, 2]

Table 2.1. Gene therapy clinical trials by indication.

Reproduced with permission from [6].

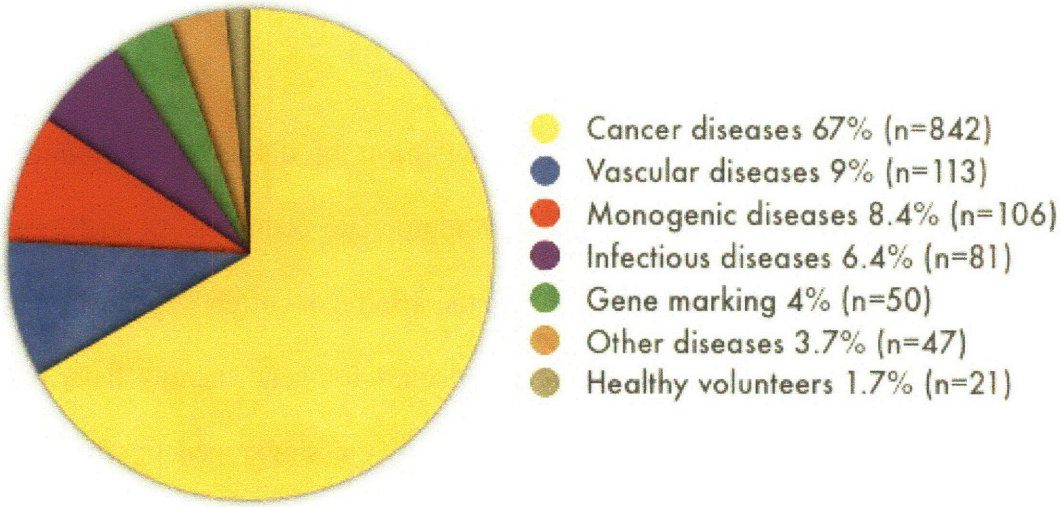

2.2 The gene delivery problem

Despite the great promise of gene therapy as a therapeutic strategy, no gene therapy protocols have been approved by the US FDA for use in clinical settings.[6-9] The most important factor limiting the clinical application of gene therapy protocols is the lack of gene delivery systems which are both safe and effective.[7-9] Traditionally, two broad classes of delivery vehicles ('vectors') have been used: viral and non-viral. Table 2.2 shows a breakdown of worldwide clinical trials for gene therapies organized by delivery vector.[6]

Table 2.2. Gene therapy clinical trials by delivery vector.

Reproduced with permission from [6].

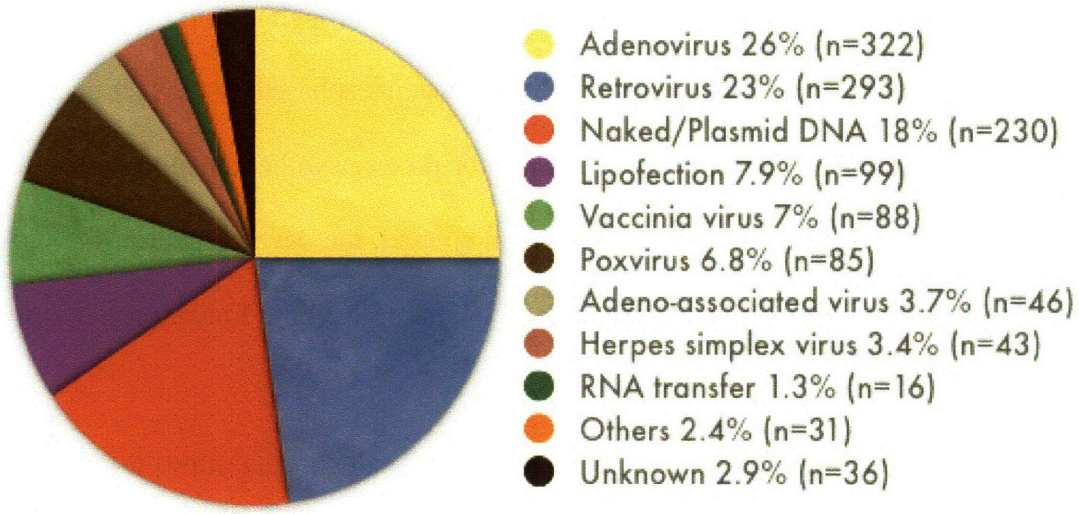

The Journal of Gene Medicine, © 2007 John Wiley and Sons Ltd www.wiley.co.uk/genmed/clinical

2.2.1 Viral Gene Delivery Vectors

Viral vectors possess highly evolved functions for overcoming the various barriers to gene transfer, and as a result typically yield high levels of both delivery and expression (frequently greater than 90% for each). As a result, viruses have become the most common vectors used in gene therapy research and clinical trials.[6] Among the over 600 current clinical trials, about 70% use recombinant viral vectors, including retroviruses, lentiviruses, adeno- and adeno-associated viruses, herpes simplex, and combinations thereof.[6, 10-16] However, viruses have significant restrictions, including immunogenicity, high risk of insertional mutagenesis, restricted cell targeting abilities, limited DNA carrying capacity, production problems, and high cost. Collectively, these restrictions make current viral vectors unsuitable for clinical use.[7-9]

2.2.2 Non-Viral Gene Delivery Vectors

The term "non-viral" gene delivery system encompasses the wide range of approaches that have been used to deliver nucleotide-based therapeutics without using viruses. Under this

heading, a suite of *electrical*[17] and *mechanical*[18-21] methods have been explored; however, the most common and versatile methods for overcoming the various biological barriers to gene transfer without the deleterious side effects of viral vectors are through the use of *chemical* methods.[9] The interest surrounding chemical gene delivery systems is based on the fact that they are generally safer than their viral counterparts and allow for precise synthetic manipulation and control.[7-9] The following paragraphs detail, in a historical context, the development of the most significant non-viral gene delivery systems used to date, including cationic lipids, proteins, and synthetic polymers.

As early as the 1950s, cationic proteins were used in high salt concentrations to condense DNA for transfer into cells. Not long after, 2-(diethylamino) ether (DEAE)-dextran and calcium phosphate were used for similar applications. While still used in laboratory *in vitro* transfections, these chemical systems are cytotoxic, unstable under physiological conditions, and inefficient delivery systems *in vivo*.[9, 22, 23]

A second wave of non-viral vectors came to prominence in the 1980s, most notably with the development of Lipofectin, an artificial, cationic lipid-based system, in 1987. Later work with these materials yielded systems based on cationic and neutral liposomes, combinations of lipids with peptides and polymeric systems, and other lipid-based systems. Lipid-based systems were among the first chemicals used in *in vivo* studies, and in fact are still used in on-going studies today; however, they have thus far been limited by significant drawbacks involving *in vivo* stability and toxicity.[24-27]

A few years later, peptide- and protein-based methods gained significant interest in the non-viral arena, particularly because they allow for precise control over molecular weight and chemical composition and can be readily functionalized with peptide-based functional domains

such as targeting ligands, membrane destabilizing peptides, and nuclear localization sequences. For example, poly-L-lysine (PLL)-based systems were used extensively in early studies in this area.[28] More recently, synthetic modifications to PLL-based systems have shown that significant transfection enhancements can be achieved using conjugated ligands for cell targeting or endosomal disruptive elements for cytoplasmic release.[29, 30] In addition to PLL-based systems, other peptides such as short derivatives of human histone or protamine, poly-L-ornithines[31], elements of DNA viruses ("pseudocapsids"), and engineered proteins have also gained significant interest and merit further investigation.[32]

While liposome-based vectors have matured to the point of widespread application in clinical trials, polymeric vectors (polyplexes) have lagged behind. This seems paradoxical, as polyplexes were used in the laboratory for insertion of exogenous DNA long before the use of lipoplexes.[33] However, it was not until the advent of polyethylenimine (PEI)-based vectors that synthetic polymers were recognized as useful materials for non-viral gene delivery applications.[34] PEI exhibited transfection efficiencies far exceeding other polyplex-based systems, primarily owing to the endosomal buffering capacity of secondary amines along its backbone. Numerous studies on second-generation PEIs have elucidated important design principles for synthetic vector design, for example, the importance of the proton sponge mechanism in orchestrating endosomal escape, the effect of cell-specific targeting via conjugated ligands, the effect of molecular weight and cross-link density on toxicity, and the effect of charge density on transfection.[35-42] Further, these systems represent some of the most efficient transfecting systems to date. In addition to first- and second-generation PEI-based systems, other linear polymeric systems have been explored as delivery vectors, including natural

polymers gelatin and chitosan, methylacrylate/methacrylamide polymers, β-cyclodextrin-containing polymers, and poly (β amino esters).[9, 43-45]

Finally, hyperbranched and dendritic macromolecules have also been a source of great interest for gene delivery applications, primarily because they can be synthesized with great control over molecular architecture and functionality as well as high levels of endosomal buffering capacity. Among the most frequently explored dendritic systems are cationic poly (amidoamine)s (PAMAM), which have been shown to complex DNA into small, toroidal particles, inhibit nuclease degradation, and promote endosomal release and transfection *in vitro* (with transfection enhancements of 10-100% relative to lipid-based reagents).[46, 47] In addition to PAMAM, other dendritic systems (e.g., PLL dendrimers) and their conjugates have also been explored, albeit in a much smaller capacity.[48]

2.2.3 Designing a New Non-Viral Gene Delivery System

The focus of the work described in this thesis on the topic of gene delivery involves the development of a new class of delivery agents for *in vivo* applications. We chose to focus on non-viral, chemical delivery systems for the following reasons: (1) chemical structures are synthetically versatile, and as such, elements imparting various functionalities (i.e. tissue targeting, steric stabilization, etc.) can be easily added and/or modified; (2) chemical delivery systems can transport much larger DNA payloads than their viral counterparts; and (3) chemical delivery systems are generally safer than their viral counterparts (for example, they can be made from biocompatible building blocks and pose little risk for adverse immune responses or insertional mutagenesis). In order to design a gene delivery system with improved properties, however, we first had to consider the major barriers limiting efficient gene delivery *in vivo*. The

following section provides an overview of these extracellular and intracellular barriers along with corresponding strategies that have been developed to overcoming them.

2.3 Overcoming extra- and intracellular barriers to efficient gene delivery using non-viral delivery systems

2.3.1 Extracellular Barriers

Extracellular barriers to systemic delivery of DNA are those that can be encountered between the site of administration and the surface of the cellular target of interest. Synthetic vectors must be able to charge neutralize and condense DNA into small, discrete particles (< 200 nm), avoid both self and non-self interactions, cause low systemic toxicity, minimize interactions with plasma proteins, evade the adaptive immune system, and selectively target specific cell populations.[9, 43] Figure 2.1 provides an overview of these extracellular barriers.

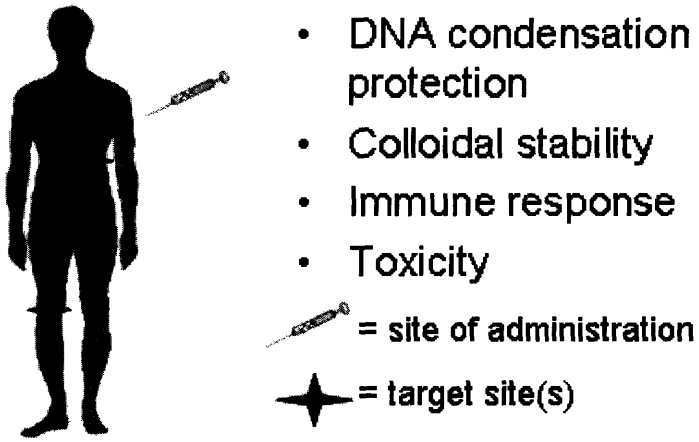

Figure 2.1. Extracellular barriers to systemic gene delivery.

Neutralization of DNA's negative charge to form condensed particles is required in order to create discrete, small particles capable of internalization by somatic cells. It is important that polyplexes be small (typically less than 200 nm) because larger particles are poorly internalized by many cells and tissues and are often rapidly removed from circulation by the

reticuloendothelial system (RES). Further, polyplexes should have a near-neutral surface charge, as highly charged particles commonly exhibit non-specific interactions with the extracellular matrix, cell membranes in non-target tissues, and plasma proteins, and are quickly removed from circulation via the phagocytotic pathway.[43]

DNA condensation and charge neutralization can be accomplished by the addition of multivalent cations (i.e., polyamines, positively-charged polymers, and peptides) which electrostatically condense DNA into rod-like, spheroidal, or toroidal nanoparticles. While charge, binding affinity, and size of polyplexes are all generally controllable experimental variables, there currently exists no optimum set of conditions for transfection. Instead, a system-specific optimization of these parameters is generally required.[43, 45, 49, 50]

Avoidance of self and non-self interactions (i.e., aggregation and absorption by non-target tissues, respectively) as well as significant increases in circulation time can be achieved by incorporating linear, flexible, hydrophilic polymers such as poly (ethylene glycol) (PEG) into polyplex formulations. See Figure 2.2.[44, 51, 52] PEG is known to sterically stabilize polyplexes and other colloidal species by creating a hydrated "brush" layer on the particle surface which can both sterically inhibit aggregation and also limit immune surveillance, permitting long circulation times.

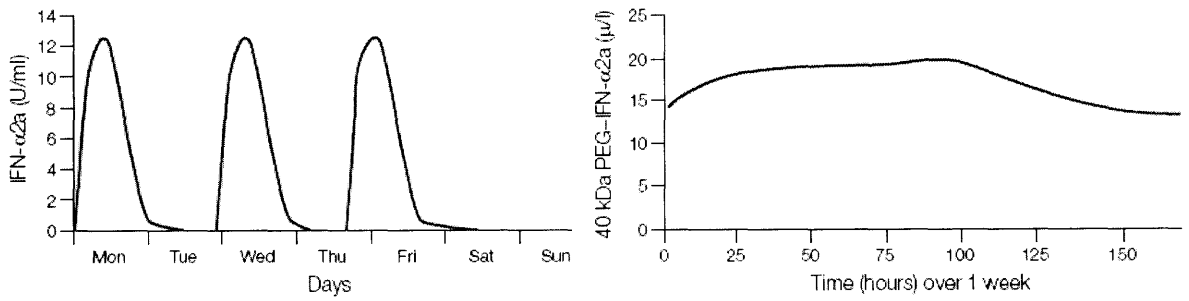

(a) **(b)**

Figure 2.2. Effect of polyethylene glycol on plasma half-life.

Plasma concentration of subcutaneously injected interferon (IFN) versus time without (a) or with (b) polyethylene glycol (PEG) conjugation. Reproduced with permission from [52].

Toxicity is generally a polymer-specific phenomenon. However, it has been shown in first generation synthetic vectors such as polyethylenimine (PEI)[53], chitosan[54], and β-cyclodextrin-containing polymers[55] to be proportional to polymer molecular weight and charge density. Further, many newer synthetic systems such as dendrimers[56], networked[57] and degradable polymers[58-61], and various PEGylated systems[44, 51, 52] demonstrate far less toxicity than first generation vectors. In sum, toxicity can generally be controlled by judicious choice of condensing polymer species and may also be minimized by incorporation of PEG.

Receptor-mediated endocytosis is one of a handful of mechanisms by which cells specifically internalize certain materials from their surroundings. Importantly, it is perhaps the most versatile and common method by which directed uptake of therapeutic materials can be targeted to specific cell populations.[43, 44, 62, 63] The steps in this process include the following: (a) binding of the particle (by specific molecular recognition) to a cell surface receptor, (b) clathrin-mediated vesicle formation, (c) clathrin depolymerization and uncoating of the internalized vesicle to form the early endosome, (d) ATP-powered influx of protons and subsequent pH decrease and ligand release, (e) recycling of plasma membrane receptors to the cell surface, and (f) trafficking of the late endosome to the lysosome for degradation of the internalized particle.[62]

Taking advantage of the receptor-meditated endocytic pathway can allow for selective targeting of ligand functionalized therapeutics (or carriers) to specific cells, a process which can both enhance therapeutic efficacy and decrease undesired side effects. Examples of ligands that have been used in targeted delivery applications are provided in Table 2.3, below.

Table 2.3. Common ligands for receptor-mediated endocytosis

Ligand	Target Cell Type
Galactose	Hepatocyte[64, 65]
Mannose	Macrophage, Dendritic cells[39, 66, 67]
αDEC-205	Dendritic cells[68]
Folate	Cancer (various)[44, 69]
Transferrin	Cancer (various)[70]
Epidermal Growth Factor	Cancer (various)[71]
Antibodies	Various[72]
Aptamers	Various[73]
Short Peptides	Various[74, 75]
Small molecules	Various[76]

In addition to receptor-mediated endocytosis, a range of additional, passive routes have also been utilized for the selective targeting of therapeutics to certain cell types. For example, non-specific adsorptive endocytosis has been cited as a mechanism by which certain polyplexes with residual positive charge and no bound ligand enter cells. In this process, the polyplexes interact with negatively charged proteoglycans of the cell membrane, a process that leads to membrane binding and internalization. However, this non-specific mechanism has several *in vivo* drawbacks, as it also favors opsonization by negatively charged blood proteins, premature blood clearance, and accumulation in "first-pass" organs such as the liver, lung, and spleen.[77] The phagocytotic pathway has been utilized for the selective targeting of therapeutics to antigen-presenting cells of the immune system, but is not useful for other somatic cell types.[78] Finally, the enhanced permeability and retention effect (EPR), wherein therapeutics passively enter cancer cells by diffusion out of leaky angiogenic vasculature, is mediated by the presence of a

polyplex component that enhances circulation time (i.e., PEG) and has been shown to be effective in the treatment of some malignant tumors.[44, 79]

2.3.2 Intracellular Barriers

Intracellular barriers to transfection include all those between the point of internalization by the target host cell and the expression of gene products. Steps in this process include cellular uptake (for example, by receptor-mediated endocytosis), endosomal escape, nuclear transport, and vector unpackaging.[9, 44] See Figure 2.3.

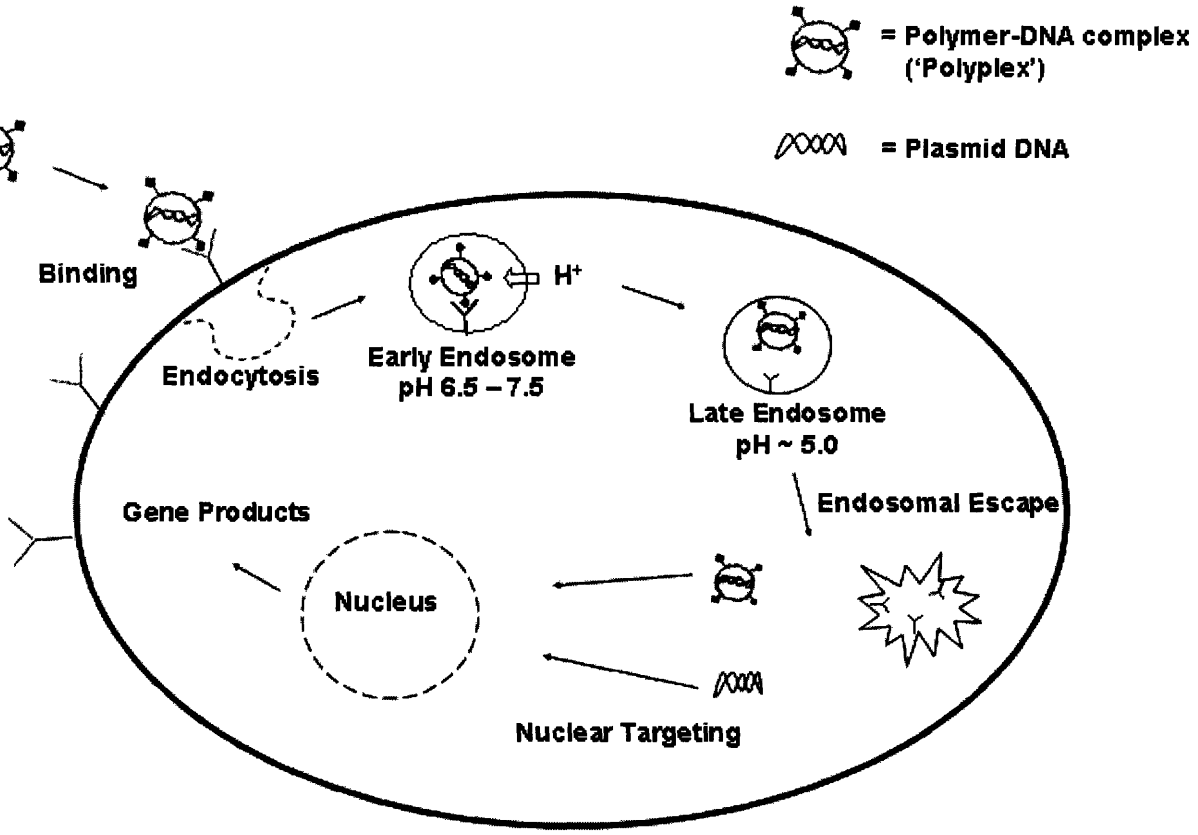

Figure 2.3. Intracellular barriers to targeted gene delivery.

Upon internalization by endocytosis, a polyplex is enveloped in an intracellular vesicle called an endosome. Over time, the pH of the endosome is lowered before it eventually fuses with a second vesicle called a lysosome, where its contents undergo hydrolytic and enzymatic

degradation. Importantly, in order for an internalized polyplex to avoid degradation, it must escape from the endosomal vesicle into the cytoplasm prior to reaching the lysosome. [62]

Endosomal escape into the cytoplasm may be orchestrated by either biologically-inspired or completely synthetic methods. In the former, fusogenic peptides or "smart" polymers can be designed to undergo a conformational shift as the endosomal pH lowers from ~6-7 (early endosome) to ~5-6 (late endosome), mimicking the method by which viruses, such as influenza (via the mHA2 capsid protein), escape lysosomal trafficking. In both the case of fusogenic peptides and "smart" polymers, the pH-triggered conformational shift results in a hydrophobic α-helical structure capable of fusing with and disrupting the plasma membrane.[80, 81] On the other hand, two completely synthetic methods have also been employed to direct endosomal escape. In the first, pH-sensitive liposomes, the pH drop triggers a change in self-organizing behavior (i.e., stable lipid bilayer at pH 7 → hexagonal-II structure at pH 5.5), which results in a structure capable of membrane fusion and disruption. Dioleoylphosphatidyl ethanolamine (DOPE) is perhaps the most well characterized material of this type.[80] Further, the most common synthetic method for endosomal escape is the so-called "proton sponge" mechanism. This mechanism, first identified by Bousiff and coworkers, involves the use of condensing agents with cationic functional groups whose pK values lie near the range of 5-6. Thus, protonation of these groups, most commonly secondary and tertiary amines, occurs as the pH of the endosome is lowered. As chloride counterions accumulate in the buffered vesicle, an osmotic pressure gradient is created across the vesicle membrane. Eventually, the membrane is destabilized as a result of this osmotic pressure gradient and the endosomal contents escape into the cytoplasm.[34] See Figure 2.4.

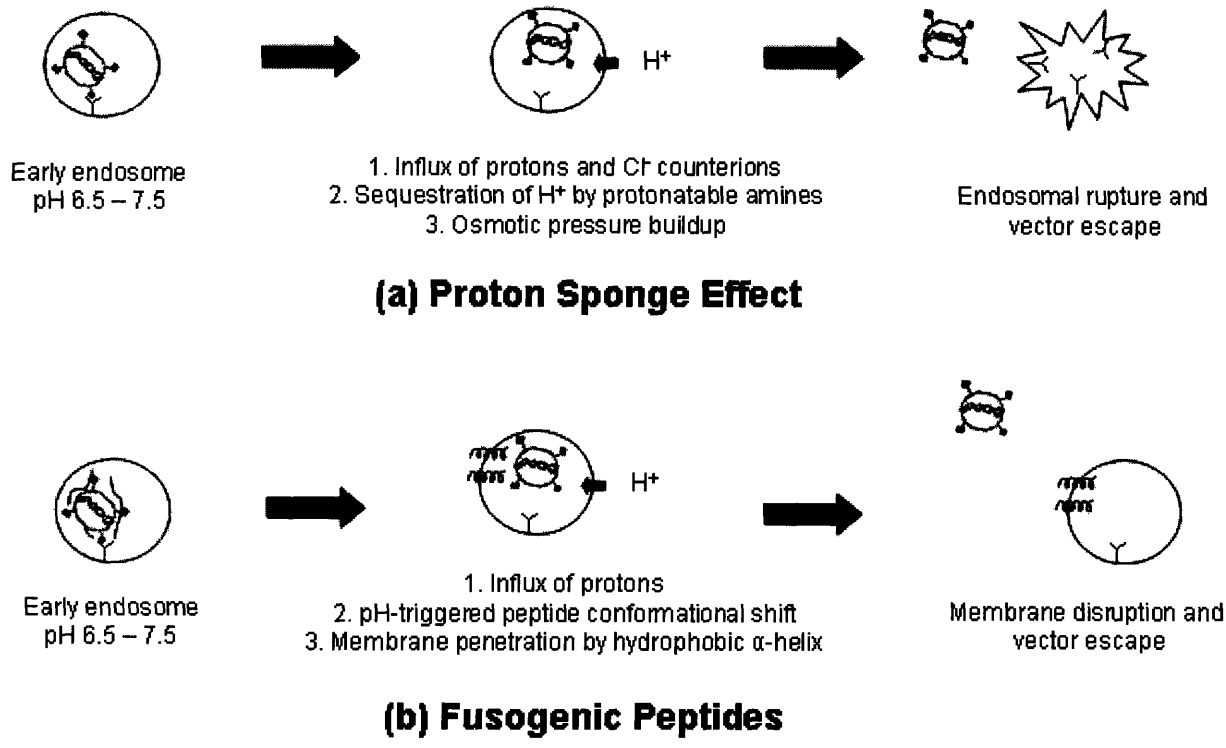

Figure 2.4. Endosomal escape mechanisms in synthetic delivery systems.

(a) Proton sponge effect. (b) Fusogenic peptides.

After entering the cytoplasm and before expression, encapsulated DNA must be partially or fully unpackaged to allow access to the nuclear transcription apparatus.[49] In support of this hypothesis, it has been observed that, for the case of linear polycations (i.e., poly-L-lysine (PLL)), the transcription efficiency is inversely related to molecular weight. It has also been demonstrated that high molecular weight (i.e., PLL 180 kDa or PEI 800 kDa)[49] or strongly charged[35] polycations result in low transfection efficiencies, probably because DNA is never released from the tightly-bound polyplex. On the contrary, lower molecular weight systems (i.e., PLL 19 kDa or PEI 25 kDa) result in much faster polyplex dissociation and higher transfection efficiencies.

It is not clear whether vector unpackaging prior to or following nuclear entry is optimal for highest transfection efficiencies. It has, however, been demonstrated that this can occur in

either the cytoplasmic or nuclear milieu.[82] Despite this uncertainty, it is likely that partial or complete vector unpackaging must precede transcription.[83] Very little work has been devoted to the development of systems with programmed mechanisms for vector unpackaging, but potential solutions include degradable, swellable, or micellar systems that favor dissociation of polymers from DNA on a physiologically relevant time scale.[57-61]

Once in the cytoplasm, DNA must be transported to the nucleus for transcription. The nucleus, which contains nearly all of the cell's genetic material and transcriptional machinery, is surrounded by two phospholipid bilayer membranes. These membranes are effectively fused at the sites of nuclear pore complexes (NPCs), which are ~125 MDa, barrel-shaped cavities composed of 50-100 different proteins.[62] Polyplexes cannot traverse the nuclear membrane and thus must be transported through the NPCs. Further, it is known that polyplexes are too large to enter through nuclear pore complexes by passive diffusion (diffusion limit ~ 9 nm).[84] It has been shown that plasmids microinjected into the cytoplasm express very poorly, while plasmids microinjected into the nucleus are highly expressed. Taken in conjunction with the known dimensions of the NPC, this data suggests that expression of exogenous DNA in nondividing cells (in which passive, mitotic nuclear entry is not possible) must require an active transport mechanism for nuclear entry.

In nature, all proteins that are found in the nucleus are synthesized in the cytoplasm. Thus, they too require an active transport mechanism for nuclear entry. One of the most well-characterized methods of assisted nuclear import is the importin pathway. This pathway involves the following steps. First, a cargo protein attached to a 5-20 basic amino acid sequence called a nuclear localization sequence (NLS) binds to importin-α and importin-β proteins (the NLS binds directly to importin-α). The importin-β portion of the trimeric complex then interacts

with specific components of the NPC, translocating the complex into the nucleoplasm by a poorly understood, ATP-dependent process. Once in the nucleoplasm, Ran-GTP interacts with importin-β, triggering release of the cargo-NLS from the trimeric complex.[62] See Figure 2.5 and Table 2.4. This strategy has been mimicked in polyplex based systems, where either the cationic polymer or DNA is bound (usually covalently) with an NLS peptide sequence for assisted nuclear import. Great enhancements in transfection (10- to 1000-fold) have been accomplished using these methods to date; however, this subset of gene therapy technology is still in its early infancy and warrants further exploration.[85-88] Finally, it is worth noting that nuclear localization strategies are designed for non-dividing cellular systems, the systems of interest in many clinical applications. However, cell-cycle-dependent transfection, in which vectors or DNA are designed for (passive) nuclear entry only during mitotic disaggregation of the nuclear membrane, may sometimes be advantageously exploited, for instance, in the case of targeting dividing brain tumor cells while avoiding non-dividing healthy cells.[77]

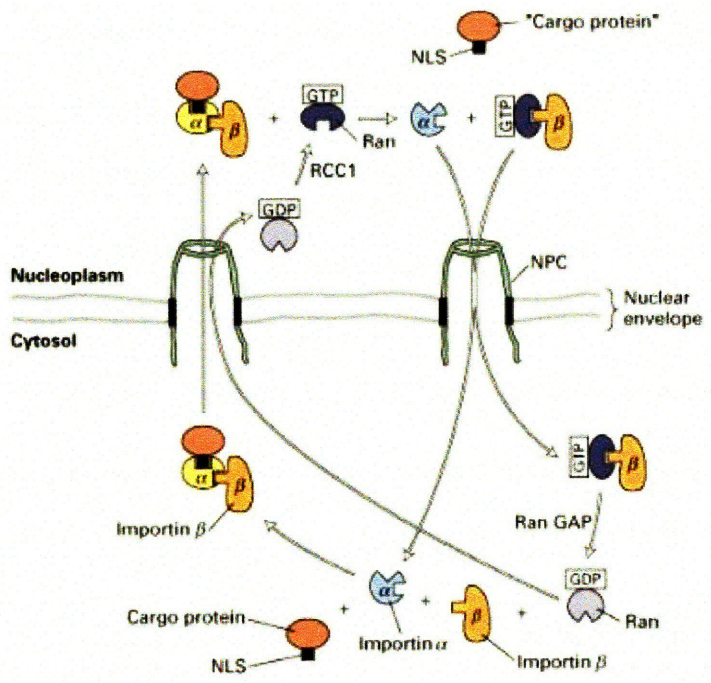

Figure 2.5. The importin pathway for nuclear import and export.

Adapted from [62].

Table 2.4. Common nuclear localization peptide sequences.

Adapted from [83-86]

Name	Sequence[a]
SV40	PKKKRKV
NF-κB	VQRKRQKLMP
OCT-6	GRKRKKRT
TFIIE-β	SKKKKTKV
TCFI-α	GKKKKRKREKL

a: peptide sequences given as single amino acid abbreviations

A summary of the major extracellular and intracellular biological barriers discussed in this section, along with the most prominent strategies for overcoming each barrier, is provided in Table 2.5, below.

Table 2.5. Common strategies for overcoming major biological barriers to gene delivery.

Barrier	Strategy
DNA condensation and protection	Cationic materials (e.g., polymers, lipids)
Avoidance of undesired interactions	Hydrophilic, flexible polymers (e.g., PEG)
Tissue targeting	Targeting ligands
	Passive targeting (e.g., phagocytosis or EPR effect)
Endosomal escape	Buffering amines ("Proton sponge effect")
	Fusogenic peptides / polymers
Vector unpackaging	Hydrolytic or reductive degradation, swelling
Nuclear import	Nuclear localization peptides

2.4 Next-generation synthetic vectors: The "artificial virus"

It is clear that a single delivery system with the ability to overcome the diverse biological barriers described above must be able to perform multiple tasks. For example, such a system must compact DNA into small particles of virus-like dimensions that can localize in targeted regions and traverse cell membranes, protect DNA cargo from degradation, shield DNA from undesired interactions with non-target tissues and the immune system, escape from endosomal vesicles, and deliver DNA to the nucleus for transcription. To accomplish these tasks, it is clear that multiple, diverse functional domains must be included in the delivery formulation, and that each domain must be able to exert its function in a way that is unhindered by the other components in the system. The term "artificial virus" has been used to describe such a multifunctional synthetic system possessing the multiple, dynamic functions of a virus, yet constructed from completely synthetic building blocks. An example of such a hypothetical system is shown in Figure 2.6.[44, 89]

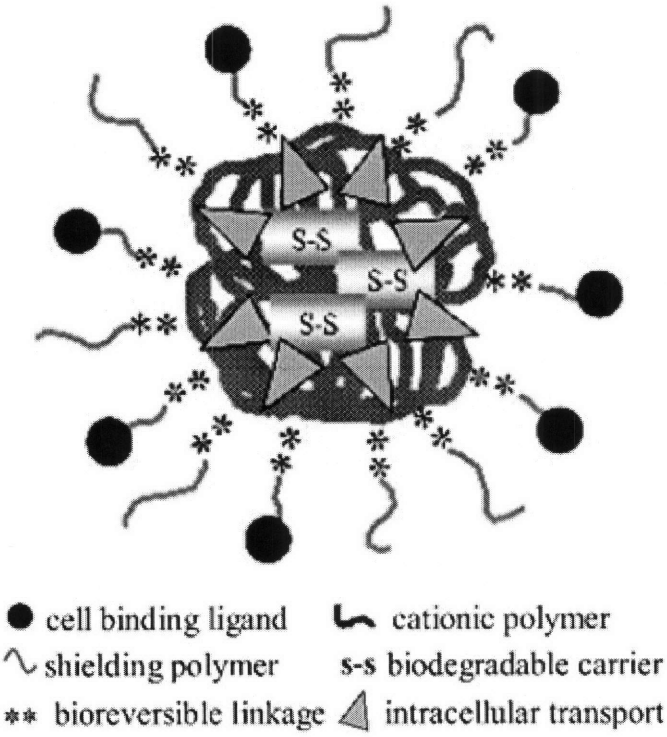

Figure 2.6. Schematic of a hypothetical "artificial virus"

Reproduced with permission from [44].

Over the past fifteen years, numerous investigators have attempted to build delivery systems with artificial virus-like properties.[44] However, there are only a few examples of truly multifunctional systems which have been designed with functionalities to overcome multiple biological barriers, and no consensus design rules have been established for the fabrication of such systems. One of the primary factors limiting progress in this area is the fact that multiple functional domains in a single system rarely behave synergistically or, for that matter, additively. The reason for this shortfall is simple: addition of new functional domains to an existing delivery system usually changes the character of existing domains.

Figure 2.7 provides an example of such a scenario. In this case, investigators were interested in using PEI as an *in vivo* delivery vehicle. However, it is well known that PEI-DNA complexes are unstable in physiological salt concentrations, which result in aggregation of

complexes and rapid clearance from circulation. In an attempt to remedy this situation, the authors modified PEI with a second polymer, PEG, which is known to stabilize colloidal suspensions by forming a dense, hydrophilic brush layer on the particle exterior, sterically inhibiting charge shielding at the particle surface and resultant particle-particle interactions (Figure 2.7(a)).[90] As shown in Figure 2.7(b), while PEGylation indeed stabilized particles against salt-induced aggregation, it also caused an undesired, 1000-fold drop in transfection efficiency *in vitro*. The reasons for this effect are likely two-fold. First, by reacting with secondary amines in the PEI main chain, the PEG modification may have imposed additional steric effects on DNA binding and condensation, which in turn effect particle size, DNA unpackaging, and direct polymer-cell membrane interactions. Second, by changing the basic character (i.e. pK_a) of secondary amines in PEI, the conjugation likely also changed their buffering and endosomolytic properties, which are known to be central to their transfection activity.[34, 35]

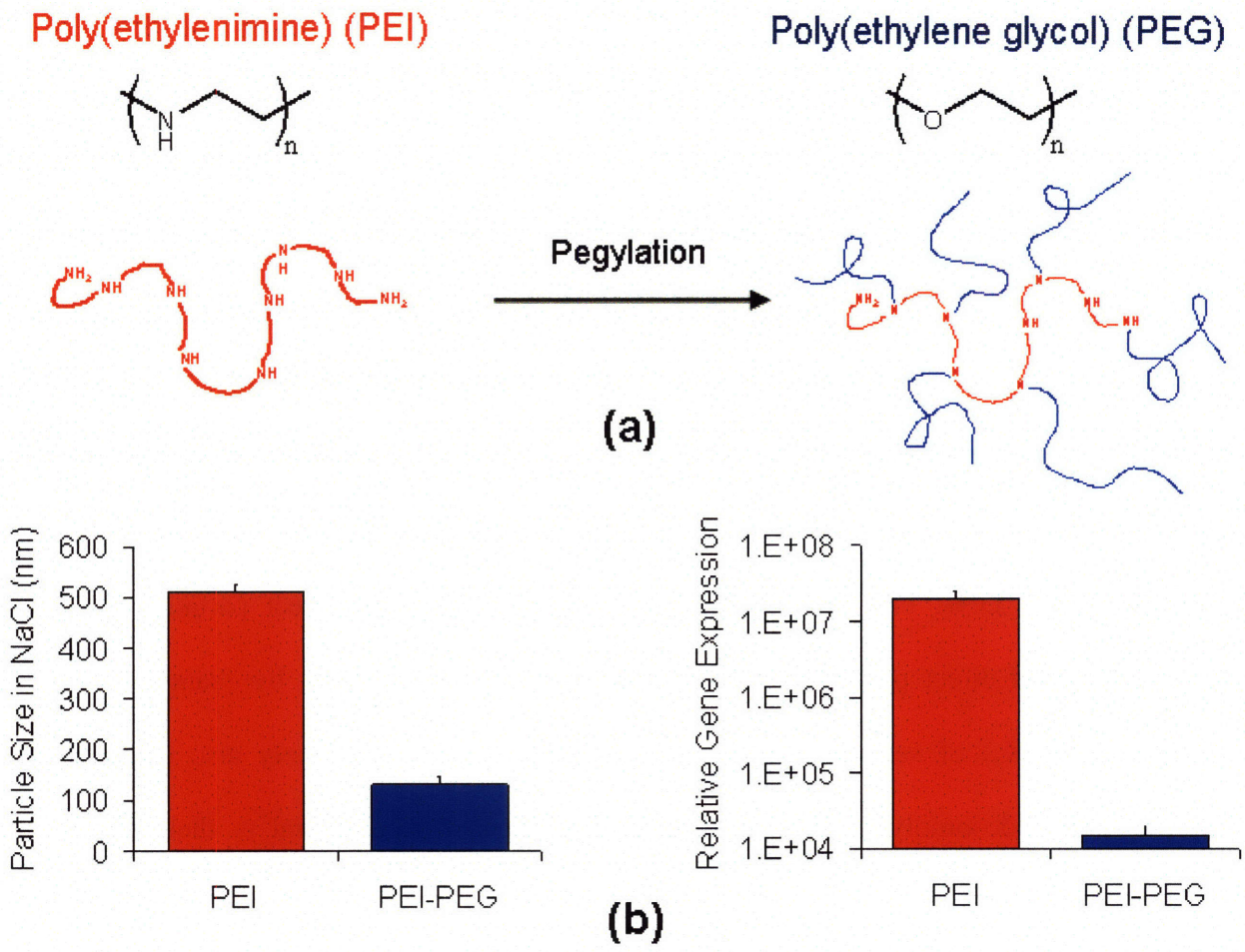

Figure 2.7. Effect of polyethylene glycol (PEG) modification of polyethylenimine (PEI) on colloidal stability and transfection.

(a) Schematic showing chemical structures of PEI and PEG as well as the PEI-PEG conjugation process (termed "PEGylation"). (b) Plots showing (i) size of polymer-DNA complexes after 1 h incubation in 10 mM NaCl and (ii) relative gene delivery efficacy of PEI and PEI-PEG conjugates.[90]

2.5 A modular delivery system

The case described above is just one of many examples in which the modification of an existing polymer structure with new domains encoding properties such as cell targeting, vector unpackaging, or steric stabilization resulted in deleterious effects on existing properties. In

response to this important limitation, we set out to design a new gene delivery system possessing multiple functional domains arranged together in a modular fashion, such that new elements could be added, modified, or removed without exerting a negative effect on the remaining properties. To achieve this, we required that functional domains be physically separated from one another. An example of such a system (possessing functional domains for DNA binding, endosomal escape, steric stabilization, and tissue or intracellular transport) is shown in Figure 2.8. In order to make this design feasible, the following criteria must be met: (1) no elements should possess overlapping functions; (2) various elements must be positioned appropriately with respect to one another so as to best facilitate the function of each; and (3) elements must be assembled using orthogonal, complementary chemistries.

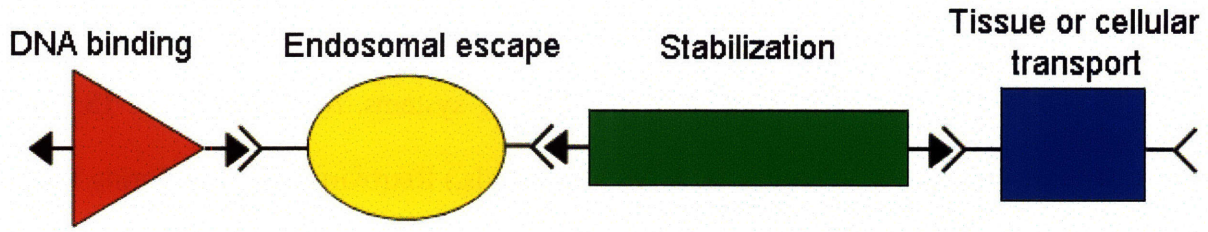

Figure 2.8. Architecture of a hypothetical modular gene delivery system.

In the following three chapters, the design and characterization of a system possessing the above characteristics will be described. Chapter 3 begins by describing the chemical architecture of a linear-dendritic "hybrid" polymer which was designed specifically to possess these characteristics and continues through the synthesis of these systems, their self-assembly with plasmid DNA, and their efficacy in *in vitro* DNA delivery experiments. Chapter 4 extends this work by using the systems developed in Chapter 3 to explore a clinically-relevant model for DNA vaccination. Finally, Chapter 5 describes a useful modification on this concept involving a new, three-step procedure for the synthesis of hybrid polymers, the functionalization of these

systems with short peptides for solid tumor targeting, and a series of *in vitro* (as well as preliminary *in vivo*) results demonstrating their efficacy.

2.6 References

1. Lemoine, N. (ed.) *Understanding Gene Therapy*. (Butterworth-Heinemann, Boston; 1999).
2. Templeton, N. & Lasic, D. (eds.) *Gene Therapy: Therapeutic Mechanisms and Strategies*. (Marcel Dekker, New York; 2000).
3. Frater, A., Fidler, S. & McClure, M. Gene therapy for AIDS and other infectious diseases. *Gene Ther* **9**, 189-213 (2002).
4. Metcalfe, B. Gene therapy for cardiovascular disorders: Is there a future? *Ann NY Acad Sci* **953**, 31-42 (2001).
5. McNeish, I. & Seckl, M. Gene therapy approaches for cancer. *Gene Ther* **9**, 87-134 (2002).
6. Journal of Gene Medicine- Gene Therapy Clinical Trials Worldwide. http://www.wiley.co.uk/genmed/clinical/. (2007).
7. Verma, I.M. & Somia, N. Gene therapy - promises, problems, and prospects. *Nature* **389**, 239-242 (1997).
8. Verma, I.M. & Weitzman, M.D. Gene therapy: Twenty-first century medicine. *Annu. Rev. Biochem.* **74**, 711-738 (2005).
9. Luo, D. & Saltzman, W. Synthetic DNA delivery systems. *Nat. Biotechnol.* **18**, 33-37 (2000).
10. Coffin, J., Hughes, S., Varmus, H. & Miller, A. (eds.) Retroviruses. (Cold Spring Harbor Laboratory Press, Plainview; 2000).
11. Vigna, E. & Naldini, L. Lentiviral vectors: excellent tools for experimental gene transfer and promising candidates for gene therapy. *J Gene Med* **2**, 308-316 (2000).
12. Brody, S.L. & Crystal, R.G. Adenovirus-Mediated in-Vivo Gene-Transfer. *Gene Therapy for Neoplastic Diseases* **716**, 90-103 (1994).
13. Monahan, P.E. & Samulski, R.J. Adeno-associated virus vectors for gene therapy: more pros than cons? *Mol Med Today* **6**, 433-440 (2000).
14. Burton, E.A., Bai, Q., Goins, W.F. & Glorioso, J.C. Targeting gene expression using HSV vectors. *Adv Drug Deliver Rev* **53**, 155-170 (2001).
15. Burton, E.A., Fink, D.J. & Glorioso, J.C. Gene delivery using herpes simplex virus vectors. *DNA Cell Biol* **21**, 915-936 (2002).
16. Lieber, A., Steinwaerder, D.S., Carlson, C.A. & Kay, M.A. Integrating adenovirus-adeno-associated virus hybrid vectors devoid of all viral genes. *J Virol* **73**, 9314-9324 (1999).
17. Wong, T.K. & Neumann, E. Electric-Field Mediated Gene-Transfer. *Biochem Bioph Res Co* **107**, 584-587 (1982).
18. Yang, N.S. & Sun, W.H. Gene Gun and Other Nonviral Approaches for Cancer Gene-Therapy. *Nature Medicine* **1**, 481-483 (1995).
19. Seiler, C. et al. Promotion of collateral growth by granulocyte-macrophage colony-stimulating factor in patients with coronary artery disease - A randomized, double-blind, placebo-controlled study. *Circulation* **104**, 2012-2017 (2001).

20. Pillai, R. et al. Ultrasonic nebulization of cationic lipid-based gene delivery systems for airway administration. *Pharmaceutical Research* **15**, 1743-1747 (1998).
21. Mann, M.J. et al. Pressure-mediated oligonucleotide transfection of rat and human cardiovascular tissues. *P Natl Acad Sci USA* **96**, 6411-6416 (1999).
22. Vaheri, A. & Pagano, J. Infectious poliovirus RNA: a sensitive method of assay. *Virology* **27**, 434-436 (1965).
23. Graham, F. & Eb, A. A new technique for the assay of infectivity of human adenovirus 5 DNA. *Virology* **52**, 456-467 (1973).
24. Lasic, D.D. & Templeton, N.S. Liposomes in gene therapy. *Adv Drug Deliver Rev* **20**, 221-266 (1996).
25. Templeton, N.S. & Lasic, D.D. New directions in liposome gene delivery. *Mol Biotechnol* **11**, 175-180 (1999).
26. Lee, R.J. & Huang, L. Lipidic vector systems for gene transfer. *Crit Rev Ther Drug* **14**, 173-206 (1997).
27. Felgner, P.L. et al. Lipofection - a Highly Efficient, Lipid-Mediated DNA-Transfection Procedure. *P Natl Acad Sci USA* **84**, 7413-7417 (1987).
28. Smith, L.C. et al. Synthetic peptide-based DNA complexes for nonviral gene delivery. *Adv Drug Deliver Rev* **30**, 115-131 (1998).
29. Zauner, W., Ogris, M. & Wagner, E. Polylysine-based transfection systems utilizing receptor-mediated delivery. *Adv Drug Deliver Rev* **30**, 97-113 (1998).
30. Wagner, E. Application of membrane-active peptides for nonviral gene delivery. *Adv Drug Deliver Rev* **38**, 279-289 (1999).
31. Ramsay, E. & Gumbleton, M. Polylysine and polyornithine gene transfer complexes: A study of complex stability and cellular uptake as a basis for their differential in-vitro transfection efficiency. *J Drug Target* **10**, 1-9 (2002).
32. Uherek, C. & Wels, W. DNA-carrier proteins for targeted gene delivery. *Adv Drug Deliver Rev* **44**, 153-166 (2000).
33. Henner, W.D., Kleber, I. & Benzinge.R Transfection of Escherichia-Coli Spheroplasts .3. Facilitation of Transfection and Stabilization of Spheroplasts by Different Basic Polymers. *J Virol* **12**, 741-747 (1973).
34. Boussif, O. et al. A versatile vector for gene and oligonucleotide transfer into cells in culture and in vivo: polyethylenimine. *Proc Natl Acad Sci U S A* **92**, 7297-7301 (1995).
35. Thomas, M. & Klibanov, A.M. Enhancing polyethylenimine's delivery of plasmid DNA into mammalian cells. *P Natl Acad Sci USA* **99**, 14640-14645 (2002).
36. Thomas, M. & Klibanov, A.M. Conjugation to gold nanoparticles enhances polyethylenimine's transfer of plasmid DNA into mammalian cells. *P Natl Acad Sci USA* **100**, 9138-9143 (2003).
37. Godbey, W.T., Ku, K.K., Hirasaki, G.J. & Mikos, A.G. Improved packing of poly(ethylenimine)/DNA complexes increases transfection efficiency. *Gene Therapy* **6**, 1380-1388 (1999).
38. Gosselin, M.A., Guo, W.J. & Lee, R.J. Efficient gene transfer using reversibly cross-linked low molecular weight polyethylenimine. *Bioconjugate Chem* **12**, 989-994 (2001).
39. Diebold, S.S., Kursa, P., Wagner, E., Cotten, M. & Zenke, M. Mannose polyethylenimine conjugates for targeted DNA delivery into dendritic cells. *Journal of Biological Chemistry* **274**, 19087-19094 (1999).

40. Ogris, M. et al. The size of DNA/transferrin-PEI complexes is an important factor for gene expression in cultured cells. *Gene Therapy* **5**, 1425-1433 (1998).
41. Wightman, L. et al. Different behavior of branched and linear polyethylenimine for gene delivery in vitro and in vivo. *J Gene Med* **3**, 362-372 (2001).
42. Gonzalez, H., Hwang, S.J. & Davis, M.E. New class of polymers for the delivery of macromolecular therapeutics. *Bioconjugate Chem* **10**, 1068-1074 (1999).
43. Davis, M.E. Non-viral gene delivery systems. *Curr Opin Biotech* **13**, 128-131 (2002).
44. Wagner, E. Strategies to improve DNA polyplexes for *in vivo* gene transfer: Will "artificial viruses" be the answer? *Pharm. Res.* **21**, 8-14 (2004).
45. Vijayanathan, V., Thomas, T. & Thomas, T.J. DNA nanoparticles and development of DNA delivery vehicles for gene therapy. *Biochemistry-Us* **41**, 14085-14094 (2002).
46. Tang, M.X., Redemann, C.T. & Szoka, F.C. In vitro gene delivery by degraded polyamidoamine dendrimers. *Bioconjugate Chem* **7**, 703-714 (1996).
47. Richardson, S.C.W., Pattrick, N.G., Man, Y.K.S., Ferruti, P. & Duncan, R. Poly(amidoamine)s as potential nonviral vectors: Ability to form interpolyelectrolyte complexes and to mediate transfection in vitro. *Biomacromolecules* **2**, 1023-1028 (2001).
48. Choi, J.S., Lee, E.J., Choi, Y.H., Jeong, Y.J. & Park, J.S. Poly(ethylene glycol)-block-poly(L-lysine) dendrimer: Novel linear polymer/dendrimer block copolymer forming a spherical water-soluble polyionic complex with DNA. *Bioconjugate Chem* **10**, 62-65 (1999).
49. Schaffer, D.V., Fidelman, N.A., Dan, N. & Lauffenburger, D.A. Vector unpacking as a potential barrier for receptor-mediated polyplex gene delivery. *Biotechnol. Bioeng.* **67**, 598-606 (2000).
50. Schaffer, D.V. & Lauffenburger, D.A. Optimization of cell surface binding enhances efficiency and specificity of molecular conjugate gene delivery. *J Biol Chem* **273**, 28004-28009 (1998).
51. Harris, J.M. & Chess, R.B. Effect of pegylation on pharmaceuticals. *Nat. Rev. Drug Discovery* **2**, 214-221 (2003).
52. Duncan, R. The dawning era of polymer therapeutics. *Nat Rev Drug Discov* **2**, 347-360 (2003).
53. Fischer, D., Bieber, T., Li, Y.X., Elsasser, H.P. & Kissel, T. A novel non-viral vector for DNA delivery based on low molecular weight, branched polyethylenimine: Effect of molecular weight on transfection efficiency and cytotoxicity. *Pharmaceutical Research* **16**, 1273-1279 (1999).
54. Richardson, S.C.W., Kolbe, H.J.V. & Duncan, R. Potential of low molecular mass chitosan as a DNA delivery system: biocompatibility, body distribution and ability to complex and protect DNA. *Int J Pharm* **178**, 231-243 (1999).
55. Hwang, S.J., Bellocq, N.C. & Davis, M.E. Effects of structure of beta-cyclodextrin-containing polymers on gene delivery. *Bioconjugate Chem* **12**, 280-290 (2001).
56. Luo, D., Haverstick, K., Belcheva, N., Han, E. & Saltzman, W.M. Poly(ethylene glycol)-conjugated PAMAM dendrimer for biocompatible, high-efficiency DNA delivery. *Macromolecules* **35**, 3456-3462 (2002).
57. Lim, Y.B., Kim, S.M., Suh, H. & Park, J.S. Biodegradable, endosome disruptive, and cationic network-type polymer as a highly efficient and nontoxic gene delivery carrier. *Bioconjugate Chem* **13**, 952-957 (2002).

58. Akinc, A., Lynn, D.M., Anderson, D.G. & Langer, R. Parallel synthesis and biophysical characterization of a degradable polymer library for gene delivery. *J Am Chem Soc* **125**, 5316-5323 (2003).
59. Anderson, D.G., Lynn, D.M. & Langer, R. Semi-automated synthesis and screening of a large library of degradable cationic polymers for gene delivery. *Angew. Chem. Int. Ed.* **42**, 3153-3158 (2003).
60. Lynn, D.M., Anderson, D.G., Putnam, D. & Langer, R. Accelerated discovery of synthetic transfection vectors: Parallel synthesis and screening of degradable polymer library. *J Am Chem Soc* **123**, 8155-8156 (2001).
61. Lynn, D.M. & Langer, R. Degradable poly(beta-amino esters): Synthesis, characterization, and self-assembly with plasmid DNA. *J Am Chem Soc* **122**, 10761-10768 (2000).
62. Lodish, H. et al. Molecular Cell Biology. (W.H. Freeman, New York; 2000).
63. Hashida, M., Nishikawa, M., Yamashita, F. & Takakura, Y. Cell-specific delivery of genes with glycosylated carriers. *Adv Drug Deliver Rev* **52**, 187-196 (2001).
64. Wu, G.Y. & Wu, C.H. Receptor-mediated gene delivery and expression in vivo. *J Biol Chem* **263**, 14621-14624 (1988).
65. Wu, G.Y. & Wu, C.H. Receptor-mediated in vitro gene transformation by a soluble DNA carrier system. *J Biol Chem* **262**, 4429-4432 (1987).
66. Ferkol, T., Perales, J.C., Mularo, F. & Hanson, R.W. Receptor-mediated gene transfer into macrophages. *Proc Natl Acad Sci U S A* **93**, 101-105 (1996).
67. Diebold, S.S., Plank, C., Cotten, M., Wagner, E. & Zenke, M. Mannose Receptor-Mediated Gene Delivery into Antigen Presenting Dendritic Cells. *In Synthetic DNA delivery systems (Eds.: D. Luo, W. M. Saltzman), Kluwer, New York* (2003).
68. Kwon, Y.J., James, E., Shastri, N. & Frechet, J.M. In vivo targeting of dendritic cells for activation of cellular immunity using vaccine carriers based on pH-responsive microparticles. *Proc Natl Acad Sci U S A* **102**, 18264-18268 (2005).
69. Zuber, G., Dauty, E., Nothisen, M., Belguise, P. & Behr, J.P. Towards synthetic viruses. *Adv Drug Deliver Rev* **52**, 245-253 (2001).
70. Wagner, E., Zenke, M., Cotten, M., Beug, H. & Birnstiel, M.L. Transferrin-Polycation Conjugates as Carriers for DNA Uptake into Cells. *P Natl Acad Sci USA* **87**, 3410-3414 (1990).
71. Chen, J.B., Gamou, S., Takayanagi, A. & Shimizu, N. A Novel Gene Delivery System Using Egf Receptor-Mediated Endocytosis. *Febs Lett* **338**, 167-169 (1994).
72. Ferkol, T., Kaetzel, C.S. & Davis, P.B. Gene-Transfer into Respiratory Epithelial-Cells by Targeting the Polymeric Immunoglobulin Receptor. *J Clin Invest* **92**, 2394-2400 (1993).
73. Farokhzad, O.C. et al. Targeted nanoparticle-aptamer bioconjugates for cancer chemotherapy in vivo. *Proc Natl Acad Sci U S A* **103**, 6315-6320 (2006).
74. Pasqualini, R. & Ruoslahti, E. Organ targeting in vivo using phage display peptide libraries. *Nature* **380**, 364-366 (1996).
75. Sergeeva, A., Kolonin, M.G., Molldrem, J.J., Pasqualini, R. & Arap, W. Display technologies: Application for the discovery of drug and gene delivery agents. *Adv Drug Deliv Rev* **58**, 1622-1654 (2006).

76. Weissleder, R., Kelly, K., Sun, E.Y., Shtatland, T. & Josephson, L. Cell-specific targeting of nanoparticles by multivalent attachment of small molecules. *Nat Biotechnol* **23**, 1418-1423 (2005).
77. Thomas, M. & Klibanov, A.M. Non-viral gene therapy: polycation-mediated DNA delivery. *Appl Microbiol Biot* **62**, 27-34 (2003).
78. Little, S.R. & Langer, R. Nonviral delivery of cancer genetic vaccines. *Adv Biochem Engin/Biotechnol* **99**, 93-118 (2005).
79. Duncan, R. The dawning era of polymer therapeutics. *Nat Rev Drug Disc* **2**, 347-360 (2003).
80. Kamiya, H., Tsuchiya, H., Yamazaki, J. & Harashima, H. Intracellular trafficking and transgene expression of viral and non-viral gene vectors. *Adv Drug Deliver Rev* **52**, 153-164 (2001).
81. Hoffman, A.S. et al. Design of "smart" polymers that can direct intracellular drug delivery. *Polym Advan Technol* **13**, 992-999 (2002).
82. Pollard, H. et al. Polyethylenimine but not cationic lipids promotes transgene delivery to the nucleus in mammalian cells. *Journal of Biological Chemistry* **273**, 7507-7511 (1998).
83. Bieber, T., Meissner, W., Kostin, S., Niemann, A. & Elsasser, H.P. Intracellular route and transcriptional competence of polyethylenimine-DNA complexes. *Journal of Controlled Release* **82**, 441-454 (2002).
84. Gasiorowski, J.Z. & Dean, D.A. Mechanisms of nuclear transport and interventions. *Adv Drug Deliver Rev* **55**, 703-716 (2003).
85. Zanta, M.A., Belguise-Valladier, P. & Behr, J.P. Gene delivery: A single nuclear localization signal peptide is sufficient to carry DNA to the cell nucleus. *P Natl Acad Sci USA* **96**, 91-96 (1999).
86. Cartier, R. & Reszka, R. Utilization of synthetic peptides containing nuclear localization signals for nonviral gene transfer systems. *Gene Therapy* **9**, 157-167 (2002).
87. Ragin, A.D., Morgan, R.A. & Chmielewski, J. Cellular import mediated by nuclear localization signal peptide sequences. *Chem Biol* **9**, 943-948 (2002).
88. Chan, C.K. & Jans, D.A. Using nuclear targeting signals to enhance non-viral gene transfer. *Immunol Cell Biol* **80**, 119-130 (2002).
89. Wagner, E., Plank, E., Zatloukal, K., Cotten, M. & Birnstiel, M.L. Influenza virus hemagglutinin HA-2 N-terminal fusogenic peptides augment gene transfer by transferrin–polylysine–DNA complexes: toward a synthetic virus-like gene-transfer vehicle. *Proc Natl Acad Sci USA* **89**, 7934-7938 (1992).
90. Sung, S.-J. et al. Effect of polyethylene glycol on gene delivery of polyethylenimine. *Biological and Pharmaceutical Bulletin* **26**, 492-500 (2003).

Chapter 3. Multifunctional linear-dendritic "hybrid" polymers for non-viral gene delivery: Design, synthesis, self-assembly with DNA, and *in vitro* DNA delivery

3.1 Introduction

To fully realize the potential for new medical advances in the post-genomic era, safe and efficient delivery systems for nucleotide-based drugs must be developed.[1] Ideally, such systems will be nontoxic, non-immunogenic, and made from building blocks that are versatile to allow for optimal delivery to a range of cells or tissues of interest. In this chapter, we describe the design, synthesis, and testing of a unique family of hierarchically structured linear-dendritic hybrid polymers that self-assemble with DNA to form stable nanoparticles with a series of concentric, functional "shells" possessing independently-tunable properties necessary for effective targeted delivery. The resultant ligand-functionalized systems demonstrate receptor-mediated delivery to targeted cells with serum stability, transfection efficiencies exceeding the most efficient commercially available polymer, poly(ethylenimine) (PEI), and low toxicity at concentrations one to two orders of magnitude higher than those at which PEI is toxic. These systems may find potential utility as targeted *in vivo* gene delivery systems for DNA or RNA-based therapies.

As described in Chapter 2, the success of gene-based therapies is dependent upon the ability to deliver genes that express key proteins when and where they are needed. As of yet, no such therapies have been approved for clinical use, primarily because of the lack of versatile, safe, and efficient gene delivery systems.[2, 3] A suite of electrical, mechanical, and modified viral delivery systems have been investigated with some success, but these systems suffer from significant drawbacks.[4-7] Notably, modified viruses often elicit severe immunogenicity, are prone to insertional mutagenesis, and are refractory to repeated administrations. Chemical delivery systems such as cationic linear polymers, dendrimers, or lipid-based reagents, while generally safer than their viral counterparts, typically lack the high efficiency or multiple functionalities required for *in vivo* administration. Moreover, even subtle synthetic modifications to these systems can dramatically influence existing biological properties.[8-10]

In this chapter, we present a new family of multifunctional gene delivery polymers based on dendritic poly(amidoamine) (PAMAM) and linear poly(ethylene glycol) (PEG) with an array of properties (i.e., blood stability, cellular targeting, DNA binding, and endosomal buffering capacity) that can be independently tuned in a modular fashion to address each of the barriers to effective gene delivery. As a proof of concept, we demonstrate the ability to independently modulate targeting and expression levels by choice of ligand and dendrimer species, respectively. Further, these systems represent a platform onto which additional functionalities may be added to impart properties such as vector unpackaging and nuclear targeting.[11, 12]

3.2 Experimental Methods

General Considerations. Bifunctional Fmoc-PEG-NHS (M_n = 3500) and $HCl \cdot NH_2$-PEG-COOH (M_n = 3400) were purchased from Nektar Therapeutics (Birmingham, AL) and used without further purification (both possessed substitution values > 99%). Methyl acrylate (99+%)

and ethylene diamine (99+%) were purchased from Sigma-Aldrich (St. Louis, MO) and distilled prior to use. D-mannosamine HCl, 1-amino-1-deoxy-β-D-galactose, and hyperbranched poly (ethylenimine) (PEI, M_n = 25000) were purchased from Sigma-Aldrich (St. Louis, MO). Plasmid DNA containing the firefly luciferase reporter gene and CMV promoter sequence (pCMV-Luc) was purchased from Elim Biopharmaceuticals (San Francisco, CA) and used without further purification. HepG2 human hepatocellular carcinoma cells and P388D1 murine macrophages were purchased from American Type Culture Collection (Manassas, VA) and grown at 37° C in 5% CO_2. HepG2 cells were grown in 90% Dulbecco's modified Eagle's medium supplemented with 10% fetal bovine serum, 100 units/mL penicillin, and 100 μg/mL streptomycin. P388D1 macrophages were grown in 90% RPMI 1640 medium supplemented with 10% fetal bovine serum, 100 units/mL penicillin, 100 μg/mL streptomycin, 2.5 mg/mL D-glucose, 10 mM HEPES, and 1 mM sodium pyruvate. Bright-Glo® luciferase assay detection kits were purchased from Promega (Madison, WI) and used according to the manufacturer's specifications. All other materials and solvents were used as received without further purification.

Instrumentation. ^{1}H NMR spectra were recorded at room temperature using a Varian Mercury 300 MHz instrument. FTIR spectra of films cast on polished KBr pellets were recorded on a Nicolet Magna-IR 550 spectrometer. A ZetaPALS dynamic light scattering detector (Brookhaven Instruments, 15 mW laser, incident beam 676 nm) was used for particle sizing. Luminescence from reporter gene expression studies was measured using a Veritas Microplate Luminometer. Optical absorbance was measured using a SpectraMax 190 microplate reader (Molecular Devices, Sunnyvale, CA).

Synthesis. Ligand-functionalized linear-dendritic polymers were synthesized as follows. Fmoc-PEG-NHS (3.5 g) was dissolved in 0.1M $NaHCO_3$ buffer (0.0375 g/mL) and pH adjusted to pH 8.5 with 1M NaOH. Each of the two sugars were dissolved separately in 0.1M $NaHCO_3$ buffer (0.03 g/mL), pH adjusted to 8.5, and added to an aliquot of dissolved polymer solution at a molar excess of 10:1 (24 h, 25° C under N_2 gas). Care was taken to combine sugar and polymer solutions immediately after dissolution of the polymer to avoid premature hydrolysis of the NHS ester. Polymers were recovered by filtration and lyophilization, dissolved in dimethylformamide (DMF, 0.1 g/mL) and added dropwise to a solution of piperdine in DMF to remove the Fmoc protecting group (20% v/v, 30 min, 25° C under N_2 gas). Following this step, polymers were recovered by precipitation in ice cold diethyl ether and dried overnight under vacuum. Dendrimer synthesis then proceeded by serial Michael addition and amidation steps via addition of methyl acrylate and ethylene diamine, respectively, as described previously.[13] In general, ligand functionalization and deprotection steps proceeded at 80-85%; all dendrimer synthetic steps proceeded with conversions of 90-100% (Figures 3.2-3.4). NMR and FTIR peaks for each of the 14 reaction products are listed below. Control polymers (no ligand) were synthesized in parallel with ligand-functionalized species using NH_2-PEG-COOH (M_n = 3400) as the starting material.

Sugar-Peg-Fmoc. ^1H NMR in $CDCl_3$: $\delta_{PEG}(CH_2CH_2O)$ = 3.66 (b); $\delta_{SUGAR}(CH_2OH)$ = 3.91 (m); $\delta_{SUGAR}(CHCH_2OH)$ = 3.5 (m); δ_{FMOC}(-CH-) = 7.25-7.8 (m). FTIR peaks, ν cm^{-1}: 3336, 2885, 1687, 1468, 1344, 1279, 1245, 1111, 964, 845.

Sugar-Peg-NH_2. ^1H NMR in $CDCl_3$: $\delta_{PEG}(CH_2CH_2O)$ = 3.62 (b); $\delta_{SUGAR}(CH_2OH)$ = 3.92 (m); $\delta_{SUGAR}(CHCH_2OH)$ = 3.51 (m). FTIR peaks, ν cm^{-1}: 3347, 2885, 1680, 1470, 1342, 1278, 1109, 964, 843.

Sugar-Peg-G0.5. ^{1}H NMR in $CDCl_3$: $\delta_{PEG}(CH_2CH_2O)$ = 3.61 (b); $\delta_{SUGAR}(CH_2OH)$ = 3.89 (m); $\delta_{SUGAR}(CHCH_2OH)$ = 3.5 (m); $\delta_{PAMAM}(CH_2COOCH_3)$ = 2.48 (m); δ_{PAMAM}(next to tertiary amines) = 2.50-2.88 (b); $\delta_{PAMAM}(CH_2COOCH_3)$ = 3.3 (m). FTIR peaks, ν cm^{-1}: 3351, 2885, 1735, 1679, 1467, 1342, 1282, 1112, 965, 844.

Sugar-Peg-G1.0. ^{1}H NMR in $CDCl_3$: $\delta_{PEG}(CH_2CH_2O)$ = 3.65 (b); $\delta_{SUGAR}(CH_2OH)$ = 3.89 (m); $\delta_{SUGAR}(CHCH_2OH)$ = 3.52 (m); $\delta_{PAMAM}(CH_2CONH)$ = 2.43 (m); δ_{PAMAM}(next to primary and tertiary amines) = 2.48-2.92 (b); $\delta_{PAMAM}(CH_2CONHCH_2)$ = 3.33 (m). FTIR peaks, ν cm^{-1}: 3336, 2887, 1682, 1471, 1342, 1283, 1111, 962, 843.

Sugar-Peg-G1.5. ^{1}H NMR in $CDCl_3$: $\delta_{PEG}(CH_2CH_2O)$ = 3.64 (b); $\delta_{SUGAR}(CH_2OH)$ = 3.88 (m); $\delta_{SUGAR}(CHCH_2OH)$ = 3.5 (m); $\delta_{PAMAM}(CH_2COOCH_3)$ = 2.45 (m); $\delta_{PAMAM}(CH_2CONH)$ = 2.15-2.4 (m); δ_{PAMAM}(next to tertiary amines) = 2.5-2.88 (b); $\delta_{PAMAM}(CH_2COOCH_3)$ = 3.6-3.7 (m); $\delta_{PAMAM}(CH_2CONHCH_2)$ = 3.32 (m). FTIR peaks, ν cm^{-1}: 3260, 2880, 1729, 1665, 1550, 1470, 1350, 1260, 1112, 960, 845.

Sugar-Peg-G2.0. ^{1}H NMR in $CDCl_3$: $\delta_{PEG}(CH_2CH_2O)$ = 3.65 (b); $\delta_{SUGAR}(CH_2OH)$ = 3.89 (m); $\delta_{SUGAR}(CHCH_2OH)$ = 3.48 (m); $\delta_{PAMAM}(CH_2CONH)$ = 2.37 (m); δ_{PAMAM}(next to primary and tertiary amines) = 2.45-3.0 (b); $\delta_{PAMAM}(CH_2CONHCH_2)$ = 3.3 (m). FTIR peaks, ν cm^{-1}: 3273, 2885, 1653, 1599, 1470, 1360, 1283, 1112, 959, 841.

Sugar-Peg-G2.5. ^{1}H NMR in $CDCl_3$: $\delta_{PEG}(CH_2CH_2O)$ = 3.66 (b); $\delta_{SUGAR}(CH_2OH)$ = 3.87 (m); $\delta_{SUGAR}(CHCH_2OH)$ = 3.52 (m); $\delta_{PAMAM}(CH_2COOCH_3)$ = 2.45 (m); $\delta_{PAMAM}(CH_2CONH)$ = 2.25-2.42 (m); δ_{PAMAM}(next to tertiary amines) = 2.5-2.95 (b); $\delta_{PAMAM}(CH_2COOCH_3)$ = 3.6-3.7 (m); $\delta_{PAMAM}(CH_2CONHCH_2)$ = 3.28 (m). FTIR peaks, ν cm^{-1}: 3252, 2881, 1736, 1666, 1552, 1467, 1354, 1252, 1113, 957, 843.

Sugar-Peg-G3.0. ^{1}H NMR in $CDCl_3$: $\delta_{PEG}(C\mathbf{H_2}C\mathbf{H_2}O)$ = 3.67 (b); $\delta_{SUGAR}(C\mathbf{H_2}OH)$ = 3.87 (m); $\delta_{SUGAR}(C\mathbf{H}CH_2OH)$ = 3.54 (m); $\delta_{PAMAM}(C\mathbf{H_2}CONH)$ = 2.38 (m); δ_{PAMAM}(next to primary and tertiary amines) = 2.5-3.1 (b); $\delta_{PAMAM}(CH_2CONHC\mathbf{H_2})$ = 3.3 (m). FTIR peaks, ν cm^{-1}: 3253, 3065, 2875, 1662, 1551, 1470, 1354, 1302, 1252, 1107, 955, 853.

Sugar-Peg-G3.5. ^{1}H NMR in $CDCl_3$: $\delta_{PEG}(C\mathbf{H_2}C\mathbf{H_2}O)$ = 3.65 (b); $\delta_{SUGAR}(C\mathbf{H_2}OH)$ = 3.88 (m); $\delta_{SUGAR}(C\mathbf{H}CH_2OH)$ = 3.55 (m); $\delta_{PAMAM}(C\mathbf{H_2}COOCH_3)$ = 2.45 (m); $\delta_{PAMAM}(C\mathbf{H_2}CONH)$ = 2.15-2.4 (m); δ_{PAMAM}(next to tertiary amines) = 2.5-3.0 (b); $\delta_{PAMAM}(CH_2COOC\mathbf{H_3})$ = 3.6-3.7 (m); $\delta_{PAMAM}(CH_2CONHC\mathbf{H_2})$ = 3.28 (m). FTIR peaks, ν cm^{-1}: 3268, 2870, 1737, 1666, 1552, 1466, 1360, 1256, 1201, 1187, 958, 845.

Sugar-Peg-G4.0. ^{1}H NMR in $CDCl_3$: $\delta_{PEG}(C\mathbf{H_2}C\mathbf{H_2}O)$ = 3.65 (b); $\delta_{SUGAR}(C\mathbf{H_2}OH)$ = 3.88 (m); $\delta_{SUGAR}(C\mathbf{H}CH_2OH)$ = 3.48 (m); $\delta_{PAMAM}(C\mathbf{H_2}CONH)$ = 2.37 (m); δ_{PAMAM}(next to primary and tertiary amines) = 2.45-3.1 (b); $\delta_{PAMAM}(CH_2CONHC\mathbf{H_2})$ = 3.27 (b). FTIR peaks, ν cm^{-1}: 3260, 3068, 2881, 1660, 1552, 1470, 1357, 1300, 1260, 1113, 954, 849.

Sugar-Peg-G4.5. ^{1}H NMR in $CDCl_3$: $\delta_{PEG}(C\mathbf{H_2}C\mathbf{H_2}O)$ = 3.67 (b); $\delta_{SUGAR}(C\mathbf{H_2}OH)$ = 3.92 (m); $\delta_{SUGAR}(C\mathbf{H}CH_2OH)$ = 3.5 (m); $\delta_{PAMAM}(C\mathbf{H_2}COOCH_3)$ = 2.45 (b); $\delta_{PAMAM}(C\mathbf{H_2}CONH)$ = 2.2-2.4 (m); δ_{PAMAM}(next to tertiary amines) = 2.5-3.2 (b); $\delta_{PAMAM}(CH_2COOC\mathbf{H_3})$ = 3.6-3.7 (m); $\delta_{PAMAM}(CH_2CONHC\mathbf{H_2})$ = 3.3 (m). FTIR peaks, ν cm^{-1}: 3272, 2873, 1740, 1665, 1556, 1469, 1362, 1260, 1200, 1184, 960, 845.

Sugar-Peg-G5.0. ^{1}H NMR in $CDCl_3$: $\delta_{PEG}(C\mathbf{H_2}C\mathbf{H_2}O)$ = 3.65 (b); $\delta_{SUGAR}(C\mathbf{H_2}OH)$ = 3.9 (m); $\delta_{SUGAR}(C\mathbf{H}CH_2OH)$ = 3.52 (m); $\delta_{PAMAM}(C\mathbf{H_2}CONH)$ = 2.4 (m); δ_{PAMAM}(next to primary and tertiary amines) = 2.5-3.0 (b); $\delta_{PAMAM}(CH_2CONHC\mathbf{H_2})$ = 3.32 (m). FTIR peaks, ν cm^{-1}: 3262, 3073, 2880, 1664, 1555, 1472, 1360, 1301, 1264, 1111, 954, 851.

Sugar-Peg-G5.5. ^{1}H NMR in $CDCl_3$: $\delta_{PEG}(\mathbf{CH_2CH_2O})$ = 3.65 (b); $\delta_{SUGAR}(\mathbf{CH_2OH})$ = 3.91 (m); $\delta_{SUGAR}(\mathbf{CH}CH_2OH)$ = 3.51 (m); $\delta_{PAMAM}(\mathbf{CH_2}COOCH_3)$ = 2.45 (b); $\delta_{PAMAM}(\mathbf{CH_2}CONH)$ = 2.2-2.4 (m); δ_{PAMAM}(next to tertiary amines) = 2.5-3.2 (b); $\delta_{PAMAM}(CH_2COOC\mathbf{H_3})$ = 3.6-3.7 (m); $\delta_{PAMAM}(CH_2CONHC\mathbf{H_2})$ = 3.3 (m). FTIR peaks, ν cm^{-1}: 3274, 2873, 1741, 1670, 1555, 1470, 1362, 1255, 1203, 1190, 960, 847.

Sugar-Peg-G6.0. ^{1}H NMR in $CDCl_3$: $\delta_{PEG}(\mathbf{CH_2CH_2O})$ = 3.66 (b); $\delta_{SUGAR}(\mathbf{CH_2OH})$ = 3.9 (m); $\delta_{SUGAR}(\mathbf{CH}CH_2OH)$ = 3.55 (m); $\delta_{PAMAM}(\mathbf{CH_2}CONH)$ = 2.4 (m); δ_{PAMAM}(next to primary and tertiary amines) = 2.6-3.0 (b); $\delta_{PAMAM}(CH_2CONHC\mathbf{H_2})$ = 3.2-3.4 (b). FTIR peaks, ν cm^{-1}: 3255, 3070, 2884, 1664, 1554, 1472, 1357, 1303, 1256, 1113, 960, 854.

Gel electrophoresis shift assays. Polyplexes were formed by combining 100 μL of DNA solution (0.1 mg/mL in 25 mM acetate buffer, pH 5.1) to 100 μL of polymer solution (concentration adjusted to reach desired concentration in 25 mM acetate buffer at pH 5.1) in an eppendorf tube and allowing 20 min for complexation. The resultant solutions were diluted in 25 mM acetate buffer and added to gels at a concentration of 100 ng DNA per well (in 20 μL volume) in 10% Ficoll 400 loading buffer (Amersham Pharmacia Biotech, Uppsala, Sweden). Gels were run at 60 V for 1 h using an Embi tec RunOne Electrophoresis Cell (San Diego, CA). Bands were visualized by ethidium bromide staining.

Dynamic light scattering (DLS). Dynamic light scattering (DLS) measurements were used to measure the size of polymer-DNA complexes. Complexes were prepared as described above. Correlation functions were collected at a scattering angle of 90°, and the sizes of particles were determined using the MAS option of the company's particle sizing software package (version 2.30) assuming the refractive index and viscosity of pure water at room temperature.

Particle sizes, obtained in triplicate, are given as effective diameters assuming a log-normal distribution.

Transmission electron microscopy (TEM). Transmission electron micrographs were obtained using a JEOL 2000FX operating at 200kV. TEM samples were prepared on 400-mesh, Formivar carbon-coated copper TEM grids by first depositing a small aliquot of the above complex solution (5 μL) onto the grid and allowing 15 minutes for evaporation of the solvent. A small drop (30 μL) of staining solution containing 0.5% RuO_4 was then placed on the sample and allowed to evaporate for 1 h prior to imaging.

Cell transfections. All transfection assays were performed in quadruplicate in accordance with the following protocol. All materials, buffers, and media were sterilized prior to use. HepG2 cells were grown in 96-well plates at an initial seeding density of 5000 cells/well in 150 μL/well of growth medium (90% Dulbecco's modified Eagle's medium supplemented with 10% fetal bovine serum, 100 units/mL penicillin, and 100 μg/mL streptomycin). P388D1 cells were grown in separate 96-well plates at an initial seeding density of 50000 cells/well in 150 μL/well of growth medium (90% RPMI 1640 medium supplemented with 10% fetal bovine serum, 100 units/mL penicillin, 100 μg/mL streptomycin, 2.5 mg/mL D-glucose, 10 mM HEPES, and 1 mM sodium pyruvate). Cells were allowed to attach and proliferate for 24 h in an incubator.

Polymers were dissolved in sterile 25 mM acetate buffer (concentrations ranging from 2-12 mg/mL) and arrayed into a 96-well plate (25 μL/well total polymer solution with concentrations adjusted as appropriate to yield polymer/DNA ratios ranging from 10:1 to 200:1). Polymer/DNA complexes were formed by the addition of 25 μL/well of 0.06 mg/mL pCMV-Luc in 25 mM acetate buffer. Polymer and DNA solutions were vigorously mixed using a

multichannel pipettor upon addition of DNA solutions and subsequently incubated for 20 min to allow for complexation. Thirty μL/well aliquots of the above complex solutions were then transferred into each well of a 96-well plate containing 200 μL/well of either serum-free Opti-MEM medium (Invitrogen Corporation, Carlsbad, CA) or 10% serum-containing growth medium. Growth medium was removed from cells and 150 μL/well of complex-plus-medium solution was added. Controls employing PEI were prepared exactly as above to yield polymer DNA ratios ranging from 0.5:1 to 10:1, and in all cases optimized formulations are reported as positive controls. Naked DNA controls were also prepared as above, and each 96-well plate included appropriate positive and negative controls as internal standards. In all cases, wells contained 587 ng DNA/well at indicated polymer/DNA ratios.

Following incubation of complex-containing medium solutions with cells for 4 h, solutions were removed and replaced with 10% serum-containing growth medium. Cells were incubated for an additional 72 h, and luciferase expression was determined using the commercially available Bright-Glo® luciferase assay kit (Promega, Madison, WI). Luminescence was quantified in solid, flat-bottom, white polypropylene 96-well plates using a bioluminescent plate reader. Luminescence was expressed in relative light units and was not normalized to total cellular protein in this assay.

Cell viability assay. Cell viability assays were performed in quadruplicate using the following protocol. HepG2 and P388D1 cells were seeded in 96-well clear, flat-bottom plates and transfected according to the procedure described above. After 72 h, cell metabolic activity was assayed using the MTT cell proliferation assay kit (ATCC, Manassas, VA). Initially, a 10 μL aliquot of MTT assay reagent was added to each well. After incubating for two hours, 100 μL of detergent reagent was added. The plate was then covered and left in the dark for 4 h, after

which optical absorbance was measured at 570 nm using a microplate absorbance reader. Background (media plus MTT assay reagent plus detergent reagent with no cells present) was subtracted from the value of each well, and all values were normalized to the value of control (untreated) cells.

3.3 Results and discussion

3.3.1 Design of linear-dendritic hybrid polymers: Modularity and hierarchical self-assembly with DNA

Linear-dendritic hybrid polymers were designed based on the hypothesis that these unique polymer architectures, which possess functionalities that are both chemically orthogonal and physically separated, could self-assemble with DNA to yield nanoparticles with an outer shell of targeting ligands accessible to cell surface receptors, a flexible, hydrophilic corona designed to prevent protein opsonization, plasma clearance, and non-specific uptake, and an interior of amine groups to promote DNA binding and escape from endosomal vesicles into the cytoplasm.[14-16] The structure of hybrid polymers, a comparison with the generic design motif described for modular polymers in Chapter 2, and a schematic depicting the self-assembly of these systems with plasmid DNA is provided in Figure 3.1.

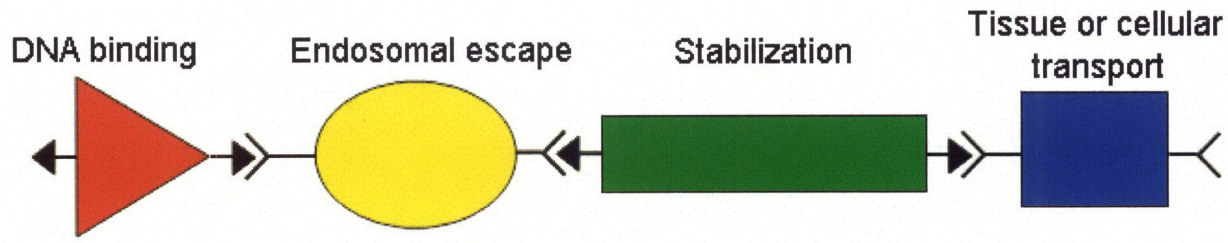
DNA binding
Endosomal escape
Stabilization
Tissue or cellular transport

(a)

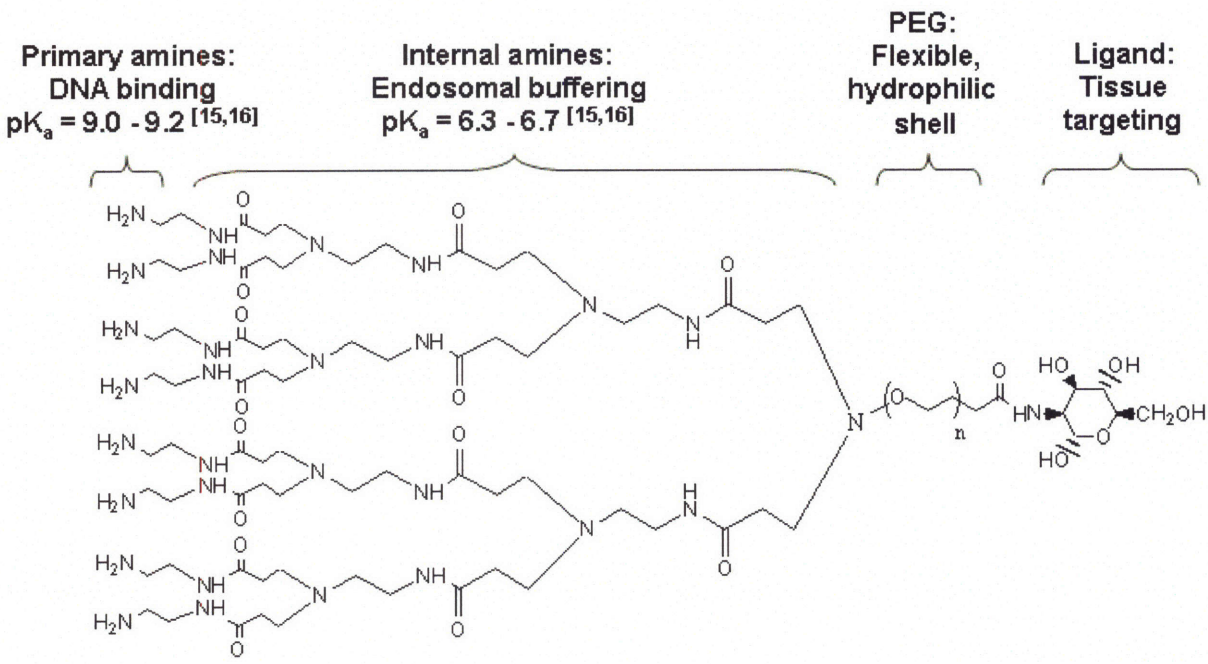
Primary amines:
DNA binding
pK$_a$ = 9.0 - 9.2 [15,16]
Internal amines:
Endosomal buffering
pK$_a$ = 6.3 - 6.7 [15,16]
PEG:
Flexible,
hydrophilic
shell
Ligand:
Tissue
targeting

(b)

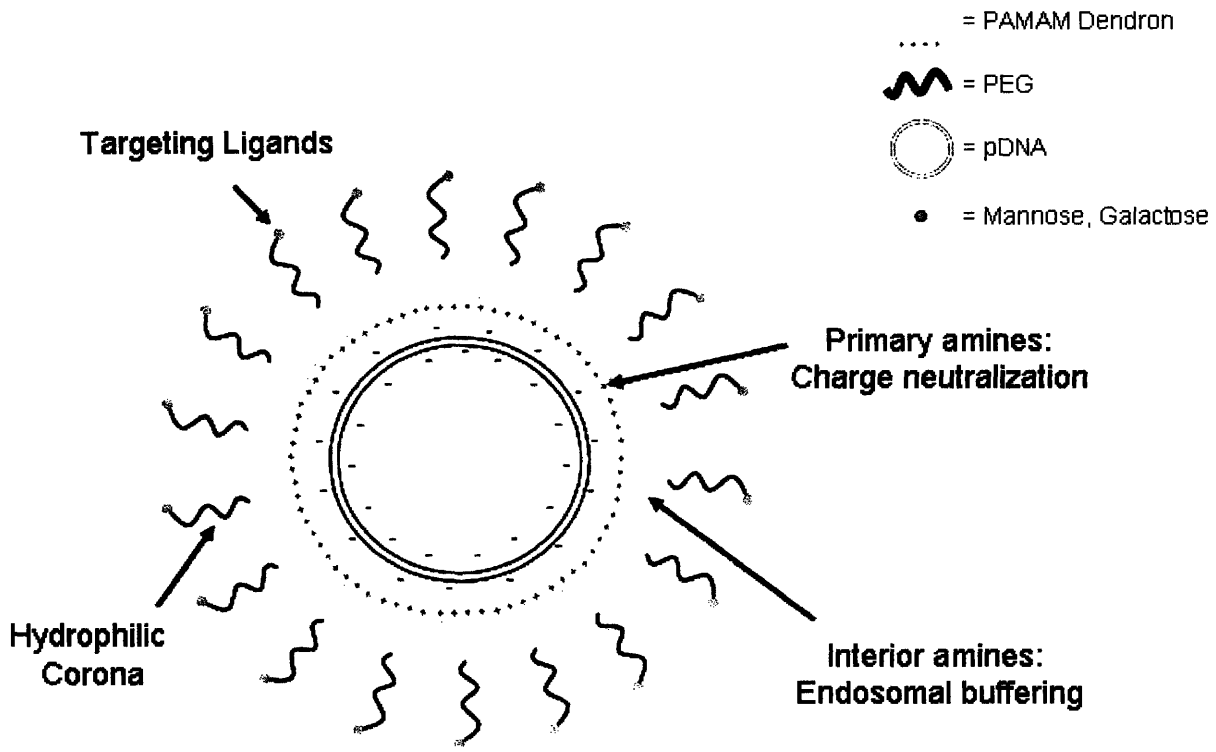

(c)

Figure 3.1. Rational design and hierarchical self-assembly of linear-dendritic polymers with plasmid DNA.

(a) Architecture of a hypothetical modular gene delivery system described in Chapter 2. (b) Molecular structure-function relationship in mannose-PEG-PAMAM G3.0. (c) Structure of linear-dendritic polyplexes showing relative positions of functional elements (not to scale).

3.3.2 Synthesis of hybrid polymers

Ligand-functionalized linear-dendritic polymers were synthesized by first conjugating an aminated targeted ligand to PEG via an NHS ester, followed by removal of the Fmoc protecting group on the opposite end of the bifunctional PEG and subsequent dendrimer growth by serial

Michael additional and amidation steps (as described previously[13]; see Figure 3.2). Physical properties of these polymers are listed in Table 3.1.

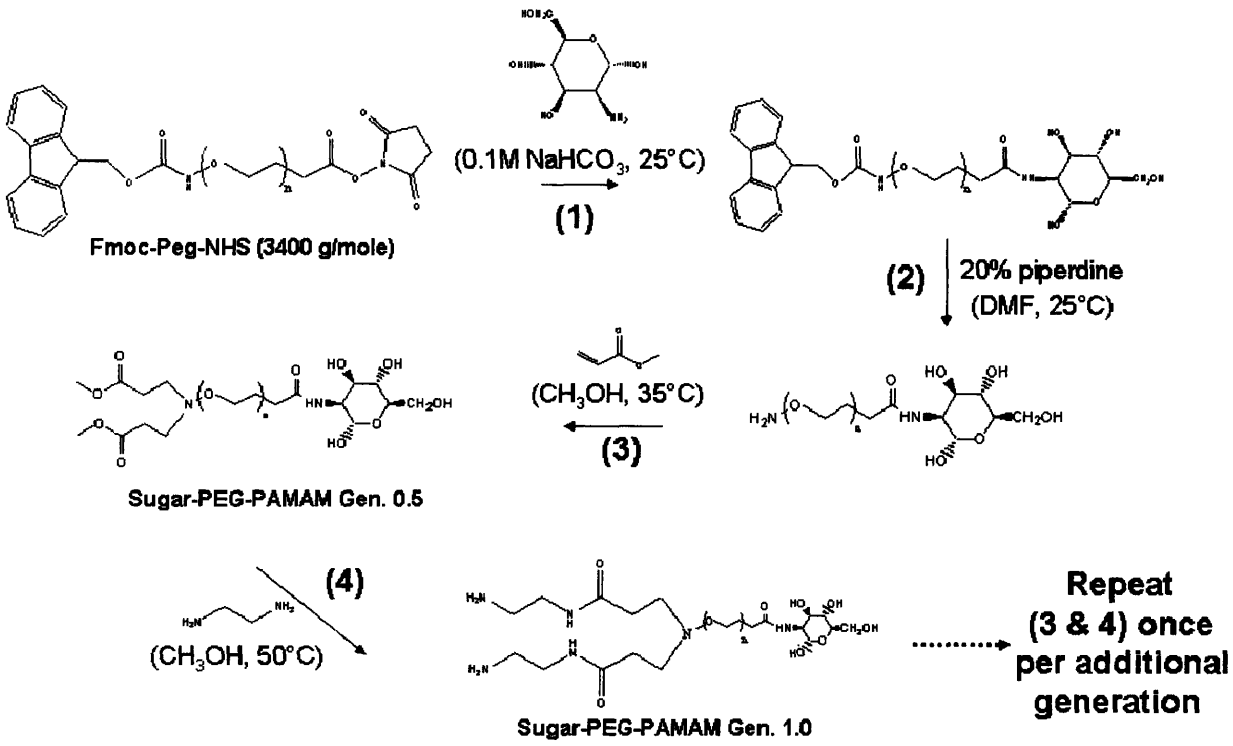

Figure 3.2. Synthesis of linear-dendritic hybrid polymers.

Table 3.1. Theoretical molecular weights and number of primary amines in ligand-functionalized PEG-PAMAM hybrid polymers used in this chapter.

Polymer	Mn (theoretical)	# of Amine End Groups
Ligand-PEG-PAMAM-G0.0	3344	1
Ligand-PEG-PAMAM-G1.0	3572	2
Ligand-PEG-PAMAM-G2.0	4028	4
Ligand-PEG-PAMAM-G3.0	4940	8
Ligand-PEG-PAMAM-G4.0	6764	16
Ligand-PEG-PAMAM-G5.0	10412	32
Ligand-PEG-PAMAM-G6.0	17708	64

In general, ligand functionalization and deprotection steps proceeded at 80-85%; all dendrimer synthetic steps proceeded with conversions of 90-100% (Figure 3.3). Qualitatively, the growth of amide (3200-3400 cm^{-1}) and carbonyl (1600-1800 cm^{-1}) peaks during dendrimer synthesis can be seen in Figure 3.4.

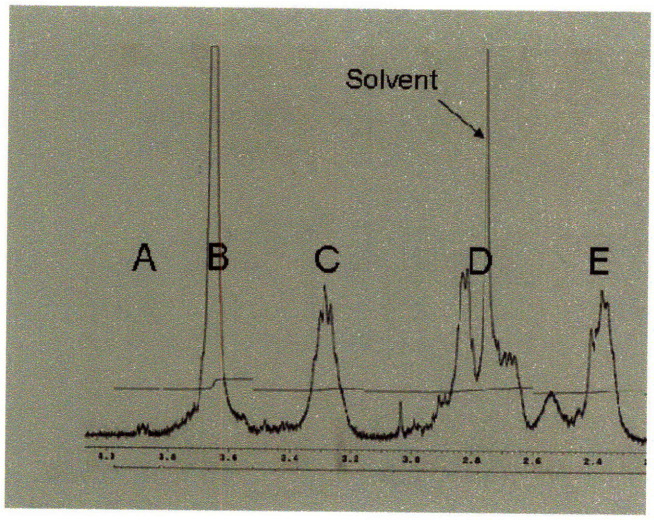

A: δ_{SUGAR}(CH2OH) = 3.88

B: δ_{PEG}(CH2CH2O) = 3.65

C: δ_{PAMAM}(CH2CONHCH2) = 3.27

D: δ_{PAMAM}(next to 1°, 3° amines) = 2.45-3.1

E: δ_{PAMAM}(CH2CONH) = 2.37

Figure 3.3. ^{1}H NMR spectrum of mannose-PEG-PAMAM-G4.0 with assigned structural peaks.

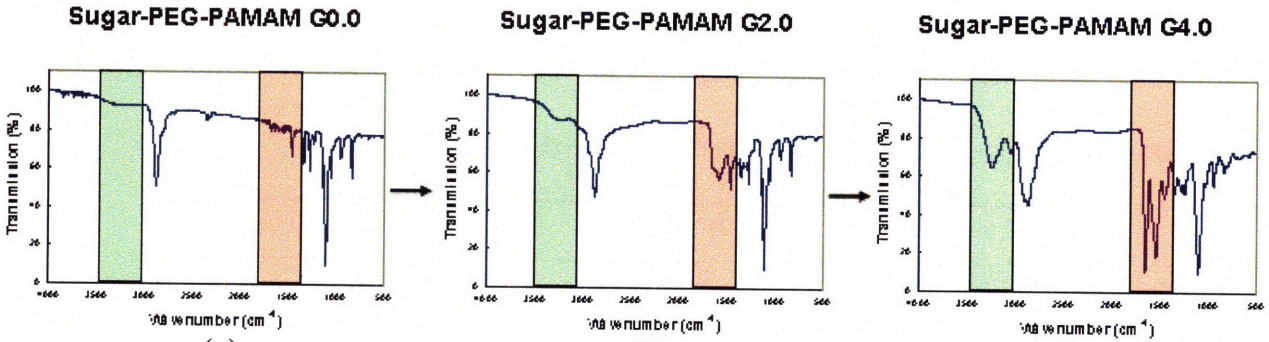

Figure 3.4. FTIR plots of transmission (%) versus wavenumber (cm^{-1}) in sugar-PEG-PAMAM G0.0, G2.0, and G4.0.

(a) G0.0, (b) G2.0, and (c) G4.0. Growth of amide (green) and carbonyl (red) peaks are highlighted (Conversion of the deprotection step was approximately 80%. Conversion at

each branching step was 90-100%.). Additional NMR and FTIR structural analysis is available in Experimental Methods.

3.3.3 Biophysical properties of polymer-DNA complexes

An array of techniques was used to probe the biophysical character of polymer/DNA complexes, or "polyplexes" (see Figure 3.5). Gel electrophoresis demonstrates binding and charge neutralization of DNA by linear-dendritic polymers incubated at mass ratios of greater than 20:1, 10:1, 5:1, 1:1, and 1:1 for generations 2.0, 3.0, 4.0, 5.0, and 6.0, respectively (pH 5.1 acetate buffer was used in all cases to ensure complete protonation of primary amines on the dendrimer periphery). The nature of this trend is consistent with intuition, as the exponentially increasing number of amines with increasing dendrimer generation results in higher charge density with increasing dendrimer size. Dynamic light scattering (DLS) suggests that polyplexes of generations 3.0, 4.0, and 6.0 average around 150 nm in diameter, under the reported cutoff of around 200 nm required for efficient cellular uptake (Figure 3.5(b)).[17] Generation 5.0 polyplexes form larger particles with DNA, a seemingly anomalous result that was nevertheless highly repeatable. The large size of G2.0 polyplexes reflects the fact that little DNA binding and charge neutralization occurred in these systems. In all cases, mass ratios ranging from 0.1 to 200 were tested and polyplex size was shown to be relatively insensitive to mass ratio above the ratio at which complexation occurs in each system, suggesting that in all cases polyplexes consist of a single DNA plasmid and that excess polymers remain dispersed in solution. Thus, particle diameters given in Figure 3.5(b) represent average diameters for an evenly weighted range of mass ratios up to 200. Finally, transmission electron micrographs (TEM) of G6.0 polyplexes show narrowly dispersed, roughly spherical complexes with an outer corona of approximately 6-8 nm, consistent with the expected size of PEG-PAMAM G6.0 (Figure 3.5(c)).[18] In all of the

above cases, complexes were formed prior to assay by incubating dilute solutions of plasmid DNA encoding firefly luciferase (6.2 kb, 2.05×10^6 g/mole, 0.1 mg/mL, 25 mM acetate buffer, pH 5.1) with equal volumes of solutions containing polymers (in 25 mM acetate buffer, pH 5.1 at appropriate concentrations to achieve the indicated mass ratios) for 20 min at room temperature.[3]

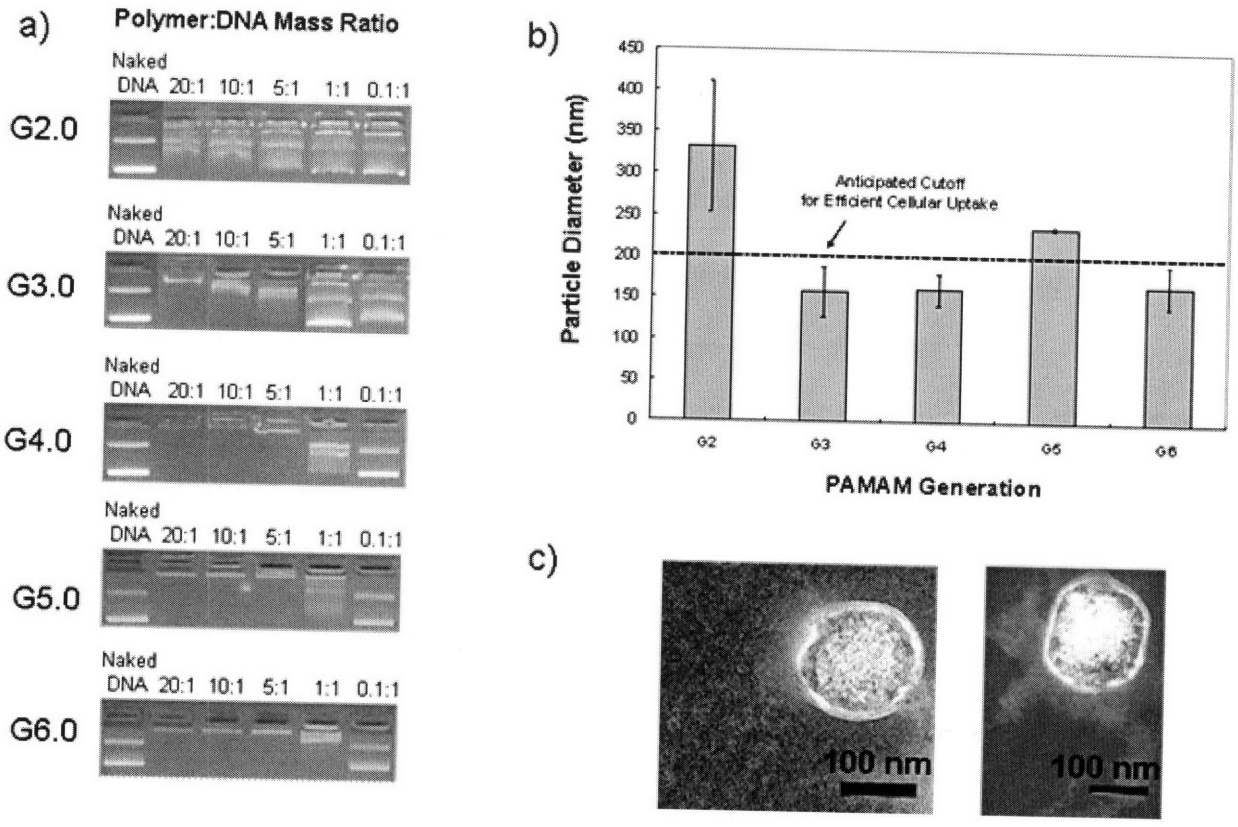

Figure 3.5. Biophysical characterization of linear-dendritic polyplexes.

(a) 1% agarose gel electrophoresis demonstrates DNA binding at indicated mass ratios. (b) Particle diameter measured via dynamic light scattering (DLS). (c) Transmission Electron Microscopy (TEM) depicts narrowly dispersed, roughly spherical particles.

3.3.4 Cell targeting, transfection, and cytotoxicity

To evaluate the ability of polyplexes to transfect target cells via receptor-mediated uptake, we transfected two cell types, P388D1 murine macrophages bearing the mannose

receptor and HepG2 human hepatocytes bearing the asialoglycoprotein receptor (for galactosylated ligands).[19-22] Transfections were performed in quadruplicate in 96-well plate format. Polymers and DNA were combined for 20 min at mass ratios ranging from 1:1 to 200:1 (polymer:DNA) in 25 mM acetate buffer, added to serum-free or 10% serum-containing medium, and incubated with cells for 4 h (587 ng DNA/well), after which the polyplex-containing medium was removed and replaced with growth medium. Cells were assayed for expression of the luciferase reporter gene at 72 h.[3] Figure 3.6(a) shows levels of luciferase reporter gene expression in macrophages (in the absence of serum) with optimized formulations of ligand-functionalized polyplexes, control polyplexes bearing no ligand, ligand-functionalized polyplexes in the presence of excess soluble ligand, and PEI. Generation 6.0, mannose-bearing polyplexes demonstrate transfection 1.6- to 1.8-fold higher than PEI, the most efficient commercially available polymer for *in vitro* transfections. Generation 5.0 polyplexes mediate reporter expression levels approximately 1.3-fold higher than PEI, while G4.0 polyplexes (as well as G3.0 and G2.0, data not shown) transfect at low levels comparable to naked DNA. The highest transfection levels were observed in polymer/DNA ratios under 50 in all systems (under 20 in G6.0), presumably owing to the effects of toxicity at high concentrations. Polyplexes with no mannose ligand exhibited significantly lower transfection efficiencies, and competitive inhibition of mannose receptors by an excess of soluble ligand virtually silenced reporter gene expression without affecting expression levels in positive and negative controls (Figure 3.6(a)). These data further support the hypothesis of cellular internalization by means of specific, receptor-mediated endocytosis. Finally, to probe the serum stability of PEGylated polyplexes, macrophages were transfected in the presence of 10% serum containing medium (Figure 3.6(b)). Four-fold transfection enhancements were observed relative to PEI, most likely owing to the

"stealth" effect imparted by PEG, which is known to reduce particle agglomeration by attenuating opsonization of serum proteins.[23]

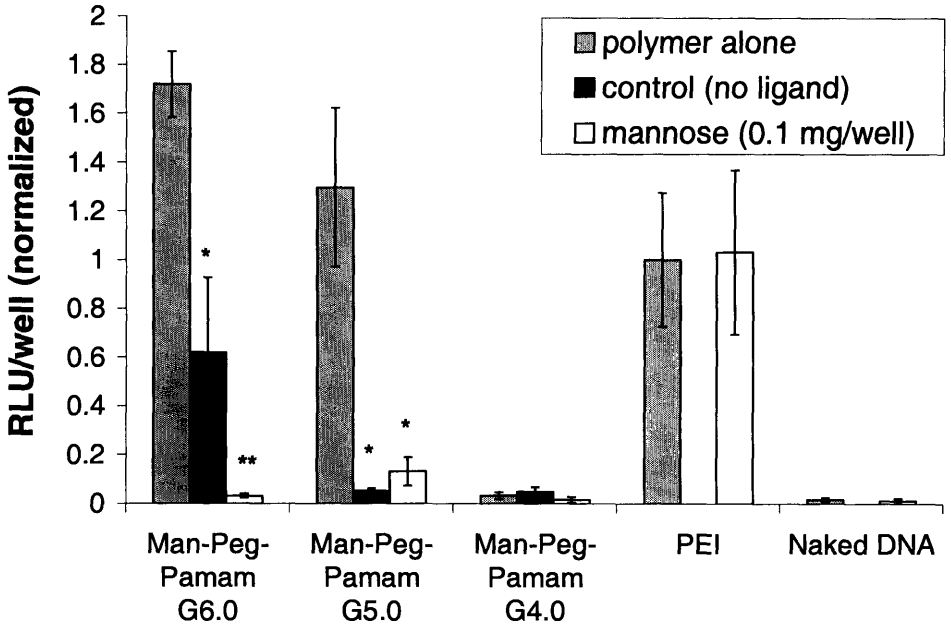

(a)

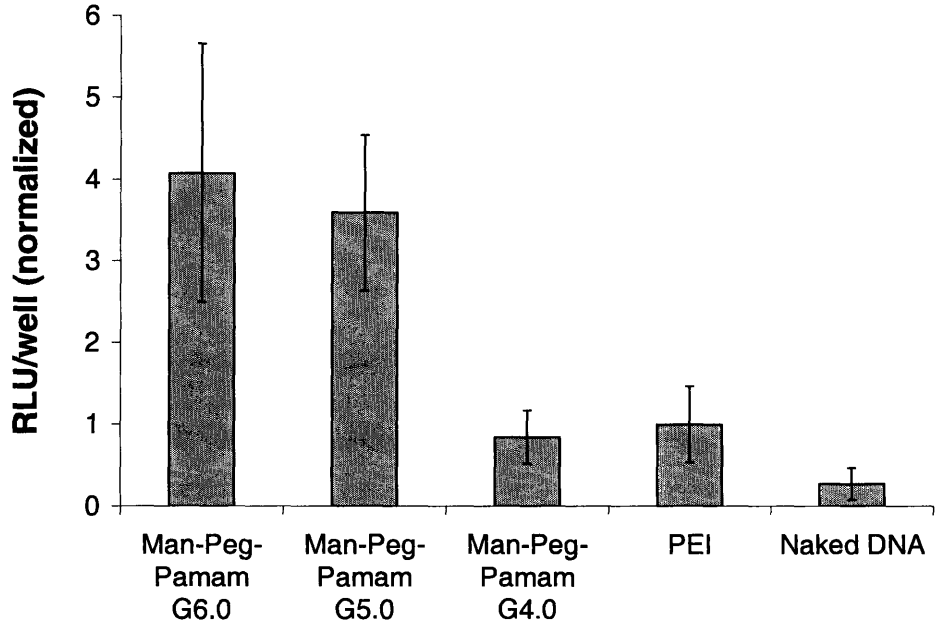

(b)

Figure 3.6. Transfection of P388D1 macrophages bearing the mannose receptor.

(a) Transfection by linear-dendritic polyplexes with and without the mannose ligand and in the presence of 0.1 mg/well soluble mannose. * indicates $p < 0.04$; ** indicates $p < 0.002$ (Two-tailed, unpaired Student's T-Test). Results normalized to an optimized formulation of PEI (2:1 PEI:DNA, serum free, no free mannose added). (b) Serum stability is demonstrated via transfection in the presence of serum proteins. Results normalized to an optimized formulation of PEI (2:1 PEI:DNA, 10% serum, no free mannose added). All results are given as average +/- standard error.

Transfection of HepG2 hepatocytes by linear-dendritic polyplexes bearing the galactose ligand is shown in Figure 3.7. In the absence of serum, optimized formulations of generation 6.0 and 4.0, ligand-functionalized polyplexes transfect significantly more efficiently ($p < 0.06$) than control polymers with no ligand (Figure 3.7(a)). Moreover, generations 6.0, 5.0, and 4.0 targeted systems mediate transfection levels within one order of magnitude of PEI in the absence of serum, and as much as eight-fold higher than PEI in the presence of serum (Figure 3.7(a) and (b)). Optimal polymer/DNA mass ratios were in the range of 100-200 for all systems studied. Taken together, these data suggest that hepatocyte-targeted polyplexes are serum stable and demonstrate enhanced transfection owing to a cell-specific, receptor-mediated process. Interestingly, expression levels were unaffected by the presence of an excess of soluble galactose, a finding that may owe to the multivalent nature of ligand binding by the asialoglycoprotein receptor, suggesting that multivalent ligand presentation via synthetic, multimeric galactose ligands may yield enhanced targeting relative to monomeric species.[24, 25]

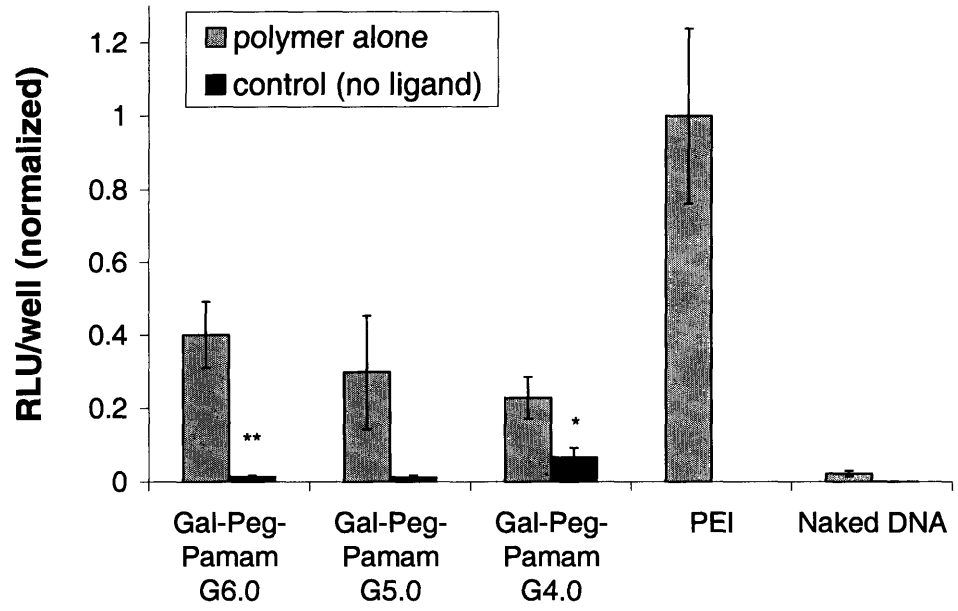

(a)

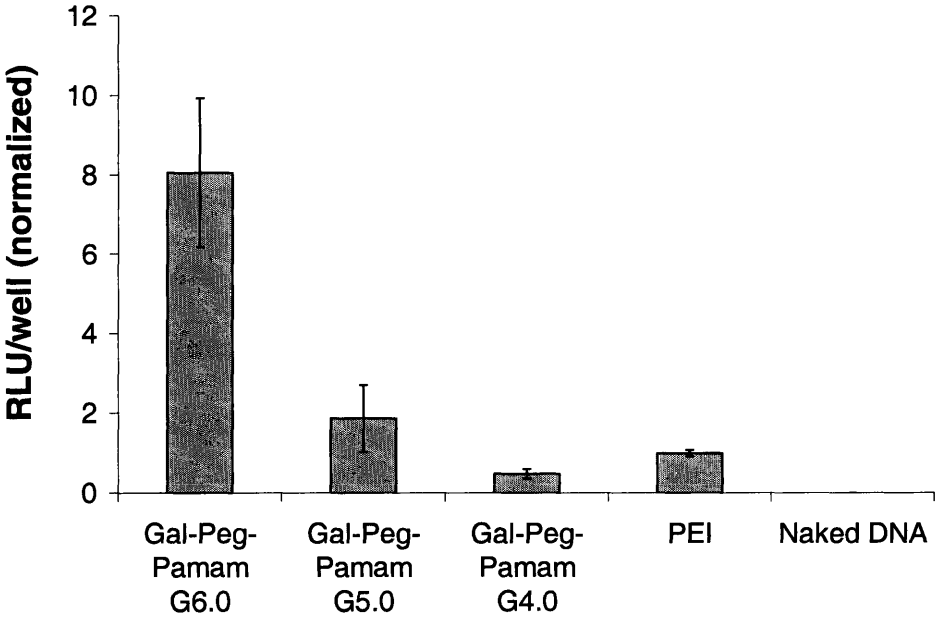

(b)

Figure 3.7. Transfection of HepG2 hepatocytes bearing the asialoglycoprotein receptor. (a) Transfection by linear-dendritic polyplexes with and without the galactose ligand * indicates $p < 0.06$; ** indicates $p < 0.03$ (Two-tailed, unpaired Student's T-Test). Results

normalized to PEI (serum free, no free galactose added) = 1.0. (b) Serum stability is demonstrated via transfection in the presence of serum proteins. Results normalized to PEI (10% serum, no free galactose added) = 1.0. All results are given as average +/- standard error.

To assess the cellular toxicity of linear-dendritic hybrid polymer-based systems, an MTT assay was performed to measure the relative viability of cells treated with varying polymer/DNA mass ratios. Cells were seeded in clear 96-well plates and transfected exactly as previously described. A range of polymer/DNA mass ratios were studied, corresponding to concentrations equal to and above those at which optimal transfection levels were observed. In P388D1 macrophages (Figure 3.8(a)), cells which we have found to be highly sensitive to environmental conditions in culture, no measurable toxicity was observed in G4.0-based systems over the entire concentration range studied. More significant toxicity was observed at high mass ratios in G5.0 (60-80% viability relative to untreated controls) and G6.0 systems (50-70%), though these toxicities were primarily observed at concentrations higher than those optimal for transfection. In HepG2 hepatocytes (Figure 3.8(b)), no measurable toxicity was observed in G4.0 and G5.0 systems at polymer/DNA mass ratios up to 200; in G6.0, moderate toxicity became apparent at ratios of 150 and above. In all cases, linear-dendritic systems failed to display toxicity until concentrations reached one to two orders of magnitude greater than those at which PEI was toxic.

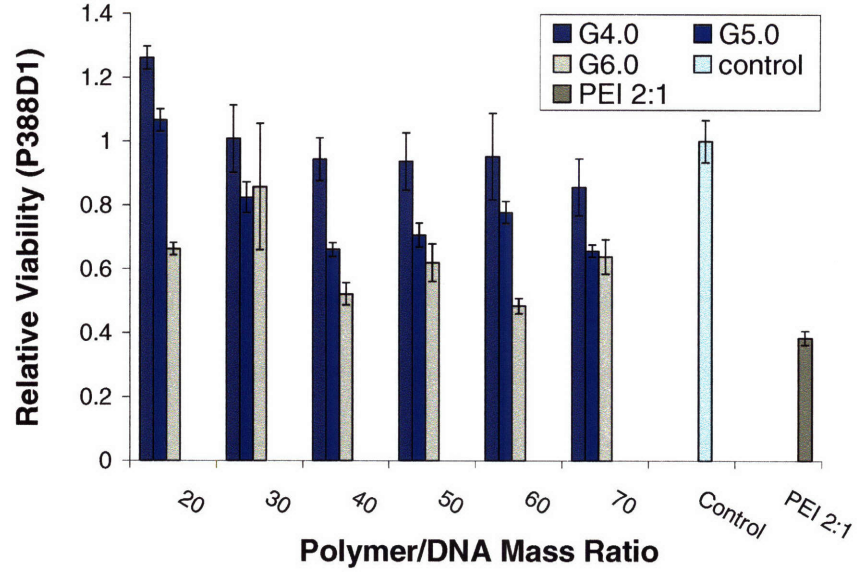

(a)

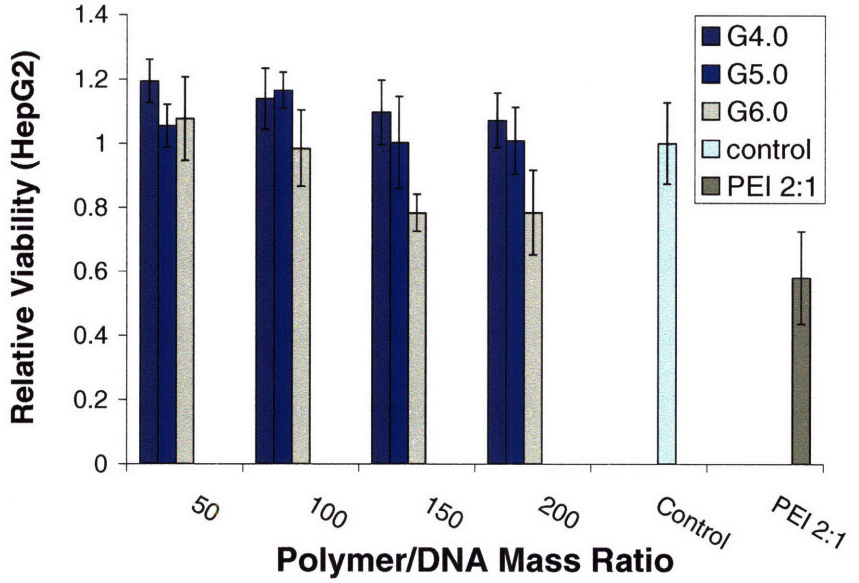

(b)

Figure 3.8. Relative viability of cells following transfection with hybrid polymers.

(a) P388D1 macrophages and (b) HepG2 hepatocytes assayed 72 h after transfection at indicated polymer/DNA mass ratios (control cells untreated). All results are given as average +/- standard error.

3.4 Summary

In this chapter, the design, synthesis, and testing of a new family of linear-dendritic hybrid polymers for their ability to deliver DNA to two distinct mammalian cell lines has been described. These hierarchically self-assembling polymers have functionalities that are physically and chemically distinct and can be independently modified. The modular nature of these systems makes them a platform from which further, serial modifications may be added to impart additional desired characteristics without substantially altering existing properties. As a proof of concept, we demonstrate the condensation of DNA by linear-dendritic polymers into nanoparticle structures with small size and robust serum stability appropriate for systemic delivery. Moreover, by presenting an outer shell of targeting ligands, these particles can transfect cells bearing targeted surface receptors with low toxicities and efficiencies exceeding the best commercially available polymer, PEI. Taken together, our data suggest that this new family of materials may find use as safe and highly efficient *in vivo* delivery agents for plasmid DNA and, potentially, other nucleotide-based therapeutics.

3.5 References

1. Verma, I.M. & Somia, N. Gene therapy - promises, problems, and prospects. *Nature* **389**, 239-242 (1997).
2. Verma, I.M. & Weitzman, M.D. Gene therapy: Twenty-first century medicine. *Annu. Rev. Biochem.* **74**, 711-738 (2005).
3. Wagner, E. Strategies to improve DNA polyplexes for *in vivo* gene transfer: Will "artificial viruses" be the answer? *Pharm. Res.* **21**, 8-14 (2004).
4. Neumann, E., Schaefer-Ridder, M., Wang, Y. & Hofschneider, P. Gene transfer into mouse lyoma cells by electroporation in high electric fields. *EMBO J.* **1**, 841-845 (1982).
5. Mehier-Humbert, S. & Guy, R.H. Physical methods for gene transfer: improving the kinetics of gene delivery into cells. *Adv. Drug Delivery Rev.* **57**, 733-753 (2005).
6. Luo, D. & Saltzman, W. Synthetic DNA delivery systems. *Nat. Biotechnol.* **18**, 33-37 (2000).
7. Glover, D.J., Lipps, H.J. & Jans, D.A. Towards safe, non-viral therapeutic gene expression in humans. *Nat. Rev. Genet.* **6**, 299-310 (2005).

8. Luo, D., Haverstick, K., Belcheva, N., Han, E. & Saltzman, W.M. Poly(ethylene glycol)-conjugated PAMAM dendrimer for biocompatible, high-efficiency DNA delivery. *Macromolecules* **35**, 3456-3462 (2002).
9. Anderson, D.G., Akinc, A., Hossain, N. & Langer, R. Structure/property studies of polymeric gene delivery using a library of poly(beta-amino esters). *Mol Ther.* **11**, 426-434 (2005).
10. Anderson, D.G., Lynn, D.M. & Langer, R. Semi-automated synthesis and screening of a large library of degradable cationic polymers for gene delivery. *Angew. Chem. Int. Ed.* **42**, 3153-3158 (2003).
11. Munkonge, F.M., Dean, D.A., Hillery, E., Griesenbach, U. & Alton, E.W. Emerging significance of plasmid DNA nuclear import in gene therapy. *Adv. Drug Delivery Rev.* **55**, 749-760 (2003).
12. Schaffer, D.V., Fidelman, N.A., Dan, N. & Lauffenburger, D.A. Vector unpacking as a potential barrier for receptor-mediated polyplex gene delivery. *Biotechnol. Bioeng.* **67**, 598-606 (2000).
13. Iyer, J., Fleming, K. & Hammond, P.T. Synthesis and Solution Properties of New Linear-Dendritic Diblock Copolymers. *Macromolecules* **31**, 8757-8765 (1998).
14. Sonawane, N.D., Szoka, F.C. & Verkman, A.S. Chloride accumulation and swelling in endosomes enhances DNA transfer by polyamine-DNA polyplexes. *J. Biol. Chem.* **278**, 44826-44831 (2003).
15. Niu, Y.H., Sun, L. & Crooks, R.A. Determination of the intrinsic proton binding constants for poly(amidoamine) dendrimers via potentiometric pH titration. *Macromolecules* **36**, 5725-5731 (2003).
16. Cakara, D., Kleimann, J. & Borkovec, M. Microscopic protonation equilibria of poly(amidoamine) dendrimers from macroscopic titrations. *Macromolecules* **36**, 4201-4207 (2003).
17. Rejman, J., Oberle, V., Zuhorn, I.S. & Hoekstra, D. Size-dependent internalization of particles via the pathways of clathrin-and caveolae-mediated endocytosis. *Biochem. J.* **377**, 159-169 (2004).
18. Tomalia, D.A. Birth of a new macromolecular architecture: dendrimers as quantized building blocks for nanoscale synthetic polymer chemistry. *Prog. Polym. Sci.* **30**, 294-324 (2005).
19. Diebold, S.S., Plank, C., Cotten, M., Wagner, E. & Zenke, M. Mannose Receptor-Mediated Gene Delivery into Antigen Presenting Dendritic Cells. *In Synthetic DNA delivery systems (Eds.: D. Luo, W. M. Saltzman), Kluwer, New York* (2003).
20. Hoflack, B. & Kornfeld, S. Lysosomal enzyme binding to mouse P388D1 macrophage membranes lacking the 215-kDa mannose 6-phosphate receptor: evidence for the existence of a second mannose 6-phosphate receptor. *Proc. Natl. Acad. Sci. U. S. A.* **82**, 4428-4432 (1985).
21. Remy, J.S., Kichler, A., Mordvinov, V., Schuber, F. & Behr, J.P. Targeted gene transfer into hepatoma cells with lipopolyamine-condensed DNA particles presenting galactose ligands: a stage toward artificial viruses. *Proc. Natl. Acad. Sci. U. S. A.* **92**, 1744-1748 (1995).
22. Stockert, R.J. The asialoglycoprotein receptor: relationships between structure, function and expression. *Physiol. Rev.* **75**, 591-609 (1995).

23. Harris, J.M. & Chess, R.B. Effect of pegylation on pharmaceuticals. *Nat. Rev. Drug Discovery* **2**, 214-221 (2003).
24. Connolly, D.T., Townsend, R.R., Kawaguchi, K., Bell, W.R. & Lee, Y.C. Binding and endocytosis of cluster glycosides by rabbit hepatocytes. Evidence for a short-circuit pathway that does not lead to degradation. *J. Biol. Chem.* **257**, 939-945 (1982).
25. Lee, Y.C. & Lee, R.T. Carbohydrate-protein interactions: Basis of glycobiology. *Acc. Chem. Res.* **28**, 321-327 (1995).

Chapter 4: Mannose-functionalized linear-dendritic hybrid polymers for the targeted delivery of DNA vaccines

4.1 Introduction

During the past century, vaccines have been responsible for the protection of millions of people against devastating diseases like smallpox, poliomyelitis, and measles. As a result, protective immunization is now recognized as the most cost-effective method for controlling and eradicating infectious diseases. Yet, despite our rapidly advancing understanding of the molecular and cellular underpinnings of the immune response, there remains a great need for vaccine technologies that are effective against HIV, hepatitis B and C, malaria, cancer, and emerging pathogens like avian influenza and weapons of bioterrorism.[1-4] In order to be useful, these new vaccines must be safe (low risk for side effects or disease transmission), scalable, and capable of stimulating both humoral and cellular arms of the immune system.[5-7] DNA vaccines are the only vaccine technology with the potential to offer all of these necessary attributes.[5-7] Thus, they have been the source of intense research interest in recent years. However, despite encouraging successes in animal trials, DNA vaccines have faired only modestly in early human clinical trials because of poor expression and adjuvancy – two problems directly related to DNA delivery. It is clear that new delivery systems which can more effectively manipulate the immune response will be necessary before this technology can be approved for clinical use. [5-8]

In order to design a better DNA vaccine, it is useful to first appreciate the mechanisms of genetic vaccination in the complex, multicellular environment of the immune system. The primary activators of adaptive immunity are antigen presenting cells (APC), which are most

commonly dendritic cells (DC's) and macrophages (MΦ's). In the immature state, APCs rapidly sample their environment, capturing and internalizing antigens at the rate of approximately one cell volume per hour.[9] After capturing an antigen, an APC will process it through one of two distinct pathways (Figure 4.1). If the antigen is endogenous (that is, produced intracellularly, as in the case of viral proteins produced by an infected APC), it will be associated in the endoplasmic reticulum with a membrane-bound molecule called Major Histocompatibility Complex class I (MHC-I), which is then shuttled to the cell surface. Once on the APC cell surface, the MHC-I-antigen complex is able to associate with T lymphocytes ("T cells") bearing the CD8 surface receptor. If accompanied by appropriate "danger" signals (surfaced proteins that are expressed by "mature" APCs), this T lymphocyte engagement will stimulate the activation and expansion of cytotoxic T lymphocyte (CTL) clones specific for this antigen, which will then remove cells from the body that are associated with this particular antigen (e.g., infected cells).[5, 10]

The second pathway for antigen presentation occurs when exogenous antigens (that is, externally produced antigens taken up by APCs) are encountered. In this case, the antigen will be internalized and broken down into small oligomeric fragments, associated with a molecule called MHC-II, and presented on the APC cell surface. The MHC-II-antigen complex is able associate with T lymphocytes bearing the CD4 surface receptor, and if accompanied by the appropriate "danger" signals, this engagement will result in the activation and expansion of T_H-lymphocytes ("helper T cells"), which stimulate, among other things, the production of antibodies specific to the antigen. Importantly, in addition to generating an immediate response to the antigen, the generation of CD8+ CTL and/or CD4+ T_H clones is thought to involve genetic

alterations in certain persisting T-cells that enhance the magnitude of the immune response in future encounters with the same antigen, the basis of prophylactic vaccination.[5, 10]

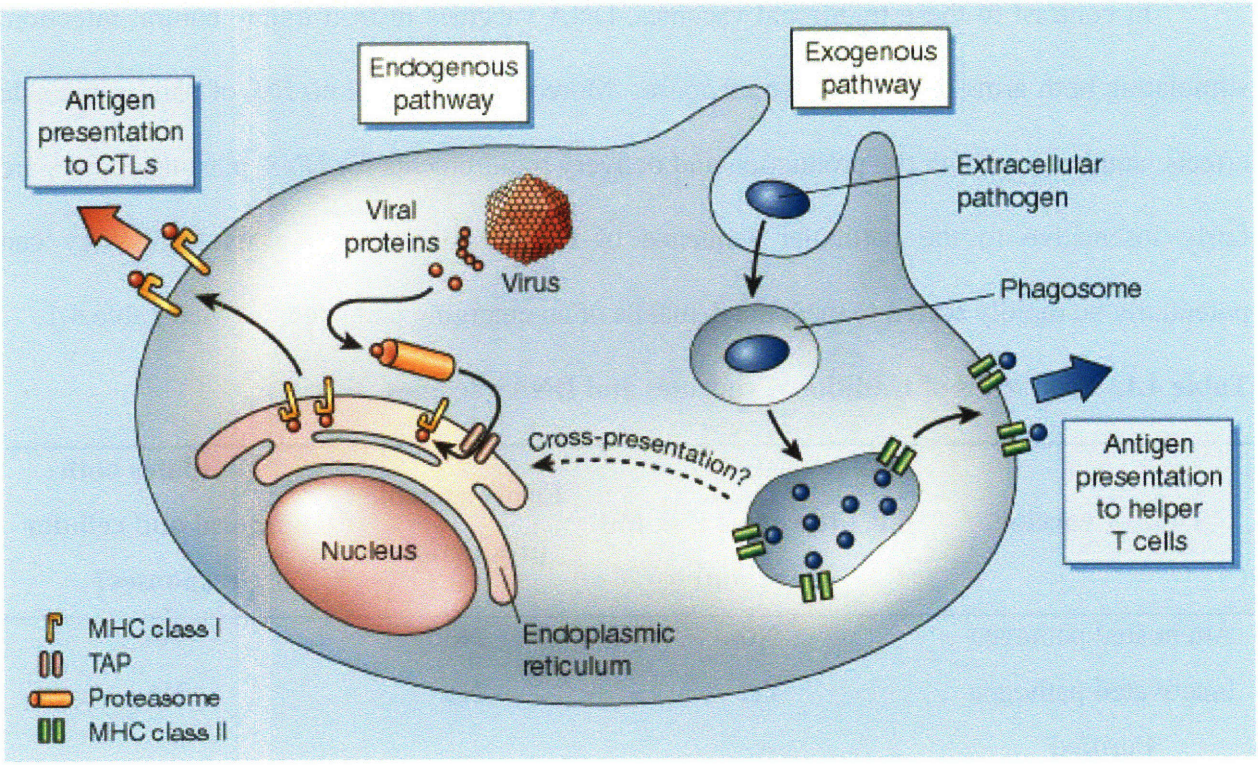

Figure 4.1. Antigen processing and presentation by antigen-presenting cells. Adapted with permission from [11].

Traditional vaccines can be divided into three major categories – attenuated pathogens, inactivated pathogens, or purified macromolecules – and the mechanism of immune stimulation varies by vaccine category. Attenuated viral or bacterial vaccines are capable of infecting cells but are unlikely to cause full blown infections. Because antigens can be both produced intracellularly by infected cells or taken up exogenously, both MHC-I and MHC-II pathways can be activated. However, while effective, attenuated vaccines are too dangerous for use against highly dangerous pathogens such as HIV because the risk of reversion to a pathogenic state, particularly in immunocompromised patients, is too great. On the other hand, completely inactivated pathogens or purified macromolecular antigens are much safer, posing virtually no

risk for full-blown infection. However, they can generally only stimulate an MHC-II (T_H cell based) response, which may be insufficient for protection against certain diseases.

In contrast to these traditional vaccines, DNA vaccines instead mimic natural infection, stimulating both arms of the immune response. Moreover, they pose no risk of pathogenic side effects, and because both the production and delivery requirements for DNA plasmid vectors are fairly insensitive to the particular sequence of the encoded antigen, this technology can potentially be rapidly scaled to meet the demands of an emerging pathogen.[5, 10] See Table 4.1.

Table 4.1. Properties of traditional vaccines and DNA vaccines.

Type of vaccine	Safe? (i.e. little or no risk for infection)	Easily scalable production?	Stimulates both humoral and cellular responses?
Attenuated pathogen	No	No	Yes
Inactivated pathogen	Yes	No	No
Purified macromolecule	Yes	Yes	No
DNA vaccine	**Yes**	**Yes**	**Yes**

A range of non-viral methods have been used to deliver DNA vaccines, including intramuscular injections of naked DNA[11-13], nanoparticles formed by the complexation of DNA with cationic lipids or polymers[5, 14], and polymeric microparticles.[15-18] However, to date none of these approaches have yielded an appropriate combination of delivery efficacy, adjuvancy, and safety to justify clinical approval. The linear-dendritic hybrid polymer DNA delivery systems developed in Chapter 3 represent a platform with unique promise for DNA vaccine delivery because they can deliver DNA in a targeted, efficient manner and can potentially be functionalized with materials to further enhance adjuvancy and expression levels. Further, it was

demonstrated that hybrid polymers functionalized with mannose can target MΦ cells through the mannose receptor, which is a pattern recognition receptor expressed on a range of APC types (including dendritic cells, the most potent APCs).[19-22]

This chapter details a series of preliminary investigations conducted to gauge the ability of mannose-functionalized hybrid polymers to deliver DNA vaccines *in vivo*. The receptor-mediated transfection of a dendritic cell line is demonstrated, as well as the elicitation of antigen-specific, primary and secondary, antibody- and cell-mediated immune responses *in vivo*. Finally, a series of recommendations for future work in this area are offered. While preliminary, the results of this study should inform and motivate future investigations on the ability of hybrid polymers to elicit protective immune responses through DNA vaccination.

4.2 Experimental Methods

General Considerations. The synthesis and characterization of mannose-functionalized and control hybrid polymers used in this study is described in detail in Chapter 3. D-mannose and hyperbranched poly (ethylenimine) (PEI, M_n = 25000) were purchased from Sigma-Aldrich (St. Louis, MO) and used without further purification. DNA plasmids encoding firefly luciferase, β-galactosidase, and the SIY-hsp65 fusion protein (pCMV-Luc, pBP2, and pCI-Neo, respectively) were purchased from Elim Biopharmaceuticals (San Francisco, CA) and used without further purification. DC2.4 dendritic cells were a generous gift from David Nguyen (Langer lab, MIT). DC2.4 cells were grown at 37° C in 5% CO_2 in 90% Dulbecco's modified Eagle's medium supplemented with 10% fetal bovine serum, 100 units/mL penicillin, 100 μg/mL streptomycin, 10 mM HEPES, 2 mM L-glutamine, and 50 μM 2-mercaptoethanol. Bright-Glo® luciferase assay detection kits were purchased from Promega (Madison, WI) and used according to the manufacturer's specifications. MTT cell proliferation assay kits were purchased from

American Type Culture Collection (ATCC, Manassas, VA) and used according to the manufacturer's specifications. C57BL/6 (B6, H-2 K^b) mice (6-10 weeks old) were purchased from Taconic Farms and cared for in compliance with the guidelines of the Massachusetts Institute of Technology.

Instrumentation. Luminescence from reporter gene expression studies was measured using a Veritas Microplate Luminometer. Optical absorbance was measured using a SpectraMax 190 microplate reader (Molecular Devices, Sunnyvale, CA). Flow cytometry was performed using a FACScan flow cytometer (Becton Dickinson).

Cell transfections. All transfection assays were performed in quadruplicate in accordance with the following protocol. All materials, buffers, and media were sterilized prior to use. DC2.4 cells were grown in 96-well plates at an initial seeding density of 10000 cells/well in 150 μL/well of growth medium. Cells were allowed to attach and proliferate for 24 h in an incubator.

Polymers were dissolved in sterile 25 mM acetate buffer (6.0 mg/mL) and arrayed into a 96-well plate (25 μL/well total polymer solution with concentrations adjusted as appropriate to yield polymer/DNA ratios ranging from 5:1 to 100:1 (m:m)). Polymer/DNA complexes were formed by the addition of 25 μL/well of 0.06 mg/mL pCMV-Luc in 25 mM acetate buffer. Polymer and DNA solutions were vigorously mixed using a multichannel pipettor upon addition of DNA solutions and subsequently incubated for 10 min to allow for complexation. Thirty μL/well aliquots of the above complex solutions were then transferred into each well of a 96-well plate containing 200 μL/well of serum-free Opti-MEM medium (Invitrogen Corporation, Carlsbad, CA). Growth medium was removed from cells and 150 μL/well of complex-plus-medium solution was added. Controls employing PEI were prepared exactly as above to yield

polymer DNA ratios ranging from 0.5:1 to 10:1 (m:m), and in all cases optimized formulations are reported as positive controls. Naked DNA controls were also prepared as above, and each 96-well plate included appropriate positive and negative controls as internal standards. In all cases, wells contained 587 ng DNA/well at indicated polymer/DNA ratios.

Following incubation of complex-containing medium solutions with cells for 8 h, solutions were removed and replaced with 10% serum-containing growth medium. Cells were incubated for an additional 24 h, and luciferase expression was determined using the commercially available Bright-Glo® luciferase assay kit (Promega, Madison, WI). Luminescence was quantified in solid, flat-bottom, white polypropylene 96-well plates using a bioluminescent plate reader. Luminescence was expressed in relative light units and was not normalized to total cellular protein in this assay.

Cell viability assay. Cell viability assays were performed in quadruplicate using the following protocol. DC2.4 cells were seeded in 96-well clear, flat-bottom plates and transfected according to the procedure described above. After 24 h, cell metabolic activity was assayed using the MTT cell proliferation assay kit (ATCC, Manassas, VA). Initially, a 15 μL aliquot of MTT assay reagent was added to each well. After incubating for two hours, 100 μL of detergent reagent was added. The plate was then covered and left in the dark for 4 h, after which optical absorbance was measured at 570 nm using a microplate absorbance reader. Background (media plus MTT assay reagent plus detergent reagent with no cells present) was subtracted from the value of each well, and all values were normalized to the value of control (untreated) cells.

***In vivo* antibody assay.** Formulations containing 100 μg DNA at a 10:1 mass ratio of polymer:DNA in 200 μL total solution volume of 25 mM sodium acetate buffer (supplemented with 5% glucose) were injected once intradermally in the back of each mouse. Negative controls

consisted of buffer only or naked DNA (100 μg DNA with no polymer), and the positive control was 50 μg recombinant β-galactosidase protein in PBS buffer. Each control was administered exactly as described above. At indicated time points, blood samples were collected from the tail vein. Anti-β-galactosidase IgG levels in serum were determined by ELISA, and the results were presented as equivalents to a monoclonal anti-β-galactosidase IgG (Calbiochem, San Diego, CA).

***In vivo* T-cell proliferation assay.** 2C T-cells were freshly isolated from the lymph nodes of 2C TCR transgenic mice (2C TCR transgenic mice were provided as a generous gift from Professor Jianzhu Chen's lab at MIT). Two million naïve 2C T-cells were injected intravenously into B6 mice. On the same day, mice were injected intradermally in the back with hybrid polymer-DNA complexes (DNA encoding SIY-hsp65, formulations prepared as described above for antibody assays) or controls. To study primary T-cell responses, the mice were sacrificed after 8 d and their lymph nodes and spleens were harvested and processed into single cell suspensions. To study secondary responses, mice were challenged with 50 μg SIY peptide (in PBS buffer) after 28 d, then sacrificed 3 d later, after which their lymph nodes and spleens were harvested and processed into single cell suspensions. In both cases, CD8+ cells and 2C T-cells were assayed by immunostaining (BD Biosciences, San Jose, CA) followed by flow cytometry (with propidium iodide gating (5 μg/mL) and collecting 100,000 total events per sample).

4.3 Results and Discussion

4.3.1 Targeted transfection of dendritic cells *in vitro*

To augment our previous data on the targeting and delivery of DNA to APCs using mannose-functionalized hybrid polymers (Chapter 3), we transfected a second type of APC:

DC2.4 dendritic cells. We chose this cell line for two reasons: First, dendritic cells are known to be the most important and potent APCs in the body.[10] Second, DC2.4 cells, like other primary and immortalized dendritic cells, are known to be highly resistant to transfection by conventional *in vitro* reagents.[23] Thus, these cells represent both an additional means of validating APC targeting *in vitro* and a stringent standard for the assessment of DNA delivery potency. Figure 4.2(a) shows that an optimized formulation of mannose-functionalized polymer – DNA complexes (20:1 polymer:DNA mass ratio) yielded transfection levels approximately 8-fold higher than polyethylenimine (PEI). Further, mannose-mediated targeting could be observed by comparison with either a control polymer (lacking the mannose ligand) or by transfection with a mannose-functionalized polymer in the presence of an excess of soluble ligand to block receptor binding. Additionally, Figure 4.2(b) shows that, in keeping with previous results using macrophages and hepatocytes (Chapter 3), significant cytotoxicity was observed only when hybrid polymers reached concentrations an order of magnitude higher than those at which PEI was toxic.

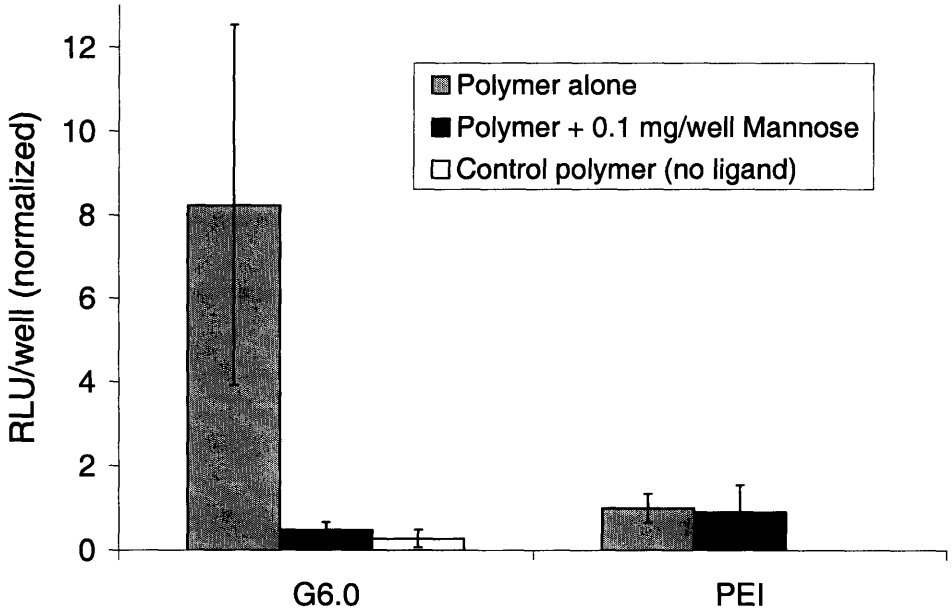

(a)

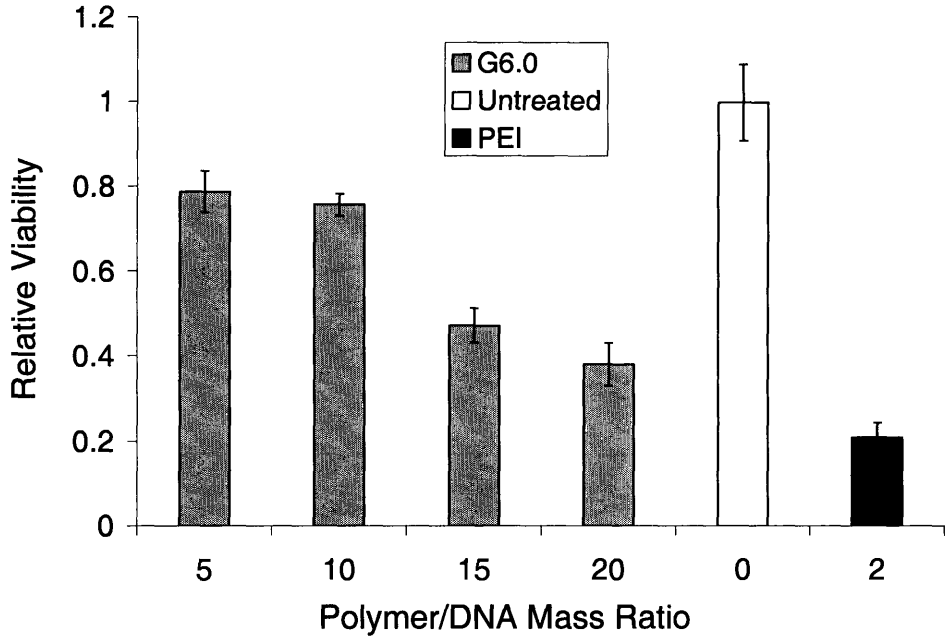

(b)

Figure 4.2. Transfection of DC2.4 dendritic cells bearing the mannose receptor.

(a) Transfection by linear-dendritic polyplexes in the presence or absence of 0.1 mg/well soluble mannose. Results are normalized to an optimized formulation of PEI (2:1

PEI:DNA, no free mannose added). (b) Relative viability of DC2.4 cells 72 h following transfection at indicated polymer/DNA mass ratios (control cells untreated). All results are given as average +/- standard error.

4.3.2 Primary and secondary humoral responses in vaccinated mice

To measure primary and secondary humoral immune responses to hybrid polymer vaccines *in vivo*, we vaccinated C57BL/6 mice (n = 5) on day 0 by intradermal (ID) injection with 100 μg of plasmid DNA encoding β-galactosidase, a model antigen (complexed with hybrid polymers at a 10:1 polymer:DNA mass ratio). Vaccination was repeated on day 28. All mice (treated and untreated) were challenged on day 56 by intraperitoneal (IP) injection with 45 μg recombinant β-galactosidase protein in PBS buffer. Serum IgG antibody levels were measured three weeks after the initial injection and three weeks after the challenge by ELISA (Figure 4.3(a)).

As shown in Figure 4.3(b), serum anti-β-galactosidase IgG levels were significantly higher in vaccinated mice than in unvaccinated mice following an antigenic challenge ($p = 0.11$). (Note: Mice vaccinated with naked DNA encoding β-galactosidase yielded serum anti-β-galactosidase IgG levels that were quantitatively similar to untreated mice.) Anti-β-galactosidase antibody levels were not significantly higher in treated versus untreated mice prior to an antigenic challenge. Data indicating that mice vaccinated with hybrid polymer DNA vaccines produce significantly higher levels of antibodies against an encoded antigen than unvaccinated mice (following an antigenic challenge) suggests that mice vaccinated against a pathogen or disease may also be better protected than unvaccinated mice.

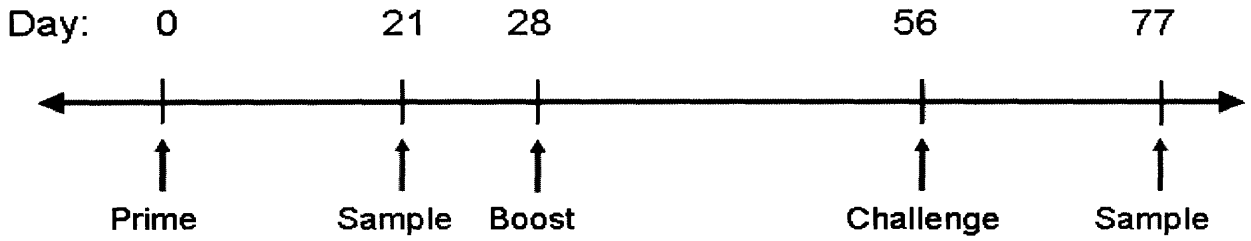

(a)

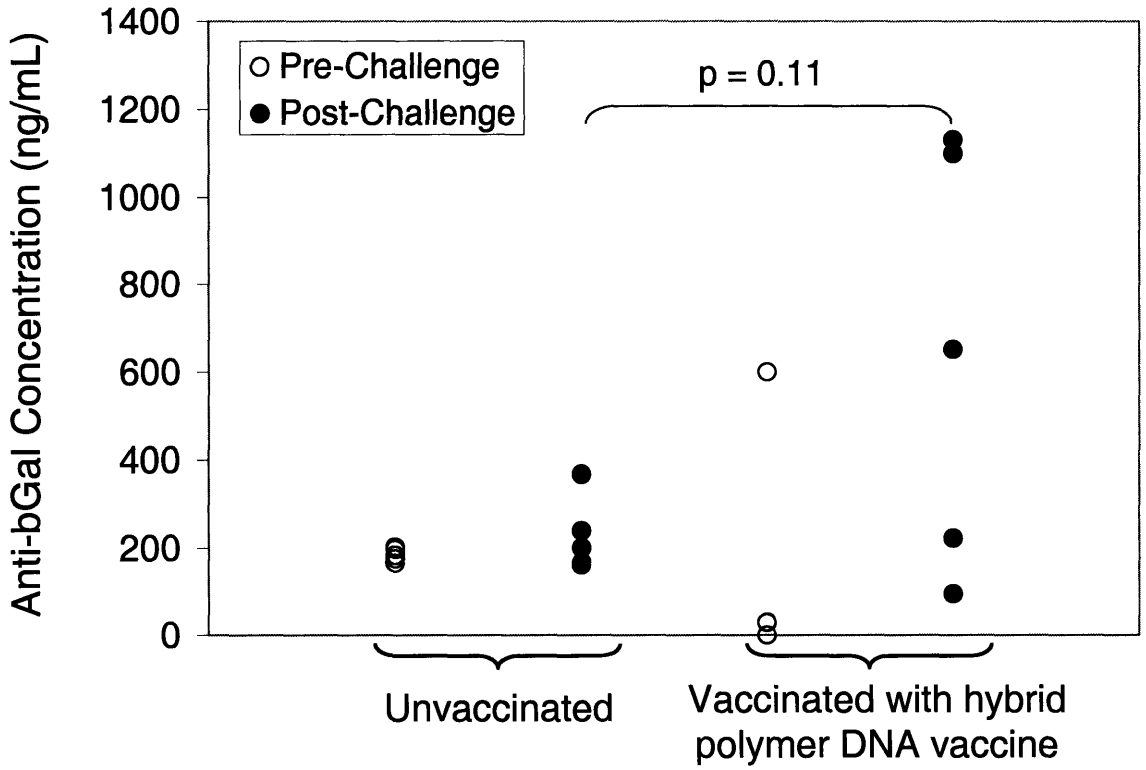

(b)

Figure 4.3. Humoral responses to hybrid polymer DNA vaccines.

(a) Experimental design. (b) Primary and secondary anti-β-galactosidase IgG levels in vaccinated and unvaccinated mice (n = 5 mice per group). Pre-challenge levels were measured three weeks after immunization. Post-challenge levels were measured three weeks after a challenge with soluble, recombinant β-galactosidase.

4.3.3 Primary and secondary cellular responses in vaccinated mice

To evaluate the ability of hybrid polymer formulations to elicit both primary and secondary cell-mediated immune responses *in vivo*, a 2C T-cell model was used. Transgenic 2C mice express a single, restricted T-cell receptor (referred to as a 2C T-cell receptor) which specifically recognizes an antigenic sequence called SIY (whose full sequence is SIYRYYGL) in complex with MHC.[24, 25] Thus, antigen-specific cellular responses in mice that have been both vaccinated against SIY and adoptively transferred 2C T-cells can be measured by clonal expansion of donor T-cells, up-regulation of early activation markers (for example, CD69) in donor T-cells, or other means.[18]

In this study, cellular responses were measured as follows. On day 0, 2C T-cells were freshly isolated from the lymph nodes of 2C mice and adoptively transferred to recipient C57BL/6 mice by retro-orbital injection. On the same day, recipient mice were vaccinated by ID injection with hybrid polymer-DNA complexes using a DNA plasmid called pCIneo-hsp65p1, which encodes the SIY antigenic sequence fused to the carboxy-terminus of heat shock protein 65 (hsp65). To measure primary responses, vaccinated and unvaccinated mice were sacrificed on day 8, and secondary lymphoid tissues (lymph nodes and spleen) were processed into single cell suspensions, stained for CD8 and Thy1.1 (a 2C T-cell-specific marker), and analyzed by flow cytometry. To measure secondary responses, vaccinated and unvaccinated mice were challenged on day 28 with an IP injection containing 50 μg of pure SIY peptide in PBS buffer on day 28, then sacrificed and analyzed as described above on day 31 (Figure 4.4(a)).

As shown in Figure 4.4(b), the sizes of both CD8+ and antigen-specific (donor) T-cell populations were significantly larger in vaccinated mice than in unvaccinated mice (by 1.5- to 2-fold) following a single vaccination. Further, following a challenge, CD8+ T cell levels were

approximately 5-fold higher than unvaccinated mice. While donor 2C T-cell levels were not measured following a challenge, the fact that CD8+ levels were further enhanced by a challenge (relative to primary responses) suggests that secondary responses are likely due, in part or in full, to the selective expansion of antigen-specific CD8+ T-cells. Together, the results in Figure 4.4 suggest that mice vaccinated with hybrid polymer DNA vaccine formulations generate antigen-specific, primary and secondary cellular responses. Moreover, these results suggest that mice vaccinated with these formulations may be better protected against pathogens or diseases than unvaccinated mice.

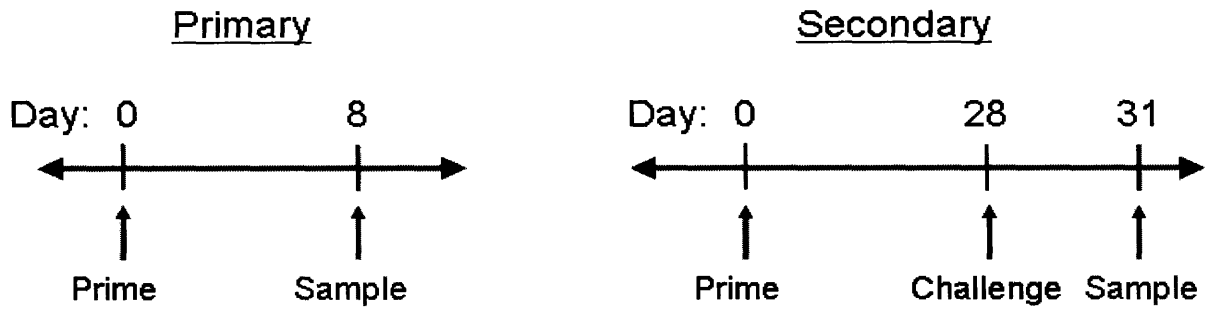

(a)

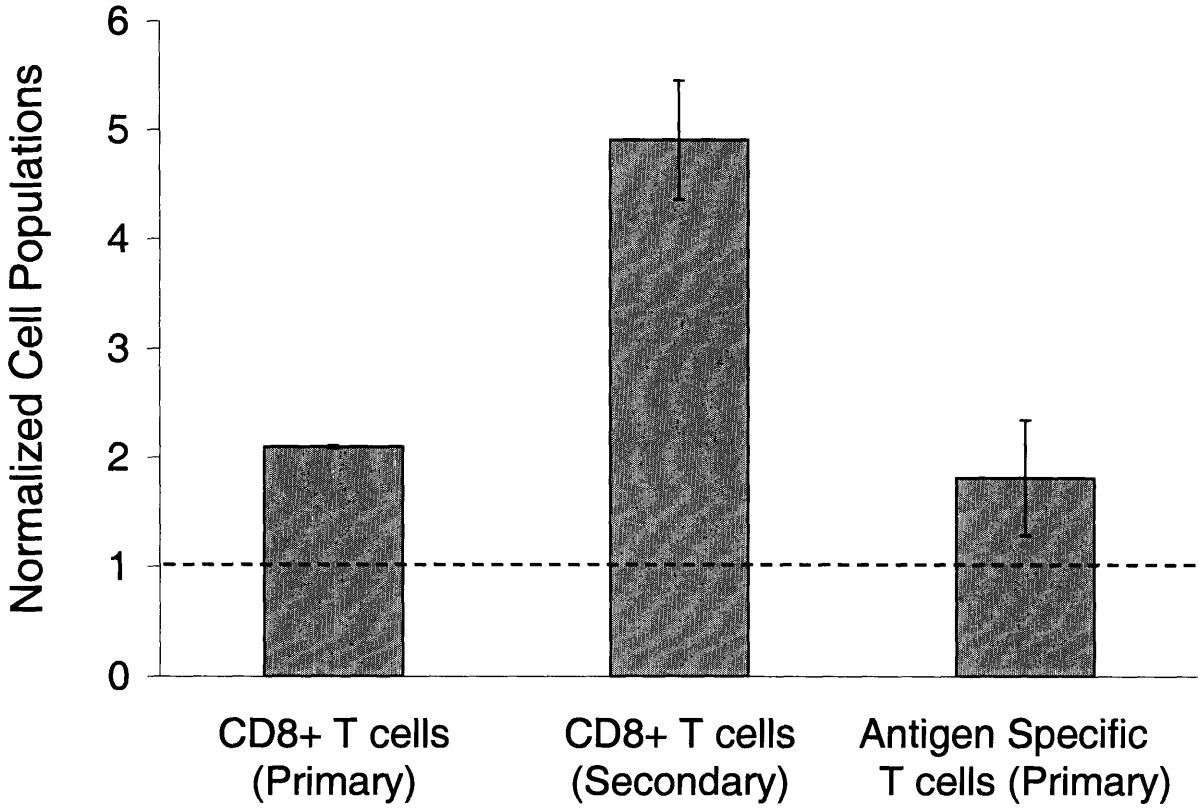

(b)

Figure 4.4. Cellular responses to hybrid polymer DNA vaccines.

(a) Experimental design. (b) Primary and secondary, CD8+ and antigen-specific T-cell levels in vaccinated mice. Each T-cell subset is normalized to the level of the same subset in an unvaccinated mouse.

4.4 Recommendations for future work

The preliminary studies described above suggest that mannose-functionalized hybrid polymers may be interesting candidates for the targeted delivery of DNA vaccines. The following passages suggest areas of future work which should further validate and explore this concept.

4.4.1 Large-scale animal studies on T-cell activation and disease protection

The T-cell activation studies described above were performed using relatively small numbers of mice (2-3 per treatment group). Follow-up studies would strongly benefit from the use of larger cohorts of animals (5 or more per treatment group), which can allow one to generate hypotheses and conclusions that are supported by statistically significant data sets. Further, to better understand the dynamics of multiple types of cells involved in the immune response (e.g., APCs, CD4+ or CD8+ T-cells, B-cells, and natural killer cells), samples from each treatment group should be stained for multiple, cell type-specific markers. Finally, one of the most convincing demonstrations of a vaccine's efficacy involves protection from a disease challenge. Established animal models exist for cancer, bacterial and viral infections, and other diseases, and the use of these models to study the potency of immune responses elicited by hybrid polymer DNA vaccines would be very useful.[10]

4.4.2 Direct observation of APC transfection *in vivo*

The ability to directly observe transgene expression in various cell types following vaccination could shed light on the roles that different cells (e.g., dendritic cells, macrophages, B-cells, etc.) play in the development of immune responses to hybrid polymer DNA vaccines. In an initial attempt to explore this topic, C57BL/6 mice were vaccinated as described above using hybrid polymer-DNA complexes encoding either green fluorescent protein (GFP) or luciferase (Luc), a non-fluorescent protein (which served as a negative control). After 48 hours, lymph nodes and spleens from all mice were processed into single cell suspensions, stained for various cell type-specific markers (for example, CD11c for dendritic cells), and analyzed by flow cytometry. Interestingly, CD11c+ dendritic cells showed markedly different morphological features and autofluorescence properties in vaccinated mice as compared to unvaccinated mice

(data not shown). However, these effects were observed in both hybrid polymer-treated groups, and as a result it was impossible to discriminate between fluorescence changes owing to GFP expression versus those owing to non-specific changes in autofluorescence. Thus, while it is clear that hybrid polymer-DNA complexes interacted with (and were likely taken up by) dendritic cells, which subsequently migrated to secondary lymphoid tissues, it is impossible to discern whether transgene expression occurred in these cells. Future experiments in this area may potentially remedy this problem by using a reporter transgene which encodes a non-native cell surface protein. It is possible to transfect cells with such a construct and then analyze expression by antibody labeling using a fluorophore (such as allophycocyanin) that can be analyzed on a fluorescence channel that yields lower levels of autofluorescence in response to changes in cell morphology.

4.4.3 Adjuvanting effects of hybrid polymers

In addition to appropriate levels of transgene expression in APCs, up-regulation of costimulatory factors on these cells during antigen presentation is also considered crucial to DNA vaccine potency.[10] Recent studies have shown that both natural and synthetic materials can act as adjuvants by causing up-regulation of costimulatory factors in APCs following exposure, an attribute which may be highly favorable for vaccine delivery systems.[17, 26-29]

Both *in vitro* and *in vivo* approaches can be used to study the adjuvanting effects of hybrid polymers. *In vitro*, immature dendritic cells may be isolated by treatment of bone marrow progenitor cells with granulocyte/macrophage colony stimulating factor (GM-CSF) using established protocols.[17] Treatment of these differentiated cells with polymer-DNA complexes (or other materials), followed by antibody staining for APC cell surface markers and up-regulated co-stimulatory factors (e.g., CD40, CD80, and CD86) can be used to measure APC

maturation in response to a given treatment.[17] *In vivo*, APC maturation can be studied by immunization, APC isolation (by processing secondary lymphoid tissues into single cell suspensions and subsequently staining for an APC marker such as CD11c), and staining for co-stimulatory factors.

Future work on hybrid polymer DNA vaccines is likely to benefit from the use of these techniques to study APC maturation, as they can be instrumental in the development of mechanistic hypotheses to explain events taking place during the vaccination process. Further, the rational modification of hybrid polymers with elements such as Toll-like receptor ligands, which can enhance the adjuvanting effects of biomaterials, may substantially improve the efficacy of these systems in vaccine delivery.[5, 30]

4.4.4 Non-specific inflammation

In several cases, significant non-specific inflammation was observed in draining lymph nodes following vaccination with hybrid polymer-DNA formulations. For example, total lymphocyte counts in draining lymph nodes 8 d after a primary vaccination with hybrid polymers were 1.5 to 3-fold higher than untreated mice (for comparison, total lymphocyte counts in mice treated with Complete Freund's Adjuvant were six-fold higher than untreated mice). Thus, the increases in total lymphocyte levels observed in our studies (Figure 4.4) are likely attributable to both specific effects (as evidenced by higher fractions of antigen-specific cells in lymph nodes of mice treated with hybrid polymer vaccine formulations as compared to untreated mice) as well as non-specific effects. Future work in this area should focus on an in-depth characterization of the role of both specific and non-specific effects in the immune response elicited by hybrid polymer delivery formulations.

4.4.5 Route and frequency of administration

Vaccines can be administered by a number of routes, including ingestion, inhalation, and injection. Within the area of injection-mediated administration alone, common routes include intravenous (IV), intraperitoneal (IP), intramuscular (IM), subcutaneous (SC), and intradermal (ID). The route of injection can play a powerful role in a vaccine's ultimate activity. For example, naked DNA encoding an antigen of interest is known to elicit only very minor immune responses if administered intravenously; however, if administered by intramuscular injection, it can produce a significant response.[11-13, 17] To further complicate the situation, it is also known that antigen persistence, or the amount of time that an antigen is accessible to the immune system, can play an important role in a vaccine's efficacy. For example, controlled release systems which release antigen over the course of several days, or repeated injections of small doses of antigen, can in some cases elicit a more powerful response than a single bolus dose.[10] Thus, when administering a new vaccine, especially one whose mechanism of action is not entirely understood, it is important to explore a range of routes and schedules of administration. Early work using hybrid polymer vaccine formulations has shown that: (1) intradermal injections yield responses that are significantly stronger than intravenous injections, and (2) repeated injections of small doses (i.e. 33 μg DNA/day for three consecutive days) can result in stronger responses than a single equivalent dose (100 μg DNA; data not shown). On the basis of these findings, it is clear that future efforts to systematically explore the effects of various routes and schedules of administration on the efficacy of hybrid polymer vaccine formulations are warranted.

4.5 Summary

In this chapter, a series of preliminary studies exploring the use of mannose-functionalized hybrid polymers for the delivery of DNA vaccines were described. These systems can efficiently deliver plasmid DNA to DC2.4 dendritic cells in a receptor-mediated fashion with toxicity that is significantly lower than PEI. *In vivo*, these systems were shown to elicit both primary and secondary, antibody- and cell-mediated immune responses that are specific to the encoded transgene. The results of this study (along with the recommendations described herein) should guide future investigations exploring the ability of hybrid polymers to elicit protective immune responses through DNA vaccination.

4.6 References

1. Koff, R. Hepatitis vaccines: recent advances. *Int. J. Parasitol.* **33**, 517-523 (2003).
2. Robinson, H. Vaccines: New hope for an AIDS vaccine. *Nat. Rev. Immunol.* **2**, 239-250 (2002).
3. Berzofsky, J.A., Ahlers, J.D. & Belyakov, I.M. Strategies for designing and optimizing new generation vaccines. *Nat Rev Immunol* **1**, 209-219 (2001).
4. Gilboa, E. The promise of cancer vaccines. *Nat. Rev. Cancer* **4**, 401-411 (2004).
5. Little, S.R. & Langer, R. Nonviral delivery of cancer genetic vaccines. *Adv Biochem Engin/Biotechnol* **99**, 93-118 (2005).
6. Forde, G. Rapid response vaccines - Does DNA offer a solution? *Nat Biotechnol* **23**, 1059-1062 (2005).
7. Donnelly, J., Wahren, B. & Liu, M. DNA vaccines: Progress and challenges. *J. Immunol.* **175**, 633-639 (2005).
8. Greenland, J.R. et al. Beta–Amino Ester Polymers Facilitate in Vivo DNA Transfection and Adjuvant Plasmid DNA Immunization. *Mol Ther* **12**, 164-170 (2005).
9. Dallal, R.M. & Lotze, M.T. *Curr Opin Immunol* **12**, 583-588 (2000).
10. Goldsby, R.A., Kindt, T.J., Kuby, J. & Osborne, B.A. Immunology, Edn. 5th. (WH Freeman, New York; 2002).
11. Wolff, J.A. et al. Direct gene transfer into mouse muscle in vivo. *Science* **247**, 1465-1468 (1990).
12. Tang, D.C., DeVit, M. & Johnston, S.A. Genetic immunization is a simple method for eliciting an immune response. *Nature* **356**, 152-154 (1992).
13. Ulmer, J.B. et al. Heterologous protection against influenza by injection of DNA encoding a viral protein. *Science* **259**, 1745-1749 (1993).
14. Gregoriadis, G., Saffie, R. & de Souza, J.B. Liposome-mediated DNA vaccination. *Febs Lett* **402**, 107-110 (1997).

15. O'Hagan, D., Singh, M. & Ulmer, J. Microparticles for the delivery of DNA vaccines. *Immunol. Rev.* **199**, 191-200 (2004).
16. Hedley, M., Curley, J. & Urban, R. Microspheres containing plasmid-encoded antigens elicit cytotoxic T-cell responses. *Nature Med* **4**, 365-368 (1998).
17. Little, S.R. et al. Poly-beta amino ester-containing microparticles enhance the activity of nonviral genetic vaccines. *Proc Natl Acad Sci U S A* **101**, 9534-9539 (2004).
18. Wang, C. et al. Molecularly engineered poly (ortho ester) microspheres for enhanced delivery of DNA vaccines. *Nat Mater* **3**, 190-196 (2004).
19. Diebold, S.S., Kursa, P., Wagner, E., Cotten, M. & Zenke, M. Mannose polyethylenimine conjugates for targeted DNA delivery into dendritic cells. *Journal of Biological Chemistry* **274**, 19087-19094 (1999).
20. Diebold, S.S., Plank, C., Cotten, M., Wagner, E. & Zenke, M. Mannose Receptor-Mediated Gene Delivery into Antigen Presenting Dendritic Cells. *In Synthetic DNA delivery systems (Eds.: D. Luo, W. M. Saltzman), Kluwer, New York* (2003).
21. Ferkol, T., Perales, J.C., Mularo, F. & Hanson, R.W. Receptor-mediated gene transfer into macrophages. *Proc Natl Acad Sci U S A* **93**, 101-105 (1996).
22. Hashida, M., Nishikawa, M., Yamashita, F. & Takakura, Y. Cell-specific delivery of genes with glycosylated carriers. *Adv Drug Deliver Rev* **52**, 187-196 (2001).
23. Nguyen, D.N., Little, S.R., Fuller, J. & Langer, R. Unpublished data. (2006).
24. Cho, B.K. et al. A proposed mechanism for the induction of cytotoxic T lymphocyte production by heat shock fusion proteins. *Immunity* **12**, 263-272 (2000).
25. Chen, J., Eisen, H.N. & Kranz, D.M. A model T-cell receptor system for studying memory T-cell development. *Microbes Infect* **5**, 233-240 (2003).
26. Babensee, J.E. & Paranjpe, A. Differential levels of dendritic cell maturation on different biomaterials used in combination products. *J Biomed Mater Res A* **74**, 503-510 (2005).
27. Yoshida, M. & Babensee, J.E. Differential effects of agarose and poly(lactic-co-glycolic acid) on dendritic cell maturation. *J Biomed Mater Res A* **79**, 393-408 (2006).
28. Yoshida, M. & Babensee, J.E. Poly(lactic-co-glycolic acid) enhances maturation of human monocyte-derived dendritic cells. *J Biomed Mater Res A* **71**, 45-54 (2004).
29. Yoshida, M., Mata, J. & Babensee, J.E. Effect of poly(lactic-co-glycolic acid) contact on maturation of murine bone marrow-derived dendritic cells. *J Biomed Mater Res A* **80**, 7-12 (2007).
30. Jain, S., Yap, W.T. & Irvine, D.J. Synthesis of protein-loaded hydrogel particles in an aqueous two-phase system for coincident antigen and CpG oligonucleotide delivery to antigen-presenting cells. *Biomacromolecules* **6**, 2590-2600 (2005).

Chapter 5: Linear-dendritic hybrid polymers functionalized with a tumor-homing peptide for targeted gene delivery to solid tumors

5.1 Introduction

Clinical applications of gene therapies are currently limited by the lack of suitable delivery systems capable of safely and efficiently delivering nucleic acid cargo to targeted tissues.[1, 2] As described in Chapter 2, a range of barriers preventing efficient systemic delivery exist, including the requirement that DNA be condensed into small, protected nanoparticle structures which can be targeted to cells or tissues of interest, interact only minimally with non-target tissues, and facilitate endosomal escape, vector unpackaging,[3] and nuclear import.[4, 5] In recent years, strategies have been devised to overcome many of these barriers. For example, cationic polymers can electrostatically bind and condense plasmid DNA; hydrophilic polymers such as poly (ethylene glycol) (PEG) can be used to sterically stabilize nanoparticles, enhance circulation times, and reduce non-specific tissue interactions; buffering amines or peptide transduction domains (e.g., the HIV TAT peptide[6]) can enhance endosomal escape; and nuclear localization sequences can direct DNA to the cell nucleus for transcription.[4, 5, 7] However, an important problem that remains is the selective targeting of gene delivery systems to tissues of interest.[8] One potential solution involves the use of peptide targeting ligands derived from combinatorial screening methodologies (such as phage display) which can selectively home to a range of healthy and diseased tissues *in vivo*.[9] Recently, these ligands have been used

successfully in the selective targeting of cytotoxic drugs,[10] pro-apoptotic peptides,[11] metalloprotease inhibitors,[12] imaging modalities,[13] and other agents to solid tumors.

In order to incorporate multiple functionalities into a single, integrated gene delivery system, we developed a family of linear-dendritic "hybrid" polymers containing linear PEG and dendritic poly(amidoamine) (PAMAM) (Chapter 3).[14] These systems contain functionalities for electrostatic DNA condensation, endosomal escape (via the proton sponge mechanism[15]), reduction of non-specific tissue interactions, and tissue targeting. Moreover, these systems have the unique attribute of modularity: because the various functional elements are physically separated, it is possible to add, modify, or remove functionalities independently. However, hybrid polymers based on PAMAM are synthesized using a labor-intensive, time-consuming process (~ 30 reaction and purification steps) that requires exposure of polymer-bound ligands to organic solvents and moderately high temperatures (> 60° C). As a result, synthesis of these systems requires weeks to months to perform, and they cannot be modified with selective targeting agents such as peptides or antibodies that are amenable to denaturation in organic solvents.

In this chapter, we demonstrate an alternative means of synthesizing hybrid polymers that is rapid (three reaction steps, two days), takes place in aqueous media at room temperature, and requires no purification steps. We use this approach to synthesize hybrid polymers modified with a peptide ligand (peptide **1**, sequence = WIFPWIQL) capable of selectively targeting glucose-regulated protein 78 kDa (GRP78) (Figure 5.1). GRP78 is a functional tumor antigen that is selectively expressed in a range of human cancers, and peptides binding to GRP78 have been used to selectively target tumors in mouse models of breast and prostate cancer and in human patient-derived tumor samples.[16-24] Here, we demonstrate that peptide **1**-modified hybrid

polymer systems can condense DNA into small nanoparticle structures and transfect cells expressing GRP78 more efficiently than branched polyethylenimine (bPEI), one of the best commercially available polymers for *in vitro* transfections. The GRP78-targeted polymers developed in this study may have direct clinical applications in cancer gene therapy. More broadly, the new synthetic approach described in this chapter may be used as a general means to rapidly synthesize high efficiency, multifunctional polymers bearing a variety of protein or peptide-based functionalities (e.g., targeting ligands, protein transduction domains, and/or nuclear localization sequences).

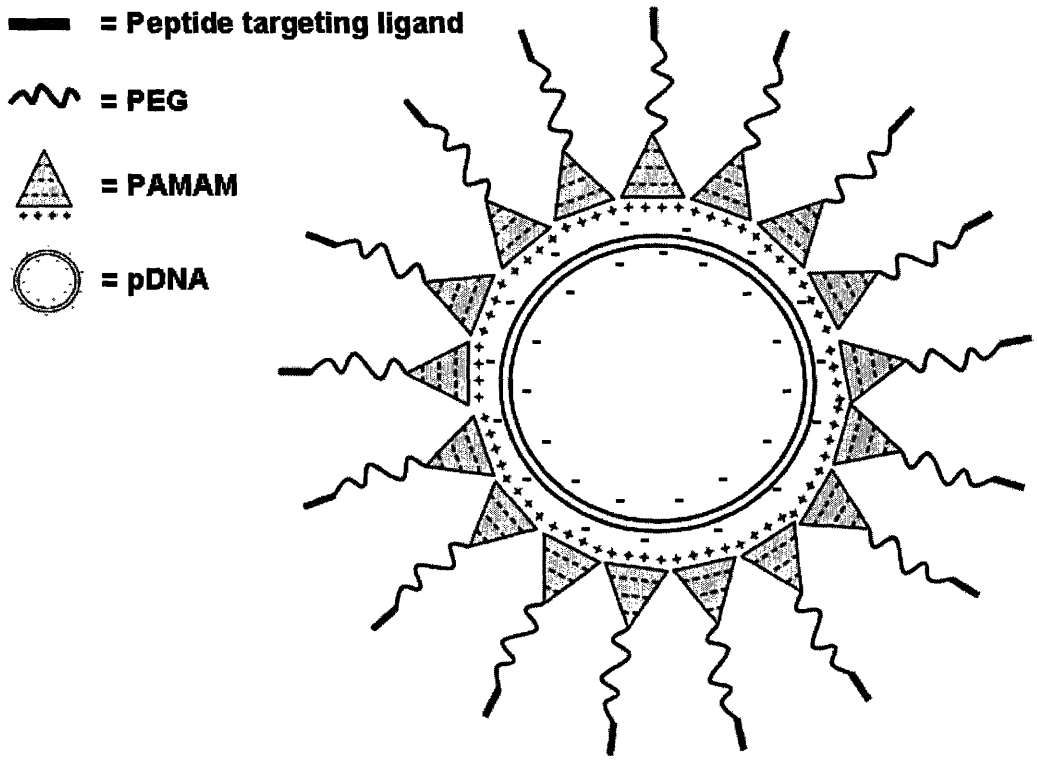

Figure 5.1. Peptide-modified hybrid polymer-DNA complexes.

5.2 Experimental Methods

General Considerations. Bifunctional Maleimide-PEG-NHS (M_n = 5278 Da, PDI = 1.0) and monofunctional mPEG-Maleimide (M_n = 5840 Da, PDI = 1.0) were purchased from

Nektar Therapeutics (Birmingham, AL) and used without further purification. Cystamine-core, generation 4.0 poly (amidoamine) (G4.0 PAMAM) dendrimers (M_n = 14308 Da, 64 primary amines per dendrimer) were obtained from Dendritic Nanotechnologies, Inc. (Mt. Pleasant, MI) and used without further purification. Peptide **1** (sequence HOOC-WIFPWIQL-NH_2) was synthesized by the MIT Biopolymers Laboratory and purified by high performance liquid chromatography (HPLC) prior to use. Hyperbranched poly (ethylenimine) (PEI, M_n = 25000), dithiothreitol (DTT), and 5,5'-dithiobis-(2-nitrobenzoic acid) (DTNB or Ellman's reagent) were purchased from Sigma-Aldrich (St. Louis, MO). Fluoraldehyde was obtained from Pierce Biotechnology, Inc. (Rockford, IL). Plasmid DNA containing the firefly luciferase reporter gene and CMV promoter sequence (pCMV-Luc) was purchased from Elim Biopharmaceuticals (San Francisco, CA) and used without further purification. A polyclonal rabbit anti-GRP78 antibody was obtained from Stressgen Biotechnologies (Victoria, British Columbia). DU145 human prostate cancer-derived cells were purchased from American Type Culture Collection (ATCC, Manassas, VA) and grown at 37° C in 5% CO_2 in 90% ATCC Eagle's minimum essential medium (with 2 mM L-glutamine and Earle's BSS adjusted to contain 1.5 g/L sodium bicarbonate, 0.1 mM non-essential amino acids, and 1.0 mM sodium pyruvate) supplemented with 10% fetal bovine serum, 100 units/mL penicillin, and 100 μg/mL streptomycin. MTT cell proliferation assay kits were also obtained from ATCC. Bright-Glo® luciferase assay detection kits were purchased from Promega (Madison, WI) and used according to the manufacturer's specifications. All other materials and solvents were used as received without further purification.

Instrumentation. ^{1}H NMR spectra were recorded at room temperature using a Varian Mercury 300 MHz instrument. Gel electrophoresis was performed using an Embi tec RunOne

Electrophoresis Cell (San Diego, CA), and gel imaging was performed using a Kodak Electrophoresis Documentation and Analysis System 120. A ZetaPALS dynamic light scattering detector (Brookhaven Instruments, Holtsville, NY; 15 mW laser, 676 nm incident beam, 90° scattering angle) was used to measure particle size and zeta potential of polymer-DNA complexes. Luminescence from reporter gene expression studies was measured using a Veritas Microplate Luminometer. Optical absorbance was measured using a SpectraMax 190 microplate reader (Molecular Devices, Sunnyvale, CA).

Synthesis. Peptide-functionalized linear-dendritic polymers were synthesized as follows. (1) Generation 4.0 (G4.0), cystamine-core PAMAM dendrimers were dissolved in 1X TAE buffer (pH 8.3), combined with a 10-fold molar excess of DTT, and stirred for 48 h under N_2 gas at room temperature. After reduction, solutions were dialyzed against pure water using a 1000 MWCO SpectraPor 7 dialysis membrane (Spectrum Laboratories, Rancho Dominguez, CA) to remove all DTT. Ellman's assay (see below) was used to verify that > 95% of dendrimers were reduced. (2) In a separate flask, Maleimide-PEG-NHS was dissolved in 1X PBS buffer (pH 7.4, 137 mM NaCl, 2.7 mM KCl, 10 mM Na_2HPO_4) and added to a solution of peptide **1** in dimethyl sulfoxide (DMSO, 99+% pure, Sigma-Aldrich) such that the reaction mixture contained equal volumes of PBS and DMSO and a 1:1 molar ratio of Maleimide-PEG-NHS and peptide **1**. The solution was stirred under N_2 gas at room temperature for 90 min. (Note: Care was taken to combine peptide and polymer solutions immediately after dissolution of the polymer to avoid premature hydrolysis of the NHS ester.) (3) Next, a solution of reduced, G4.0 PAMAM dendron in pure water was adjusted to 1X PBS buffer concentration using 10X concentrated PBS stock and added to the solution from (2) to achieve a final molar ratio of peptide:PEG:G4.0 dendron of 1:1:1. This reaction was stirred under N_2 gas at room temperature for 48 h. Following synthesis,

hybrid polymers were dialyzed against pure water to remove buffers and trace amounts of DMSO (MWCO 1000). Control polymers (no ligand) were synthesized in parallel with ligand-functionalized species using an analogous protocol and mPEG-Maleimide (M_n = 5800) as the starting material.

Structural characterization. Ellman's assay was used to quantify free thiols in solution.[25] Briefly, Ellman's reagent (DTNB) was dissolved in 1X TAE buffer at 1 mg/mL. In each well of a clear, 96-well plate, 7.1 μL of DTNB solution was combined with 75 μL of pure TAE buffer and 17.9 μL of the thiol-containing solution to be measured. The solutions were allowed to incubate for 20 min in the dark at room temperature before measuring absorbance at 412 nm. A standard curve was generated using cysteine at concentrations ranging from 0 to 1.5 mM. All conditions were measured in triplicate, averaged, and compared with the standard curve to determine free thiol concentrations.

The fluoraldehyde assay was used to quantify free amines in solution.[26] In each assay, 200 μL of amine-containing solution was added to 2.0 mL of fluoraldehyde reagent. After 5 min of dark incubation, the absorbance was measured at 338 nm. A standard curve was generated using solutions containing known concentrations of the species to be detected (peptide **1**) in a 50/50 mixture of DMSO and PBS buffer (v/v).

NMR was used to further characterize reactants and products. Results are as follows:

^{1}H NMR of peptide **1** in DMSO-d_6: 8.65 (s), 8.4 (s), 8.2 (s), 8.05 (s), 7.9 (s), 7.75 (s), 7.5 (s), 7.3 (s), 6.8-7.2 (m), 4.8 (s), 4.2-4.6 (s), 3.75 (s), 3.5 (m), 3.3 (s), 3.0 (m), 2.8 (s), 2.2 (s), 1.8 (s), 1.7 (m), 1.5 (s), 1.3 (s), 0.6-1.2 (m).

^{1}H NMR of Maleimide-PEG-NHS in DMSO-d_6: $\delta_{PEG}(CH_2CH_2O)$ = 3.73 (s); $\delta_{PEG}(CH_2CH_2O)$ = 3.60 (b); $\delta_{PEG}(CH_2CH_2O)$ = 3.4 (s); $\delta_{MALEIMIDE}(COCHCHCO)$ = 3.26 (s), $\delta_{NHS}(COCH_2CH_2CO)$ = 2.8-2.92 (s).

^{1}H NMR of Maleimide-PEG-Peptide in DMSO-d_6: $\delta_{PEG}(CH_2CH_2O)$ = 3.73 (s); $\delta_{PEG}(CH_2CH_2O)$ = 3.59 (b); $\delta_{PEG}(CH_2CH_2O)$ = 3.39 (s); $\delta_{MALEIMIDE}(COCHCHCO)$ = 3.26 (s); $\delta_{PEPTIDE}$ = 8.05 (s), 7.9 (s), 7.75 (s), 7.5 (s), 7.3 (s), 6.8-7.2 (m), 4.8 (s), 4.2-4.6 (s), 3.0 (m), 2.8 (s), 2.2 (s), 1.8 (s), 1.7 (m), 1.5 (s), 1.3 (s), 0.6-1.2 (m).

^{1}H NMR of G4.0 PAMAM in CD_3OD: $\delta_{PAMAM}(-CH_2CONHCH_2CH_2NR_2-)$ = 3.27 (b); $\delta_{PAMAM}(-CH_2CONHCH_2CH_2NH_2)$ = 3.24 (b); $\delta_{PAMAM}(-NCH_2CH_2CONH-)$ = 2.75 (b); $\delta_{PAMAM}(-CH_2CONHCH_2CH_2NH_2)$ = 2.7 (m); $\delta_{PAMAM}(-CH_2CONHCH_2CH_2NR_2-)$ = 2.53 (m); $\delta_{PAMAM}(-NCH_2CH_2CONH-)$ = 2.32 (m).

^{1}H NMR of final conjugate (peptide-PEG-PAMAM G4.0) in D_2O: $\delta_{PEPTIDE}$ = 3.8-4.2 (s), 3.45-3.55 (s), 3.04-3.12 (s), 1.0-2.3 (s); $\delta_{PEG}(CH_2CH_2O)$ = 3.55-3.78 (b); $\delta_{PAMAM}(-CH_2CONHCH_2CH_2NR_2-)$ = 3.36 (b); $\delta_{PAMAM}(-CH_2CONHCH_2CH_2NH_2)$ = 3.25 (b); $\delta_{PAMAM}(-NCH_2CH_2CONH-)$ = 2.95 (b); $\delta_{PAMAM}(-CH_2CONHCH_2CH_2NH_2)$ = 2.77 (m); $\delta_{PAMAM}(-CH_2CONHCH_2CH_2NR_2-)$ = 2.57 (m); $\delta_{PAMAM}(-NCH_2CH_2CONH-)$ = 2.4 (b).

Gel electrophoresis shift assays. Polyplexes were formed by combining 100 μL of DNA solution (0.1 mg/mL in 25 mM acetate buffer, pH 5.1) to 100 μL of polymer solution (concentration adjusted to reach desired concentration in 25 mM acetate buffer at pH 5.1) in an eppendorf tube and allowing 20 min for complexation. The resultant solutions were diluted in 25 mM acetate buffer and added to gels at a concentration of 100 ng DNA per well (in 20 μL

volume) in 10% Ficoll 400 loading buffer (Amersham Pharmacia Biotech, Uppsala, Sweden). Gels were run at 65 V for 2 h. Bands were visualized by ethidium bromide staining.

Dynamic light scattering (DLS). Dynamic light scattering (DLS) was used to measure the size and zeta potential of polymer-DNA complexes. Complexes were prepared as described above. Correlation functions were collected at a scattering angle of 90°, and the sizes of particles were determined using the MAS option of the BIC particle sizing software package (version 2.30) assuming the refractive index and viscosity of pure water at room temperature. Particle sizes are given as effective diameters assuming a log-normal distribution. Zeta potentials were calculated from electrophoretic mobilities of complexes using the BIC PALS zeta potential analysis software incorporating the Smoluchowsky model for aqueous colloidal dispersions.

Cell transfections. All transfection assays were performed in quadruplicate in accordance with the following protocol. All materials, buffers, and media were sterilized prior to use. DU145 cells were grown in 96-well plates at an initial seeding density of 10000 cells/well in 150 μL/well of growth medium. Cells were allowed to attach and proliferate for 24 h in an incubator.

Polymers were dissolved in sterile 25 mM acetate buffer (6.0 mg/mL) and arrayed into a 96-well plate (25 μL/well total polymer solution with concentrations adjusted as appropriate to yield polymer/DNA ratios ranging from 5:1 to 100:1 (m:m)). Polymer/DNA complexes were formed by the addition of 25 μL/well of 0.06 mg/mL pCMV-Luc in 25 mM acetate buffer. Polymer and DNA solutions were vigorously mixed using a multichannel pipettor upon addition of DNA solutions and subsequently incubated for 10 min to allow for complexation. Thirty μL/well aliquots of the above complex solutions were then transferred into each well of a 96-well plate containing 200 μL/well of serum-free Opti-MEM medium (Invitrogen Corporation,

Carlsbad, CA). Growth medium was removed from cells and 150 μL/well of complex-plus-medium solution was added. Controls employing PEI were prepared exactly as above to yield polymer DNA ratios ranging from 0.5:1 to 10:1 (m:m), and in all cases optimized formulations are reported as positive controls. Naked DNA controls were also prepared as above, and each 96-well plate included appropriate positive and negative controls as internal standards. In all cases, wells contained 587 ng DNA/well at indicated polymer/DNA ratios.

Following incubation of complex-containing medium solutions with cells for 4 h, solutions were removed and replaced with 10% serum-containing growth medium. Cells were incubated for an additional 72 h, and luciferase expression was determined using the commercially available Bright-Glo® luciferase assay kit (Promega, Madison, WI). Luminescence was quantified in solid, flat-bottom, white polypropylene 96-well plates using a bioluminescent plate reader. Luminescence was expressed in relative light units and was not normalized to total cellular protein in this assay.

Cell viability assay. Cell viability assays were performed in quadruplicate using the following protocol. DU145 cells were seeded in 96-well clear, flat-bottom plates and transfected according to the procedure described above. After 72 h, cell metabolic activity was assayed using the MTT cell proliferation assay kit (ATCC, Manassas, VA). Initially, a 10 μL aliquot of MTT assay reagent was added to each well. After incubating for two hours, 100 μL of detergent reagent was added. The plate was then covered and left in the dark for 4 h, after which optical absorbance was measured at 570 nm using a microplate absorbance reader. Background (media plus MTT assay reagent plus detergent reagent with no cells present) was subtracted from the value of each well, and all values were normalized to the value of control (untreated) cells.

***In vivo* tumor targeting and transgene expression assay.** Tumor-bearing mice were established and bioluminescence imaging performed as previously described.[13,24,27,28] Mice were anesthetized by intraperitoneal administration of Avertin or by gas (2% isoflurane and 98% oxygen) inhalation. The EF43-*FGF4* mouse mammary tumor cells (5×10^4) expressing GRP78 were implanted subcutaneously into 6-week-old female BALB/c immunocompetent mice.[13] When tumors reached a size in excess of 150 mm^3, mice received a single intravenous polymer-DNA complexes or pure saline (negative control). Polymer-DNA complexes consisted of 100 μg DNA (pCMV-Luc) complexed with 2.0 mg of peptide-PEG-G4.0 in 200 μL of 25 mM sodium acetate buffer supplemented with 5% glucose. To image reporter gene expression, tumor-bearing mice received a single dose (150 mg/kg, intraperitoneal) of the substrate D-luciferin (Xenogen). Photonic emission was imaged using an IVIS 200 *In Vivo* Imaging System (Xenogen). Imaging parameters included image acquisition time: 1 min; binning: 2; no filter; f/stop: 1; field of view: 10 cm. Regions of interest were defined manually over the tumors for measuring signal intensities. All mice were cared for in compliance with the standards and practices of the University of Texas-M.D. Anderson Cancer Center.

5.3 Results and Discussion

5.3.1 Synthesis of hybrid polymers

The synthesis of hybrid polymers bearing peptide- or protein-based ligands requires that the synthesis be performed in aqueous solution at moderate temperature and pH. The synthetic approach developed in this work is shown in Figure 5.2, and makes use of the commercial availability of cystamine-core PAMAM dendrimers, which can be reduced to yield dendrons with a single, free thiol in the interior. Briefly, dendrimers were first reduced by addition to a molar excess of dithiothreitol (DTT) followed by dialysis against pure water to remove the

reducing agent. Ellman's assay was used to quantify the fraction of dendrimers reduced prior to the PEG conjugation (see Experimental Methods). In a separate vessel, peptide **1** was added to a bifunctional Maleimide-PEG-NHS ester for 90 minutes, followed by addition to a molar equivalent of reduced dendrimer at pH 7.4 (phosphate buffered saline) with stirring for 24-48 hours to yield the final conjugate. Note that peptide **1** was dissolved in dimethylsulfoxide prior to the PEG conjugation reaction because it is insoluble in water.

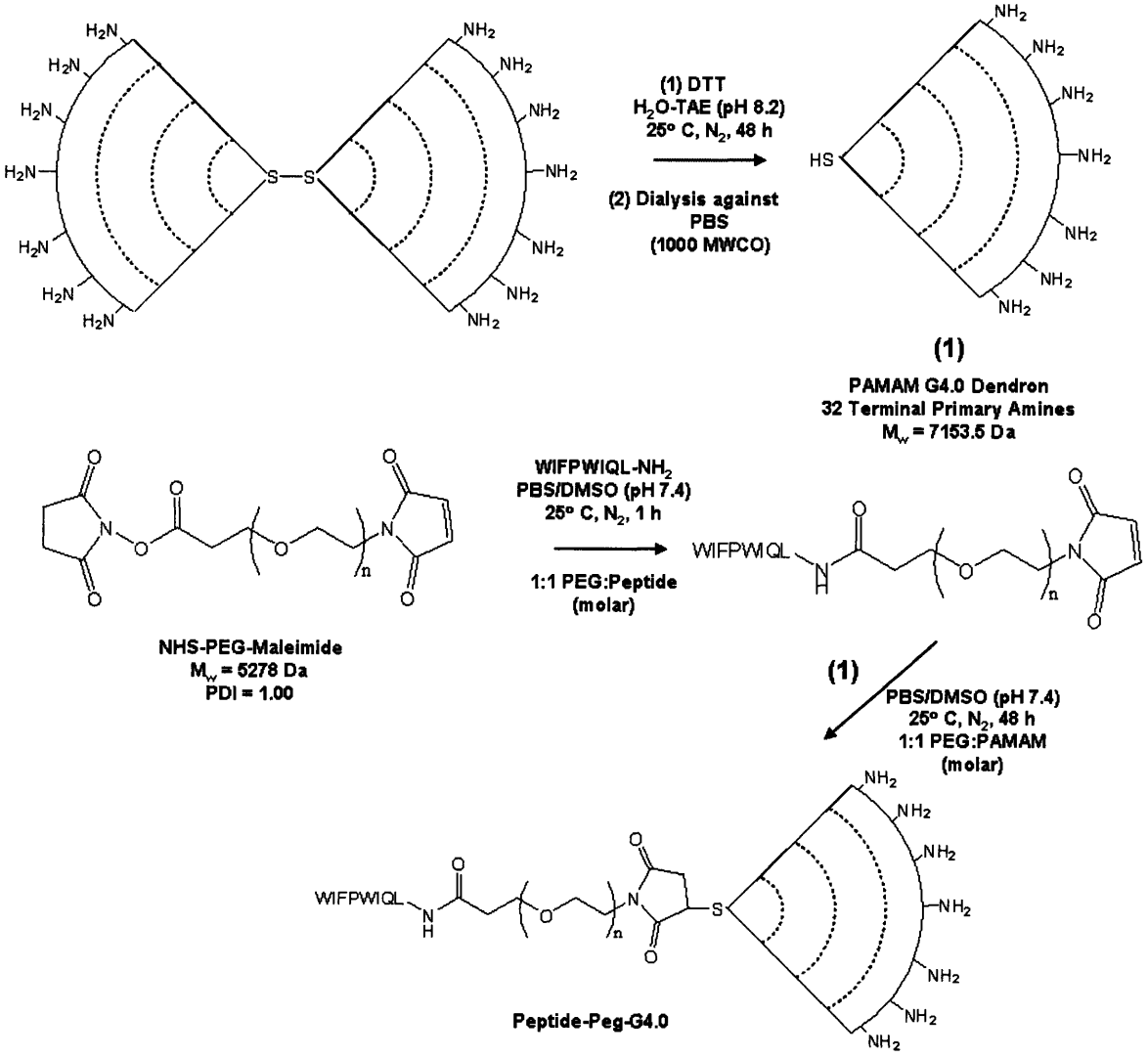

Figure 5.2. Synthesis of peptide-functionalized hybrid polymers.

Table 5.1 provides a quantitative analysis of the conversions achieved in each step of the hybrid polymer synthesis. All PAMAM reduction reactions proceeded at conversions of 95-100% (based on total thiol concentration as measured by Ellman's method). The peptide-PEG conjugation reaction proceeded at 78% conversion (Figure 5.3), and the final PEG-PAMAM conjugation step went at 74% conversion (based on the disappearance of thiols). To ensure that the disappearance of free thiol groups during the PEG-PAMAM conjugation step was a result of a reaction with the maleimide group instead of reformation dendritic disulfides, a sample of the final product was incubated overnight with a 10-fold molar excess of DTT, dialyzed, and analyzed again for thiol content. No additional thiols were observed, suggesting that the disappearance of free thiols during the PEG-PAMAM conjugation reaction was due exclusively to the formation of stable thioether linkages with the maleimide group. Additionally, each conjugation step was also verified using NMR (see Experimental Methods).

Table 5.1. Conversions of reduction and conjugation reactions.

Reaction	Percent Conversion (%)
Dendrimer reduction	>95[a]
Peptide-PEG conjugation	78[b]
PAMAM-PEG conjugation	74[a]

a: Ellman's method. b: Fluoraldehyde method.

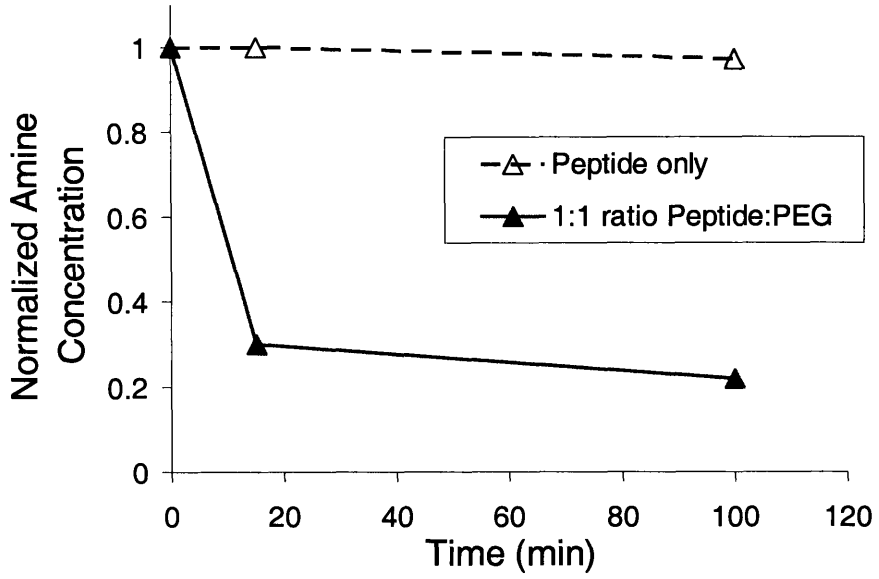

Figure 5.3. Conjugation of peptide 1 to NHS-PEG-Maleimide as monitored by fluoraldehyde assay. Peptide contains only one primary amine (N-terminus).

5.3.2 Physical properties of hybrid polymer-DNA complexes

A range of techniques was used to measure the physical properties of polymer-DNA complexes. In Figure 5.4(a), gel electrophoresis demonstrates binding and charge neutralization of plasmid DNA (pCMV-Luciferase) by hybrid polymers at polymer:DNA mass ratios of greater than 1:1, with complete charge neutralization occurring at mass ratios equal to or greater than 5:1. Zeta potential measurements indicate that complexes formed at polymer:DNA ratios of up to 40:1 have low, positive zeta potentials (Figure 5.4(b)), and dynamic light scattering shows that small particles (<210 nm) are formed with diameters equal to or less than the reported cutoff of ~ 200 nm for efficient cellular uptake (Figure 5.4(c)).[29] Particle size showed some sensitivity to the polymer:DNA mass ratio, with small ratios yielding smaller (~ 140-150 nm) particles and larger ratios yielding slightly larger particles (180-210 nm), likely due to increased steric or charge repulsion in complexes formed at high mass ratios. All general, the physical properties of

hybrid polymer-DNA complexes described here were in close agreement with those of hybrid polymers synthesized by divergent growth (Chapter 3).

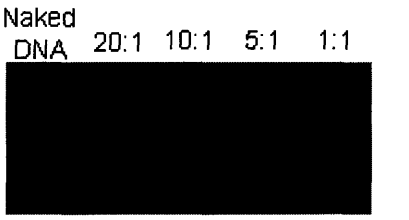

(a)

Polymer : DNA Ratio (m:m)	Zeta Potential (mV)
10:1	7 ± 2
20:1	8 ± 4
40:1	6 ± 1
60:1	11 ± 1
PEI 10:1	12 ± 5

(b)

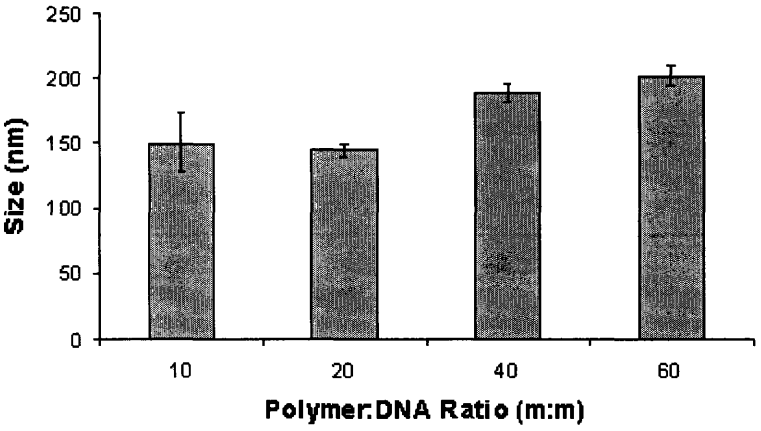

(c)

Figure 5.4. Physical properties of hybrid polymer-DNA complexes.

(a) 1% agarose gel electrophoresis demonstrates DNA binding at indicated mass ratios. (b) Zeta potential and (c) particle diameter measured by dynamic light scattering (DLS).

5.3.3 Targeted DNA delivery by peptide-functionalized hybrid polymers

Hybrid polymers developed in this study were functionalized with a peptide that selectively targets GRP78, a functional tumor antigen identified through epitope mapping of the humoral immune response in human cancer patients.[22] GRP78 confers a protective cellular response against stress conditions in solid tumors, and GRP78 expressed at the cell surface of cancer cells has been used to target peptide ligands to both mouse models of human cancers as well as human patient-derived samples.[16-24] To test for the ability of peptide-functionalized hybrid polymers to target and deliver plasmid DNA to cells expressing GRP78, we transfected

DU145 cells, which have been shown to bind and internalize peptide **1** in a GRP78-dependent manner.[24] Our results show that peptide-functionalized hybrid polymers can transfect DU145 cells at levels nearly 10-fold higher than an optimized formulation of branched, 25 kDa PEI. Moreover, this process is receptor-mediated, as evidenced by the fact that cells transfected using polymers lacking a peptide ligand, as well as cells transfected with peptide-functionalized polymers in the presence of polyclonal anti-GRP78 antiserum (to block receptor-ligand binding), yielded significantly lower levels of transfection (Figure 5.5).

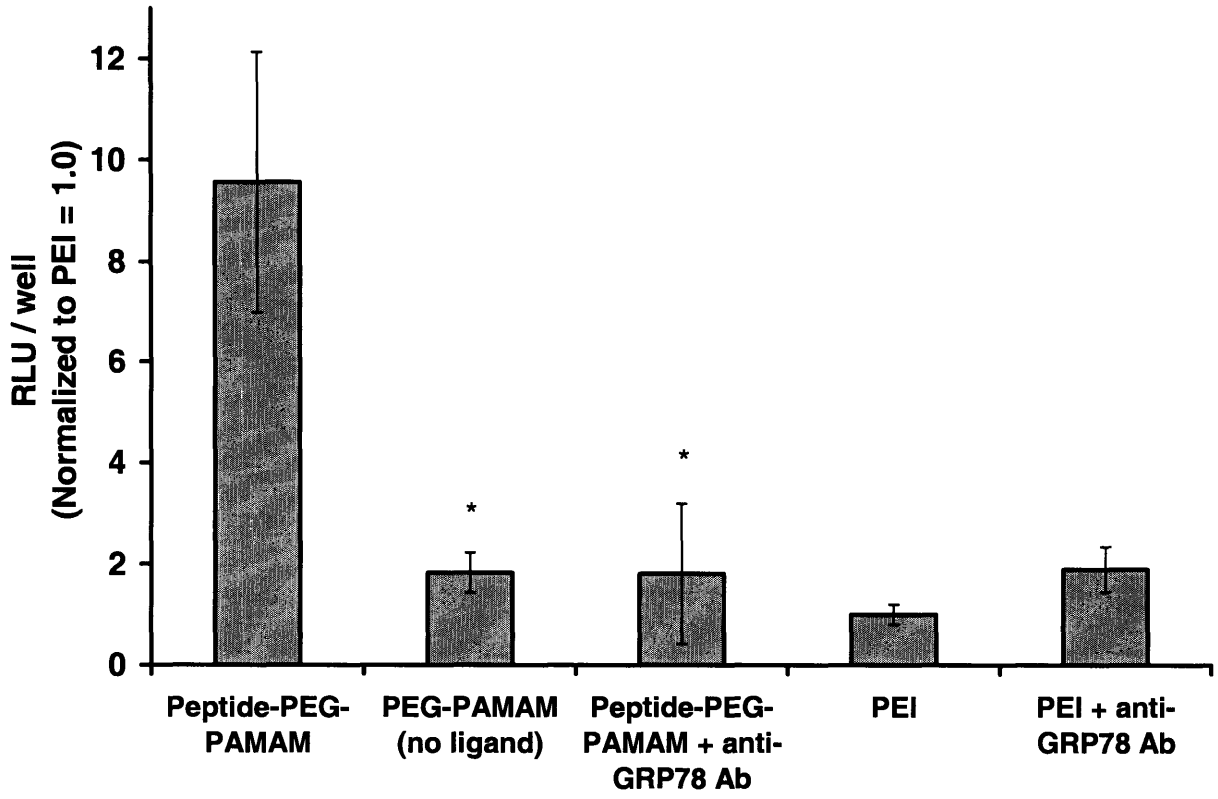

Figure 5.5. Transfection of DU145 prostate carcinoma cells expressing GRP78 with peptide-modified hybrid polymers.

Polymers with and without the peptide ligand, and peptide-modified polymers transfecting in the presence of polyclonal anti-GRP78 antiserum to block receptor binding, are shown.[24]

*** indicates $p < 0.1$. Results normalized to an optimized formulation of PEI (2:1 PEI:DNA ratio (m:m)). All results are given as average +/- standard error.**

5.3.4 *In vivo* bioluminescence imaging of transgene expression in tumor xenografts

To investigate the delivery of DNA to solid tumors following systemic administration of peptide-PEG-G4.0-DNA complexes, we used an established model based on EF43-*FGF4* mouse mammary tumors (expressing GRP-78) established in immunocompetent BALB/c mice, combined with bioluminescence imaging of luciferase transgene expression.[13] Briefly, tumors were established by subcutaneous injection of 5×10^4 EF43-*FGF4* tumor cells. When tumors reached sizes greater than 150 mm^3, mice were administered a single, intravenous injection of either saline (negative control) or hybrid polymer-DNA (pCMV-Luc) complexes at a mass ratio of 20:1 (polymer:DNA). Forty-eight hours following administration, mice were anesthetized, injected with D-luciferin, and imaged using a Xenogen IVIS 200 *In Vivo* Imaging System. Preliminary results demonstrate that, in comparison with controls, mice treated with peptide-functionalized hybrid polymers show significant transgene expression in regions surrounding the exterior of the tumor while showing lower expression in non-target tissues as well as the central, necrotic core of tumors. A representative image is shown in Figure 5.6.

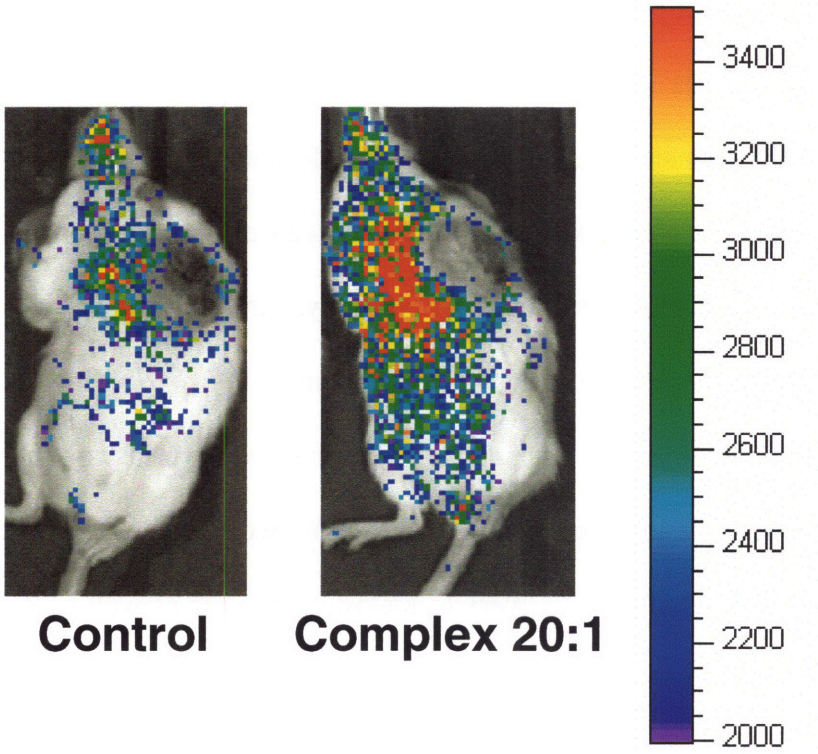

Figure 5.6. *In vivo* bioluminescence imaging of luciferase expression in EF43-*FGF4* mouse mammary tumors established in immunocompetent BALB/c mice.

Mice were treated with a single, intravenous injection of either saline (control) or peptide-PEG-G4.0-pCMV-Luc polymer-DNA complexes (20:1 polymer:DNA mass ratio) 48 h prior to imaging. Intensity scale at right indicates relative light units (RLU). The absence of signal in the core of the tumor is a result of the fact that large tumors have developed necrotic cores.

5.4 Summary

In this chapter, a new synthetic approach yielding hybrid polymers is described. This approach is rapid (three reaction steps, two days), takes place in near-neutral pH, room temperature, aqueous conditions which are compatible with the use of sensitive biological agents, and in some cases can be performed without the need for additional purification steps.

Using this approach, we synthesized hybrid polymers functionalized with short peptides which bind to glucose-regulated protein-78 kDa (GRP-78), a tumor associated antigen that is selectively expressed by a range of human cancers. These peptide-functionalized hybrid polymer systems form small, electrostatic complexes with DNA and can efficiently transfect cells expressing GRP-78 in a receptor-mediated fashion. Finally, preliminary *in vivo* bioluminescence imaging experiments performed using mice bearing EF43-*FGF4* tumors demonstrate that a single, intravenous injection of peptide-functionalized hybrid polymer systems can lead to transient, tumor-specific transgene expression. Future work in this area will focus on bioluminescence imaging of targeted gene delivery to metastatic tumors as well as the delivery of "suicide" transgenes to solid tumors.

5.5 References

1. Verma, I.M. & Somia, N. Gene therapy - promises, problems, and prospects. *Nature* **389**, 239-242 (1997).
2. Verma, I.M. & Weitzman, M.D. Gene therapy: Twenty-first century medicine. *Annu. Rev. Biochem.* **74**, 711-738 (2005).
3. Schaffer, D.V., Fidelman, N.A., Dan, N. & Lauffenburger, D.A. Vector unpacking as a potential barrier for receptor-mediated polyplex gene delivery. *Biotechnol. Bioeng.* **67**, 598-606 (2000).
4. Wagner, E. Strategies to improve DNA polyplexes for *in vivo* gene transfer: Will "artificial viruses" be the answer? *Pharm. Res.* **21**, 8-14 (2004).
5. Luo, D. & Saltzman, W. Synthetic DNA delivery systems. *Nat. Biotechnol.* **18**, 33-37 (2000).
6. Plank, C., Zauner, W. & Wagner, E. Application of membrane-active peptides for drug and gene delivery across cellular membranes. *Adv Drug Deliver Rev* **34**, 21-35 (1998).
7. Putnam, D. Polymers for gene delivery across length scales. *Nat Mater* **5**, 439-451 (2006).
8. Schaffer, D.V. & Lauffenburger, D.A. Targeted synthetic gene delivery vectors. *Curr Opin Mol Ther* **2**, 155-161 (2000).
9. Sergeeva, A., Kolonin, M.G., Molldrem, J.J., Pasqualini, R. & Arap, W. Display technologies: Application for the discovery of drug and gene delivery agents. *Adv Drug Deliv Rev* **58**, 1622-1654 (2006).
10. Arap, W., Pasqualini, R. & Ruoslahti, E. Cancer treatment by targeted drug delivery to tumor vasculature in a mouse model. *Science* **279**, 377-380 (1998).
11. Ellerby, H.M. et al. Anti-cancer activity of targeted pro-apoptotic peptides. *Nat Med* **5**, 1032-1038 (1999).

12. Koivunen, E. et al. Integrin-binding peptides derived from phage display libraries. *Methods Mol Biol* **129**, 3-17 (1999).
13. Hajitou, A. et al. A hybrid vector for ligand-directed tumor targeting and molecular imaging. *Cell* **125**, 385-398 (2006).
14. Wood, K.C., Little, S.R., Langer, R. & Hammond, P.T. A family of hierarchically self-assembling linear-dendritic hybrid polymers for targeted efficient gene delivery. *Angew Chem Int Ed* **44**, 6704-6708 (2005).
15. Sonawane, N.D., Szoka, F.C. & Verkman, A.S. Chloride accumulation and swelling in endosomes enhances DNA transfer by polyamine-DNA polyplexes. *J. Biol. Chem.* **278**, 44826-44831 (2003).
16. Jamora, C., Dennert, G. & Lee, A.S. Inhibition of tumor progression by suppression of stress protein GRP78/BiP induction in fibrosarcoma B/C10ME. *Proc Natl Acad Sci U S A* **93**, 7690-7694 (1996).
17. Koong, A.C., Chen, E.Y., Lee, A.S., Brown, J.M. & Giaccia, A.J. Increased cytotoxicity of chronic hypoxic cells by molecular inhibition of GRP78 induction. *Int J Radiat Oncol Biol Phys* **28**, 661-666 (1994).
18. Li, L.J. et al. Establishment of a Chinese hamster ovary cell line that expresses grp78 antisense transcripts and suppresses A23187 induction of both GRP78 and GRP94. *J Cell Physiol* **153**, 575-582 (1992).
19. Miyake, H., Hara, I., Arakawa, S. & Kamidono, S. Stress protein GRP78 prevents apoptosis induced by calcium ionophore, ionomycin, but not by glycosylation inhibitor, tunicamycin, in human prostate cancer cells. *J Cell Biochem* **77**, 396-408 (2000).
20. Reddy, R.K. et al. Endoplasmic reticulum chaperone protein GRP78 protects cells from apoptosis induced by topoisomerase inhibitors: role of ATP binding site in suppression of caspase-7 activation. *J Biol Chem* **278**, 20915-20924 (2003).
21. Sugawara, S., Takeda, K., Lee, A. & Dennert, G. Suppression of stress protein GRP78 induction in tumor B/C10ME eliminates resistance to cell mediated cytotoxicity. *Cancer Res* **53**, 6001-6005 (1993).
22. Mintz, P.J. et al. Fingerprinting the circulating repertoire of antibodies from cancer patients. *Nat Biotechnol* **21**, 57-63 (2003).
23. Shin, B.K. et al. Global profiling of the cell surface proteome of cancer cells uncovers an abundance of proteins with chaperone function. *J Biol Chem* **278**, 7607-7616 (2003).
24. Arap, M.A. et al. Cell surface expression of the stress response chaperone GRP78 enables tumor targeting by circulating ligands. *Cancer Cell* **6**, 275-284 (2004).
25. Riddles, P.W., Blakeley, R.L. & Zerner, B. Reassessment of Ellman's reagent. *Methods Enzymol* **91**, 49-60 (1983).
26. Roth, M. Fluorescence reaction for amino acids. *Anal Chem* **43**, 880-882 (1971).
27. Hajitou, A. et al. Down-regulation of vascular endothelial growth factor by tissue inhibitor of metalloproteinase-2: effect on in vivo mammary tumor growth and angiogenesis. *Cancer Res* **61**, 3450-3457 (2001).
28. Marchio, S. et al. Aminopeptidase A is a functional target in angiogenic blood vessels. *Cancer Cell* **5**, 151-162 (2004).
29. Rejman, J., Oberle, V., Zuhorn, I.S. & Hoekstra, D. Size-dependent internalization of particles via the pathways of clathrin-and caveolae-mediated endocytosis. *Biochem. J.* **377**, 159-169 (2004).

Chapter 6: Local drug delivery and drug-medical device combinations

6.1 Local drug delivery

In clinical settings, drugs are administered through a range of diverse routes, including oral, intravenous, subcutaneous, intramuscular, sublingual, topical (nasal, cutaneous, aural, and ocular), and other local routes.[1] While the goal of many approaches is to achieve systemic drug bioavailability, local administration seeks instead to provide therapeutic drug concentrations only to discrete target sites for times sufficient to achieve a desired pharmacological outcome.[2] In some cases, local delivery strategies can have important advantages over systemic drug therapy (see Table 6.1). As a result, local drug delivery strategies have found use in treatments for conditions such as thrombosis, ocular diseases, infection, inflammation, osteomyelitis, and cancer.[2-5]

Table 6.1 Advantages of local drug administration strategies over systemic approaches (adapted from [2])

1	Lower doses required
2	Greater control over toxicity and bioavailability of dose
3	Lower risk of promoting antibiotic resistance
4	Longer duration of drug release
5	Potential for combining local and systemic drugs with differing kinetics
6	Applicability to drug-medical device combinations
7	Avoidance of systemic exposure and undesired systemic side effects
8	Direct treatment for device-related problems (e.g. tissue integration, infection, etc.)

6.2 Drug-medical device combinations

A prominent example of the utility of local drug administration involves the recent development of drug-medical device combinations as implantable therapeutics. Combining drugs with medical devices has been demonstrated as a means for overcoming several long-standing clinical hurdles related to complications associated with device implantation such as infection and poor tissue integration. In particular, several early applications have demonstrated that drug-medical device combinations can achieve mutually reinforcing effects that are superior to the administration of the same drug and device in their conventional, separate forms.[2, 6-10] For example, drug-eluting stents have demonstrated dramatically reduced rates of restenosis compared to conventional, bare metal stents in several large clinical trials,[7, 8, 11] and central venous catheters coated with antimicrobial agents have led to significantly reduced risk of catheter-related bloodstream infections in both preclinical and clinical studies.[9, 10, 12-15] Both the European Union and United States Food and Drug Administration have established new guidelines governing the approval of such combination products for human clinical administration, and the market for such products is expected to reach $9.5 billion USD by 2009.[2,6] Examples of drug-device combinations approved by the US FDA are listed in Table 6.2, below.

Table 6.2. Examples of recent FDA-approved drug-medical device combinations (ref. [2])

Name	Company	Device Type
Cordis CYPHER™	Johnson & Johnson	DES
TAXUS Express^{2}™	Boston Scientific	DES
ARROWgard™	Arrow International	CVC
BioGuard Spectrum™	Cook Critical Care	CVC
LubriSil I.C.™	C.R. Bard	UC
Simplex P™	Stryker Osteonics	BC

DES: Drug-eluting stent; CVC: Central venous catheter; UC: Urinary catheter; BC: Bone cement

6.3 Traditional fabrication of drug-medical device combinations

Local drug delivery systems, including those used in drug-medical device combinations, are most frequently fabricated using one of three approaches: (1) simple coating of a device or substrate with a drug by ab- or adsorption;[9, 12, 16] (2) incorporation of a drug into a bulk polymer matrix either alone or in combination with a device;[11, 17] (3) direct incorporation of a drug into a device during or after fabrication.[2, 4, 13]

While each method has shown promise in certain applications, each also has drawbacks. For example, simple drug coating typically requires derivatization of drug molecules with ionic functional groups prior to surface coating to promote surface adsorption, which may alter drug activity and bioavailability.[9, 16] Additionally, this method allows for little control over drug loading and release kinetics, particularly when long-term release is desired.[2, 9, 16] Incorporation of drugs into bulk polymer matrices, on the other hand, can allow for much greater control over

release kinetics. However, uniformly depositing bulk polymeric coatings onto medical devices, which commonly possess small features (on the micrometer length scale) and non-planar geometries, can be challenging.[2, 11, 17] As a result, achieving uniformity of coating and drug release while preserving the properties of the underlying device can be challenging. Finally, direct incorporation of drugs into devices or substrates places limits on total mass loading because of gross effects on the device's physical properties, and also frequently requires that drugs be stable in the non-aqueous or high temperature environments used in materials fabrication.[2] As a result, there is currently a significant amount of research and commercial interest in the development of drug delivery approaches which can allow for extended release, encapsulation and release of biological drugs (e.g., proteins, antibodies, and nucleic acids), release of multi-drug or multi-dose schedules, responsiveness to a variety of environmental stimuli, and integration with existing medical device technologies.[4, 5, 18-20]

The following three chapters describe our initial attempts to develop a set of general strategies for fabricating systems with the properties described above. Specifically, we sought to develop controlled release systems that can be applied to existing implantable devices without placing restrictions on the size, shape, or surface chemistry of the device, that can allow for the delivery of drugs with varying chemical structures (e.g., small molecules, nucleic acids, and proteins), and that are amenable to the controlled release of multiple agents with well-controlled kinetics. The layer-by-layer (LbL) directed self-assembly technique was chosen as the primary tool for this work. The scientific basis for this technique, our rationale for using it for these applications, and a preview of our work in this area will be described in the following section.

6.4 Drug-device combinations using layer-by-layer self-assembly

6.4.1 Layer-by-layer self assembly

Since their introduction in 1992, self-assembled layer-by-layer (LbL) thin films have been the source of an extraordinary amount of interest in the materials science and engineering community because of their well-controlled physicochemical properties, ease of processing, and versatility (particularly with regard to materials selection and applications).[21, 22] Compared with other techniques for fabricating nanoscale coatings and thin films (e.g., Langmuir-Blodgett and chemisorption techniques), the LbL technique allows for significantly greater flexibility with regard to materials selection, substrate chemistry, and resultant bulk and surface properties.[22-24] LbL films are formed by the sequential adsorption of materials containing complementary functional groups onto a solid substrate, as illustrated in Figure 6.1 for the specific case of oppositely charged polymers.[21, 22] Complementary interactions driving LbL assembly are most commonly ionic in nature (using polyanionic and polycationic materials), but can also be extended to include hydrogen bonding[25-28], van der Waals forces[29], and biomolecular recognition.[30] Layer-by-layer assemblies can be deposited onto substrates ranging from large area surfaces to nanoscopic colloidal materials using processes such as dip coating[21, 22], colloidal adsorption[31], and spin coating.[32] As described in Figure 6.1 for a typical dip coating process, a substrate (e.g., glass or silicon) is first dipped into a solution containing a charged species, rinsed to remove purely physically bound species, dipped again into a solution containing the oppositely charged species (e.g., polyanion), and rinsed again. This process is repeated as desired to build up a film one molecular layer at a time, resulting in composite assemblies whose composition, thickness, surface, and other properties can be precisely manipulated.[22-24] As a result of this versatility, LbL systems have been constructed using materials that extend beyond

simple polyelectrolytes to include anything that either possesses, or can be encapsulated in a "carrier" species that possesses, the appropriate charged or functional group (e.g., dendrimers, micelles, nanoparticles). Thus, materials such as inorganics[24], uncharged small molecules[33], proteins[34], polysaccharides[35, 36], and enzymes[37] have all been used in LbL assemblies, with the latter three examples demonstrating little to no loss of functional activity. Because of their versatility, LbL systems have been used in applications which include sensors, semi-permeable membranes, electrochromic devices, solid-state electrolytes, patterned arrays, and biological interfaces.[22-24]

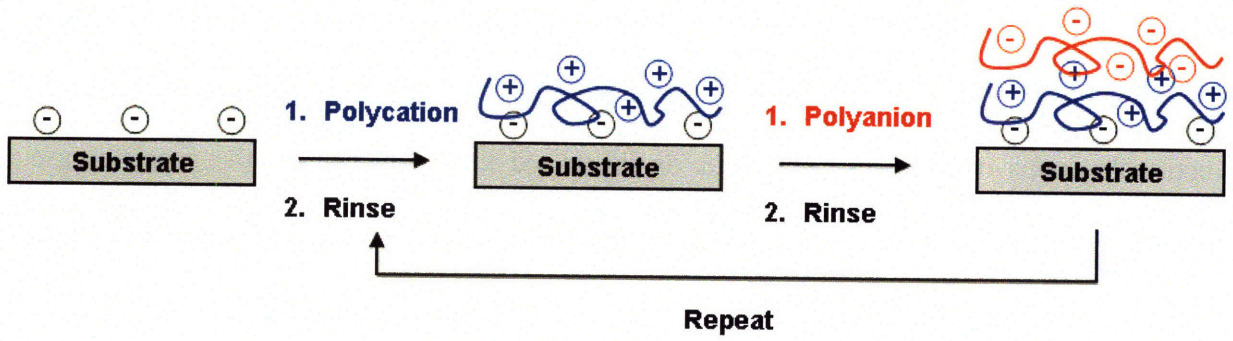

Figure 6.1. Layer-by-layer deposition.

6.4.2 Layer-by-layer systems in drug delivery

LbL thin films have also been investigated extensively for drug delivery applications in recent years based on the hypothesis that their highly tunable properties may lead to controllable drug release behavior. In early work, Sukhishvili, et al. demonstrated the release of fluorescent dyes from hydrogen bonded films containing weak poly(acids), which dissolve immediately in response to changes in environmental pH.[27, 38] Similarly, Schüler and coworkers demonstrated the NaCl-induced degradation of LBL thin films at very high ionic strengths.[39]

Later, Caruso and others pioneered the use of core-shell architectures for the encapsulation and release of various drugs. In these studies, LBL thin films were first deposited onto colloids followed by extraction of the colloidal template to yield hollow microcapsules.[40] The resultant systems can be loaded with enzymes[41, 42], dyes[33], ions[43], or small molecules[33, 44, 45] for controlled release applications.

In an alternative approach, Rubner and coworkers developed porous LBL thin films for encapsulation and pH-triggered release of poorly water soluble small molecules.[46, 47] In these studies, two general strategies were employed. In the first, small, charged molecules such as dyes were loaded into films via electrostatic interactions with unbound, oppositely charged functional groups within the films. In this arrangement, a subsequent pH change results in the release of the entrapped small molecule.[46] In the second strategy, uniform pores with high affinity for small organic molecules were formed throughout the film via a simple, post-deposition process. Pore affinity was shown to be effectively reversed by a second pH-induced conformational shift, resulting in release of the entrapped drug.[47]

While the approaches outlined above represent the first steps toward the realization of LBL drug delivery systems, each possesses drawbacks. For example, hydrogen bonded LBL systems are often highly unstable at near neutral pH and degrade on time scales that are too rapid for most controlled release applications. Salt-induced multilayer degradation requires salt concentrations (0.6-5.0 M) which are considerably higher than most physiological environments. Most colloidal core-shell structures are not amenable to device or materials coatings and rely on diffusion of drugs through the shell as the primary release mechanism, thus limiting their ability to respond rapidly to physiological triggers such as pH. Finally, while porous LBL systems are strong candidates for the delivery of small organic molecules, they are not suitable for the

delivery of larger protein- and polysaccharide-based drugs. Perhaps most importantly, none of the above mentioned technologies offers a clear mechanism for controlling the sequence by which incorporated species are released.

6.4.3 Programmable disassembly of layer-by-layer films

The focus of our work in this area is on the development of LbL films capable of *disassembling* to release their components in controlled ways (Figure 6.2). This new approach could possess the following unique attributes relative to the approaches described previously:

1. Broad applicability to existing implantable devices. LbL films can be conformally deposited onto a range of substrates without regard to substrate geometry, size, or surface chemistry.[22-24] As such, these materials may be use in the coating of materials ranging from large area, implantable devices (i.e., prosthetics, sutures, stints, and tissue engineering scaffolds) to circulating micro- or nanoscopic colloids.

2. Compatibility with a range of chemical and drug structures. LbL films can be used to encapsulate a diverse range of molecular species, from uncharged small molecules to large proteins, thus making them attractive candidates for a wide range of delivery applications.[33,34,48-50] Moreover, these films are constructed using all-aqueous processing conditions, and as a result can be used to encapsulate functional proteins with little to no loss of functional activity.[34, 37, 51, 52]

3. Potential utility in multi-drug or multi-dose release applications. The fabrication of LbL structures through "bottom-up" assembly suggests that it may be possible to build LbL architectures containing multiple, physically separated components (i.e. drugs). Combining such architectural control with top-down film disassembly could result in films capable of releasing

complex schedules of drugs, a highly desirable technology that is only currently available in a very limited spectrum of materials.[4, 18, 19] Moreover, the ability to exert fine-scale control over the nature and relative abundance of different chemical components in a single film suggests an additional means for controlling disassembly kinetics.

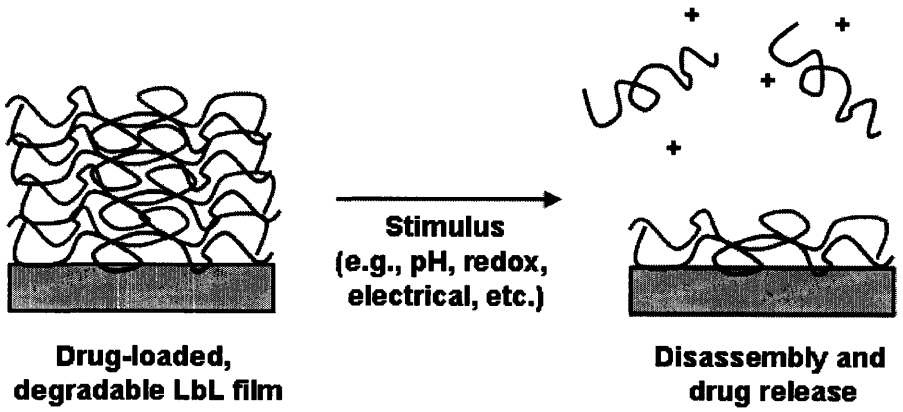

Figure 6.2. Concept of controlled disassembly of LbL thin films for controlled release applications.

Our initial efforts in this area focused on (1) the development and use of different chemical stimuli to trigger disassembly of LbL films, and (2) control over architectural features and resultant release behavior in single- and multi-drug containing films. In Chapter 7, a proof-of-concept study demonstrating the passive, pH-dependent, hydrolytic degradation of LbL films built using a degradable poly (β amino ester) will be discussed.[53] In Chapter 8, this work will be extended to include both the extended release of a single drug as well as the development of films capable of releasing multiple drugs either in series or in parallel.[54] Finally, Chapter 9 will describe the development of a similar class of degradable LbL films which, instead of degrading by passive hydrolysis, make use of a remotely-controllable, electrochemical stimulus to trigger degradation and drug release.[55]

6.5 References

1. Ansel, H., Popovich, N., Loyd, V. & Allen, J. Pharmaceutical dosage forms and drug delivery systems, Edn. 6th. (Williams and Wilkins, 1995).
2. Wu, P. & Grainger, D.W. Drug/device combinations for local drug therapies and infection prophylaxis. *Biomaterials* 27, 2450-2467 (2006).
3. Langer, R. Drug delivery and targeting. *Nature* 398, 5-10 (1998).
4. LaVan, D.A., McGuire, T. & Langer, R. Small-scale systems for in vivo drug delivery. *Nat Biotechnol* 21, 1184-1191 (2003).
5. Langer, R. Drugs on target. *Science* 293, 58-59 (2001).
6. Dubin, C. A one-two punch: drug/medical device combination products are taking healthcare in a new direction. Is the pharmaceutical industry prepared? *Drug Deliv Technol* 4 (2004).
7. Moses, J.W. et al. Sirolimus-eluting stents versus standard stents in patients with stenosis in a native coronary artery. *N Engl J Med* 349, 1315-1323 (2003).
8. Morice, M.C. et al. A randomized comparison of a sirolimus-eluting stent with a standard stent for coronary revascularization. *N Engl J Med* 346, 1773-1780 (2002).
9. Pai, M., Pendland, S. & Danziger, L. Antimicrobial-coated/bonded and -impregnated intravascular catheters. *Ann Pharmacother* 35, 1255-1263 (2001).
10. Veenstra, D.L., Saint, S., Saha, S., Lumley, T. & Sullivan, S.D. Efficacy of antiseptic-impregnated central venous catheters in preventing catheter-related bloodstream infection: a meta-analysis. *JAMA* 281, 261-267 (1999).
11. Rodgers, C. Drug-eluting stents: role of stent design, delivery vehicle, and drug selection. *Rev Cardiovasc Med* 3, S10-15 (2002).
12. Kamal, G.D., Pfaller, M.A., Rempe, L.E. & Jebson, P.J. Reduced intravascular catheter infection by antibiotic bonding. A prospective, randomized, controlled trial. *JAMA* 265, 2364-2368 (1991).
13. Zhang, X. Anti-infective coatings reduce device-related infections. *Antimicrob/Anti-infect Mater*, 149-180 (2000).
14. Raad, II & Hanna, H.A. Intravascular catheter-related infections: new horizons and recent advances. *Arch Intern Med* 162, 871-878 (2002).
15. Raad, I. et al. Central venous catheters coated with minocycline and rifampin for the prevention of catheter-related colonization and bloodstream infections. A randomized, double-blind trial. The Texas Medical Center Catheter Study Group. *Ann Intern Med* 127, 267-274 (1997).
16. Greco, R.S. & Harvey, R.A. The role of antibiotic bonding in the prevention of vascular prosthetic infections. *Ann Surg* 195, 168-171 (1982).
17. Hwang, C.W., Wu, D. & Edelman, E.R. Impact of transport and drug properties on the local pharmacology of drug-eluting stents. *Int J Cardiovasc Intervent* 5, 7-12 (2003).
18. Richards-Grayson, A. et al. Multi-pulse drug delivery from a resorbable polymeric microchip device. *Nature Materials* 2, 767-772 (2003).
19. Santini, J.T., Cima, M.J. & Langer, R. A controlled-release microchip. *Nature* 397, 335-338 (1999).
20. Staples, M., Daniel, K., Cima, M.J. & Langer, R. Application of micro- and nano-electromechanical devices to drug delivery. *Pharm Res* 23, 847-863 (2006).

21. Decher, G., Hong, J. & Schmitt, J. Buildup of ultrathin multilayer films by a self-assembly process: Consecutively alternating adsorption of anionic and cationic polyelectrolytes on charged surfaces. *Thin Solid Films* 210, 831-835 (1992).
22. Decher, G. Fuzzy nanoassemblies: Toward layered polymeric multicomposites. *Science* 277, 1232-1237 (1997).
23. Hammond, P.T. Recent explorations in electrostatic multilayer thin film assembly. *Colloid Interface Sci* 4, 430-432 (2000).
24. Hammond, P.T. Form and function in multilayer assembly: New applications at the nanoscale. *Adv Mater* 16, 1271-1293 (2004).
25. Stockton, W.B. & Rubner, M.F. Molecular-level processing of conjugated polymers .4. Layer-by-layer manipulation of polyaniline via hydrogen-bonding interactions. *Macromolecules* 30, 2717-2725 (1997).
26. Wang, L. et al. Multilayer assemblies of poly(4-vinylpyridine) bearing an osmium complex and poly(acrylic acid) via hydrogen bonding. *Macromol Chem Phys* 200, 1523-1527 (1999).
27. Sukhishvili, S. & Granick, S. Layered, erasable, ultrathin polymer films. *J Am Chem Soc* 122, 9550-9551 (2000).
28. Yang, S.Y. & Rubner, M.F. Micropatterning of polymer thin films with pH-sensitive and cross-linkable hydrogen-bonded polyelectrolyte multilayers. *Journal of the American Chemical Society* 124, 2100-2101 (2002).
29. Kotov, N. Layer-by-layer self-assembly: The contribution of hydrophobic interactions. *Nanostruct Mater* 12, 789-796 (1999).
30. Cui, X. et al. Layer-by-layer assembly of multilayer films composed of avidin and biotin-labeled antibody for immunosensing. *Biosens Bioelectron* 18, 59-67 (2003).
31. Donath, E., Sukhorukov, G.B., Caruso, F., Davis, S.A. & Mohwald, H. Novel hollow polymer shells by colloid-templated assembly of polyelectrolytes. *Angew Chem Int Edit* 37, 2202-2205 (1998).
32. Chiarelli, P.A. et al. Controlled fabrication of polyelectrolyte multilayer thin films using spin-assembly. *Advanced Materials* 13, 1167-+ (2001).
33. Caruso, F., Yang, W., Trau, D. & Renneberg, R. Microencapsulation of uncharged low molecular weight organic materials by polyelectrolyte multilayer self-assembly. *Langmuir* 16, 8932-8936 (2000).
34. Lvov, Y., K, A., I, I. & T, K. Assembly of multicomponent protein films by means of electrostatic layer-by-layer adsorption. *J Am Chem Soc* 117, 6117-6123 (1995).
35. Thierry, B., Winnik, F., Merhi, Y. & Tabrizian, M. Nanocoatings onto arteries via layer-by-layer deposition: Toward the in vivo repair of damaged blood vessels. *J Am Chem Soc* 125, 7494-7495 (2003).
36. Thierry, B., Winnik, F.M., Merhi, Y., Silver, J. & Tabrizian, M. Bioactive coatings of endovascular stents based on polyelectrolyte multilayers. *Biomacromolecules* 4, 1564-1571 (2003).
37. Onda, M., Lvov, Y., Ariga, K. & Kunitake, T. Sequential actions of glucose oxidase and peroxidase in molecular films assembled by layer-by-layer alternate adsorption. *Biotechnology and Bioengineering* 51, 163-167 (1996).
38. Sukhishvili, S. & Granick, S. Layered, erasable polymer multilayers formed by hydrogen-bonded sequential self-assembly. *Macromolecules* 35, 301-310 (2002).

39. Schuler, C. & Caruso, F. Decomposable hollow biopolymer-based capsules. *Biomacromolecules* 2, 921-926 (2001).
40. Caruso, F., Caruso, R. & Mohwald, H. Nanoengineering of inorganic and hybrid hollow spheres by colloidal templating. *Science* 282, 1111-1114 (1998).
41. Caruso, F. & Schuler, C. Enzyme multilayers on colloid particles: Assembly, stability, and enzymatic activity. *Langmuir* 16, 9595-9603 (2000).
42. Caruso, F., Trau, D., Mohwald, H. & Renneberg, R. Enzyme encapsulation in layer-by-layer engineered polymer multilayer capsules. *Langmuir* 16, 1485-1488 (2000).
43. Sukhorukov, G.B., Brumen, M., Donath, E. & Mohwald, H. Hollow polyelectrolyte shells: Exclusion of polymers and donnan equilibrium. *J Phys Chem B* 103, 6434-6440 (1999).
44. Shi, X. & Caruso, F. Release behavior of thin-walled microcapsules composed of polyelectrolyte multilayers. *Langmuir* 17, 2036-2042 (2001).
45. Antipov, A., Sukhorukov, G., Donath, E. & Mohwald, H. Sustained release properties of polyelectrolyte multilayer capsules. *J Phys Chem B* 105, 2281 (2001).
46. Chung, A.J. & F, R.M. Methods of loading and releasing low molecular weight cationic molecules in weak polyelectrolyte multilayer films. *Langmuir* 18, 1176-1183 (2002).
47. Hiller, J.A. & Rubner, M.F. Reversible molecular memory and pH-switchable swelling transitions in polyelectrolyte multilayers. *Macromolecules* 36, 4078-4083 (2003).
48. Lynn, D.M. Layers of opportunity: nanostructured polymer assemblies for the delivery of macromolecular therapeutics. *Soft Matter* 2, 269-273 (2006).
49. Vazquez, E., DeWitt, D.M., Hammond, P.T. & Lynn, D.M. Construction of hydrolytically-degradable thin films via layer-by-layer deposition of degradable polyelectrolytes. *J Am Chem Soc* 124, 13992-13993 (2002).
50. Zhang, J., Chua, L.S. & Lynn, D.M. Multilayered thin films that sustain the release of functional DNA under physiological conditions. *Langmuir* 20, 8015-8021 (2004).
51. Decher, G., Lehr, B., Lowack, K., Lvov, Y. & Schmitt, J. New Nanocomposite Films for Biosensors - Layer-by-Layer Adsorbed Films of Polyelectrolytes, Proteins or DNA. *Biosens Bioelectron* 9, 677-684 (1994).
52. MacDonald, M. & Hammond, P. Unpublished data. (2007).
53. Wood, K.C., Boedicker, J.Q., Lynn, D.M. & Hammond, P.T. Tunable drug release from hydrolytically degradable layer-by-layer thin films. *Langmuir* 21, 1603-1609 (2005).
54. Wood, K.C., Chuang, H.F., Batten, R.D., Lynn, D.M. & Hammond, P.T. Controlling interlayer diffusion to achieve sustained, multiagent delivery from layer-by-layer thin films. *Proc Natl Acad Sci USA* 103, 10207-10212 (2006).
55. Wood, K. et al. Electroactive controlled release thin films. *Submitted* (2007).

Chapter 7: Hydrolytically degradable layer-by-layer thin films: Assembly, degradation, and release of a single drug

7.1 Introduction

Over the past several years, the field of drug delivery has advanced considerably, resulting in new controlled and sustained release systems. These systems allow for enhanced targeting, improved pharmacokinetics, lower toxicity, and improved patient convenience. In sum, these advances have led to both entirely new disease treatments and great improvements on traditional therapies.[1] However, many challenges still exist, notably the development of improved systems which are versatile, highly responsive, and capable of encapsulating an ever-increasing range of drug types.

As reviewed in Chapter 6, self-assembled polyelectrolyte layer-by-layer (LbL) thin film technology has been extensively developed over the past decade. These multilayer systems, formed by the sequential adsorption of oppositely charged polyelectrolytes onto a solid substrate, can be constructed with nanometer scale control over morphology, molecular architecture, and surface properties.[2-4] In the area of biomaterials alone, these versatile systems have been used to create novel biosensors[5], membranes[6], arrays[7], and bioactive or biocompatible coatings[8-12], among other things. Further, these films have been shown to effectively encapsulate a range of functional biomolecules, including uncharged small molecules[13], proteins[14], polysaccharides[15, 16], and enzymes[17], without substantial loss in activity.

LbL thin films have been investigated extensively for drug delivery applications in recent years based on the hypothesis that their highly tunable properties may lead to controllable drug release behavior. Despite significant progress on several fronts, there has been very little progress in the development of systems which can be engineered to disassemble and release their contents in response to physiologically-relevant environmental conditions. Such systems, if developed, could potentially be used to deliver drugs from the surfaces of a range of biomaterials, including those with both large and small area surfaces (e.g., prosthetic devices and nanoscopic colloids, respectively), diverse surface chemistries, and non-planar geometries. Additionally, the all-aqueous construction of LbL films makes them amenable to the encapsulation of a wide range of therapeutics, from small molecules to proteins. Finally, and perhaps most significantly, the ability to build complex spatial architectures into these self-contained, biodegradable systems could potentially render them useful for the timed release of complex schedules of drugs.

As an initial step toward the creation of films which degrade passively under physiologically-relevant environmental conditions, the focus of this chapter is to examine the hydrolytic degradation of, and associated drug release from, LbL thin films formed by the alternating deposition of a degradable, cationic poly (β amino ester)[18] (polymer **1**, Figure 7.1) and a series of model polysaccharide therapeutics, including heparin, low molecular weight heparin, and chondroitin sulfate. Polymer **1**, which possesses the dual requisite functionalities of charge (via tertiary amine groups) and hydrolytic lability (via main chain ester groups), was chosen on the basis of its relatively slow degradation rate at acidic pH ($t_{1/2}$ > 10 h at pH 5.1, 37° C).[18] Further, it is known to form electrostatic complexes with both free and adsorbed polyanions, and both the polymer and its degradation products have been shown to cause low

cytotoxicity relative to poly(ethylenimine) (PEI), a common synthetic polymer used in biological applications.[18, 19] In a previous work[20], Lynn, Hammond and colleagues demonstrated that polymer 1 can be incorporated into LbL thin films, which then degrade in a manner that appears to be top-down at pH 7.4 (the desired behavior for most sustained release applications).[21] In this chapter, we examine the incorporation of a spectrum of model polysaccharide drugs, including heparin, low molecular weight heparins, and chondroitin sulfate, into polymer 1-based LbL thin films. The degradation of drug-loaded films at a range of pH values is studied, and we observe highly consistent, pseudo-first-order degradation kinetics. Finally, the controlled release of ^{3}H-labeled heparin from these degradable systems is demonstrated.

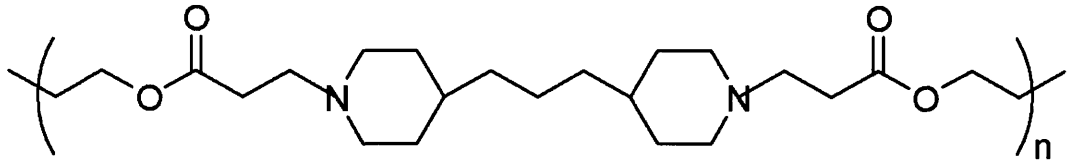

Polymer 1

Figure 7.1. Chemical structure of a repeat unit of the degradable poly (β amino ester) (polymer 1) used in this work.

(M_n = 10,000, PDI = 2.0).[18]

7.2 Experimental Methods

General Considerations. Silicon substrates (3 cm x 2 cm) were rinsed with methanol and deionized water, dried under a stream of dry nitrogen, and plasma etched prior to use using a Harrick PDC-32G plasma cleaner. Thin film deposition was performed using a Carl Zeiss HMS Series Programmable Slide Stainer. Ellipsometric measurements were conducted using a Gaertner Variable Angle Ellipsometer (6328 nm, 70° incident angle) and accompanying Gaertner

Ellipsometer Measurement Program (GEMP) Version 1.2 software interface. Fourier Transform Infrared Spectroscopy (FTIR) spectra were recorded using a Nicolet Magna IR 550 Series II Spectrometer. Zinc selenide substrates were used for transmission FTIR analysis, and were prepared using the same method employed for silicon substrates. Radiolabeled ^{3}H-heparin used in drug release experiments was quantified using a Tri-carb liquid scintillation counter (Model U2200). The amount of radiolabel in each sample vial was measured using a ^{3}H counting protocol which was shown to be highly accurate over a broad concentration range (30-100,000 DPM/mL) in calibration experiments performed prior to drug release.

Materials. Polymer **1** (M_n = 10000) was synthesized as previously described.[18] Heparin sodium salt (M_n = 12500) and low molecular weight heparin (Centaxarin®, M_n = 6000) were obtained from Celsus Laboratories (Cincinnati, OH). Chondroitin sulfate sodium salt (M_n = 60000) was obtained from VWR Scientific (Edison, NJ). Silicon wafers (test grade n-type) were purchased from Silicon Quest (Santa Clara, CA). Linear poly(ethylenimine) (LPEI, M_n = 25000) was received from Polysciences, Inc. Poly (sodium 4-styrenesulfonate) (PSS, M_n = 1000000) was purchased from Sigma-Aldrich (St. Louis, MO). ^{3}H-heparin sodium salt was obtained from American Radiolabeled Chemicals, Inc (1 mCi total, 0.30 mCi/mg, M_n = 12500). All materials and solvents were used as received without further purification.

Preparation of Polyelectrolyte Solutions. Dipping solutions containing polymer **1** were made at a concentration of 5 mM with respect to the polymer repeat unit in acetate buffer (100 mM, pH 5.1). Heparin, low molecular weight heparin, and chondroitin sulfate dipping solutions were prepared in acetate buffer (100 mM, pH 5.1) at concentrations of 10 mM with respect to the polymer repeat unit of interest. Nondegradable base layers were deposited from dipping solutions of LPEI and PSS in deionized water pH adjusted to 4.25 and 4.75, respectively.

Deionized water used to prepare all solutions was obtained using a Milli-Q Plus (Bedford, MA) at 18.2 MΩ. For degradation experiments, PBS buffer (pH 7.4, 137 mM NaCl, 2.7 mM KCl, 10 mM Na_2HPO_4) and sodium acetate buffer (pH 5.1, 100 mM) were used. For degradation experiments conducted at pH 6.2, sodium acetate buffer was pH adjusted by dropwise addition of NaOH (1 N), yielding a final salt concentration of approximately 200 mM.

Polyelectrolyte Deposition. All polyelectrolyte LbL thin films were constructed as follows according to the alternate dipping method.[2, 22] A ten bilayer nondegradable base film ($(LPEI/PSS)_{10}$) was deposited by submerging plasma treated silicon substrates in an LPEI dipping solution for 5 minutes, then a cascade rinse cycle consisting of three deionized water rinsing baths (15, 30, and 45 seconds, respectively). Substrates were then submerged in a PSS dipping solution for 5 minutes followed by the same cascade rinsing cycle, and the entire process was repeated ten times. Next, degradable films were deposited on the existing polyanion-terminated base layer by repeating the above procedure 20 times using polymer **1** as the polycationic species and either heparin, low molecular weight heparin, or chondroitin sulfate as the polyanionic species. Following deposition, films were immediately removed from the final rinsing bath and dried thoroughly under a stream of dry nitrogen gas. Film thickness was determined by ellipsometry at ten different predetermined locations on the film surface after deposition of both the nondegradable base layer and the degradable layer. All measurements were performed in triplicate.

Fourier transform infrared spectroscopy (FTIR). LbL thin films were removed following the deposition of every second bilayer (and subsequent cascade rinse), dried under a stream of dry nitrogen, and FTIR spectra were recorded between 4000 and 500 cm^{-1} (baseline subtraction mode).

Measurement of Thin Film Degradation. All film degradation studies were performed as follows. Films were immersed in 20 mL of the appropriate buffer solution in a screw top glass vial and tightly sealed. At designated times, films were removed, dried thoroughly under a stream of dry nitrogen, and thickness was measured using ellipsometry at ten predetermined locations on the film surface (measurements were performed in triplicate). Following measurements, films were reimmersed in buffer solutions and resealed.

Measurement of Drug Release. Radiolabeled ^{3}H-heparin sodium salt (2.48 g, 0.32 mCi/mg) was reconstituted in deionized water to form a stock solution containing 172 μCi/mL. In the drug release experiment, a ^{3}H-heparin labeled dipping solution was prepared by dissolving 1 mL of radiolabeled stock solution in 30 mL of heparin sodium salt solution (10 mM in sodium acetate buffer, as above). The LbL deposition procedure was then performed, also as above. Following deposition, ^{3}H-heparin labeled films were immersed in 50 mL PBS buffer for 1000 minutes. A 1 mL sample was extracted every 30 minutes and analyzed by adding 5 mL of ScintiSafe Plus 50% (Fisher Scientific, Atlanta, GA) prior to measurement. Degradation vials were tightly capped between sample extractions to prevent evaporation of the buffer solution. Raw data (disintegrations per minute, DPM) were converted to micrograms (μg) of heparin using the conversion factor 2.2 x 10^{6} DPM = 1 μCi = 3.3 μg ^{3}H-heparin. Finally, the total heparin release from a single film was calculated according to the following equation:

$$M_i = \left(\left(C_i \times V_i\right) + \left(1mL\right)\sum_{j=1}^{i-1} C_j \right)\left(345\right) \qquad (1)$$

where M_i (μg) is the total cumulative mass released from the film as of measurement *i*, C_i (μg/mL) is the concentration of sample *i*, V_i (mL) is the total volume of the degradation bath prior to measurement *i*, $(1mL)\sum_{j=1}^{i-1} C_j$ is the total mass in previously extracted samples, and 345 is

equal to the mass ratio of total heparin to ^{3}H-labeled heparin in the dipping solution (i.e., in the degradable film).

7.3 Results and Discussion

7.3.1 Analysis of Thin Film Construction

Films were constructed on planar silicon substrates using the alternate dipping method.[2, 22] In all cases, degradable films were assembled on 10 bilayers of nondegradable (LPEI/PSS) (terminating in PSS) to ensure a uniform surface charge for the deposition of polymer **1**. Dilute aqueous solutions of polymer **1** and model polyanions in acetate buffer (100 mM, pH 5.1) were used for the construction of degradable thin films. Films were dried immediately after completion of the dipping process to avoid premature degradation. All dipping conditions were chosen judiciously to avoid the range of conditions for which degradation of polymer **1** occurs rapidly.

As shown in Figure 7.2(a), $(LPEI/PSS)_{10}$ base layers formed smooth films on the surface of the substrate (ca. 400 Å), and as such contributed little to the roughness of the final films. Degradable multilayers were constructed from 20 bilayers of (polymer **1**/X), where X is a model polyanion (e.g., heparin, low molecular weight heparin, or chondroitin sulfate). Degradable multilayers were observed to form an even, conformal coating on the substrate, as evidenced by their modest roughness (error bars represent one standard deviation in film thickness measurements) and a lack of defects observable by ellipsometry. Degradable multilayers could be reproducibly fabricated, as multiple films constructed under similar deposition conditions (e.g., dipping solution pH and ionic strength) were observed to possess nearly identical thickness and surface roughness values. Finally, it is worth noting that each of the three model polyanions used in this study formed degradable multilayer films with similar thickness and roughness

values, an effect that is attributable to their similarities with respect to chemical structure and relative number of strong and weak acid groups.

It should be noted that error bars depicted in Figure 7.2(a) (as well as Figure 7.3(a-b)) represent one standard deviation in film thickness based on measurements taken at ten predetermined locations on the film surface. In contrast, the standard deviation of multiple thickness measurements taken at a single location was less than 10 Å. Thus, error bars can be interpreted as a measure of the roughness of films rather than an indication of the intrinsic error of the analytical device.

As shown in Figure 7.2(b), the LbL deposition process was monitored using FTIR for the case of (polymer **1**/heparin)$_{20}$ films. Specifically, the absorbance from sulfonic acid groups (heparin) at 1035 cm^{-1} and carbonyl groups at 1730 cm^{-1} (heparin, polymer **1**) was measured after the deposition of every second bilayer. All measurements were taken from the same spot on the surface of the film in transmission mode on IR-transparent, zinc selenide substrates. FTIR absorbance was used to measure film growth because it is known to scale approximately linearly with mass in the low wavenumber regime, and while it can only give a relative measure of film thickness, it is not as sensitive to variations in the surface roughness and refractive index of the film as ellipsometry. The observed increase in absorbance with increasing number of bilayers is indicative of the LbL deposition process. The exponential nature of this trend suggests exponential growth behavior, a commonly observed phenomenon.[23-25] (Note that each data set in Figure 7.2(b) can be fit to an exponential regression with $R^2 > 0.96$.) This behavior seems to be especially prevalent in systems comprised of biologically-derived polyanions.[26-29] Explanations of the exact mechanism responsible for exponential growth vary. One explanation, offered for the case of deposition from high ionic strength solutions, states that exponential growth is due to

increasing surface roughness, which in turn presents increasing surface area that permits the deposition of greater amounts of material at each step.[23] In a second explanation, diffusion into and out of the film is cited.[26-29] In our studies, the second mechanism is most likely to be the major contributor to the exponential growth behavior observed, namely because (1) roughness does not increase with increasing number of bilayers (data not shown), (2) the multivalent nature of heparin repeat units contributes to strong electrostatic repulsion along the polymer backbone and an extended (non-globular) conformation in solution, (3) deposition is performed at low ionic strengths, and (4) exponential growth behavior owing to diffusion has been rigorously verified in systems containing hyaluronan[26-29], and other polysaccharides with chemical structures highly similar to that of heparin. Further investigation and verification of the phenomenon of exponential growth in degradable LbL films is warranted, as this may have important ramifications for drug loading and release behavior from these constructs.

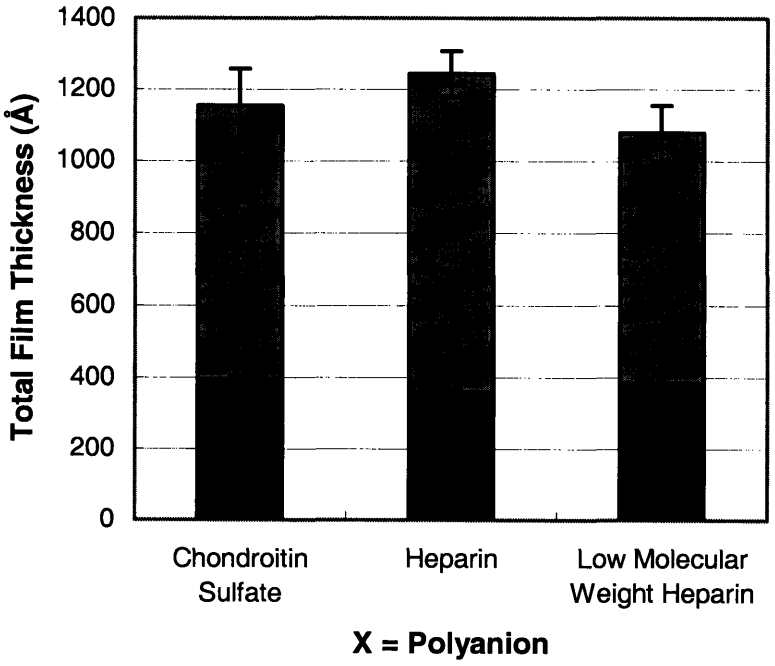

(a)

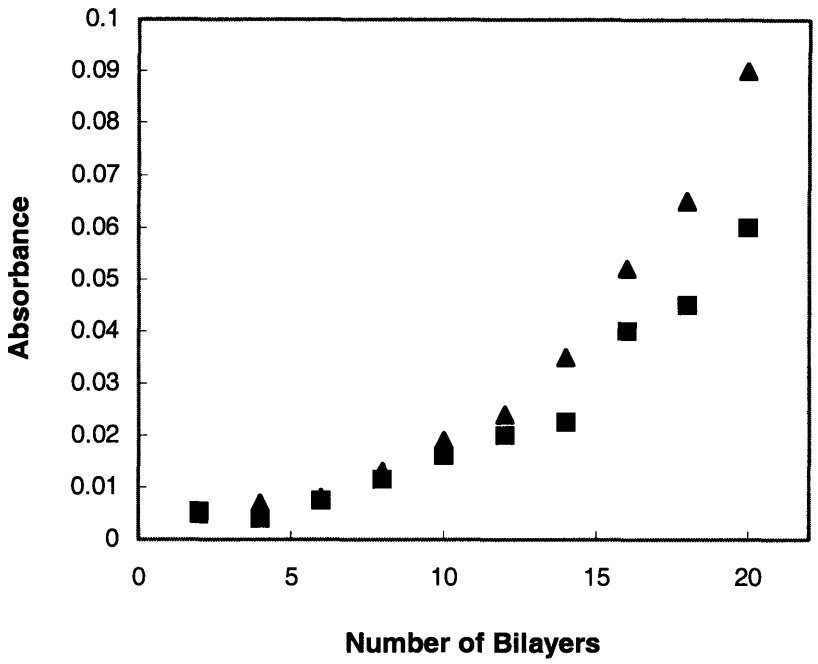

(b)

Figure 7.2. Construction of degradable layer-by-layer thin films.

(a) Average film thickness. $(LPEI/PSS)_{10}$ base layers are represented by dark gray and $(polymer\ 1/X)_{20}$ degradable layers by light gray. Five representative films were used to determine the average in each case. Error bars represent the average standard deviation of the measured thickness values at ten predetermined locations on the surface of the films. (b) Measured FTIR absorbance versus number of bilayers for sulfonic acid (triangle, heparin, 1035 cm^{-1}) and carbonyl (square, polymer 1/heparin, 1730 cm^{-1}) functional groups in the (polymer 1/heparin) system. Measurements were performed in duplicate (discrepancies were within 0.005 absorbance units). The $(LPEI/PSS)_{10}$ base layer spectrum was taken as a baseline and subtracted in all cases.

7.3.2 Analysis of Thin Film Degradation

All thin film degradation studies were performed by immersing a single film-coated substrate in a sealed vial containing 20 mL of buffered solution. At indicated time points, films were removed and dried under a stream of dry nitrogen. Film thickness was then measured by ellipsometry, followed by reimmersion of the film in the appropriate buffer solution. The pH of buffered solutions was checked throughout the degradation process to ensure that it remained constant.

Figure 7.3(a) shows the change in film thickness in (polymer **1**/X)$_{20}$ films with time following immersion in phosphate buffered saline at pH 7.4. All films demonstrate swelling to 2-8% above their original thickness during the first 0.5-2.0 hours following submersion. Most likely, this behavior reflects a balance between hydrolysis and swelling immediately following immersion of the dry films. Following this brief swelling period, films reach saturation and hydrolysis begins to act as the dominant factor effecting film thickness. Accordingly, film thickness decreases at a constant rate (approximately 0.8, 0.7, and 1.0 Å/min for heparin, low molecular weight heparin, and chondroitin sulfate-based systems, respectively). Finally, film degradation was observed to cease in all cases when the degradable (polymer **1**/X)$_{20}$ film had degraded completely, leaving only the nondegradable (LPEI/PSS)$_{10}$ base layer. Base layers were stable in all pH environments for at least 200 days.

Figure 7.3(b) shows the degradation of (polymer **1**/X)$_{20}$ films at pH 6.2. As in the case of degradation at pH 7.4, films initially swell up to 10% above their original thickness. Interestingly, this swelling period occurs during the first 10-30 hours following submersion in the pH 6.2 environment, a significantly longer swelling time (by approximately 10-fold) than was observed in the pH 7.4 environment. Most likely, this is a reflection of slower hydrolysis in

this less basic environment. After this period of initial swelling, films degrade again at a constant, measurable rate (approximately 0.05, and 0.04 Å/min for heparin and chondroitin sulfate-based systems, respectively). As in the case above, film degradation ceased in all cases following complete degradation of the polymer **1**/X film, leaving behind only the nondegradable $(LPEI/PSS)_{10}$ base layer. Interestingly, polymer **1**-based films were completely stable (no measurable degradation) for over one to two weeks when immersed in 0.1 M acetate buffer at pH 5.1. Further, degradation rates of 0.004 – 0.005 Å/min were observed in both polymer **1**/heparin and polymer **1**/low molecular weight heparin systems, and complete degradation of 1000 Å films occurred after 140 - 160 days at pH 5.1 (data not shown).

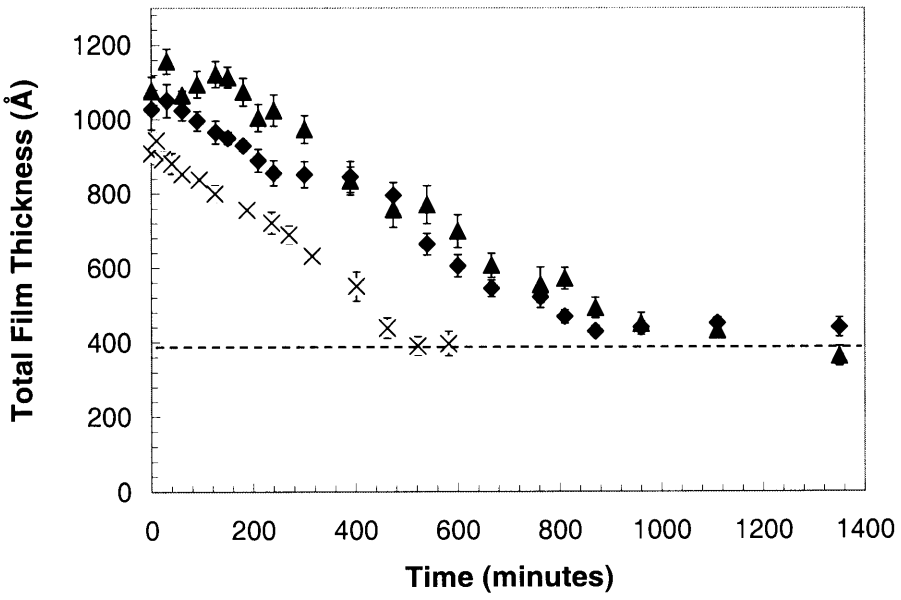

(a)

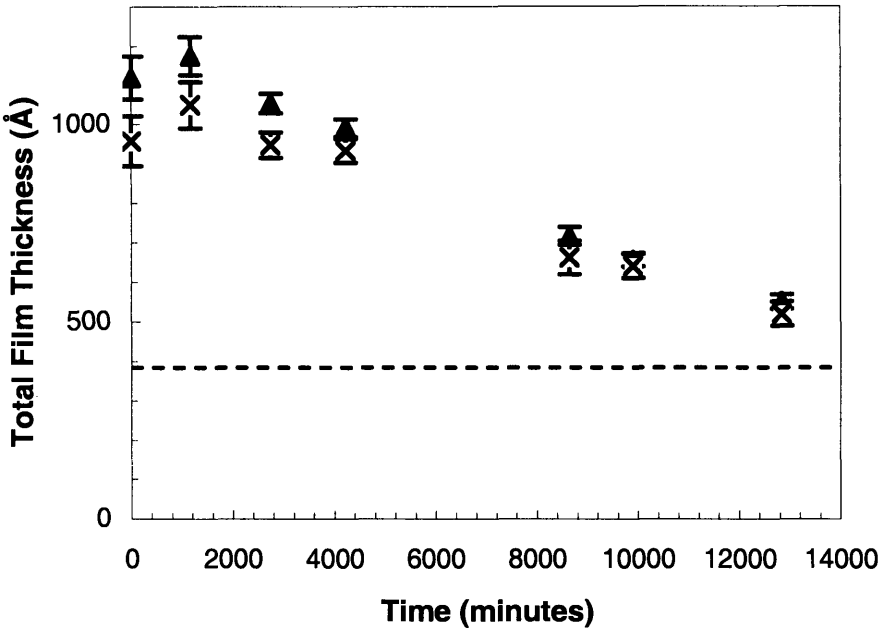

(b)

Figure 7.3. Total film thickness versus degradation time for degradable films as a function of pH.

$(LPEI/PSS)_{10}$ + (polymer $1/X)_{20}$ systems at (a) pH 7.4 and (b) pH 6.2. Model polysaccharides represented by X include heparin (triangle), low molecular weight heparin (diamond), and chondroitin sulfate (×). Dashed lines represent the approximate thickness (± 20 Å) of nondegradable base layers. Error bars represent one standard deviation of the measured thickness values at ten predetermined locations on the surface of the film. As such, error bars provide an indication of the surface roughness of films (standard deviation of multiple thickness measurements taken at a single location was less than 10 Å).

7.3.3 Pseudo-First-Order Degradation Behavior

Polymer **1** and other amine-containing polyesters are known to degrade more rapidly in basic environments than acidic environments. Consistent with this, degradation half-times for polymer **1** in solution have been reported to range from less than 2 h at pH 7.4 to 7 h at pH 5.1.[18]

It has been speculated that the exact mechanism of hydrolysis of poly (amino esters) may involve attack by both the free hydroxyl ion and intramolecular nucleophilic amines, though the latter effect is most likely less significant in polymer **1** because of the hindered reactivity of tertiary amines in the polymer backbone.[30, 31] The degradation rate of polymer **1**-based LbL thin films, also more rapid in basic environments, is influenced by the rate of diffusion of the reactant hydroxyl species from the bulk aqueous phase to the film surface, the rate of hydrolysis of the immobilized species on the film surface, and the rate of diffusion of the hydrolysis products from the film surface into the bulk. Further, degradation of polymer **1**-based films may also be influenced by diffusion and reaction within the bulk of the film. However, despite these complexities film degradation behavior at all pH conditions was observed to be linearly proportional to the concentration of hydroxyl ion species in the aqueous (bulk) environment, suggesting that the degradation behavior may be modeled as pseudo-first-order. A pseudo-first-order reaction rate constant, k_{obs}, relating the film degradation rate to the concentration of free hydroxyl ions, can be calculated from the degradation data at any pH. Using the degradation at pH 7.4 as a basis, k_{obs} was found to be equal to $3.3(5) \times 10^6$ Å min^{-1} M^{-1}. Further, using this reaction rate constant, the degradation behavior at pH 6.2 and 5.1 can be accurately predicted to within 10%. Utilitizing the highly tunable and predictable rate of degradation and drug release from LbL thin films as a basis, we are currently working to develop constructs capable of more complex, timed drug release profiles.

7.3.4 Drug Release from Degradable LbL Thin Films

To measure drug release from degradable LbL thin films, ^{3}H-heparin loaded films were constructed by adding of a known quantity of radiolabeled heparin to the deposition solution, then constructing films as described above. ^{3}H-heparin with the same molecular weight and

chemical composition as the unlabeled heparin was chosen so as to most closely reflect the deposition of the unlabeled species studied in all previous figures. ^{3}H-heparin loaded films were then immersed in 50 mL of buffer solution in a 200 mL sealed flask. At indicated time points, 1 mL samples of the buffer solution were extracted and analyzed for ^{3}H-heparin content, and total heparin release was determined by multiplying by the ratio of total to ^{3}H-labeled heparin in the original dipping solution. All release experiments were performed at least in duplicate, and highly reproducible results were obtained (i.e., release profiles from multiple film samples were quantitatively and qualitatively similar).

Figure 7.4(a) shows the heparin release profile at pH 7.4. Unlike the film degradation profile, the drug release profile is nonlinear. During the first 100 minutes, a period of rapid drug release is observed, most likely owing to the rapid release of material on the outermost layer of the film (the terminal layer in all films is composed of the polyanion species). Following the first 100 minutes, the drug release rate was observed to gradually decline until effectively approaching zero over the final 150 minutes of degradation. Figure 7.4(b) shows the heparin release profile at pH 6.2. Again, a period of rapid drug release from the outermost layer of the film was initially observed, followed by steadily declining drug release rates over the final 70-80% of the degradation period. Taken together with Figures 7.2(b) and 7.3, these data suggest an interesting hypothesis with respect to the composition and drug release properties of degradable heparin-loaded thin films. The quantity of heparin in each layer of the progressively growing film appears to increase exponentially with the number of bilayers. As a result, we postulate that the films are heavily loaded with heparin in the outermost layers and only sparsely loaded in the innermost layers (Figure 7.2(b)). The exposure of heparin-loaded films to the degradation buffer solution appears to result in the rapid release of the thick, outermost heparin layer, followed by

the steady release of heparin from adjacent, underlying layers as the film degrades from the top-down. After 40-50% of the film has degraded, the remaining intact film is composed of increasingly thinner layers, which release decreasing amounts of drug with time.

For a more complete description of the composition and drug release properties of these systems, one must also consider that, despite nonlinear growth and drug release properties, film thickness was observed to decrease linearly with time. This suggests that polymer **1** is evenly dispersed throughout the films, without regard to the thickness of a particular bilayer. This may be attributable to the ability of polymer **1** to diffuse substantially during the film construction process, effectively suppressing any variations in its concentration with respect to position within the film. Interestingly, this observed behavior closely reflects the mechanistic hypothesis first postulated by Voegel, Schaaf, and coworkers. In systems containing biologically-derived polyanions (e.g., hyaluronan) similar in structure to heparin, they observed film growth behavior that can be briefly described as follows. Upon each dipping step, the polycation was observed to diffuse into and throughout the entire film. The polycation could then diffuse out toward the surface of the film during each successive rinsing step. As the polycation continues to diffuse out of the film during the polyanion dipping step, it encounters the incoming polyanion, forming a new layer. The amount of material in each successive layer is proportional to the amount of polycation diffusing out of the film during the build-up step, and thus the thickness of each successive layer grows "exponentially".[26-29] Interestingly, dye-labeling experiments performed on these systems suggest that the polyanion is not able to diffuse throughout the film as the polycation does, resulting in films composed of stratified layers of polyanion of increasing layer thickness and a homogeneous concentration of diffuse polycation.[29]

Our analysis of the polymer **1**/heparin system appears to support this mechanistic hypothesis of exponential growth and interlayer diffusion. Namely, the combination of nonlinear growth and release with linear degradation suggests that the quantity of heparin increases with increasing numbers of bilayers while the concentration of the degradable polycation does not vary with position. Further, our previous atomic force microscopy (AFM) studies involving the polymer **1**/PSS system indicate that surface roughness values of partially eroded films (RMS roughness = 6.9 nm) were less than the thickness of a single bilayer (~10 nm) and were consistent over 1 μm^2 portions of the films.[20] Nevertheless, it remains possible that an alternative degradation mechanism may be controlling the observed behavior. In light of this, we are currently exploring the deposition and degradation of polymer **1**-based thin films, as well as the possible interlayer diffusion of various species within these constructs, in greater detail with the aim of better understanding and possibly augmenting the mechanistic hypothesis described above.

In summary, the data presented in Figure 7.4 provide interesting clues about the architecture of polymer **1**/heparin LbL films and a tool for improving the design and drug release profiles from these constructs.

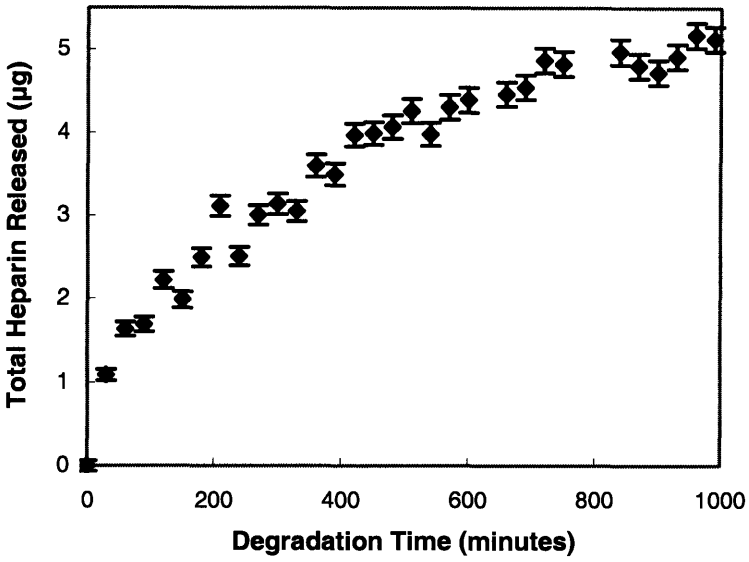

(a)

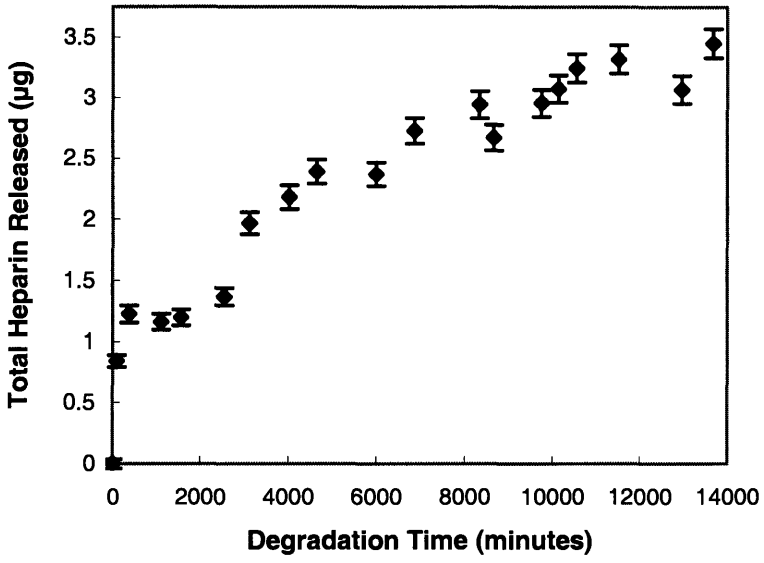

(b)

Figure 7.4. ^{3}H-Heparin release from degradable thin films as a function of pH.

Results show release from (polymer 1/heparin)$_{20}$ thin films at (a) pH 7.4 and (b) pH 6.2. One milliliter samples were extracted from the degradation buffer solution every thirty

minutes and DPM (disintegrations per minute) values were converted to cumulative micrograms of heparin released using equation (1). Error bars indicate one standard deviation in the measured DPM values.

7.4 Summary

In this chapter, we have examined the construction, degradation, and drug release properties of degradable LbL thin films containing a series of model therapeutic polysaccharides alternately deposited with a degradable, cationic poly (β amino ester) (polymer **1**). Twenty bilayer degradable films, deposited on nondegradable $(LPEI/PSS)_{10}$ base films to promote uniform adhesion, appear to grow exponentially during the deposition process, with the resultant films exhibiting consistent thickness and surface roughness. Films exhibited linear degradation profiles following an initial swelling period, where both the rate of degradation and the duration of the swelling period were proportional to the concentration of hydroxyl ions in the degradation environment. Degradation kinetics of these polymer **1**-based films can be predicted (±10%) at various pH conditions using a highly simplified, pseudo-first-order kinetic model. Finally, heparin release from degradable LbL thin films was nonlinear, instead exhibiting distinct regimes which we believe may correspond to the degradation of layers of decreasing thickness from the top-down. Our data provide interesting information about the morphology and architecture of these degradable LbL systems and represents a platform from which we may explore the controlled release of other drug types (i.e., proteins or small molecules). Further, as the LbL technique allows for a high degree of control over film thickness and spatial composition, we may eventually be able to use this technique for the fabrication of controlled release systems capable of administering complex, multi-dose or multi-drug schedules from systems ranging from implantable devices to circulating particles.

7.5 References

1. Langer, R. Drug delivery and targeting. *Nature* **398**, 5-10 (1998).
2. Decher, G. Fuzzy nanoassemblies: Toward layered polymeric multicomposites. *Science* **277**, 1232-1237 (1997).
3. Hammond, P.T. Recent explorations in electrostatic multilayer thin film assembly. *Colloid Interface Sci* **4**, 430-432 (2000).
4. Hammond, P.T. Form and function in multilayer assembly: New applications at the nanoscale. *Adv Mater* **16**, 1271-1293 (2004).
5. Decher, G., Lehr, B., Lowack, K., Lvov, Y. & Schmitt, J. New Nanocomposite Films for Biosensors - Layer-by-Layer Adsorbed Films of Polyelectrolytes, Proteins or DNA. *Biosens Bioelectron* **9**, 677-684 (1994).
6. Kim, B. & Bruening, M. pH-dependent growth and morphology of multilayer dendrimer/poly(acrylic acid) films. *Langmuir* **19**, 94-99 (2003).
7. Berg, M., Yang, S., Hammond, P. & MF, R. Controlling mammalian cell interactions on patterned polyelectrolyte multilayer surfaces. *Langmuir* **20**, 1362-1368 (2004).
8. Chluba, J. et al. Peptide hormone covalently bound to polyelectrolytes and embedded into multilayer architectures conserving full biological activity. *Biomacromolecules* **2**, 800-805 (2001).
9. Serizawa, T., Yamaguchi, M., Matsuyama, T. & Akashi, M. Alternating bioactivity of polymeric layer-by-layer assemblies: Anti- vs procoagulation of human blood on chitosan and dextran sulfate layers. *Biomacromolecules* **1**, 306-309 (2000).
10. Elbert, D., Herbert, C. & Hubbell, J. Thin polymer layers formed by polyelectrolyte multilayer techniques on biological surfaces. *Langmuir* **15**, 5355-5362 (1999).
11. Tryoen-Toth, P. et al. Viability, adhesion, and bone phenotype of osteoblast-like cells on polyelectrolyte multilayer films. *J Biomed Mater Res* **60**, 657 (2002).
12. Jessel, N. et al. Bioactive coatings based on a polyelectrolyte multilayer architecture functionalized by embedded proteins. *Advanced Materials* **15**, 692-695 (2003).
13. Caruso, F., Yang, W., Trau, D. & Renneberg, R. Microencapsulation of uncharged low molecular weight organic materials by polyelectrolyte multilayer self-assembly. *Langmuir* **16**, 8932-8936 (2000).
14. Lvov, Y., K, A., I, I. & T, K. Assembly of multicomponent protein films by means of electrostatic layer-by-layer adsorption. *J Am Chem Soc* **117**, 6117-6123 (1995).
15. Thierry, B., Winnik, F., Merhi, Y. & Tabrizian, M. Nanocoatings onto arteries via layer-by-layer deposition: Toward the in vivo repair of damaged blood vessels. *J Am Chem Soc* **125**, 7494-7495 (2003).
16. Thierry, B., Winnik, F.M., Merhi, Y., Silver, J. & Tabrizian, M. Bioactive coatings of endovascular stents based on polyelectrolyte multilayers. *Biomacromolecules* **4**, 1564-1571 (2003).
17. Onda, M., Lvov, Y., Ariga, K. & Kunitake, T. Sequential actions of glucose oxidase and peroxidase in molecular films assembled by layer-by-layer alternate adsorption. *Biotechnology and Bioengineering* **51**, 163-167 (1996).
18. Lynn, D. & Langer, R. Degradable poly(beta-amino esters): Synthesis, characterization, and self-assembly with plasmid DNA. *J Am Chem Soc* **122**, 10761-10768 (2000).
19. Boussif, O. et al. A versatile vector for gene and oligonucleotide transfer into cells in culture and in vivo: polyethylenimine. *Proc Natl Acad Sci U S A* **92**, 7297-7301 (1995).

20. Vazquez, E., DeWitt, D.M., Hammond, P.T. & Lynn, D.M. Construction of hydrolytically-degradable thin films via layer-by-layer deposition of degradable polyelectrolytes. *J Am Chem Soc* **124**, 13992-13993 (2002).
21. Langer, R. & Peppas, N. Origins and development of biomedical engineering within chemical engineering. *AIChE J* **49**, 2990-3006 (2003).
22. Decher, G., Hong, J. & Schmitt, J. Buildup of ultrathin multilayer films by a self-assembly process: Consecutively alternating adsorption of anionic and cationic polyelectrolytes on charged surfaces. *Thin Solid Films* **210**, 831-835 (1992).
23. Ruths, J., Essler, F., Decher, G. & Riegler, H. Polyelectrolytes I: Polyanion/polycation multilayers at the air/monolayer/water interface as elements for quantitative polymer adsorption studies and preparation of hetero-superlattices on solid surfaces. *Langmuir* **16**, 8871-8878 (2000).
24. Clark, S., Montague, M. & Hammond, P. Selective deposition in multilayer assembly: SAMs as molecular templates. *Supramolecular Science* **4**, 141-146 (1997).
25. McAloney, R., Sinyor, M., Dudnik, V. & Goh, M. Atomic force microscopy studies of salt effects on polyelectrolyte multilayer film morphology. *Langmuir* **17**, 6655-6663 (2001).
26. Richert, L. et al. Layer by layer buildup of polysaccharide films: Physical chemistry and cellular adhesion aspects. *Langmuir* **20**, 448-458 (2004).
27. Lavalle, P. et al. Comparison of the structure of polyelectrolyte multilayer films exhibiting a linear and an exponential growth regime: An in situ atomic force microscopy study. *Macromolecules* **35**, 4458-4465 (2002).
28. Picart, C. et al. Buildup mechanism for poly(L-lysine)/hyaluronic acid films onto a solid surface. *Langmuir* **17**, 7414-7424 (2001).
29. Picart, C. et al. Molecular basis for the explanation of the exponential growth of polyelectrolyte multilayers. *Proc Natl Acad Sci USA* **99**, 12531-12535 (2002).
30. Lim, Y., Choi, Y. & Park, J.-S. A self-destroying polycationic polymer: Biodegradable poly(4-hydroxy-L-proline ester). *J Am Chem Soc* **121**, 5633-5639 (1999).
31. Lim, Y.-B., Kim, C.-H., Kim, K., Kim, S. & Park, J.-S. Development of a safe gene delivery system using biodegradable polymer, poly[alpha-(4-aminobutyl)-L-glycolic acid]. *J Am Chem Soc* **122**, 6524-6525 (2000).

Chapter 8: Hydrolytically degradable layer-by-layer thin films: Controlling interlayer diffusion to achieve sustained, multi-agent release

8.1 Introduction

The ability to engineer surfaces which present multiple functionalities when and where they are needed could lead to important advances in electro-optical devices, separations, and biomaterials.[1, 2] For example, in the area of drug delivery there is a need for low-cost "smart" coatings that balance the ability to release complex drug profiles with the flexibility of incorporation into a range of biomaterials, including those with large area sizes or non-planar geometries such as pins, sutures, prosthetic bones, devices, and microparticles. The layer-by-layer (LbL) electrostatic assembly technique is ideally suited for such applications because it allows for absolute control over the order in which multiple functional elements are incorporated into a growing film.[3] However, the development of truly stratified, multicompartment LbL films has been largely unsuccessful with many biomacromolecules because of the phenomenon of interlayer diffusion, which results in blended structures lacking regular, controlled order.[4] In this chapter, we systematically probe a range of strategies designed to solve this problem by placing physical barriers between various components within a single film to control interlayer diffusion. We measure the effect of each type of barrier using a novel system consisting of a hydrolytically

degradable polymer (Polymer **1**, Figure 8.2) alternately deposited with a series of radiolabeled polyelectrolytes. Top-down film degradation results in the release of components in a sequence which reflects their relative positions in the film; thus, we can quantify the effects of various barrier strategies aimed at limiting diffusion behavior. Using this approach, we uncover for the first time a set of strategies which allow for the production of compartmentalized films capable of passively releasing complex, tuned release profiles. In addition to uncovering fundamental strategies to control interlayer diffusion in LbL films, this work may lead to important applications in drug delivery by allowing for the fabrication of nanoscale materials coatings capable of releasing sustained, multi-drug schedules from surfaces of virtually any composition or geometry under physiological conditions.

As described in Chapter 6, the layer-by-layer (LbL) electrostatic assembly technique entails the sequential adsorption of monolayers of oppositely charged polymers, colloids, or other materials onto a solid substrate to form a cohesive, ionically crosslinked thin film.[3] Multilayers can be deposited rapidly and inexpensively atop large area surfaces of any geometry while allowing for nanometer scale control over a range of physical properties.[3, 5] Further, the all-aqueous processing of LbL systems allows for the incorporation of sensitive biomolecules such as proteins and DNA.[6-10] More broadly, the technique can also be extended to include any molecular species that is either charged or that can be encapsulated in a charged "carrier" (i.e., dendrimer, micelle, chaperone, or nanoparticle), thus making it possible to incorporate a wide range of species without regard to molecular weight or intrinsic charge. On the basis of these attributes, we hypothesized that degradable LbL systems based on a hydrolytically degradable polyion such as Polymer **1** might be useful for a range of drug delivery applications, particularly those which involve the release of complex schedules of drugs (Figure 8.1).[11-13] However,

though promising, this technology has been limited because of the inability to control the relative positions and distributions of multiple species residing within a single film, resulting in highly disorganized architectures.[14] The phenomenon responsible for this lack of control is referred to as interlayer diffusion, the tendency of some species to diffuse throughout LbL systems during the deposition process. All polyelectrolytes fall into one of two broad classes with respect to interlayer diffusion: diffusing polyelectrolytes (for example, many polypeptides and polysaccharides) are able to rapidly diffuse throughout LbL architectures during assembly, resulting in poorly organized, blended structures, while non-diffusing polyelectrolytes (for example, many synthetic, strong polyelectrolytes) cannot, resulting in spatially organized structures wherein each deposited species is only able to interact with neighboring layers in close proximity (usually 2-3 layers).[4]

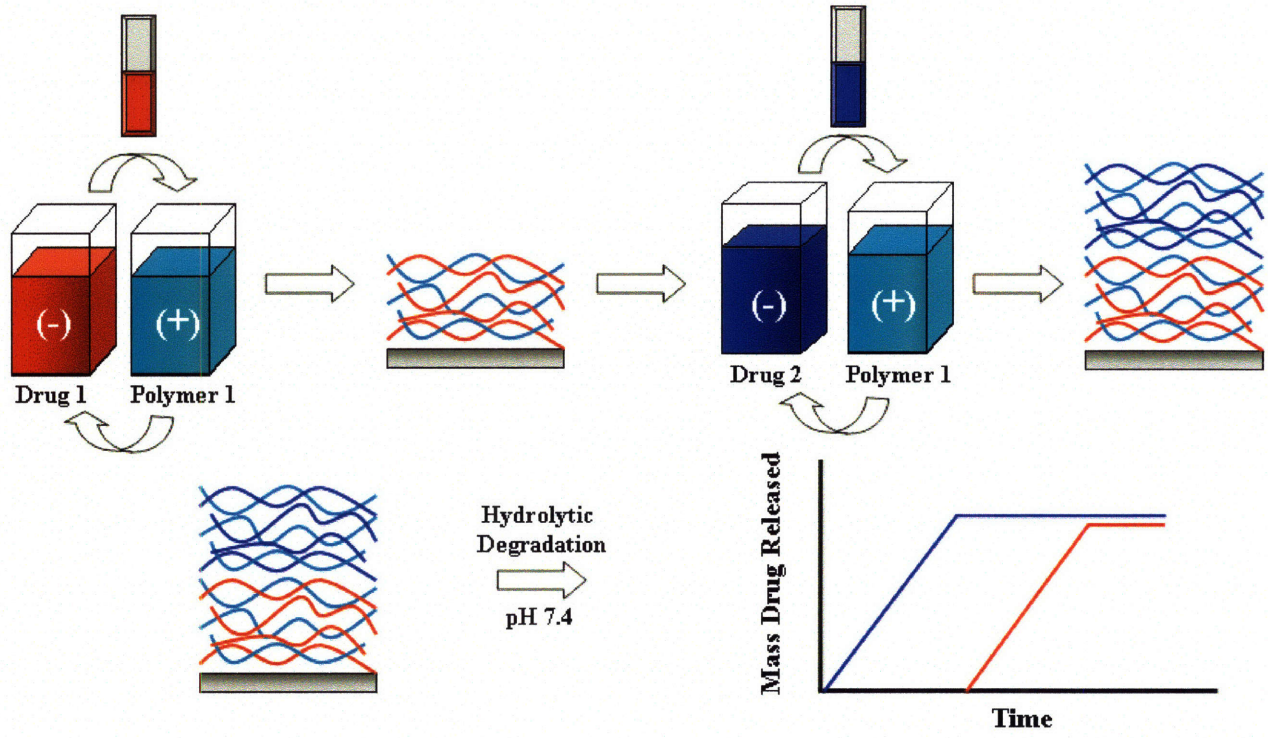

Figure 8.1. Schematic depicting hypothetical drug release profiles from hydrolytically degradable LbL thin films with controlled architectures.

In this chapter, we examine the effects of various physical barrier strategies on both diffusing and non-diffusing systems by tracking the release of radiolabeled polyelectrolytes which exhibit either extensive diffusing behavior (heparin, HEP) or non-diffusing behavior (dextran sulfate, DS) when incorporated into LbL structures. We show that covalently cross-linked barriers deposited between the two labeled components can effectively block interlayer diffusion, leading to compartmentalized structures. In contrast, even very large numbers of ionically cross-linked (degradable or non-degradable) barrier layers cannot block interlayer diffusion. By connecting interlayer diffusion with ultimate film architecture and release properties, and by further studying the fabrication parameters which allow us to control interlayer diffusion, we uncover a set of guiding principles which should significantly aid future

attempts to build highly organized LbL structures. Further, the demonstration that these films can release multiple agents either in parallel or in series may have important implications for drug delivery and controlled release materials.

8.2 Experimental Methods

Materials. Polymer **1** (M_n = 10000) was synthesized as previously described.[15] Heparin sodium salt (M_n = 12500) was obtained from Celsus Laboratories (Cincinnati, OH). Dextran sulfate sodium salt (M_n = 8000), poly (sodium 4-styrenesulfonate) (SPS, M_n = 1000000), poly (allylamine hydrochloride) (PAH, M_n = 70000), and poly (diallyldimethylammonium chloride) (PDAC, M_n = 100000) were obtained from Sigma-Aldrich (St. Louis, MO). Linear poly(ethylenimine) (LPEI, M_n = 25000) and poly (acrylic acid) (PAA, M_n = 90000) were purchased from Polysciences, Inc (Warrington, PA). Silicon wafers (test grade n-type) were purchased from Silicon Quest (Santa Clara, CA). ^{3}H-heparin sodium salt (1 mCi, 0.30 mCi/mg, M_n = 12500) and ^{14}C-dextran sulfate sodium salt (100 μCi, 1.5 mCi/g, M_n = 8000) were obtained from American Radiolabeled Chemicals, Inc. Radiolabeled and corresponding unlabeled polymers were chosen with similar molecular weights and polydispersities in order to mimic the behavior of the unlabeled species as closely as possible. All materials and solvents were used as received without further purification.

General Considerations. A Harrick PDC-32G plasma cleaner was used to etch silicon substrates (3 cm x 2 cm) following rinsing with methanol and deionized water and drying under a stream of dry nitrogen. Layer-by-layer thin films were deposited using an automated Carl Zeiss HMS Series Programmable Slide Stainer. Absorbances from growing films were measured using Fourier Transform Infrared Spectroscopy (FTIR) using a Nicolet Magna IR 550 Series II Spectrometer. Zinc selenide substrates used for transmission FTIR analysis were

prepared using the same method employed for silicon substrates. Ellipsometric measurements for film thickness were conducted using a Gaertner Variable Angle Ellipsometer (6328 nm, 70° incident angle) and Gaertner Ellipsometer Measurement Program (GEMP) Version 1.2 software interface. The release of radiolabeled polymers was quantified using a Tri-carb liquid scintillation counter (Model U2200). The amount of radiolabel in each sample vial was measured using ^{3}H, ^{14}C, and dual counting protocols, each of which were shown to be both consistent and highly accurate over a broad concentration range (30-100,000 DPM/mL) in calibration experiments performed prior to drug release. Thermal cross-linking of (PAH/PAA) films was performed by incubating films in a Yamoto DVS400 gravity convection oven at 215° C for indicated time intervals.

Thin Film Fabrication. All films were constructed from dilute aqueous solutions (2-10 mM) using the alternating dipping method.[3] All polymers used in degradable thin films were prepared in 100 mM acetate buffer at pH 5.1 to avoid the conditions under which polymer **1** degrades rapidly ($t_{1/2}$ > 10 h at pH 5.1, 37° C).[15] Nondegradable base layers were deposited from dipping solutions of LPEI and SPS in deionized water pH adjusted to 4.25 and 4.75, respectively. Deionized water used to prepare all solutions was obtained using a Milli-Q Plus (Bedford, MA) at 18.2 MΩ. For degradation experiments, 1X PBS buffer (pH 7.4, 137 mM NaCl, 2.7 mM KCl, 10 mM Na_2HPO_4) was used. Films used in this study were constructed on either silicon (for ellipsometry and degradation studies) or zinc selenide (for transmission mode FTIR) planar substrates. In all cases, degradable, polymer **1**-based films were constructed directly on top of ten bilayer, nondegradable base films containing linear poly(ethylenimine) (LPEI) and sulfonated poly(styrene) (SPS) to ensure uniform adhesion to the substrate. Following

deposition, films were removed from rinsing baths and dried thoroughly under a stream of dry nitrogen to avoid premature degradation.

Thin Film Degradation Studies. All film degradation studies were performed as follows. Films were immersed in 20 mL of the appropriate buffer solution in a screw top glass vial and tightly sealed. At designated times, films were removed, dried thoroughly under a stream of dry nitrogen, and thickness was measured using ellipsometry at ten predetermined locations on the film surface (measurements were performed in triplicate). Following measurements, films were reimmersed in buffer solutions and resealed.

Release Studies. For drug release experiments, radiolabeled LbL thin films were first constructed by alternately depositing polymer **1** and the indicated radiolabeled drug(s). Radiolabled deposition solutions containing ^{3}H-heparin were prepared by combining 1 mL of 50 μCi/mL ^{3}H-heparin (0.30 mCi/mg, M_n = 12500) with 35 mL of 100 mM acetate buffer. Unlabeled heparin (M_n = 12500) was added to bring the total concentration of heparin (unlabeled plus labeled) to 2 mg/mL (1.5-2 μCi/mL ^{3}H). Radiolabled deposition solutions containing ^{14}C-dextran sulfate were similarly prepared by combining ^{14}C-dextran sulfate (1.5 mCi/g, M_n = 8000), unlabeled dextran sulfate (M_n = 8000), and 100 mM acetate buffer to yield a total concentration of dextran sulfate (unlabeled plus labeled) to 2 mg/mL (1 μCi/mL ^{14}C). After fabrication of the indicated films, drug release experiments were performed by immersing each film in 50 mL 1X PBS buffer in a 200 mL screw top vial. A 1 mL sample was extracted at indicated time points and analyzed by adding 5 mL of ScintiSafe Plus 50% (Fisher Scientific, Atlanta, GA) prior to measurement. Degradation vials were tightly capped between sample extractions to prevent evaporation of the buffer solution. Raw data (disintegrations per minute, DPM) were converted to micrograms (μg) of drug released using the conversion factor 2.2 x 10^{6}

DPM = 1 μCi, the specific radioactivity of the drug, and our knowledge of the ratio of total drug to labeled drug in the deposition solution.[13]

8.3 Results and Discussion

8.3.1 Build up and release properties of single component films

As a basis for these studies, we selected two radiolabeled polysaccharides, heparin (HEP) and dextran sulfate (DS), which exhibit growth behavior associated with diffusive and non-diffusive species, respectively.[4] Figure 8.2(a) is a plot of the transmission mode FTIR absorbance recorded from films containing either (polymer **1**/Hep) or (polymer **1**/DS). Specifically, the absorbances from sulfonic acid groups at 1035 cm^{-1} (heparin) and 1017 cm^{-1} (dextran sulfate) were measured after the deposition of indicated bilayers. All measurements were taken from the same spot on the surface of the film in transmission mode on IR-transparent, zinc selenide substrates. The inset shows the film thickness versus number of deposited bilayers for a (polymer **1**/DS) film. Both FTIR and ellipsometry demonstrate that the quantity of DS incorporated into the film is linearly proportional to the number of adsorption cycles, a commonly observed characteristic of many LbL systems. Linear build-up behavior is characteristic of films whose constituent polyions adsorb directly onto the film surface during each deposition step. Interlayer diffusion does not occur in these systems, which as a result form spatially organized structures wherein species deposited at a given step are only able to interact with neighboring species that are in close proximity (e.g., 2-3 layers).[3, 16, 17] On the other hand, heparin-based films exhibit an exponential increase in absorbance with increasing numbers of adsorbed layers. Exponentially growing films, which are most commonly composed of hydrophilic polyelectrolytes or biologically-derived materials (i.e., peptides and polysaccharides), are poorly organized, blended architectures characterized by the complete "in"

and "out" diffusion of adsorbing species throughout the growing film during the film's assembly process.[4, 18-20] A series of recent studies offer mechanistic explanations[20, 21] and direct evidence[4] for this process, wherein a species deposited at a given step can reside in any position throughout the film.

Figure 8.2(b) depicts the chemical structures of the repeat units of polymer **1**, HEP, and DS, the three polymers used in this study. Polymer **1** is a cationic, degradable poly (β amino ester) synthesized by the conjugate addition-step polymerization of a diamine and a diacrylate; it represents one member of a library of over 2350 degradable poly (β amino esters) recently synthesized and screened for their abilities to deliver DNA to cells in culture.[22] Both model drug compounds, HEP and DS, are polysaccharides that possess similar structural attributes, including strong (sulfonic) acid groups on each repeat unit and relatively low molecular weights.

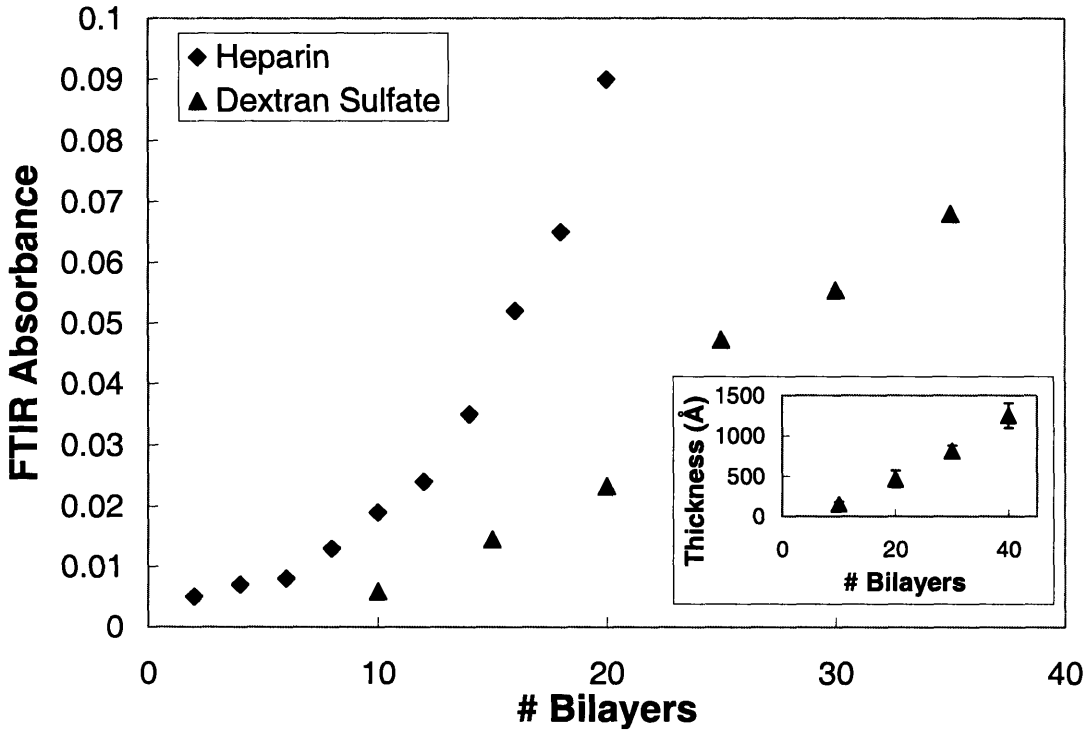

(a)

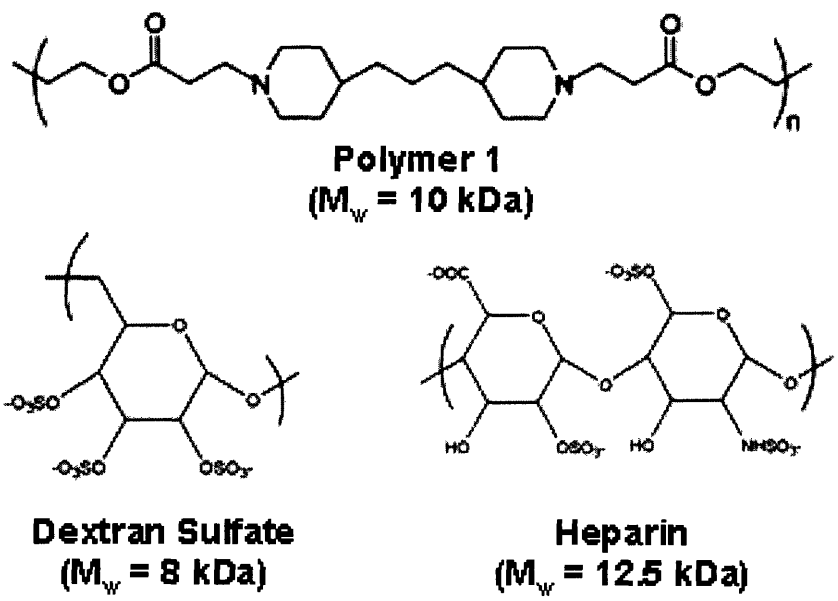

(b)

Figure 8.2. Assembly of LbL films exhibiting linear or exponential growth.

(a) A plot of FTIR absorbance versus number of thin film bilayers demonstrates layer-by-layer assembly of (polymer 1/heparin) (diamond) and (polymer 1/dextran sulfate) (triangle) films exhibiting exponential and linear growth, respectively. (Inset: Thickness versus number of bilayers for (polymer 1/dextran sulfate) films.) (b) Chemical structures of degradable polymer and model drugs used in this chapter.

To better understand the degradation and release behavior exhibited by the two model polyelectrolytes, we simultaneously measured release and degradation of single component films containing each species. Figures 8.3(a) and 8.3(b) show degradation and release from 20 bilayer (polymer 1/HEP) and (polymer 1/DS) systems, respectively, following immersion in PBS buffer at pH 7.4. As previously documented, complete degradation and consequent release from (polymer 1/HEP) systems occurred within 20 hours. Film thickness was observed to decrease linearly following a brief swelling period of 0.5-2.0 h on first exposure to aqueous solution.[13]

DS-based films exhibited similar degradation and release behavior, though with kinetics approximately five-fold slower than their HEP-based counterparts. The initial release observed in both cases within the first few hours of degradation likely reflects passive release from the surface, as the outermost layer of each film consists of the labeled compound. The fact that this effect is more pronounced in the case of heparin likely reflects the presence of interlayer diffusion, which results in a thick outer layer of diffusible material at the film surface.[4] Interestingly, in both cases film thickness was observed to decrease linearly with time; further, the apparent roughness of the film surface, taken from the standard deviation in film thickness measured at 10 predetermined spots on the surface, was observed to remain constant, or even decrease, with time. Taken together, these data suggest top-down surface erosion of the films; one would anticipate that patchy or bulk degradation would result in a much larger standard deviation and nonlinear degradation behavior. (Recent AFM investigations also provide further physical support to the mechanism of top-down degradation.[11, 23]) Given the linear degradation and surface erosion observed in both sets of thin films, the vastly different kinetics of degradation and release exhibited by these two systems reflect differences in film organization, wherein the diffusive character of HEP contributes to loose gradient films with larger quantities of HEP in the top layers, in comparison to their relatively more stratified, and more densely ion-crosslinked DS counterparts that have a constant distribution of DS throughout the film.

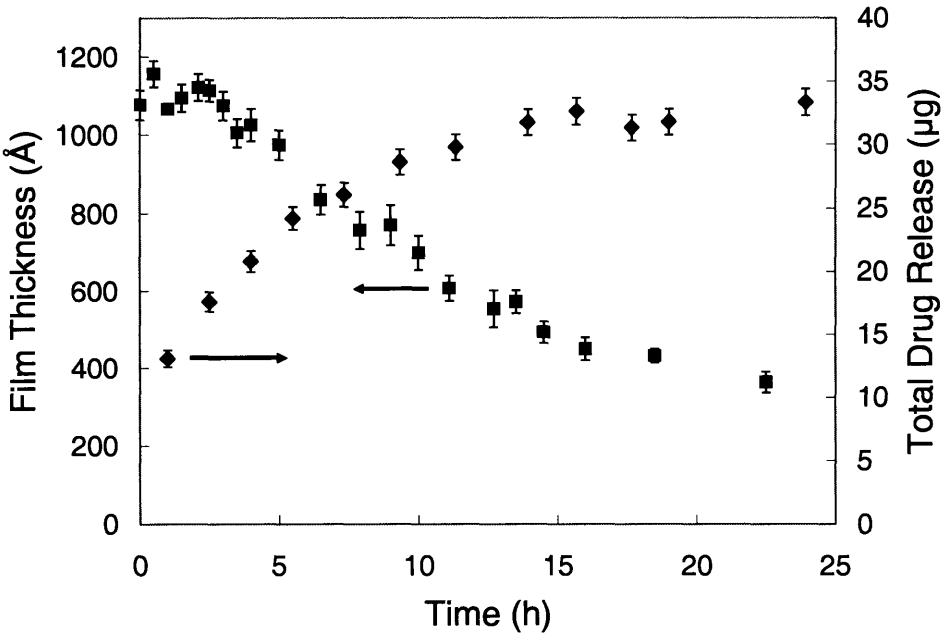

(a)

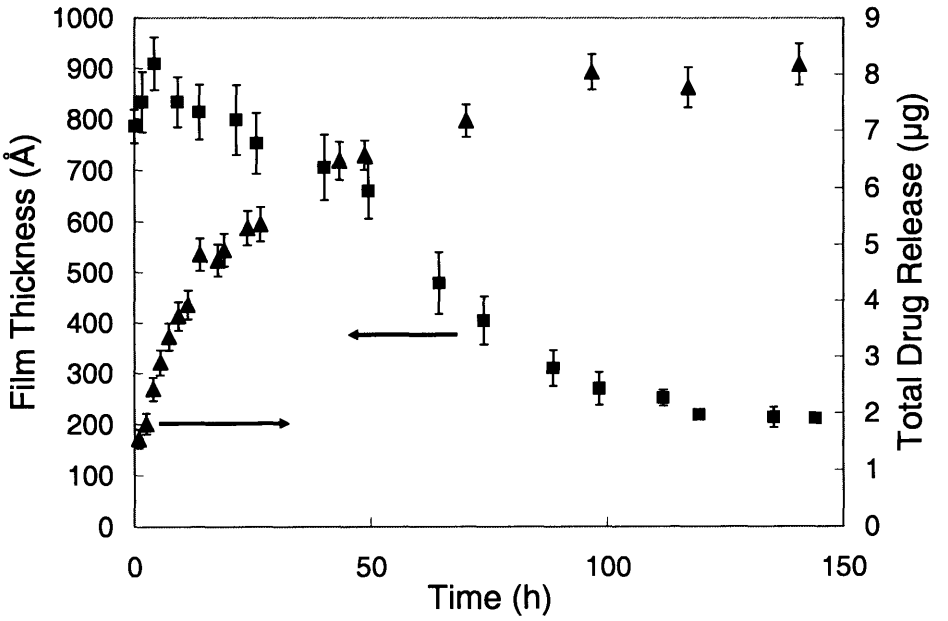

(b)

Figure 8.3. Degradation (square) and drug release (triangle) from single component films. (a) (polymer 1/HEP)$_{20}$. (b) (polymer 1/DS)$_{20}$.

To further verify that release occurs by means of surface erosion, and to explore the relationship between interlayer diffusion and release properties of degradable LbL constructs, we constructed a series of 20, 50, and 80 bilayer films containing either (polymer **1**/HEP) (Figure 8.4(a)) or (polymer **1**/DS) (Figure 8.4(b)). For the case of (polymer **1**/HEP) systems, the release behavior reflects intuition for the case of an exponentially growing system with top-down degradation behavior. The slope of the release curve differs dramatically between films of varying thickness, a reflection of the fact that exponentially growing systems result in the formation of disorganized films with increasing amounts of the diffusible species (HEP) at each deposition step (initial release rates of 0.4, 3.7, and 7.9 $\mu g/cm^2 \cdot h$ were observed for 20, 50, and 80 bilayer films, respectively). Moreover, each HEP-based system was observed to release its contents rapidly (in less than 20 h) without regard to its thickness, again a likely reflection of the fact that the majority of the model polyelectrolyte is contained in the upper layers following multiple deposition cycles.[4] In sharp contrast, release from (polymer **1**/DS) films of increasing thickness results in all cases in an initial phase of linear release followed by a "leveling off" as degradation is completed. Interestingly, as might be expected for the case of top-down release from a series of linearly growing films, we observed that all three films released DS at a relatively equivalent rate during the linear release phase (release rates of 0.07, 0.06, and 0.08 $\mu g/cm^2 \cdot h$ were observed for 20, 50, and 80 bilayer films, respectively), and that the duration of this linear release phase was proportional to the number of deposited bilayers (20 h, 49 h, and 97 h for 20, 50, and 80 bilayer films, respectively). The slow release kinetics of these systems likely reflects the higher effective ionic crosslink density of the thin films and much lower interlayer diffusivity of the model polyelectrolyte within the multilayer matrix. Importantly, these data suggest that the hydrolytic degradation of LbL systems can provide quantitative new

insights into the architecture and organization of these films. Moreover, this demonstration suggests that the duration of time over which release occurs can be broadly tuned in linearly growing (non-diffusing) systems simply by changing the number of deposited layers.

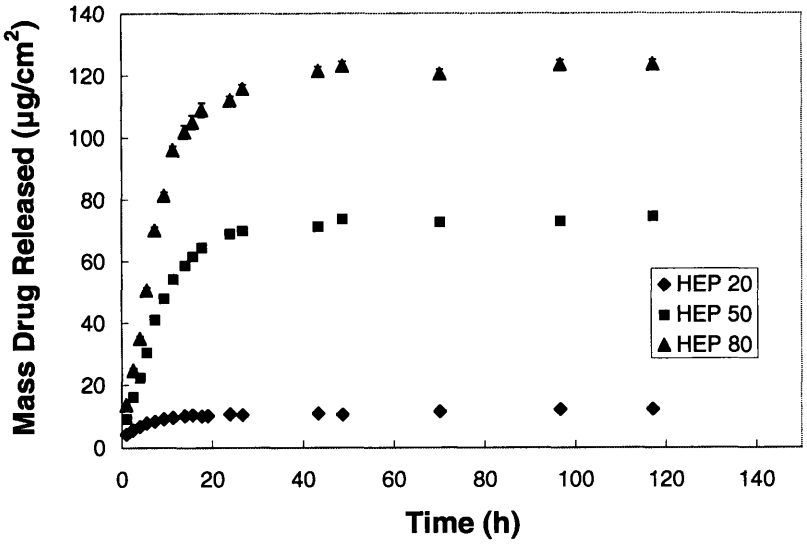

(a)

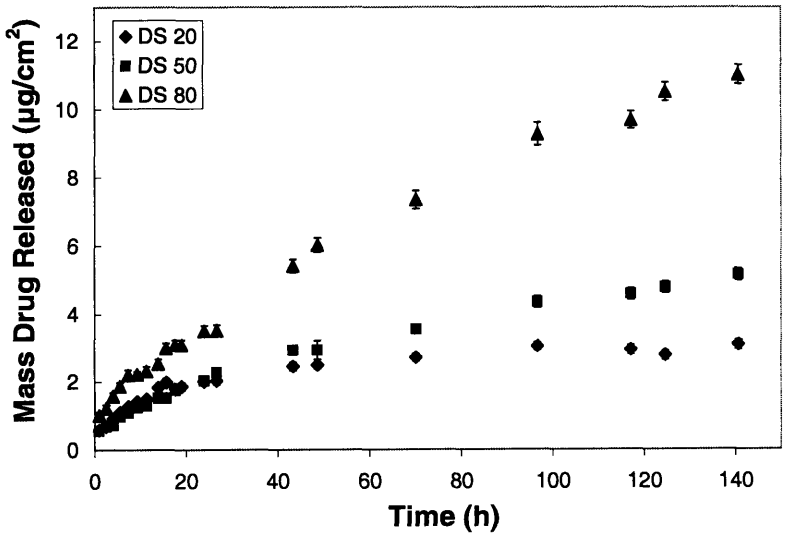

(b)

Figure 8.4 Release from 20 (diamond), 50 (square), and 80 (triangle) bilayer films versus time.

(a) Heparin-containing films exhibiting exponential growth, and (b) dextran sulfate films exhibiting linear growth (release is surface area normalized; error bars are small).

8.3.2 Controlling interlayer diffusion to modulate multi-agent release profiles

Having demonstrated the ability of hydrolytically degradable LbL thin films to act as a probe to gain quantitative insight into film organization and architecture, we next sought to evaluate a range of strategies to control the relative positions of multiple, labeled species within a single film by constructing physical barriers to separate the two components. We constructed films containing first 20-40 base layers of polymer **1**/HEP, followed by a set of "barrier" layers consisting of either polymer **1**/SPS (degradable), PDAC/SPS (non-degradable), thermally cross-linked PAH/PAA, or nothing at all, and finally a set of 20-40 surface layers of polymer **1**/DS. In similar fashion, we also constructed films identical to these, only with the order of the labeled components reversed (DS base layers and HEP surface layers). See Figure 8.5.

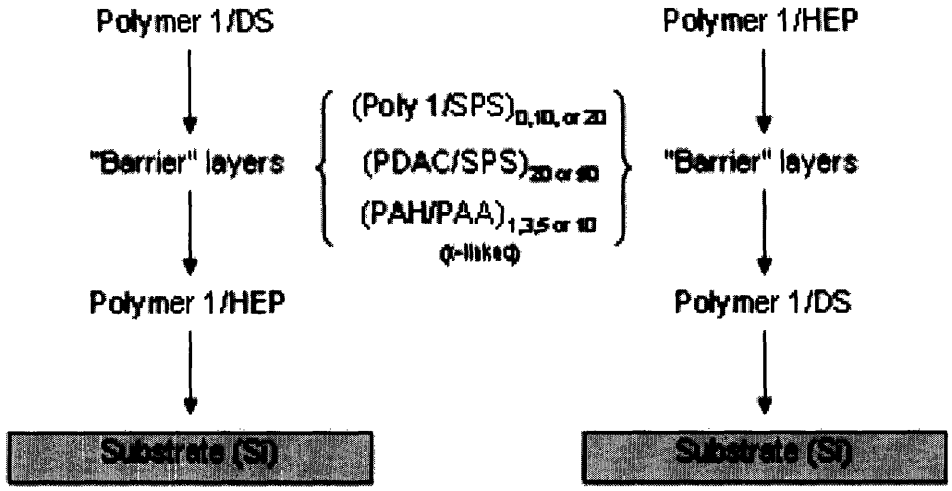

Figure 8.5. Schematic depicting strategies used to construct physical barriers to control interlayer diffusion in multi-component films.

As shown in Figure 8.6, when a base layer of polymer **1**/DS was coated with a single bilayer of PAH/PAA (covalently cross-linked for 20 min at 215° C), followed by the deposition of polymer **1**/HEP, we observed a multi-stage, serial release of first the surface heparin followed by the underlying DS. Thus, the use of a single covalently cross-linked PAH/PAA layer was sufficient to separate the two components when deposited onto the surface of the linearly growing polymer **1**/DS system, as evidenced by the two-stage release profile. Following the approximately 25 h time delay, underlying DS was released with a linear profile. Interestingly, the average rate of DS release was approximately 60% slower than that observed in corresponding films without covalently cross-linked barrier layers. This work constitutes the first observation of such a two-part release profile from fully electrostatically assembled thin film constructs; moreover, to our knowledge, this is the first demonstration of the use of covalently cross-linked barrier layers to physically separate the constituents in a multi-component degradable thin film. Additional experiments using single and multiple cross-linked PAH/PAA barrier layers show that both the duration of the release delay and the rate of release following this delay can be broadly controlled using this approach. For example, multiple layers of (PAH/PAA) cross-linked for longer than 1.5 h (at 215° C) virtually halted the release of all underlying DS (no release of DS was observed for up to 45 days). This result may have important and direct applications in drug delivery, as it suggests that both the timing and rate of release of an underlying species can be broadly controlled using as little as a single cross-linked bilayer. Interestingly, we also found that when the order of the two labeled components was reversed (HEP as the base layer and DS as the surface layer) it was no longer possible to achieve serial release of the two components using cross-linked spacer layers, suggesting that the nature

of the base film onto which the cross-linked barrier layer is absorbed influences the final properties of the barrier layer (Figure 8.7).

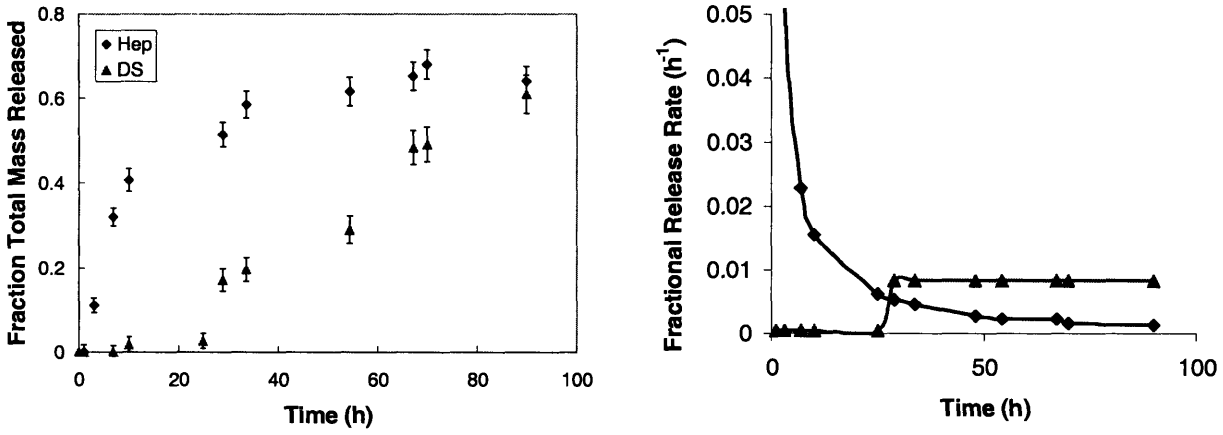

(a) (b)

Figure 8.6. Dextran sulfate (base layer, triangle) and heparin (surface layer, diamond)-loaded layers separated by a single, cross-linked layer of (PAH/PAA) exhibit sequential release.

(a) Fraction of mass released versus degradation time. (b) Fractional release rate versus time.

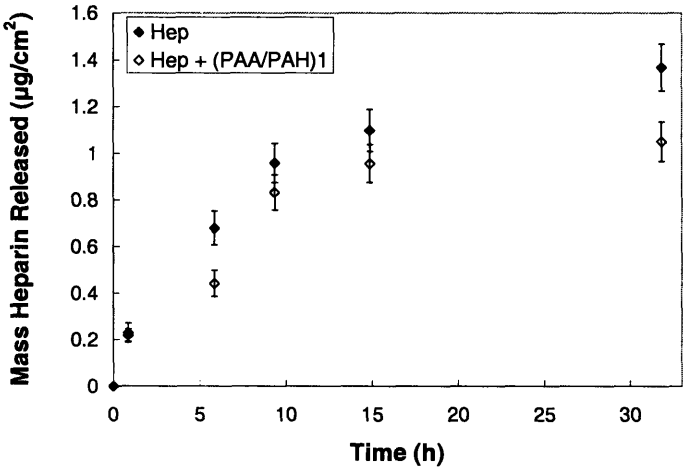

Figure 8.7. A single cross-linked layer of (PAH/PAA) does not significantly delay the release of underlying heparin.

Release of heparin-loaded films coated with a single layer of (PAH/PAA) cross-linked for 45 min at 215° C (filled diamond) is compared with untreated heparin-loaded films (open diamonds).

Remarkably, all of the non-covalent (noncrosslinked) barrier layers designed to physically separate the HEP and DS systems (Figure 8.5) resulted in simultaneous release of both components (see Figures 8.9-8.16). In most cases the barrier layers failed to even slow the release of the initially deposited base layers (Figure 8.8). To further verify these findings, the above series of films was repeated at a range of fabrication conditions (pH, ionic strength, number of deposited barrier layers), yet all resulted in simultaneous, rapid release in every case studied (data not shown). These data suggest that noncovalent, electrostatically-assembled barrier layers cannot block interlayer diffusion and thus cannot be used to create compartmentalized structures involving diffusive polyelectrolytes. This finding is particularly interesting in light of a recent study which showed that compartmentalized films containing linearly and exponentially growing regions could be constructed simply by depositing different films directly on top of one other.[24] The incongruities between this study and ours could be a result of a number of factors, including different polymer systems, molecular weights, and deposition conditions; moreover, they suggest that factors outside of the nature of growth that a given system exhibits may powerfully influence the final film architecture.

To more clearly demonstrate the effect of barrier layers on the average release rate from the aforementioned two-component systems, release rate is normalized and charted versus the type of barrier layer used in Figure 8.8. In Figure 8.8(a), it is apparent that the average release rate (taken as the average slope of the initial, linear portion of the release curve) of systems composed of an underlying layer of linearly-growing DS can be broadly controlled using both

multiple layers of a nondegradable system PDAC/SPS or as little as a single layer of cross-linked PAH/PAA. Further, by tuning any of the parameters affecting the degree of cross-linking (e.g., cross-linking time, temperature, number of cross-linked layers), the release rate can be dramatically altered (cross-linking times of greater than 1.5 h at 215° C, as well as barriers containing more than five cross-linked layers, resulted in one to two order of magnitude decreases in release rate) (data not shown). Thus, milder cross-linking conditions (such as lower temperatures) may allow for a greater degree of flexibility in tailoring release profiles. Further, aqueous, chemical cross-linking techniques using common biochemical reagents such as carbodiimides may represent a suitable alternative to thermal cross-linking when low temperature fabrication is required. Nevertheless, these proof-of-principle studies suggest that sampling a range of approaches to control the release of underlying species can yield effective results, particularly when the underlying species lacks the ability to diffuse throughout the film.

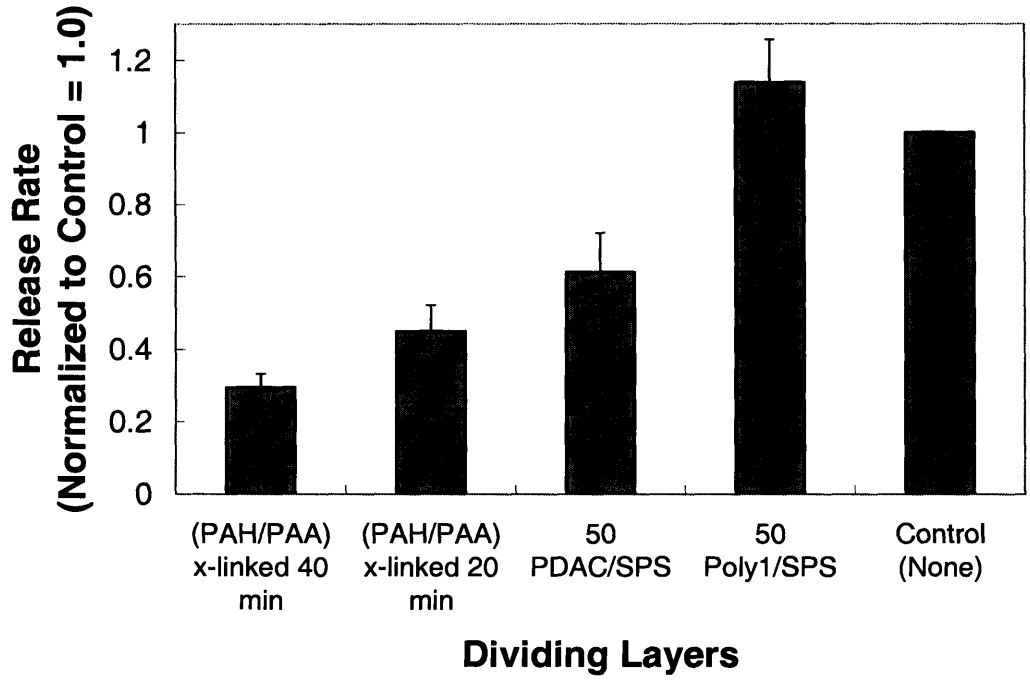

(a)

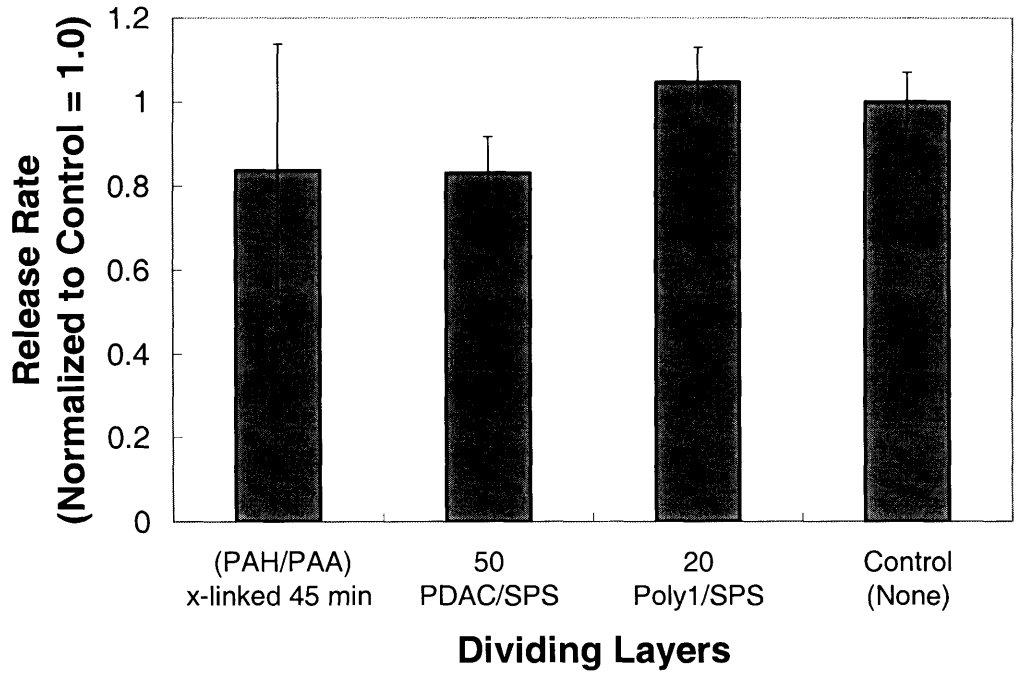

(b)

Figure 8.8. Normalized release rates from films coated with various blocking layers. Normalized initial average release rate (μg/h-cm^2) from base films containing (a) dextran sulfate and (b) heparin coated with no separation layers (control), or with a single layer of (PAH/PAA) cross-linked at 215° C for variable times, non-degradable (PDAC/SPS), or degradable (Poly1/SPS). Initial average release rates were calculated from the average slope of the linear portion of the mass released versus time curve during the first 50 h (dextran sulfate) or 10 h (heparin) of degradation.

Taken together, the data in Figures 8.6-8.8 yield a set of interesting hypotheses with respect to diffusion and release from multi-component, hydrolytically degradable LbL films. First, when initially deposited layers contain a highly diffusible species such as HEP, subsequent deposition of additional layers has little to no effect on its release, as the diffusible species is likely able to migrate through even tightly interacting networks within the film, effectively

ensuring that it always resides near the film surface.[4] However, when initially deposited layers contain a linearly growing species such as DS, subsequent deposition of new species can have a significant impact on its release, as the linearly growing system provides a structural substratum on which a tightly interacting network of barrier layers can be formed (which can then serve to hinder its release during degradation by physically separating it from subsequently adsorbed species). We demonstrate that a relatively simple understanding of the nature of build up and diffusion within a given system can allow one to engineer stratified, multicompartment architectures with complex release profiles, and that these profiles can be broadly controlled to suit the demands of a particular application.

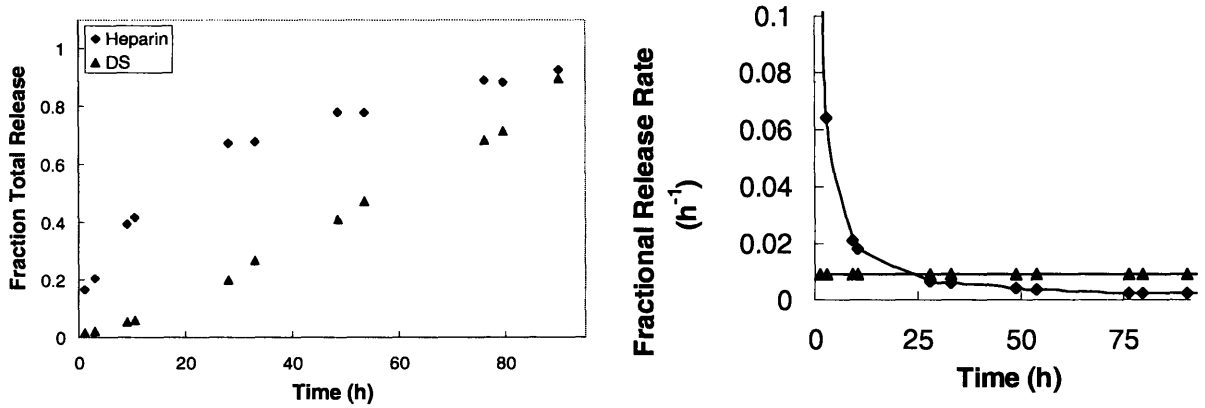

Figure 8.9. Heparin (base layer, diamond) and dextran sulfate (surface layer, triangle)-loaded layers, without dividing layers, sustain simultaneous release.

(a) Fraction of mass released versus degradation time (error bars are small). (b) Fractional release rate versus time.

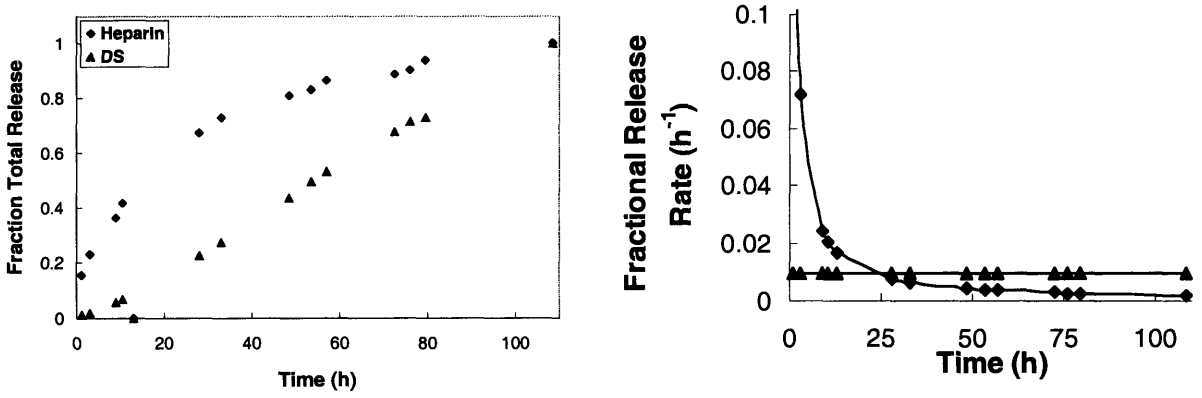

(a) (b)

Figure 8.10. Heparin (base layer, diamond) and dextran sulfate (surface layer, triangle)-loaded layers, separated by (Poly1/SPS)$_{20}$ degradable dividing layers, sustain simultaneous release.

(a) Fraction of mass released versus degradation time (error bars are small). (b) Fractional release rate versus time.

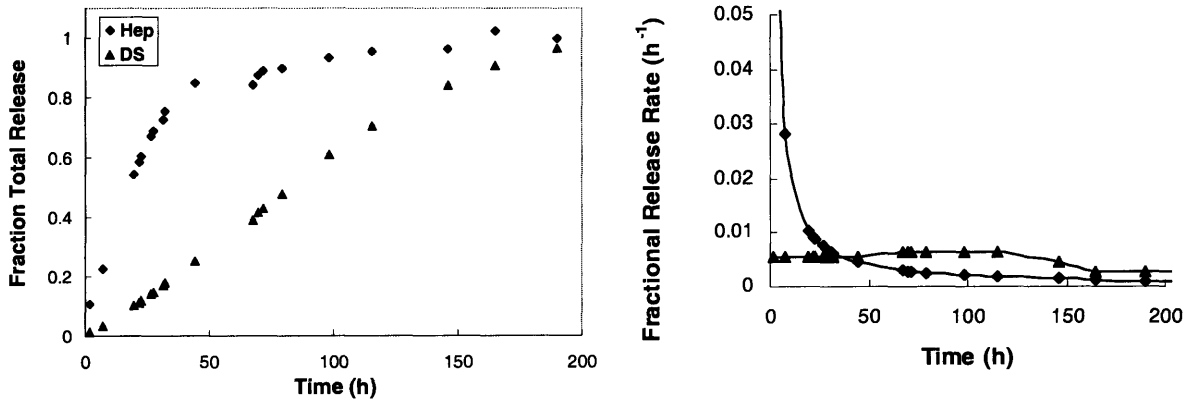

(a) (b)

Figure 8.11. Heparin (base layer, diamond) and dextran sulfate (surface layer, triangle)-loaded layers, separated by (PDAC/SPS)$_{50}$ non-degradable dividing layers, sustain simultaneous release.

(a) Fraction of mass released versus degradation time (error bars are small). (b) Fractional release rate versus time.

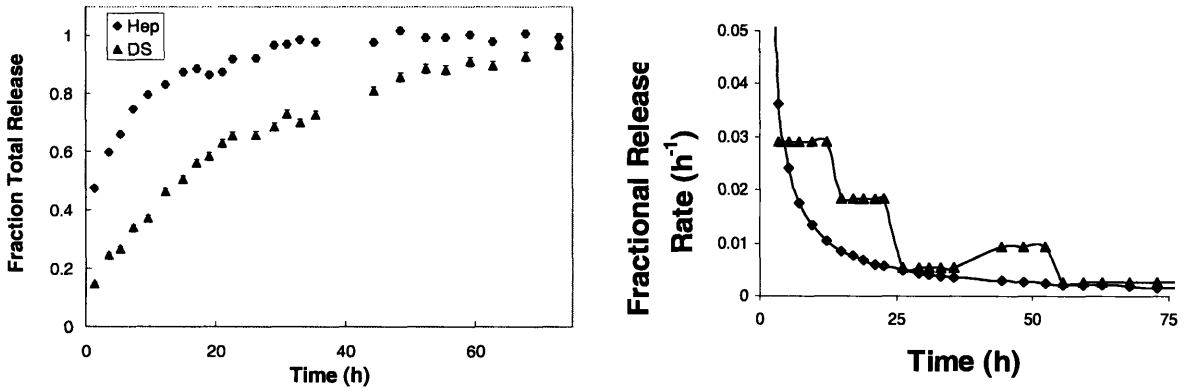

(a) (b)

Figure 8.12. Dextran sulfate (base layer, triangle) and heparin (surface layer, diamond)-loaded layers, without dividing layers, sustain simultaneous release.

(a) Fraction of mass released versus degradation time (error bars are small). (b) Fractional release rate versus time.

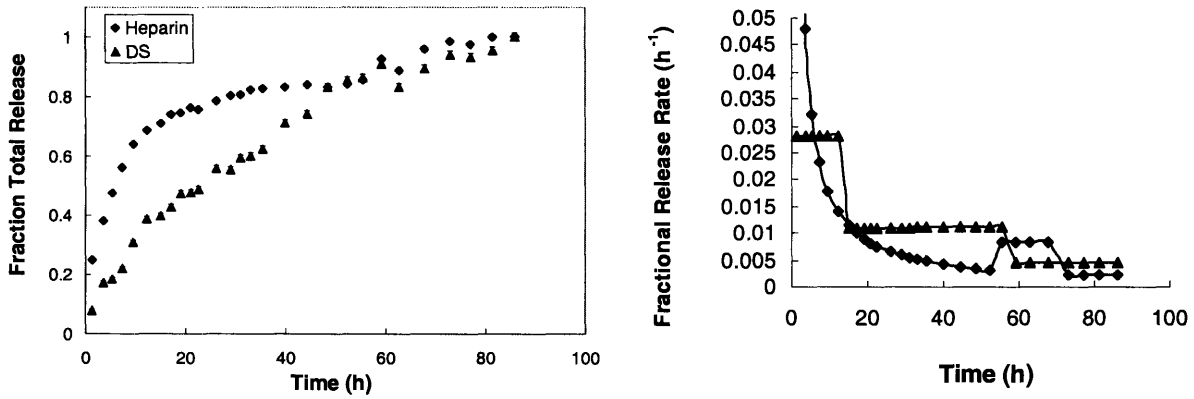

(a) (b)

Figure 8.13. Dextran sulfate (base layer, triangle) and heparin (surface layer, diamond)-loaded layers, separated by 50 (Poly1/SPS) degradable dividing layers, sustain simultaneous release.

(a) Fraction of mass released versus degradation time (error bars are small). (b) Fractional release rate versus time.

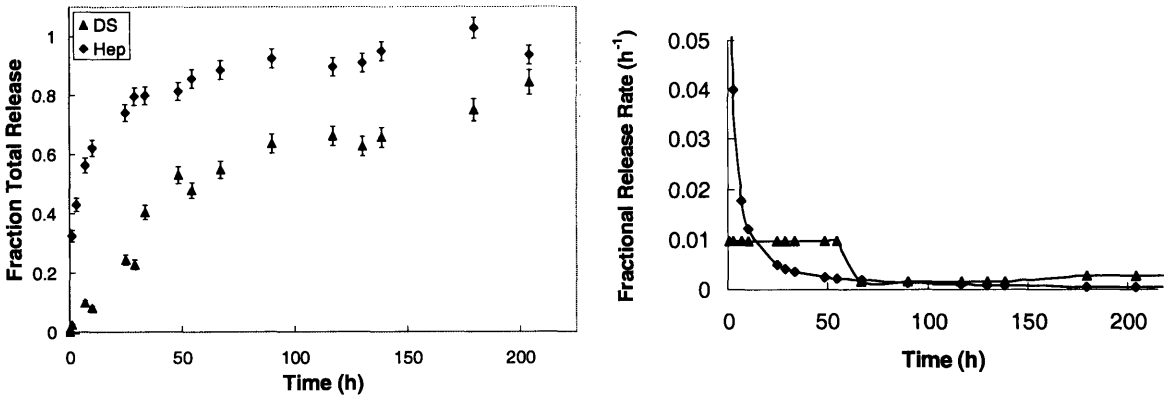

(a) (b)

Figure 8.14. Dextran sulfate (base layer, triangle) and heparin (surface layer, diamond)-loaded layers, separated by 50 (PDAC/SPS) non-degradable dividing layers, sustain simultaneous release.

(a) Fraction of mass released versus degradation time. (b) Fractional release rate versus time.

8.4 Conclusions

In this chapter, we systematically probe a series of strategies designed to physically separate multiple components within a layer-by-layer film by blocking interlayer diffusion. We measure the effect of each type of barrier using a novel experimental system consisting of a hydrolytically degradable polymer alternately deposited with a series of radiolabeled polyelectrolytes. Using this approach, we uncover for the first time a set of strategies which allow for the production of compartmentalized, or stratified, films capable of releasing complex, tuned release profiles. In particular, we show covalently cross-linked barriers can effectively block interlayer diffusion, leading to compartmentalized structures, while even very large

numbers of ionically cross-linked (degradable or non-degradable) barrier layers cannot block interlayer diffusion. Perhaps most interestingly, we demonstrate that wide ranging materials properties can be obtained from a single, relatively simple set of materials by judiciously applying strategies to control interlayer diffusion. Combining the attributes of the LbL processing technique – which allows for the rapid, all-aqueous, conformal, highly uniform and tunable fabrication of nanoscale coatings – with the ability to spatially order active agents and control release kinetics for multiple species may yield significant new opportunities in drug delivery, separations, electro-optical materials, and other fields.

8.5 References

1. Hammond, P.T. Form and function in multilayer assembly: New applications at the nanoscale. *Adv Mater* **16**, 1271-1293 (2004).
2. Anderson, D., Burdick, J. & Langer, R. Smart Biomaterials. *Science* **305**, 1923-1924 (2004).
3. Decher, G. Fuzzy nanoassemblies: Toward layered polymeric multicomposites. *Science* **277**, 1232-1237 (1997).
4. Picart, C. et al. Molecular basis for the explanation of the exponential growth of polyelectrolyte multilayers. *Proc Natl Acad Sci USA* **99**, 12531-12535 (2002).
5. Hammond, P.T. Recent explorations in electrostatic multilayer thin film assembly. *Colloid Interface Sci* **4**, 430-432 (2000).
6. Caruso, F., Yang, W., Trau, D. & Renneberg, R. Microencapsulation of uncharged low molecular weight organic materials by polyelectrolyte multilayer self-assembly. *Langmuir* **16**, 8932-8936 (2000).
7. Onda, M., Lvov, Y., Ariga, K. & Kunitake, T. Sequential actions of glucose oxidase and peroxidase in molecular films assembled by layer-by-layer alternate adsorption. *Biotechnology and Bioengineering* **51**, 163-167 (1996).
8. Lvov, Y., K, A., I, I. & T, K. Assembly of multicomponent protein films by means of electrostatic layer-by-layer adsorption. *J Am Chem Soc* **117**, 6117-6123 (1995).
9. Thierry, B., Winnik, F., Merhi, Y. & Tabrizian, M. Nanocoatings onto arteries via layer-by-layer deposition: Toward the in vivo repair of damaged blood vessels. *J Am Chem Soc* **125**, 7494-7495 (2003).
10. Jessel, N. et al. Bioactive coatings based on a polyelectrolyte multilayer architecture functionalized by embedded proteins. *Advanced Materials* **15**, 692-695 (2003).
11. Vazquez, E., DeWitt, D.M., Hammond, P.T. & Lynn, D.M. Construction of hydrolytically-degradable thin films via layer-by-layer deposition of degradable polyelectrolytes. *J Am Chem Soc* **124**, 13992-13993 (2002).
12. Zhang, J., Chua, L.S. & Lynn, D.M. Multilayered thin films that sustain the release of functional DNA under physiological conditions. *Langmuir* **20**, 8015-8021 (2004).

13. Wood, K.C., Boedicker, J.Q., Lynn, D.M. & Hammond, P.T. Tunable drug release from hydrolytically degradable layer-by-layer thin films. *Langmuir* **21**, 1603-1609 (2005).
14. Jewell, C.M., Zhang, J., Fredin, N.J. & Lynn, D.M. Multilayered polyelectrolyte films promote the direct and localized delivery of DNA to cells. *J Control Release* **106**, 214-223 (2005).
15. Lynn, D. & Langer, R. Degradable poly(beta-amino esters): Synthesis, characterization, and self-assembly with plasmid DNA. *J Am Chem Soc* **122**, 10761-10768 (2000).
16. Hübsch, E. et al. Controlling the growth regime of polyelectrolyte multilayer films: Changing from exponential to linear growth by adjusting the composition of polyelectrolyte mixtures. *Langmuir* **20**, 1980-1985 (2004).
17. Lösche, M., Schmitt, J., Decher, G., Bouvman, W. & Kjaer, K. Detailed Structure of Molecularly Thin Polyelectrolyte Multilayer Films on Solid Substrates as Revealed by Neutron Reflectometry. *Macromolecules* **31**, 8893-8906 (1998).
18. Elbert, D., Herbert, C. & Hubbell, J. Thin polymer layers formed by polyelectrolyte multilayer techniques on biological surfaces. *Langmuir* **15**, 5355-5362 (1999).
19. Picart, C. et al. Buildup mechanism for poly(L-lysine)/hyaluronic acid films onto a solid surface. *Langmuir* **17**, 7414-7424 (2001).
20. Lavalle, P. et al. Comparison of the structure of polyelectrolyte multilayer films exhibiting a linear and an exponential growth regime: An in situ atomic force microscopy study. *Macromolecules* **35**, 4458-4465 (2002).
21. Lavalle, P. et al. Modeling the buildup of polyelectrolyte multilayer films having exponential growth. *J Phys Chem B* **108**, 635-648 (2004).
22. Anderson, D.G., Lynn, D.M. & Langer, R. Semi-automated synthesis and screening of a large library of degradable cationic polymers for gene delivery. *Angew. Chem. Int. Ed.* **42**, 3153-3158 (2003).
23. Fredin, N., Zhang, J. & Lynn, D. Surface Analysis of Erodible Multilayered Polyelectrolyte Films: Nanometer-Scale Structure and Erosion Profiles. *Langmuir* **21**, 5803-5811 (2005).
24. Garza, J. et al. Multicompartment films made of alternate polyelectrolyte multilayers of exponential and linear growth. *Langmuir* **20**, 7298-7302 (2004).

Chapter 9: Electroactive controlled release thin films

9.1 Introduction

Recently, great interest has centered on the development of 'smart' controlled release systems capable of administering drugs in response to external stimuli such as electric or magnetic fields for use in applications such as controlled release implants ('pharmacy-on-a-chip').[1-3] Toward these goals, microfabricated devices have been developed which make use of micrometer-scale pumps, channels, and wells to deliver drugs on demand.[1-5] However, while these technologies have resulted in encouraging new treatment possibilities, several challenges still remain. For example, the direct integration into non-planar, functional or structural implants such as arterial stents, medical sutures, and bone prostheses is challenging, as photolithographic and micromachining techniques are primarily developed for planar, silicon-based substrates.[6] Further, the multi-step processing of these devices can be both time consuming and expensive.[7]

In this chapter, we extend the concept of layer-by-layer (LbL) thin films for controlled release applications to include a new class of films which degrade to release their contents in response to a small applied voltage (1.25 V). These "active" controlled release systems possess many of the benefits of LbL films described in Chapters 6-8 (e.g., ability to conformally coat a range of substrates, nanoscale control over various architectural features, and all-aqueous processing); moreover, they also allow for external control of drug release through electrochemical modulation of film stability using an electroactive component that is both non-toxic and approved by the US FDA for use in humans.

Electroactive thin films are constructed using the layer-by-layer (LbL) directed self-assembly technique which, as previously described, utilizes the alternating adsorption of materials containing complementary charged or functional groups onto a solid substrate to form thin films.[8] This method can be used to create highly tunable, conformal thin films with nanometer-scale control over film composition and structure. The only criteria for inclusion in an LbL thin film is that the species of interest either possess, or that it be encapsulated in a 'carrier' species (i.e., nanoparticle, micelle, dendrimer, etc.) that possesses the desired complementary functional group. Thus, a wide range of components including polymers, proteins, nucleic acids, small molecules, and nanoparticles have been incorporated into these assemblies, which can further be constructed in a range of interesting geometries and patterns.[9, 10] As a result of this versatility, LbL thin films have been used in a variety of drug delivery applications, most notably as coatings that can release drugs passively[11-13] or in response to environmental changes such as pH or ionic strength.[14-22]

The electroactive component of films described in this chapter is Prussian Blue (PB), a non-toxic, FDA-approved inorganic iron hexacyanoferrate compound that is well known for its electrochromic,[23] electrochemical,[24] and magnetic properties.[25] PB exhibits a number of stable oxidation states known colloquially as Prussian White (PW), Prussian Blue (PB), Berlin Green (BG), and Prussian Brown (PX), in order of increasing oxidation state. These states are all negatively charged with the exception of PX, which is neutral.[26] PB can be synthesized in the form of polydisperse, anionic nanoparticles (median size 4-5 nm) which are stable in aqueous solution.[27] Applying a potential of +1.25 V (compared to SCE) switches these materials between the PB (negative) and PX (neutral) states.[26]

Here, we demonstrate that by applying a low voltage to PB nanoparticle-based LbL thin films, and thus changing the PB oxidation state from negative to zero-valent, we can induce rapid film destabilization and controlled release of the film's components. This destabilization is believed to be based on the loss of electroneutrality occurring within the film following the PB to PX transition, resulting in the repulsion of adjacent, like-charged layers. Destabilization is associated with swelling and then release of the film's components into solution, and we quantify this controlled release using a model, radiolabeled drug (^{14}C-dextran sulfate). We further show that this release is well-controlled; that is, removal of the oxidizing potential results in restabilization of the remaining film. Finally, as a measure of biocompatibility we demonstrate that PB particles exhibit no measurable toxicity on a panel of mammalian cell lines at concentrations up to 1.0 mg/mL. Together, this technology represents a new robust, inexpensive, and versatile platform for the fabrication of nanostructured, field-activated (remote-controlled) drug delivery systems.

9.2 Experimental Methods

Materials. Dextran sulfate sodium salt (M_n = 8000) was obtained from Sigma-Aldrich (St. Louis, MO). ^{14}C-dextran sulfate sodium salt (100 μCi, 1.5 mCi/g, M_n = 8000) was obtained from American Radiolabeled Chemicals, Inc (St. Louis, MO). Radiolabeled and corresponding unlabeled polymers were chosen with similar molecular weights and polydispersities in order to mimic the behavior of the unlabeled species as closely as possible. Linear poly(ethylenimine) (LPEI, M_n = 25000) was received from Polysciences, Inc. $FeCl_2$, potassium ferricyanide, and KCl were purchased from Aldrich. All materials and solvents were used as received without further purification.

Synthesis of PB nanoparticles. Briefly, 35 mL of 10 mM aqueous $FeCl_2$ (Aldrich) was added dropwise to an equivalent volume of 50 mM potassium ferricyanide (Aldrich) and 50 mM KCl, agitated for 1 min, and filtered continuously with deionized water (with magnetic stirring) against a 3000 Da MWCO regenerated cellulose membrane. Permeate solutions (containing ten or more equivalent volumes) were yellow, suggesting that only the excess potassium ferricyanide along with a trivial amount of PB may have passed through the membrane. The retentate solution was collected, pH adjusted to 4 by addition of potassium hydrogen phthalate buffer, and used immediately in LbL assembly.[27]

Preparation of electrolyte solutions. LbL films were assembled on conducting ITO-coated glass substrates (Delta Technologies, 0.7 cm × 5 cm, 6 Ω/square) for profilometry, deconstruction, and drug release studies. ITO-glass substrates were cleaned via ultrasonication in dicholormethane, acetone, methanol, and deionized water for 15 min each, followed by a 5 min oxygen plasma etch (Harrick PCD 32G) to ensure that the surfaces were clean and abundant in hydroxyl groups. Dextran sulfate and LPEI dipping solutions were prepared at concentrations of 10 mM with respect to the polymer repeat unit in acetate buffer (100 mM, pH 5.1) and deionized water (pH 4.25 by addition of HCl), respectively. Deionized water used to prepare all solutions was obtained using a Milli-Q Plus (Bedford, MA) at 18.2 MΩ.

Thin film deposition. LBL films were constructed as follows according to the alternate dipping method using an automated Carl Zeiss HMS Series Programmable Slide Stainer.[8] Briefly, pretreated substrates were submerged in an LPEI dipping solution for 10 minutes followed by a cascade rinse cycle consisting of three deionized water rinsing baths (15, 30, and 45 seconds, respectively). Substrates were then submerged in a PB dispersion for 10 minutes followed by the same cascade rinsing cycle, and the entire process was repeated as desired to

construct (LPEI/PB) films with desired numbers of layer pairs. Tetralayer films containing LPEI/dextran sulfate/LPEI/PB were constructed using the same general protocol; however, in this case, the PB dipping step alternated with a dextran sulfate dipping step (10 min with cascade rinse cycle). Following deposition, films were immediately removed from the final rinsing bath and dried thoroughly under a stream of dry nitrogen gas. Film thickness and deconstruction experiments on conducting ITO-glass substrates were conducted using a Tencor P10 profilometer by scoring the film and profiling the score. A tip force of 5 mg was used to avoid penetrating the underlying ITO film.

Electrochemical degradation of thin films. Electrochemical deconstruction studies were performed using an EG&G 263 A potentiostat/galvanostat. The electrolyte was a 10 mM KCl solution. Approximately 0.3 cm^2 was used, the reference electrode was a K-type saturated calomel electrode, and the counter electrode was a piece of Pt foil (2.5 cm × 2.5 cm).

Drug release. For drug release experiments, films were formed using a radiolabeled ^{14}C-dextran sulfate sodium salt (100 μCi, 1.5 μCi/mg) dipping solution at a concentration of 4 μCi/mL. The LBL deposition procedure was then performed as described above. Following deposition, ^{14}C-dextran sulfate labeled films were immersed in 100 mL of 10 mM KCl, and electrochemical deconstruction was performed by applying square wave potentials, also as described above. In all cases, films were first immersed for 10 min prior to application of potential, and no passive release was observed. A 1 mL sample was extracted at indicated time points and analyzed for radioactive ^{14}C content by adding 5 mL of ScintiSafe Plus 50% (Fisher Scientific, Atlanta, GA) prior to measurement. Raw data (disintegrations per minute per mL, DPM/mL) were converted to micrograms per mL (μg/mL) of ^{14}C-dextran sulfate using the

conversion factor 2.2 x 10^6 DPM = 1 μCi = 0.67 mg ^{14}C-dextran sulfate. Finally, the total dextran sulfate release from a single film was calculated according to the following equation:

$$M_i = C_i \times V_i + (1mL)\sum_{j=1}^{i-1} C_j \qquad (1)$$

where M_i (μg) is the total cumulative mass released from the film as of measurement i, C_i (μg/mL) is the concentration of sample i, V_i (mL) is the total volume of the deconstruction bath prior to measurement i, and $(1mL)\sum_{j=1}^{i-1} C_j$ is the total mass in previously extracted samples.

Cell viability. Cell viability assays were performed in triplicate using the following protocol. All materials, buffers, and reagents were sterilized prior to use. Cell culture reagents were purchased from Invitrogen Corporation (Carlsbad, CA) and MTT viability assay kits were obtained from American Type Culture Collection (Manassas, VA). Focus HCC cells were grown in 96-well plates at an initial seeding density of 5000 cells/well in 150 μL/well of growth medium (90% modified Eagle's medium supplemented with 10% fetal bovine serum, 100 units/mL penicillin, and 100 μg/mL streptomycin, 0.1 mM non-essential amino acids, 1 mM sodium pyruvate, and 2 mM L-glutamine). HeLa cells were grown in 96-well plates at an initial seeding density of 10000 cells/well in 150 μL/well of growth medium (90% modified Eagle's medium supplemented with 10% fetal bovine serum, 100 units/mL penicillin, and 100 μg/mL streptomycin, 0.1 mM non-essential amino acids, 1 mM sodium pyruvate, and 2 mM L-glutamine). Cos-7 cells were grown in 96-well plates at an initial seeding density of 15000 cells/well in 150 μL/well of growth medium (90% Dulbecco's modified Eagle's medium supplemented with 10% fetal bovine serum, 100 units/mL penicillin, and 100 μg/mL

streptomycin). After seeding, cells were allowed to attach and proliferate for 24 h in an incubator (37° C, 5% CO_2). A sterile, 10X concentrated PBS buffer solution was added to an aqueous suspension of PB nanoparticles to yield a final solution containing 1.125 mg/mL PB, 137 mM NaCl, 2.7 mM KCl, and 10 mM Na_2HPO_4 at pH 7.4. Growth media were removed from cells and replaced with the above suspension of PB particles diluted in Opti-MEM (Invitrogen) at concentrations ranging from 0 mg/mL to 1.0 mg/mL PB. In parallel, cells were also incubated with carrier solutions alone (Opti-MEM plus an equivalent concentration of PBS without PB particles) to account for toxicity associated with the carrier solution only. Cells were incubated with the solutions for 4 h, after which solutions were removed and replaced with growth media. After 72 h, cell metabolic activity was assayed using the MTT cell proliferation assay kit (ATCC, Manassas, VA). Initially, a 10 μL aliquot of MTT assay reagent was added to each well. After incubating for two hours, 100 μL of detergent reagent was added. The plate was then covered and left in the dark for 4 h, after which optical absorbance was measured at 570 nm using a SpectraMax 190 microplate reader (Molecular Devices, Sunnyvale, CA). Background (media plus MTT assay reagent plus detergent reagent with no cells present) was subtracted from the value of each well, and all values were normalized to the value of control (untreated) cells. In similar fashion, the toxicity of an equivalent amount of PBS buffer in Opti-MEM (with no PB) was calculated. Values reported in Figure 9.8 represent the normalized viability of PB-treated cells divided by the normalized viability of cells treated with equivalent amounts of pure PBS (to account for the toxicity of PBS itself).

9.3 Results and discussion

9.3.1 Fabrication of electroactive thin films

Figure 9.1(a) outlines the process for constructing electroactive LbL thin films based on PB. A glass substrate coated with a conducting film of indium tin oxide (ITO) is first dipped in a solution containing a cationic drug or drug-containing 'carrier' species, then rinsed in deionized water. Next, the substrate is dipped into an aqueous PB solution at pH 4 and rinsed again in deionized water. The process is repeated to build up a multilayer nanocomposite film with desired properties (see Experimental Methods). Controlled film deconstruction occurs upon the application of an electrochemical potential of 1.25 V, "switching" PB to the neutral PX state and releasing the encapsulated species. Removing the potential reduces the particles back to the anionic PB state, allowing one the ability to switch the assembly back and forth between stable and unstable states.

Figure 9.1(b) depicts the structure of 'soluble' PB, $KFe^{III}[Fe^{II}(CN)_6]$. Potassium inclusions in this form of PB can dissociate in aqueous solutions, resulting in a net negative charge on the particle surface which renders nanoparticles stable in solution. PB nanoparticles are formed via the room temperature, aqueous-phase reaction that occurs upon the addition of a molar excess of potassium ferricyanide to iron(II) chloride (see Methods). This synthesis and purification procedure yielded dark blue, aqueous suspensions that were stable in the absence of sonication or chemical stabilizers.

Figure 9.1(c) shows the linear build-up of the tetralayer system containing linear poly(ethylenimine) (LPEI)/dextran sulfate/LPEI/PB used in this study (measured by profilometry and UV-Visual spectroscopy). Tetralayer systems, rather than traditional bilayer systems, were

used in order to encapsulate and release ^{14}C-dextran sulfate (DS), our negatively charged model drug species. The thickness of an average tetralayer was 4.2 ± 0.6 nm. (This value reflects the average of five data points taken at various positions on the surface of the film.) Films were observed to grow linearly in thickness with increasing numbers of layers. The linear growth behavior observed in these systems may have important implications for the controlled delivery of precise quantities of drugs, as the thickness (and mass) of a given layer can be precisely predicted with no dependence on the thickness of the underlying film, resulting in facile control over drug payloads.

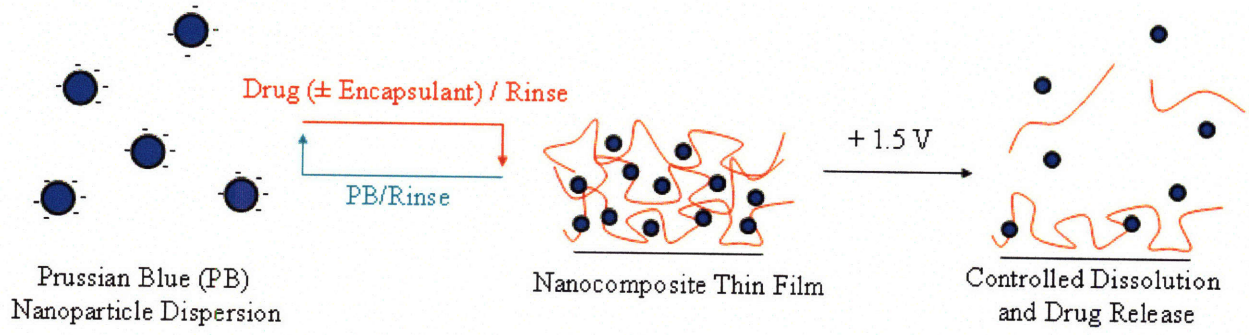

(a)

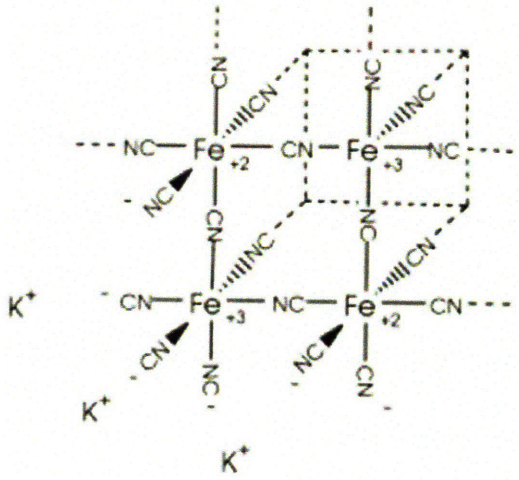

(b)

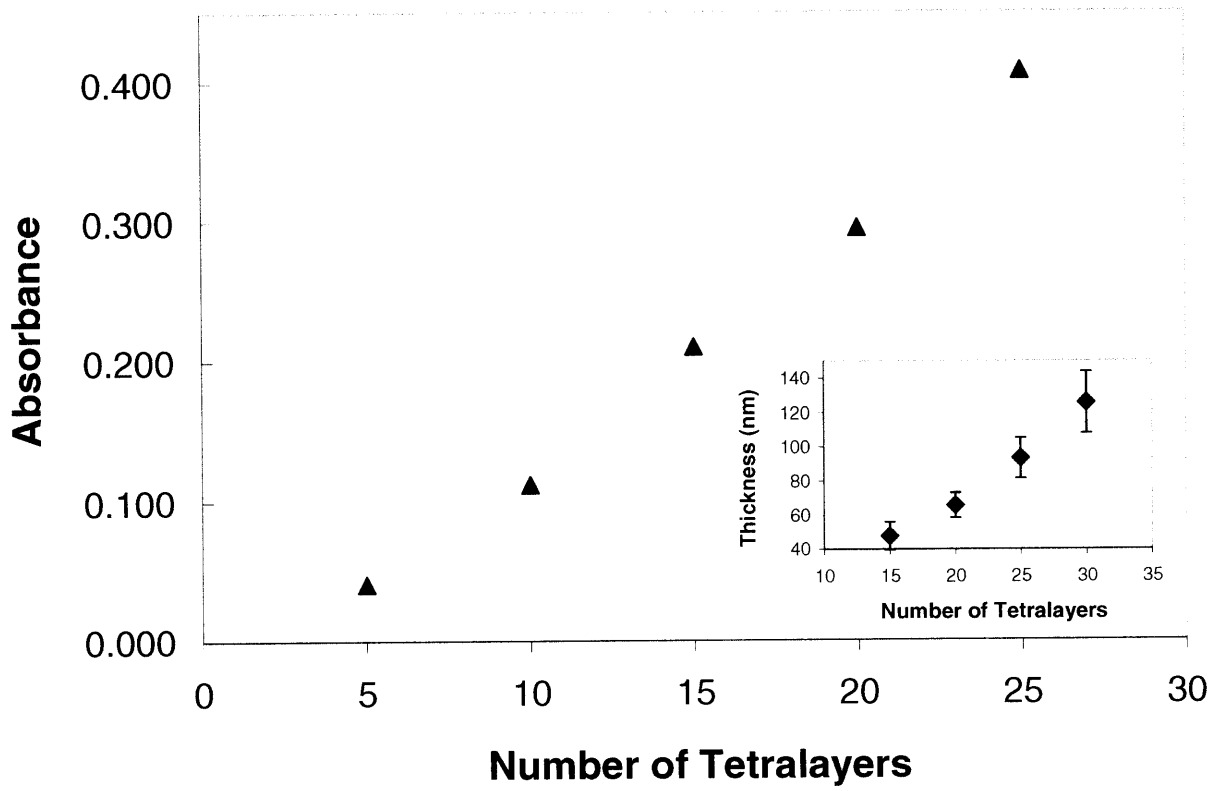

(c)

Figure 9.1. Fabrication of LbL nanocomposite thin films based on PB.

(a) Generalized schematic detailing the assembly and deconstruction of drug-containing PB nanocomposites. (b) Structure of PB. (c) Absorbance at 700 nm versus number of deposited tetralayers for the (PB/LPEI/DS/LPEI) system as determined by UV-Visual spectroscopy. (Insert: Film thickness versus number of deposited tetralayers for the (PB/LPEI/DS/LPEI) system as determined by profilometry. Measurements were performed at five predetermined spots on the surface of the films, and error bars represent one standard deviation in measured values.)

9.3.2 Electroactive degradation of films

Figure 9.2 shows the deconstruction of $(LPEI/DS/LPEI/PB)_{30}$ tetralayer films under the influence of an applied voltage held constant at 1.25 V, as monitored by UV-Visual spectroscopy (PB exhibits an absorbance maximum at ~ 700 nm). Absorbance from PB-containing films was observed to decrease with increasing amounts of time at 1.25 V (Figure 9.2(a)). Quantitatively, absorbance at 700 nm was observed to decline rapidly during the first 5-10 minutes, reaching a value equal to 54% of that of the original film by 10 minutes (see Figure 9.2(b)). Thereafter, absorbance continued to decrease, reaching a value of 38.5% of the original film by 20 min, 18.2% by 60 min, and 10.4% by 90 min. Absorbance measurements taken from a control film (0 V) showed no decrease in color, suggesting that PB loss is directly related to film instabilities that are stimulated by the applied potential. Further, control experiments using films containing only LPEI and DS show that no degradation or drug release occurs in the presence of an applied potential when PB is absent from the system, suggesting that film destabilization is mediated by voltage-induced switching of PB (data not shown).

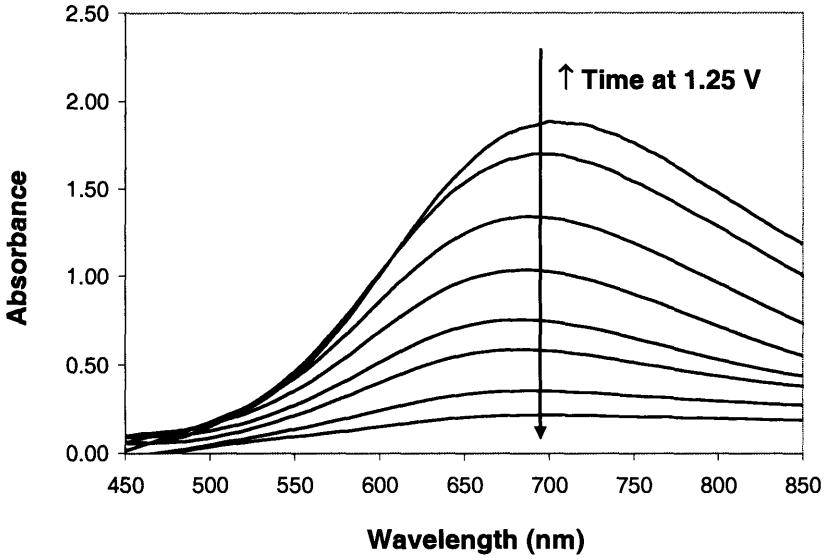

(a)

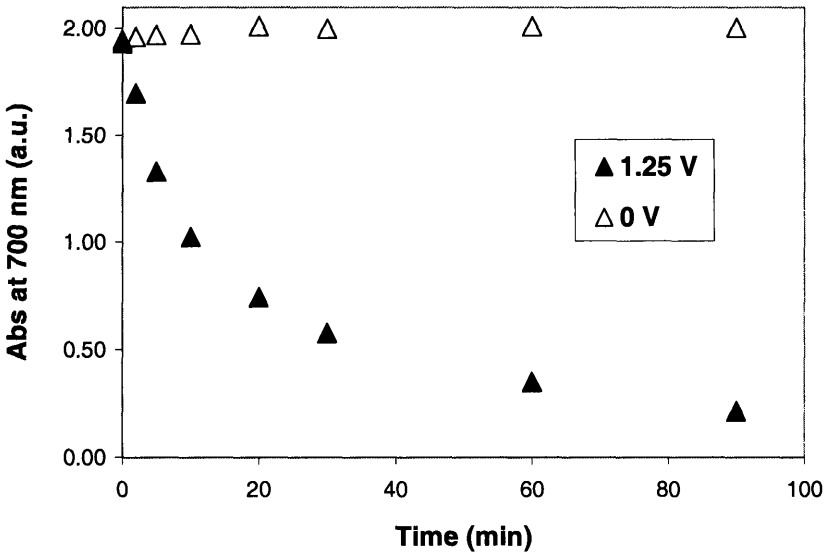

(b)

Figure 9.2. Electrochemical deconstruction of PB-containing thin films.

(a) Absorbance spectrum showing decreasing PB absorbance with increasing time at 1.25 V. (b) Absorbance (700 nm) versus time for films with (filled triangles) and without (open triangles) an applied potential.

To measure the effect of an applied potential on film thickness, and specifically to determine if PB loss correlated with deconstruction of the film, PB-containing films were exposed to a constant potential of 1.25 V and thickness was measured with respect to time using profilometry (Figure 9.3). In all PB-containing films studies, film thickness was observed to decrease rapidly at early times (1-5 min) followed by a more gradual decrease at later times (5 – 60 min), kinetics which reflect the time scales for PB loss described above. Further, in all systems, thickness was observed to decay until reaching 10-20% of the original film thickness, suggesting that some residual material was remaining on the surface of the substrate. In $(LPEI/DS/LPEI/PB)_{30}$ tetralayer films, thickness decayed to 80% of the original film after 1 min at 1.25 V, 50% after 5 min, and 20% after 60 min (not shown). In $(LPEI/PB)_{20}$ systems, destabilization occurred on a more rapid time scale, reaching 43% in under 1 min and 20% in under 4 min. The shorter time scales required for destabilization in $(LPEI/PB)_{20}$ systems likely reflects the fact that these films lose all cohesive electrostatic interactions following the PB to PX transition, resulting in rapid deconstruction relative to $(LPEI/PB/LPEI/DS)_{30}$ systems, which retain some stable electrostatic interactions (from LPEI and DS) in the presence of an applied potential.

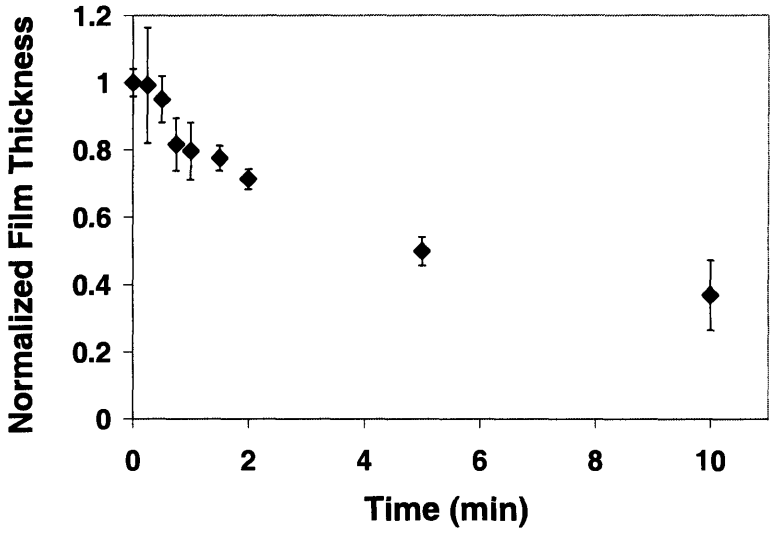

(a)

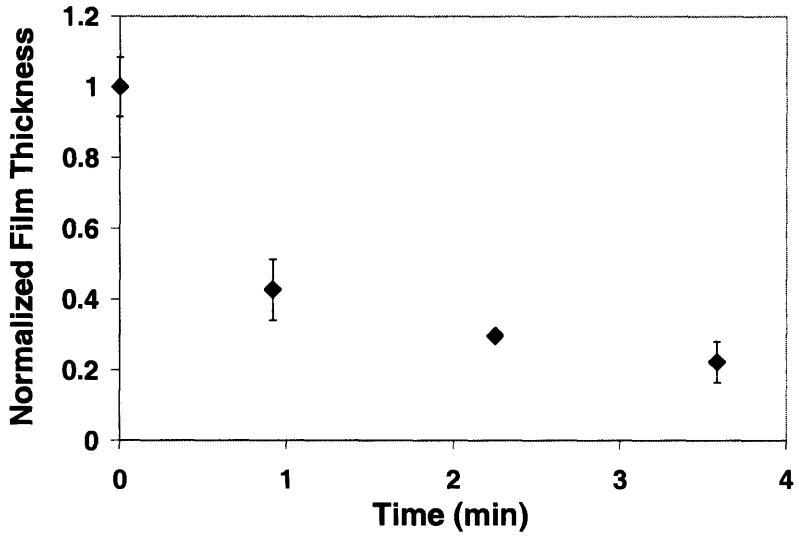

(b)

Figure 9.3. Normalized thickness of PB-containing films versus time at a constant potential of 1.25 V.

(a) Total film thickness versus time with constant potential held at 1.25 V. (a) $(LPEI/DS/LPEI/PB)_{30}$ films; (b) $(LPEI/PB)_{20}$ films. Error bars represent one standard

deviation of the measured thickness values at five predetermined locations on the surface of the film. As such, error bars provide an indication of the surface roughness of films (standard deviation of multiple thickness measurements taken at a single location was less than 10 Å).

9.3.3 Single and multi-film drug release

To determine if the electrochemical destabilization of PB-containing films causes drug release into solution, we built films containing a radiolabled, model drug compound, ^{14}C-DS. Figure 9.4 shows that these systems release the drug rapidly following the application of potential, with kinetics that are in agreement with film degradation. It appears on the basis of this data that PB-containing films are quickly destabilized by an applied potential, resulting in rapid film deconstruction and drug release. To verify that release occurs only in the presence of an applied potential, we soaked films in a solution identical to those used in the deconstruction experiments (10 mM KCl) and observed no significant drug release.

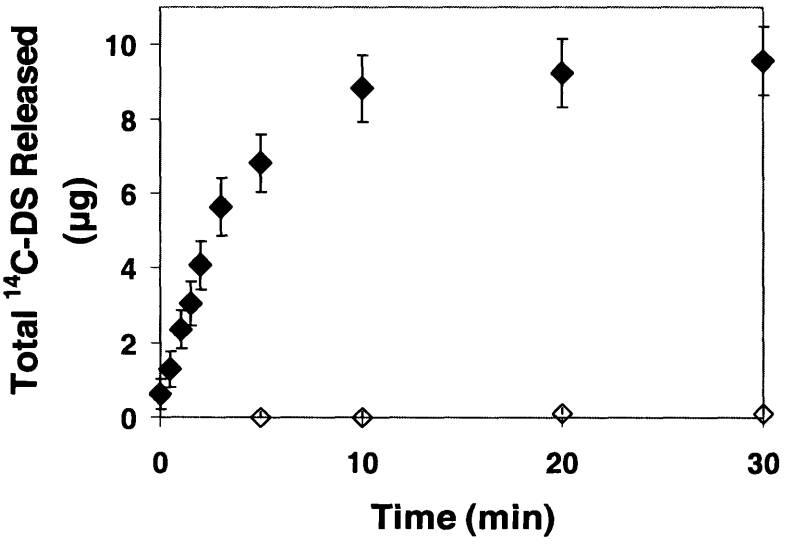

Figure 9.4. Drug release from a single film held at a constant potential of 1.25 V.

^{14}C-Dextran sulfate release from $(LPEI/DS/LPEI/PB)_{30}$ films. Films held constant at 1.25 V (closed diamonds) or no applied potential (open diamonds; error bars are small) are shown. All error bars represent one standard deviation in measured values.

The ability of PB-containing thin films to release their contents only in response to a small applied potential suggests that these systems might be interesting materials for implantable pharmacy-on-a-chip applications.[1] For example, existing patterning and machining techniques could be used to array multiple films onto individually addressable electrodes on a single substrate, and the application of a potential to individual films could result in the release of an active species from one film at a time. As a simple proof of this concept, we placed two $(LPEI/DS/LPEI/PB)_{30}$ films in a release bath, then applied a potential of 1.25 V to each film individually. As shown in Figure 9.5, this results in the release of the contents of the first film followed by the contents of the second film.

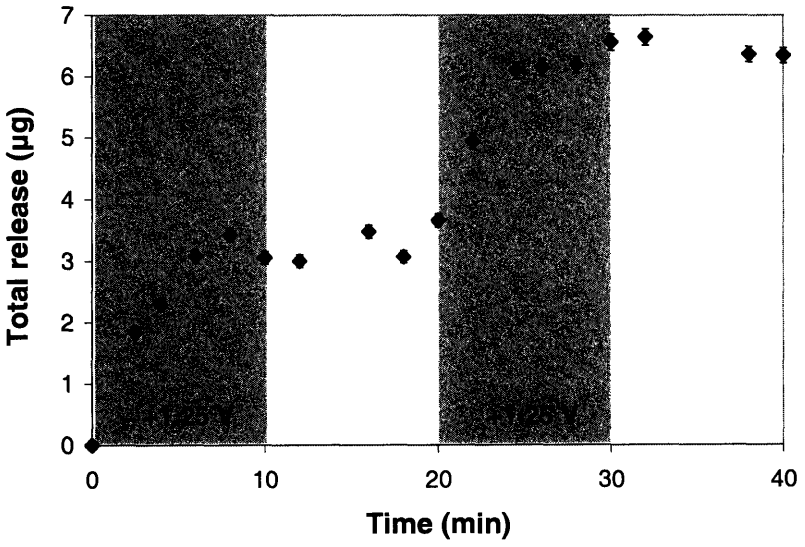

(a)

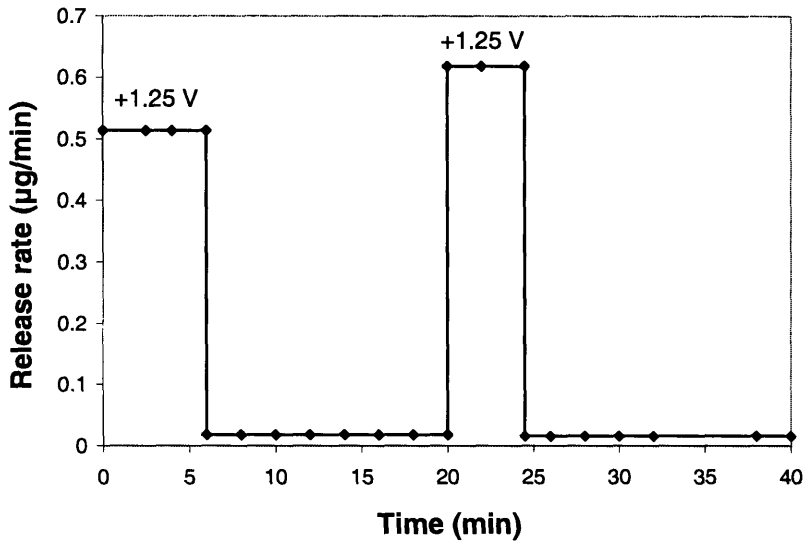

(b)

Figure 9.5. Serial release from multiple films in a single solution.

(a) ^{14}C-Dextran sulfate release from two $(LPEI/DS/LPEI/PB)_{30}$ films. A potential was applied to one film for 10 min, followed by 10 min with no applied potential. Next, the process was repeated with a second film in the same degradation bath. Periods during which a potential was applied are shaded. All error bars represent one standard deviation in measured values. (b) Release rate versus time for the films in part (a).

9.3.4 Reversible destabilization of a single film

To more closely examine the kinetics of film deconstruction, we measured drug release from representative 30 tetralayer LPEI/^{14}C-dextran sulfate/LPI/PB systems under the influence of a square wave potential of 1.25 V for varying amounts of time. All films used in these studies were deposited onto identical 2.45 cm^2, ITO-coated glass substrates from the same dipping solutions in order to ensure uniform thickness and drug loading. Figure 9.6(a) shows the release due to 10 s and 1 min square wave intervals at 1.25 V. Application of the oxidizing potential for

very short intervals (10 s) is not sufficient to significantly destabilize the film, likely because diffusion of polyelectrolytes out of the destabilized structure is the rate-limiting process (PB redox switching times are less than 1 s).[27] Thus, only a relatively small amount of ^{14}C-dextran sulfate was released. A longer interval (1 min) at the oxidizing potential results in significantly greater total drug release. Further, in both cases the drug release was observed to stop shortly after removing the potential, suggesting that films can become restabilized. In Figure 9.6(b) the drug release in response to differing time intervals at 1.25 V is shown. Films release significantly more drug following 10 min and 30 min intervals than shorter 10 s or 1 min intervals, an indication of the reversible nature of film destabilization. Further, 10 min and 30 min intervals result in similar quantities of drug release with similar kinetics (data not shown), suggesting that all of the available drug was released within the first 10 min. This is in agreement with the data in Figure 9.4, which shows that ~10 min at a 1.25 V potential is sufficient to achieve complete release from 30 tetralayer systems used in this study. To examine the reversible nature of film destabilization in response to an applied potential, a single film was exposed to two 1 min intervals at 1.25 V, separated by a 14 min interval with no applied potential (Figure 9.6(c) and (d)). From this data, it is apparent that films are rapidly destabilized in the presence of an applied potential, then restabilized when the potential is removed. This process is reversible, as reapplication of a potential can again destabilize the film. Thus, the stability (and drug release properties) of PB-based films can be precisely controlled electrochemically. In drug delivery applications, this reversible stability may allow for fine-tuned control over doses administered from implanted films.

Together, the data in Figure 9.6 suggests the following conclusions: (1) the process of destabilization can be reversed by removing the oxidizing potential and reactivated by re-

applying the oxidizing potential so long as each occurs prior to complete film deconstruction; (2) diffusion of the film's components out of the destabilized film structure is a rate-limiting step in drug release; and (3) deconstruction and release from 30 tetralayer systems studied in this chapter is completed in fewer than 10 min when held at constant potential.

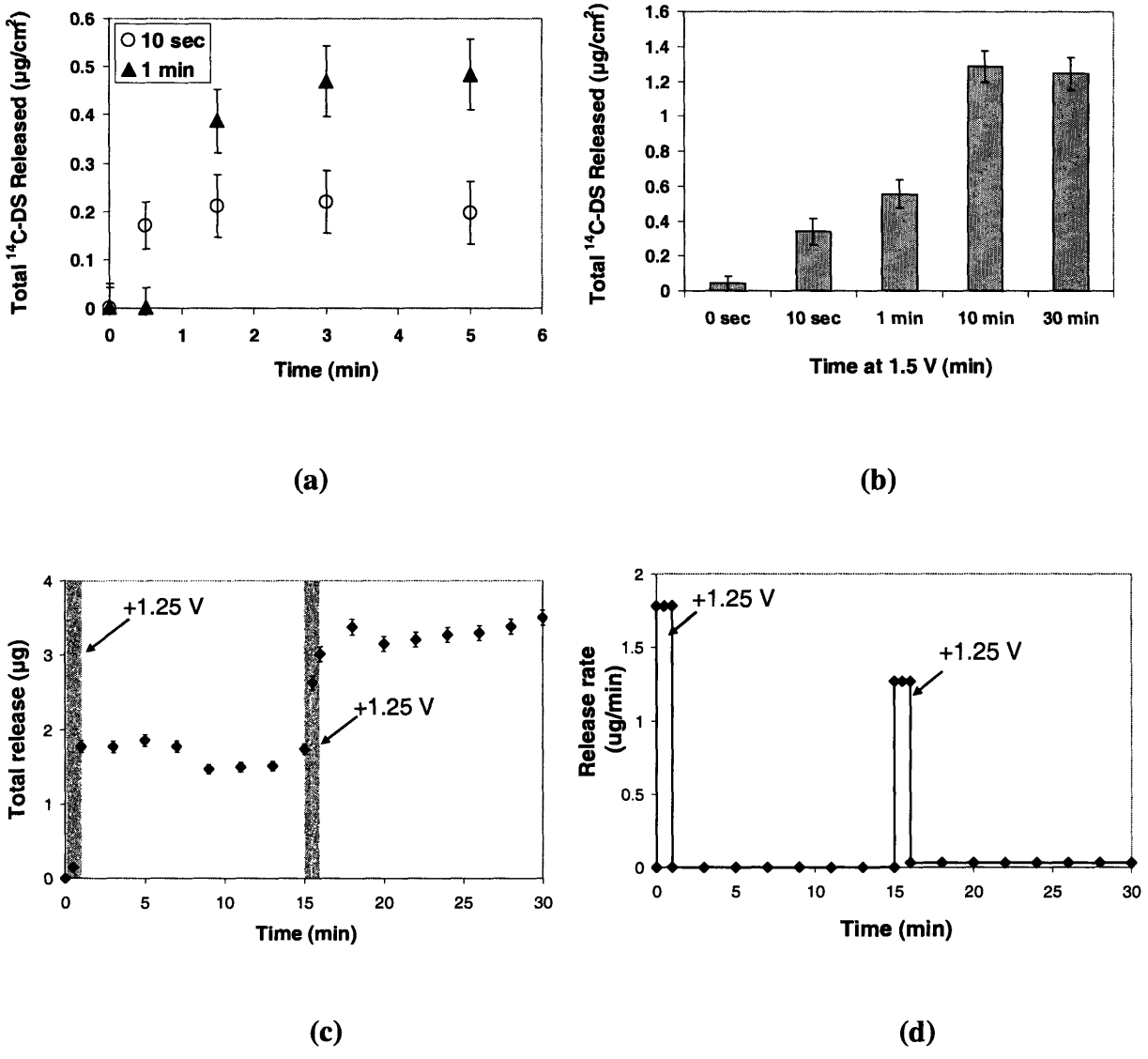

Figure 9.6. Reversible destabilization of PB-containing thin films.

(a) ^{14}C-Dextran sulfate release after applying potential for 10 s and 1 min intervals. (b) Total ^{14}C-dextran sulfate release from equivalent samples held at the oxidizing potential for

varying times. (c) ^{14}C-dextran sulfate release from a single film held at 1.25 V for 1 min intervals at t = 0 and t = 15 min. (d) Release rate from film shown in (c). In all cases, error bars indicate one standard deviation.

9.3.5 Surface analysis

An interesting phenomenon that we observed in all cases is that film thickness decreased by only ~80%, leaving behind a fraction of the film on the substrate surface even after holding the oxidizing potential constant for long amounts of time (e.g., 1-2 h). We hypothesize that the remaining material is composed of oxidized hydrophobic PX particles which aggregate at the substrate-liquid interface. To investigate this phenomenon, we used Atomic Force Microscopy (AFM). Before degradation, the film surface exhibits small, regular surface features that likely reflect a monolayer of nanoparticles on the film surface. Following degradation, the film surface becomes rougher, and larger aggregates become visible (data not shown). This data supports the hypothesis that oxidized hydrophobic PX particles aggregate at the substrate surface following degradation.

9.3.6 Toxicity of Prussian Blue

Finally, as a measure of the biocompatibility of PB nanoparticles, we measured their toxicity on a panel of mammalian cell lines, including hepatocellular carcinoma (HCC), ovarian cancer (HeLa), and kidney fibroblast (Cos-7) cells, using a conventional MTT assay. The MTT assay measures the effect of added substances on cell growth and metabolism, and is commonly used as an *in vitro* measure of toxicity.[28] Interestingly, PB particles caused no observable toxicity at all concentrations tested (up to 1.0 mg/mL) (Figure 9.7). These findings are not entirely surprising, as PB is known to cause no adverse health effects in humans and was

approved by the US FDA in 2003 for the treatment of radiation contamination and heavy metal poisoning.[29]

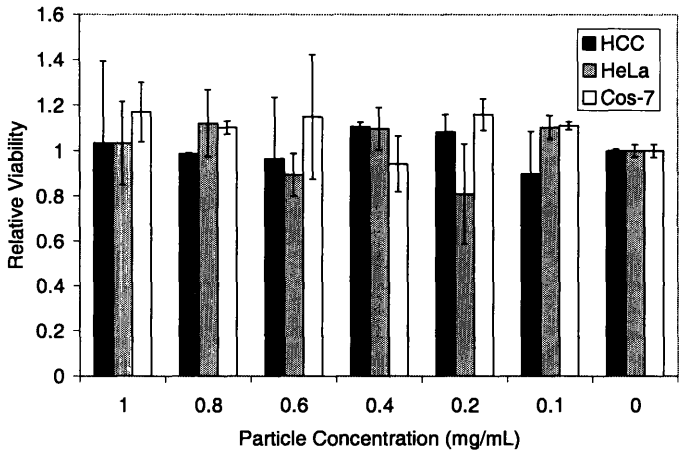

Figure 9.7. MTT assay for cellular toxicity indicates that PB nanoparticles exhibit no toxicity on three different cell lines at concentrations up to 1.0 mg/mL.
Error bars represent one standard deviation in measured values.

9.4 Summary

We have demonstrated a new approach for constructing nanostructured thin films capable of releasing precise quantities of chemicals on demand in response to a small electrochemical stimulus. Further, we have shown that the films are stable enough to release a fraction of their contents, then restabilize upon removal of the applied potential. The LbL technique is sufficiently general to allow for the incorporation of chemicals of any structure (small molecules, macromolecules, charged and uncharged species, etc.) into these systems, alone or in conjunction with a 'carrier' species.[8-10] As a simple proof of principle, we have studied the (LPEI/dextran sulfate/LPEI/PB) system, in which the model chemical species of interest (dextran sulfate) is alternately deposited (in conjunction with a 'carrier' species, LPEI) with the electroactive

component, PB. Similar model drug species that are currently under study include heparin sulfate and a range of charged proteins.[17, 30] Finally, we have outlined a mechanistic hypothesis to explain the deconstruction process occurring in these systems, whereby an electrochemical signal oxidizes the nanoparticles to the PX state, resulting in loss of particle charge and destabilization of the film through self-repulsion of the polycation species. We expect that these electroactive controlled release thin films may find interesting applications in fields including drug delivery, tissue engineering, medical diagnostics, analytical chemistry, and chemical detection. Further, using the various thin film patterning techniques developed in recent years, we suggest that these materials may eventually be arrayed to produce multi-drug or multi-dose 'smart' devices.[1]

9.5 References

1. LaVan, D.A., McGuire, T. & Langer, R. Small-scale systems for in vivo drug delivery. *Nat Biotechnol* **21**, 1184-1191 (2003).
2. Santini, J.T., Richards, A.C., Scheidt, R., Cima, M.J. & Langer, R. Microchips as controlled drug-delivery devices. *Angew Chem Int Ed* **39**, 2396-2407 (2000).
3. Santini, J.T., Cima, M.J. & Langer, R. A controlled-release microchip. *Nature* **397**, 335-338 (1999).
4. Razzacki, S.Z., Thwar, P.K., Yang, M., Ugaz, V.M. & Burns, M.A. Integrated microsystems for controlled drug delivery. *Adv Drug Deliv Rev* **56**, 185-198 (2004).
5. Staples, M., Daniel, K., Cima, M.J. & Langer, R. Application of micro- and nano-electromechanical devices to drug delivery. *Pharm Res* **23**, 847-863 (2006).
6. Reed, M.L. et al. Micromechanical devices for intravascular drug delivery. *J Pharm Sci* **87**, 1387-1394 (1998).
7. Duffy, D.C., McDonald, J.C., Schueller, O.J.A. & Whitesides, G.M. Rapid Prototyping of Microfluidic Systems in Poly(dimethylsiloxane). *Anal Chem* **70**, 4947-4984 (1998).
8. Decher, G. Fuzzy nanoassemblies: Toward layered polymeric multicomposites. *Science* **277**, 1232-1237 (1997).
9. Hammond, P.T. Recent explorations in electrostatic multilayer thin film assembly. *Colloid Interface Sci* **4**, 430-432 (2000).
10. Hammond, P.T. Form and function in multilayer assembly: New applications at the nanoscale. *Adv Mater* **16**, 1271-1293 (2004).
11. Caruso, F. & Schuler, C. Enzyme multilayers on colloid particles: Assembly, stability, and enzymatic activity. *Langmuir* **16**, 9595-9603 (2000).

12. Shi, X. & Caruso, F. Release behavior of thin-walled microcapsules composed of polyelectrolyte multilayers. *Langmuir* **17**, 2036-2042 (2001).
13. Sukhorukov, G.B., Brumen, M., Donath, E. & Mohwald, H. Hollow polyelectrolyte shells: Exclusion of polymers and donnan equilibrium. *J Phys Chem B* **103**, 6434-6440 (1999).
14. Jewell, C.M., Zhang, J., Fredin, N.J. & Lynn, D.M. Multilayered polyelectrolyte films promote the direct and localized delivery of DNA to cells. *J Control Release* **106**, 214-223 (2005).
15. Vazquez, E., DeWitt, D.M., Hammond, P.T. & Lynn, D.M. Construction of hydrolytically-degradable thin films via layer-by-layer deposition of degradable polyelectrolytes. *J Am Chem Soc* **124**, 13992-13993 (2002).
16. Wood, K.C., Boedicker, J.Q., Lynn, D.M. & Hammond, P.T. Tunable drug release from hydrolytically degradable layer-by-layer thin films. *Langmuir* **21**, 1603-1609 (2005).
17. Wood, K.C., Chuang, H.F., Batten, R.D., Lynn, D.M. & Hammond, P.T. Controlling interlayer diffusion to achieve sustained, multiagent delivery from layer-by-layer thin films. *Proc Natl Acad Sci USA* **103**, 10207-10212 (2006).
18. Zhang, J., Chua, L.S. & Lynn, D.M. Multilayered thin films that sustain the release of functional DNA under physiological conditions. *Langmuir* **20**, 8015-8021 (2004).
19. Chung, A.J. & F, R.M. Methods of loading and releasing low molecular weight cationic molecules in weak polyelectrolyte multilayer films. *Langmuir* **18**, 1176-1183 (2002).
20. Hiller, J.A. & Rubner, M.F. Reversible molecular memory and pH-switchable swelling transitions in polyelectrolyte multilayers. *Macromolecules* **36**, 4078-4083 (2003).
21. Ma, Y., Dong, W.F., Hempenius, M.A., Mohwald, H. & Vancso, G.J. Redox-controlled molecular permeability of composite-wall microcapsules. *Nat Mater* **5**, 724-729 (2006).
22. Schuler, C. & Caruso, F. Decomposable hollow biopolymer-based capsules. *Biomacromolecules* **2**, 921-926 (2001).
23. Mortimer, R.J. Electrochromic materials. *Chem Soc Rev* **26**, 147-156 (1993).
24. Karyakin, A.A., Gltelmacher, O.V. & Karyakin, E.E. Prussian blue-based first-generation biosensor - A sensitive amperometric electrode for glucose. *Anal Chem* **67**, 2419-2423 (1995).
25. Mingotaud, C., Lafuente, C., Amiell, J. & Delhaes, P. Ferromagnetic Langmuir-Blodgett film based on Prussian Blue. *Langmuir* **15**, 289-292 (1999).
26. Neff, V.D. Electrochemical oxidation and reduction of thin-films of Prussian Blue. *J Electrochem Soc* **125**, 886-887 (1978).
27. DeLongchamp, D.M. & Hammond, P.T. High-contrast electrochromism and controllable dissolution of assembled Prussian blue/polymer nanocomposites. *Adv Func Mater* **14**, 224-232 (2004).
28. Hansen, M.B., Nielsen, S.E. & Berg, K. Re-examination and further development of a precise and rapid dye method for measuring cell growth/cell kill. *J Immunol Methods* **119**, 203-210 (1989).
29. Pearce, J. Studies of any toxicological effects of Prussian Blue compounds in mammals - A review. *Food Chem Toxicol* **32**, 577-582 (1994).
30. Wood, K.C., MacDonald, M.L., Smith, R.C., Chuang, H.F. & Hammond, P.T. Unpublished data. (2007).

Chapter 10: Summary and future work

10.1 Summary

The main objective of the work in this thesis was to design new polymeric structures for gene and drug delivery applications. An emphasis was placed on controlling both molecular structure and supramolecular self-assembly behavior in these systems based on the hypothesis that fine control over architectural features could yield superior properties as compared to conventional, bulk materials.

In the first part of this thesis (Chapters 2-5), the design and synthesis of a family of linear-dendritic "hybrid" polymers for gene delivery applications was described. These systems are unique in that they possess multiple, complimentary functional domains which are assembled in a modular fashion. Chapters 2-3 describe the initial design and characterization of these systems, including: the divergent synthesis of hybrid polymers; hierarchical self-assembly of polymers with plasmid DNA to yield small (~ 150 nm), spherical, electrostatic complexes; the targeted transfection of cells in culture; and the low cytotoxicity of hybrid polymers *in vitro*.[1] Chapter 4 described a series of initial experiments toward the use of hybrid polymers for the delivery of DNA vaccines, including the targeted, efficient transfection of dendritic cells in culture as well as the elicitation of both primary and secondary, cellular and humoral responses specific to an encoded transgene. Finally, Chapter 5 described an alternative synthetic approach for hybrid polymers which is rapid (three steps, two days) and takes place at room temperature in neutral pH, aqueous solutions. As a result, unlike the original divergent synthesis of hybrid polymers, this new approach allows for the use of biological targeting ligands such as peptides,

proteins, and antibodies. This method was utilized to synthesize hybrid polymers functionalized with a tumor-homing peptide which can efficiently target and transfect cells expressing glucose-regulated protein-78 kDa (GRP-78), a known tumor-associated antigen. Further, preliminary results demonstrating the potential utility of these systems for targeted gene delivery to solid tumors *in vivo* was shown.[2]

In the second part of this thesis (Chapters 6-9), the development of degradable layer-by-layer (LbL) thin films was described. These systems, formed by the directed self-assembly of systems containing charged or complementary functional groups onto a solid substrate, were of interest for two major reasons. First, they are conformal and have the ability to coat virtually any surface without regard to size, shape, or chemical composition. Second, the LbL technique allows for absolute control over the order in which multiple components are deposited onto a growing film, suggesting that the film composition and resultant release properties of one or more species can be controlled. Following a brief overview of the LbL technique in Chapter 6, Chapter 7 described an initial attempt to construct degradable LbL films using a hydrolytically-labile poly (β amino ester). The thickness of these nanoscale thin films decreases linearly with time at a rate that is proportional to the concentration of hydroxyl ions in solution, suggesting that hydrolysis (rather than dissolution or decomplexation) controls film degradation. Further, drug release occurs on time scales which are in quantitative agreement with film degradation.[3] In Chapter 8, the concept of drug release from hydrolytically degradable LbL films was extended in several ways. First, it was demonstrated that the amount of drug incorporated into a film and, in some cases, the duration of time over which a drug is released are proportional to the number of adsorbed layers. Second, the effects of interlayer diffusion of drugs were explored in detail; namely, a connection between interlayer diffusion, final film architecture, and drug release

behavior was established. Third, the release of multiple drugs from a single film, both in series and in parallel, was demonstrated. In particular, it was shown that the serial release of multiple drugs requires that drug-containing layers be physically separated, a property which can be controlled using cross-linked blocking layers.[4] Finally, Chapter 9 explored an alternative means of destabilizing LbL films based on an active, electrochemical stimulus. LbL films containing Prussian Blue, an iron hexacyanoferrate material, can undergo reversible destabilization in the presence of a small applied potential (1.25 V), resulting in drug release which can be precisely controlled. The process of destabilization is reversible in these systems, and they are made from active components which are both non-toxic and FDA approved for use in humans.[5] Together, LbL systems which degrade by both hydrolytic and electrochemical means represent exciting candidates for a host of drug delivery applications.

10.2 Future Work

The materials and methodologies developed in this thesis warrant further investigation in several ways. In the area of hybrid polymer gene delivery systems, the new synthesis technique described in Chapter 5 (linear dendritic coupling) should enable a range of new opportunities, particularly involving the use of biologically-derived functional domains such as targeting ligands. Four areas for future exploration are proposed below.

1. *Pre-clinical animal studies.* Preliminary studies demonstrating the promise of hybrid polymer systems for both the *in vivo* delivery of DNA vaccines and direct tumor targeting should be augmented with more comprehensive, large scale animal studies. In the former area, a more thorough study of the activation of cell-based immune responses using hybrid polymers, an investigation of the adjuvanting effects of these systems, and a study involving the use of these

systems for protective vaccination against a robust, clinically-relevant disease challenge are each warranted. In the area of direct tumor targeting, a large animal study exploring the use of peptide-functionalized hybrid polymers for the delivery of both reporter (i.e. luciferase) and "suicide" (i.e. Herpes simplex virus-thymidine kinase, HSV*tk*[6]) transgenes to solid tumors is also warranted.

2. *Engineering new functionalities.* Hybrid polymers provide an excellent platform for the testing of additional or modified functional domains, such as nuclear localization peptides, membrane destabilizing peptides, and degradable polymer chemistries, which may significantly enhance the activity of these delivery systems.[7, 8] Mechanistic studies on the effect of such additions on targeting and intracellular trafficking of complexes, and ultimately on transgene expression, would provide important insight into the behavior and engineering of these systems.

3. *Toxin potentiation.* A series of preliminary experiments conducted in collaboration with the Wittrup group at MIT have explored the conjugation of hybrid polymers to single chain variable fragments (scFv) that were engineered to bind to tumor-associated antigens.[9] These conjugates will be used for the targeted delivery of both DNA and protein-based toxins to solid tumors. In the former area, targeted gene delivery will be explored in a manner analogous to the work described in Chapter 5. In the latter area, we will be studying the ability of hybrid polymers to potentiate the toxicity of gelonin, a naturally-occurring toxin found in plants which functions by cleaving ribosomal RNA. Gelonin is highly toxic in the cytosolic compartment of cells, where studies have shown that even a single molecule of toxin can destroy an entire cell. However, it is non-toxic in the extracellular environment and lacks a mechanism for cellular entry. Thus, its use as a therapeutic requires that it be actively transported to the cytosol.[10, 11] As described in Part I, PAMAM dendrimers are known to be effective intracellular delivery agents

because of their ability to promote endosomal escape via the proton sponge mechanism.[12] By conjugating PAMAM dendrimers to an scFv that is selectively internalized by cells expressing tumor-associated antigens, it may be possible to selectively potentiate the toxicity of co-administered gelonin in tumors (using co-administration with either free gelonin or a gelonin-scFv fusion protein). Preliminary experiments examining the synthesis and purification of scFv-hybrid polymer conjugates and their ability to potentiate gelonin toxicity *in vitro* have yielded promising results and warrant further exploration.

4. *Product purification.* Each of areas described above will benefit from the continued development of purification protocols which allow for the isolation of pure samples of hybrid polymers. In some cases, the products of linear-dendritic coupling reactions can be relatively pure, obviating the need for extensive purification. However, it is clear that the isolation of pure samples would allow for a more clear inference of structure-property relationships in these materials, as well as potentially improved properties.

In the area of degradable LbL thin films, the studies described in Chapters 6-9 demonstrate the use of these systems for the controlled release of one or more species in response to both passive (hydrolytic) and active (electrochemical) stimuli. A range of additional studies are warranted, including investigations aimed at better understanding and manipulating physicochemical properties of these systems as well as studies involving distinct therapeutic applications. Three areas of primary emphasis are described below:

1. *Approaching therapeutic applications.* The studies described in this thesis shed light on the fact that even subtle changes in drug or polymer structure and film assembly or degradation conditions can significantly alter release properties of degradable LbL systems.

Thus, future studies aimed at therapeutic applications of these systems should focus largely (if not exclusively) on the encapsulation and release of relevant drug compounds in environments that mimic physiological conditions, rather than model drug compounds in "unnatural" environments (for example, buffered saline at room temperature). After studying the properties of drug-containing film systems *in vitro* (with an emphasis on establishing desired drug release kinetics and efficacy), studies should progress as rapidly as possible toward *in vivo* studies which can both provide a more realistic appraisal of a system's therapeutic efficacy and also shed light on important issues related to biocompatibility.

2. *Understanding and manipulating physicochemical properties of degradable films.* As described above, we have observed that subtle factors regarding polymer structure, assembly conditions, and other parameters can strongly influence final film properties.[4] A large, systematic study of the effects of a range of fabrication conditions on resultant film properties should be undertaken in conjunction with quantitative analysis and physical/mathematical modeling to better understand these phenomena. In addition to leading to a better understanding of the film assembly process, these studies could reveal important factors which can be manipulated to improve film stability and release behavior.

3. *Multi-drug or multi-dose release from "stacked" or arrayed films.* The LbL technique allows for precise control over the order in which multiple components are incorporated into a growing film. Thus, it may be possible to exploit this process to construct multicompartment, striated structures comprised of "stacked" layers, each containing a different drug component.[13-15] The surface-mediated degradation of such a film could then lead to the release of multiple drugs or doses in a predefined manner.[16, 17] However, despite the simplicity of this concept, it has been difficult to experimentally engineer systems with such properties.

This is most likely attributable to the phenomenon of interlayer diffusion, a phenomenon which results in the migration of one or more components throughout a film structure. In Chapter 8, a strategy for controlling interlayer diffusion based on thermally cross-linked blocking layers was discussed. However, the development of additional strategies to create striated film structures by blocking interlayer diffusion is warranted, as the approach used in Chapter 8 involves high temperatures and chemistries which are not compatible with a large number of drugs. An alternative approach to "stacked" multicompartment films involves the patterning of surfaces with multiple features possessing differential drug release properties.[18, 19] Such an approach could also be used to achieve complex, multi-drug or multi-dose release profiles. Thus, additional research exploring (1) techniques for controlling interlayer diffusion to create multicompartment film structures capable of releasing multiple components, and (2) two-dimensional patterning of multiple films with differential release properties are both warranted.

10.3 References

1. Wood, K.C., Little, S.R., Langer, R. & Hammond, P.T. A family of hierarchically self-assembling linear-dendritic hybrid polymers for targeted efficient gene delivery. *Angew Chem Int Ed* **44**, 6704-6708 (2005).
2. Wood, K.C., Azarin, S.M., Langer, R. & Hammond, P.T. Tumor-selective nonviral gene delivery using linear-dendritic hybrid polymers functionalized with a tumor-homing peptide. *Manuscript in Preparation* (2007).
3. Wood, K.C., Boedicker, J.Q., Lynn, D.M. & Hammond, P.T. Tunable drug release from hydrolytically degradable layer-by-layer thin films. *Langmuir* **21**, 1603-1609 (2005).
4. Wood, K.C., Chuang, H.F., Batten, R.D., Lynn, D.M. & Hammond, P.T. Controlling interlayer diffusion to achieve sustained, multi-agent drug delivery from layer-by-layer thin films. *Proc Natl Acad Sci USA* **103**, 10207-10212 (2006).
5. Wood, K.C. et al. Electroactive controlled release thin films. *Submitted* (2007).
6. Hajitou, A. et al. A hybrid vector for ligand-directed tumor targeting and molecular imaging. *Cell* **125**, 385-398 (2006).
7. Wagner, E. Strategies to improve DNA polyplexes for *in vivo* gene transfer: Will "artificial viruses" be the answer? *Pharm. Res.* **21**, 8-14 (2004).
8. Luo, D. & Saltzman, W. Synthetic DNA delivery systems. *Nat. Biotechnol.* **18**, 33-37 (2000).

9. Graff, C., Chester, K., Begent, R. & Wittrup, K. Directed evolution of an anti-carcinoembryonic antigen scFv with a 4-day monovalent dissociation helf-time at 37° C. *Protein Engineering, Design, and Selection* **17**, 293-304 (2004).
10. Sandvig, K. & van Deurs, B. Delivery into cells: lessons learned from plant and bacterial toxins. *Gene Ther* **12**, 865-872 (2005).
11. Kuehne, J. & Murphy, R.M. Synthesis and characterization of membrane-active GALA-OKT9 conjugates. *Bioconjugate Chem* **12**, 742-749 (2001).
12. Sonawane, N.D., Szoka, F.C. & Verkman, A.S. Chloride accumulation and swelling in endosomes enhances DNA transfer by polyamine-DNA polyplexes. *J. Biol. Chem.* **278**, 44826-44831 (2003).
13. Nolte, A.J., Rubner, M.F. & Cohen, R.E. Creating effective refractive index gradients within polyelectrolyte multilayer films: molecularly assembled rugate filters. *Langmuir* **20**, 3304-3310 (2004).
14. Wang, T.C., Cohen, R.E. & Rubner, M.F. Metallodielectric photonic structures based on polyelectrolyte multilayers. *Advanced Materials* **14**, 1534 (2002).
15. Garza, J. et al. Multicompartment films made of alternate polyelectrolyte multilayers of exponential and linear growth. *Langmuir* **20**, 7298-7302 (2004).
16. Wood, K.C., Boedicker, J.Q., Lynn, D.M. & Hammond, P.T. Tunable drug release from hydrolytically degradable layer-by-layer thin films. *Langmuir* **21**, 1603-1609 (2005).
17. Wood, K.C., Chuang, H.F., Batten, R.D., Lynn, D.M. & Hammond, P.T. Controlling interlayer diffusion to achieve sustained, multiagent delivery from layer-by-layer thin films. *Proc Natl Acad Sci USA* **103**, 10207-10212 (2006).
18. Hammond, P.T. Recent explorations in electrostatic multilayer thin film assembly. *Colloid Interface Sci* **4**, 430-432 (2000).
19. Hammond, P.T. Form and function in multilayer assembly: New applications at the nanoscale. *Adv Mater* **16**, 1271-1293 (2004).